Isolation, structure determination, and chemical synthesis of acyl glucoses from *Solanum pennellii* and investigation of their biological activities

(*Solanum pennellii* 由来の新規アシルグルコースの単離、構造決定、化学合成、およびその生物活性の生物有機化学的研究)

A dissertation submitted to the Global Education Program for AgriScience Frontiers, Graduate School of Agriculture, Hokkaido University.

By

MASIMBULA VIDANALAGE RISHNI SAMINDIKA MASIMBULA

Laboratory of Natural Product Chemistry
Unit of Applied Biochemistry
Frontiers in Biosciences
Graduate School of Agriculture
Hokkaido University

September 2022

ACKNOWLEDGEMENT

A new direction in my life started with undertaking the doctoral course at the Graduate School of Agriculture, Hokkaido University. I would like to take a chance here to acknowledge the loving people who were always around with me providing guidance and assistance to make this dream come true.

First and foremost, I am honored to express my deepest gratitude to Prof. Hideyuki Matsuura for his excellent guidance, suggestions, comments, invaluable patience, and understanding. Without his enormous support, this journey will never come true. I am deeply indebted to my first M.Sc. supervisor Prof. Kosaku Takahashi for making the path to study in Japan. The word cannot express the support received from Assist. Prof. Naoki Kitaoka during this period. My deepest appreciation goes to Prof. Makoto Hashimoto, Prof. Kosaku Takahashi, and Assist. Prof. Naoki Kitaoka for reviewing my thesis and providing me with valuable suggestions to improve the quality of my study. I am extremely grateful to my defense committee for who generously provided knowledge and expertise. I would like to thank the Ajinomoto Scholarship Foundation and Hokkaido University DX Doctoral Fellowship for providing me the financial support. My deep appreciation goes to Dr. Sarath Bandara who shared the information about the Laboratory of Natural Product Chemistry, Graduate School of Agriculture, Hokkaido University.

I would like to extend my sincere thanks to all the academic and non-academic staff in the Graduate school for Agriculture, Hokkaido University. I am also thankful to Dr. E. Fukushi and Mr. Y. Takata for their assistance in obtaining the spectroscopic data. Next, I would like to pass on many thanks to all my friends in the laboratory for the countless

support given to me all the time. My gratitude goes to Ms. Yuka Konishi, Mr. Naoshige Kuwata, Mr. Tanaka Genta, and Ms. Shiori Itou for helping me to adjust to Japan when I came to Sapporo for the first time. Their effort to teach me Japanese was countless.

I am extremely grateful to my loving parents and my brothers for always being with me in love, support, and encouragement to follow my dreams. I would like to express my gratitude to my loving daughter, Miyuki Godigamuwa for making me refresh all the time with her beautiful smile and eyes filling with love. Lastly, I would like to mention, my loving husband, Kasun Godigamuwa who has been by my side always, and without him, I could not be able to achieve success on this journey in the first place.

DECLARATION

I do hereby clear that the work reported in this project thesis was extensively carried out by me under the supervision of Professor, Hideyuki Matsuura. It describes the results of my own independent research except where due reference has been made in the text. No part of this project thesis has been submitted earlier or concurrently for the same or any other degree.

Date: 2022/07/26 Name: Masimbula Vidanalage Rishni

Samindika Masimbula

TABLE OF CONTENT

LIST OF FIGURES viii

LIST OF TABLES x

LIST OF SCHEMES xi

LIST OF ABBRIVIATIONS xii

CHAPTER 1 1

GENERAL INTRODUCTION 1

1.1. Acyl sugars 3

1.2. Acyl sugar biosynthesis 5

1.3. Biological activities of acyl sugars 9

1.4. *Solanum pennellii* plant 9

1.5. Aims and objectives 12

CHAPTER 2 13

ISOLATION, IDENTIFICATION, AND STRUCTURE DETERMINATION OF ACYL GLUCOSES FROM *Solanum pennellii* 13

2.1. Introduction 13

2.2. Objective 15

2.3. Experimental procedures 16

2.3.1. Plant materials 16

2.3.2. Extraction and isolation 16

2.4. Results and discussion 18

2.4.1. Isolation and structure determination of dibenzyl pennelliiside D 18

2.4.2. Debenzylation 20

2.5. Conclusions 28

CHAPTER 3 29

CHEMICAL SYNTHESIS OF ACYL GLUCOSES 29

3.1. Introduction 29

3.2. Objectives 31

3.3. Experimental procedures 32

3.3.1. Total synthesis of (*S*) and (*R*) isomers of pennelliiside D 32

3.3.1.1. Synthesis of 1-*O*-benzyl-2,3,4,6-*O*-tetraacetyl-*β*-D-glucose (**4**) 32

3.3.2. Synthesis of dibenzyl pennelliisides A and B 41

3.4. Results and discussion 50

3.4.1. Total synthesis of pennelliiside D 50

3.4.2. Synthesis of the benzylated derivative of pennelliisides A and B 52

3.5. Conclusions 61

CHAPTER 4 62

BIOLOGICAL ACTIVITIES OF ACYL GLUCOSES 62

4.1. Introduction 62

4.2. Objectives 64

4.3. Experimental procedure 65

4.3.1. Rooth-growth inhibitory test....65
4.3.2. Water stress treatment....65
4.3.3. Treatment of airborne MeSA and MeJA....66
4.4. Results and discussion....68
4.4.1. Root-growth inhibitory effect....68
4.4.2. Responses to water stress....68
4.4.3. Responses to airborne MeSA and MeJA....69
4.5. Conclusions....74
CHAPTER 5....75
CONCLUSIONS....75
CHAPTER 6....78
GENERAL EXPERIMENTAL PROCEDURES....78
6.1. Equipment and their conditions....78
6.2. LC-TOF-MS analysis condition for airborne MeSA and MeJA, and water stress treatments....79
REFERENCES....81
APPENDIX I: FD-MASS DATA....95
APPENDIX II: NMR SPECTRA....116

LIST OF FIGURES

Figure 1. Structures of acyl sugars.....3

Figure 2. Acyl sugar biosynthesis in *Solanum pennellii*.....7

Figure 3. Acyl sucrose from *S. lycopersicum* and *P. axillaris*.....8

Figure 4. *Solanum pennellii* plant.....10

Figure 5. Types of trichomes in *S. pennellii*.....11

Figure 6. Mechanism of α and β anomerization of acyl glucoses.....14

Figure 7. Structures of pennelliiside D and its benzylated derivative 23

Figure 8. Important resonances of compound **2**.....24

Figure 9. Structures of pennelliisides A and B, and their benzylated derivatives 31

Figure 10. Expanded key ^{1}H-NMR spectrum for the H-A4 resonances of natural dibenzyl pennelliiside D (**2**) and its synthesized isomers (*S*/*R*).....55

Figure 11. The absolute configuration of pennelliiside D and its benzylated derivative. 56

Figure 12. Plants treated with water stress.....66

Figure 13. Experimental setup for the airborne MeSA/MeJA treatment.....67

Figure 14. Root growth inhibitory effect of pennelliiside D (**1**) and its constituent fatty acids.. 70

Figure 15. Photographs of root growth inhibitory effect of pennelliiside D (**1**) and 2-methylbutanoic acid.....71

Figure 16. Evaluation of pennelliisides A-D in *S. pennellii* upon water stress. 72

Figure 17. Evaluation of pennelliiside D in *S. pennellii* upon airborne MeSA and MeJA. 73

LIST OF TABLES

Table 1. ^{1}H NMR (500 MHz) and ^{13}C NMR (126 MHz) spectroscopic data of natural dibenzyl pennelliiside D (**2**) in C_6D_6 (δ in ppm, *J* in Hz) 25

Table 2. ^{1}H NMR (500 MHz) and ^{13}C NMR (126 MHz) spectroscopic data of natural pennelliiside D (**1**) in $CDCl_3$ (δ in ppm, *J* in Hz).....26

Table 3. ^{1}H NMR (500 MHz) and ^{13}C NMR (126 MHz) spectroscopic data of synthesized (*S*) and (*R*) isomers of dibenzyl pennelliiside D (**2**) in C_6D_6 (δ in ppm, *J* in Hz).....57

Table 4. ^{1}H NMR (500 MHz) and ^{13}C NMR (126 MHz) spectroscopic data of synthesized (*S*) isomer of pennelliiside D (**1**) in $CDCl_3$ (δ in ppm, *J* in Hz).....58

Table 5. LC-TOF-MS analysis condition 79

LIST OF SCHEMES

Scheme 1. Reaction of acyl glucose with TriBOT 15

Scheme 2. Removal of benzyl ether 27

Scheme 3. Total synthesis of dibenzyl pennelliiside D 59

Scheme 4. Synthesis of dibenzyl pennelliisides A and B. 60

LIST OF ABBRIVIATIONS

S. pennellii	: *Solanum pennellii*
S. lycopersicum	: *Solanum lycopersicum*
HPLC	: Hight performance liquid chromatography
UPLC MS/MS	: Ultra performance liquid chromatography-tandem mass spectrometry
UHPLC-HR-MS	: Ultrahigh-performance liquid chromatography-high resolution mass spectrometry
HRFD-MS	: High-resolution field desorption mass spectrometry
LC-TOF-MS	: Liquid chromatography time-of-flight mass spectroscopy
NMR	: Nuclear magnetic resonance
A. thaliana	: *Arabidopsis thaliana*
JA	: Jasmonic acid
MeJA	: Methyl jasmonate
SA	: Salicylic acid
MeSA	: Methyl salicylate
IPMS	: Isopropylmalate synthase
ASAT	: Acyl sugar acyltransferases
SlASAT	: *S. lycopersicum* acyl sugar acyltransferases
P. axillaris	: *Petunia axillaris*
FD	: Field desorption
TriBOT	: 2,4,6-tris(benzyloxy)-1,3,5-triazine
DMF	: Dimethylformamide

DCC	: Dicyclohexylcarbodiimide
DMAP	: 4-Dimethylaminopyridine
TFA	: Trifluoroacetic acid
Et_3SiH	: Triethylsilane

CHAPTER 1

GENERAL INTRODUCTION

Plants live in complex environments where they expose to countless stresses. Their life is tremendously vulnerable. To stand against abiotic and biotic stresses, plants have their own defense systems and they produce thousands of specialized metabolites known as secondary metabolites through various biosynthesis pathways [1]. These secondary metabolites have vast structural and functional diversity. Acyl sugars, terpenoids, flavonoids, and alkaloids are some examples of structurally and functionally diverse secondary metabolites. Depending on the types and strength of stresses or interactions, biosynthesis of these metabolites progresses quickly, and the chemical products induce various biological phenomena such as plant-to-plant communication or response to biotic or abiotic stresses in the environment.

Plant accumulate and store these chemical products in specific structures [2]. The surface of many plants mainly, leaves and stems, has hair-like sticky epidermal structures called trichomes. The size of trichomes is from a few microns to centimeters [3]. They differ in size, shape, number of cells, morphology, and composition [4]. Generally, trichomes are divided into two categories based on their shape, and they can be grouped into glandular and non-glandular trichomes [2]. Their capacity to produce, store, and release a large number of specialized metabolites is remarkable. In the trichomes, plants synthesize various classes of acyl glucoses [4], terpenoids [5], polyphenolic compounds [6], flavonoids [7,8], alkaloids [9], etc. It is well known that trichome-produced secondary metabolites are commercially valuable as natural pesticides, pharmaceuticals, fragrances, and food additives [10,11].

When considering the history of biochemistry, the idea that plants produce secondary metabolites to protect themselves from environmental stresses came out in the 19th century [4]. Interest in the identification of secondary metabolites and their biosynthesis pathways arose in the late 19th century. However, there was little interest in the identification of secondary metabolites produced in trichomes and elucidation of their biosynthesis pathways. With the development of biochemistry and analytical techniques, scientists became more aware of the commercial advantages of these compounds and became more interested to isolate and identify those compounds in recent years.

Acyl sugars known as sugar esters are one of a class of non-volatile secondary metabolites stored in trichomes. They account for a major amount among other secondary metabolites in trichomes. Particularly, *Solanum pennellii* LA0716, a wild-type tomato plant, accumulates acyl sugars nearly 20% of its leaf dry weight [12] while tobacco accumulates up to 17% of its leaf dry weight [13]. However, although there are studies related to the biosynthesis of acyl sugars, their full discovery is yet to be discovered [14]. This is due to the availability of vast diversity of acyl sugars. Although several types of acyl sugars have been identified in *S. pennellii* [15], due to the vast diversity many compounds are remained to be identified.

In the present study, isolation, identification, and structural elucidation of acyl sugars produced by *S. pennellii* were performed. Moreover, chemical syntheses of the identified compounds were conducted. Finally, using the synthesized compounds their biological roles were investigated.

1.1. Acyl sugars

The core of acyl sugars is either disaccharide sucrose or glucose, which is attached to straight or branched-chain fatty acid moieties via an *O*-acylation (Figure 1) [16]. Acyl sugars have been reported in several plant families such as Solanaceae, Martyniaceae, Rosaceae, Geraniaceae, Caryophyllaceae, and Brassicaceae [14,17]. In the Solanaceae family, it has been reported in Solanum [18], Nicotina [19], Datura [20], and Petunia [3]. Glandular trichomes within the genus Solanum, which include tomato, potato, and eggplant produce and store acyl sugars [21]. In most cases, acyl sugars have mono-, di-, or tri-fatty acid moieties having a length from carbon two to twelve [22]. Cultivated tomato species of *Solanum lycopersicum* produce so-called F-type acyl sucroses which contain a single acyl group at the furanose ring, and two or three acyl moieties at the pyranose ring [23–25]. In contrast, *Solanum habrochaites* and *S. pennellii* accumulate so-called P-type acyl sucroses which contain two or three acyl groups at the pyranose ring [26].

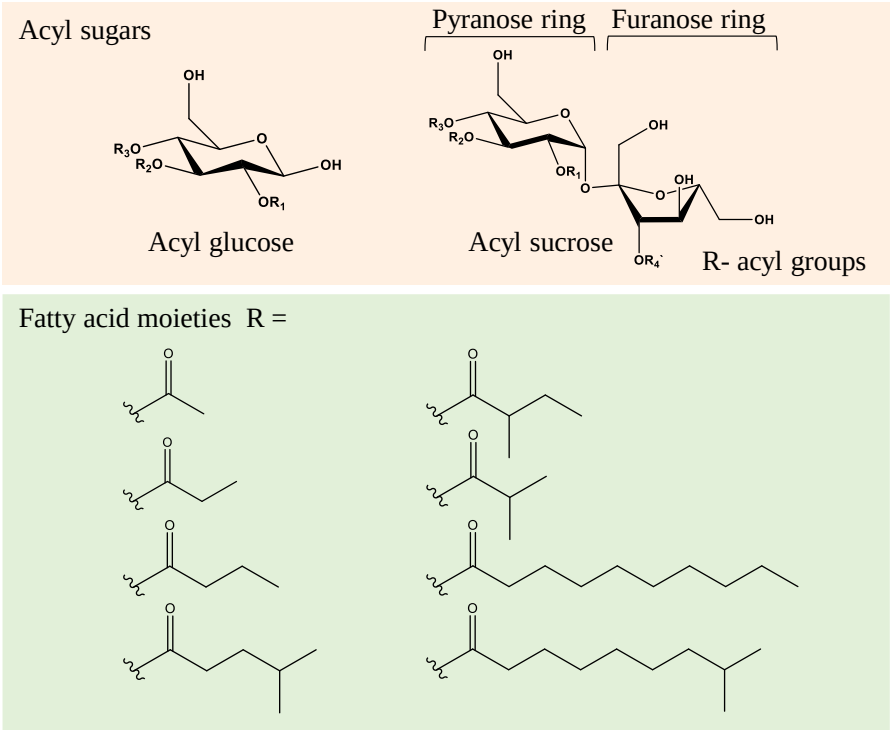

Figure 1. Structures of acyl sugars

Biosynthesis of acyl sugars has been well studied and documented in tomato [3,19] and tobacco species [23,27]. However, a comprehensive understanding of biosynthesis in all species is yet to be discovered. This becomes complex due to having many numerical numbers of different types of acyl sugar structures. Among tomato species, investigation of the biosynthesis of acyl sugars has been paid attention mostly in *S. lycopersicum* and *S. pennellii*, especially in *S. pennellii* accession of LA0716 [14]. Most of the previous studies on acyl sugars have focused on the metabolism of acyl sugars [21,28], the identification of enzymes that synthesize acyl sugars [16,29–31], and their roles as herbivores [32]. Shapiro et al., 1993 [33] have investigated fifteen accessions of *Lycopersicon pennellii* and four accessions of *L. pennellii var. puberulum* for the variability of acyl sugar production corresponding to the geographical distribution. Lybrand et al., 2020 [21] revealed that *S. pennellii* accumulates a mixture of acyl sugars that contained at least thirteen unique structures by using ultrahigh-performance liquid chromatography-high resolution mass spectrometry (UHPLC-HR-MS) and nuclear magnetic resonance (NMR) spectroscopy. In some studies, structural identification of acyl sugars has been conducted for Nicotiana species [34–38]. Although there are some studies related to identifying the fatty acid moieties present in the acyl glucose or acyl sucrose and their composition, most of the studies have been conducted using liquid chromatography or gas chromatography which gave a rough idea [15,21,39,40]. Only a few studies have determined the exact structure of acyl glucoses based on NMR spectroscopy in *S. pennellii* [28,41]. Although Liu et al., 2017 [42] have identified more than hundreds of acyl sugars from Petunia species; *Petunia axillaris, Petunia exserta*, and *Petunia integrifolia*, they could only elucidate the structure of fourteen neutral acyl sucroses and fifteen malonate acyl sucroses using NMR spectroscopy. Although many variabilities in acyl sugars were detected so far,

isolation and elucidation of their chemical structures still remain to be difficult. This is because of the anomerization (α to β and vice versa) at the C-1 position (anomeric carbon) in the glucose [43,44]. Information on detailed structures of acyl sugars is essential to understand the biosynthesis of acyl sugars.

1.2. Acyl sugar biosynthesis

In order to understand how fatty acids are composed and how acyl sugars can use in industrial applications, knowledge of the biosynthesis of acyl sugars is essential. Up to date, some genes related to the biosynthesis of acyl sugars have been identified. However, how those genes are involved in the assembly of fatty acids to the core sugar is elusive since the availability of a huge number of different fatty acids.

Based on the references available so far, biosynthesis of acyl sugars can be explained in two phases: (1) formation of acyl CoAs, and (2) esterification of acetyl groups to sugars [45]. Figure 2 explains the biosynthesis pathway of acyl sugars in *S. pennellii*. Acyl CoA synthetase (ACS), enoyl CoA hydratase (ECH), and isopropylmalate synthase 3 (IPMS3) are involved in the generation of different types of fatty acids CoAs [30]. Based on the comparative and biochemical approaches, it was reported that the IPMS3 enzyme involves in producing 2-methylproponoic acid and 3-methylbutanoic acid in *S. pennellii* accessions [30,46]. In addition to that, Fan et al., 2020 [29] have reported two non-homologous genes; acyl sugar acyl-CoA synthetase (*AACS*) and acyl sugar enoyl-CoA hydratase (*AECH*) from chromosome 7 that involve in producing medium-chain fatty acids in acyl sugar biosynthesis. These two genes are only activated at the tip of trichomes. Acyl-transferase2 (AT2) has been identified as an enzyme involved in the esterification of acetyl (C2) group into major detectable tetra-acyl sucroses of cultivated tomato *S. lycopersicum* cv. M82 [23].

The main tomato acyl sugar biosynthesis pathway is the esterification of acetyl groups into the core sucrose. This process is mainly controlled by four enzymes of acyl sugar acyltransferases (ASAT1-ASAT4) which are specifically secreted in the tip of the trichomes [23]. However, it was reported that only three ASAT1-ASAT3 are involved in *S. pennellii* (Figure 2) [24,45,46], while cultivated tomato (*S. lycopersicum*) produces tri- and tetra-acyl sucroses using *S. lycopersicum* acyl sugar acyltrasferase (SlASAT1 to SlASAT4) [29,39]. These enzymes belong to the BAHD acyltransferase superfamily [named according to the first letter of four characterized enzymes of the family: BEAT (benzylalcohol *O*-acetyltransferase) from *Clarkia breweri*, AHCT (anthocyanin *O*-hydroxycinnamoyltransferases) from *Petunia*, *Senecio*, *Gentiana*, *Perilla*, and *Lavandula*, HCBT (anthranilate *N*-hydroxycinnamoyl/benzoyltransferase) from *Dianthus caryophyllus*, and DAT (deacetylvindoline 4-*O*-acetyltransferas) from *Catharanthus roseus*] [46–50]. In *S. pennellii*, at first, ASAT1 transfers the acyl group from its coenzyme A (CoA) to the R_3 position of sucrose to yield monoacylated sucrose. Secondly, ASAT3 transfers the acyl group to the R_1 position in sucrose to give diacylated sucrose followed by transferring the acyl group by ASAT2 to the R_2 position in sucrose to give triacylated acyl sucrose [21] (Figure 2). Based on the previous studies, the structure of acyl groups was identified as straight or branched chain, typically short chain, C_4 - C_5, and medium chain, C_{10} - C_{12} [51,52]. Slocombe et al., 2008 [19] have reported two modes of elongation of branched-chain fatty acids using isotope feeding studies. They have found that elongation of two carbons in tomato species: *S. pennellii* and *Datura metel* via fatty acid synthase, and elongation of one carbon in tobacco, *Nicotina,* and *petunia* species via -keto acid. Elongation of branched-chain fatty acid occurs through branched-chain keto acid dehydrogenase [3]. However, how these enzymes are involved in fatty acid synthesis is yet to be

discovered. Additionally, acylsucrose fructofuranosidase 1 (ASFF1) was reported as an invertase to create acyl glucose from acyl sucrose [18]. Rapid turnover of acyl sucrose is catalyzed by acylsugar acylhyrolases (ASHs) to recreate mono-, and di-acyl sucroses [30].

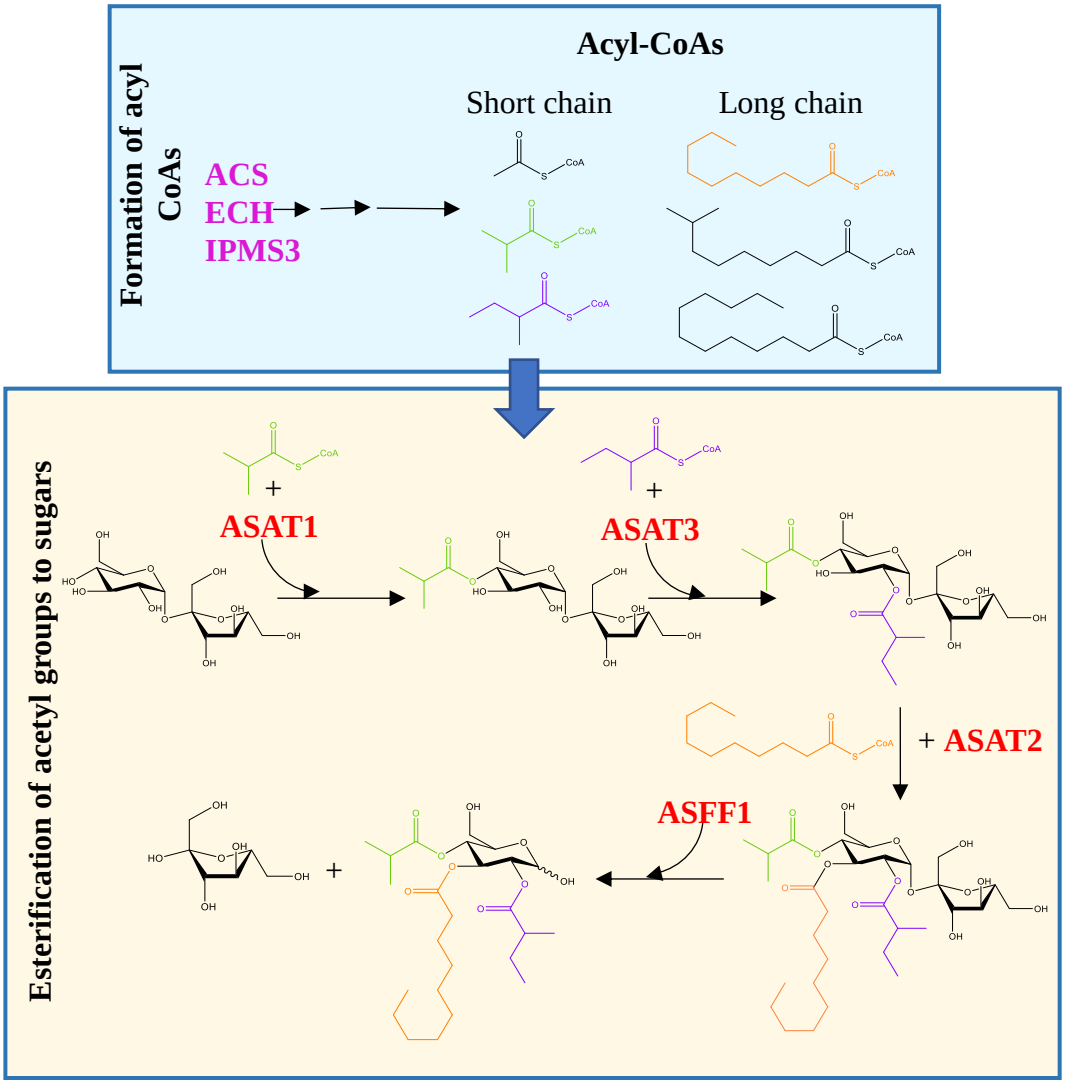

Figure 2. Acyl sugar biosynthesis in *Solanum pennellii*

However, this order of esterification of acyl groups to sucrose is not always the same in plants even within the same family. Notably, their chemical structures also seem to

be different. For example, in the Solanaceae family member of *S. lycopersicum*, tetra acyl sucrose is produced by esterifying acyl groups in order of R_3, R_2, R_4', and R_1 by SlASAT1, SlASAT2, SlASAT3, and SlASAT4 respectively (Figure 3A) [13,22–24,43]. In contrast, the addition of acyl groups occurs in order of R_1, R_2, R_3, R_4, and R_1` in Petunia species of *P. axillaris* [39] (Figure 3B).

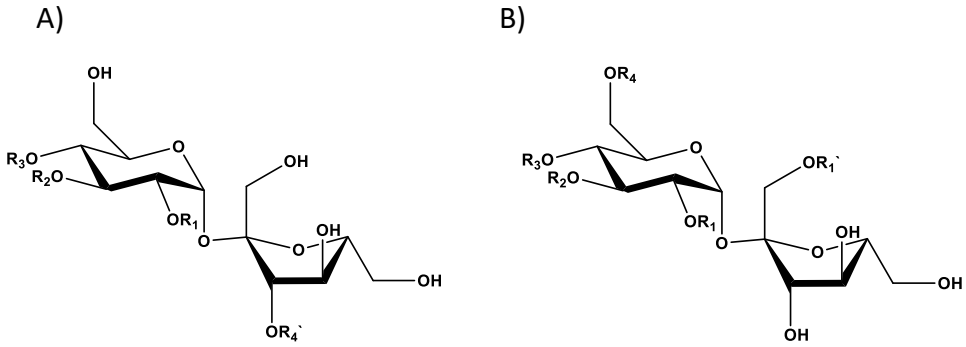

Figure 3. Acyl sucrose from *S. lycopersicum* and *P. axillaris*. (A) Chemical structure of acyl sucrose from *S. lycopersicum*; (B) Chemical structure of acyl sucrose from *P. axillaris* (Nadakuduti et al., 2017 [39]).

When considering a single species, its acyl sugar biosynthesis seems to be simple, thus it was possible to carry out the acyl sugar biosynthesis pathway in a test tube by simply adding ASATs enzymes to sucrose and acyl CoAs [16]. However, it is not simple always as we see because of having a wide variety of acyl sugar profiles. As long as the identification of acyl sugars is carried out, it will be possible to fully discover acyl sugar biosynthesis genes and their metabolic diversity.

1.3. Biological activities of acyl sugars

The biological activities of acyl sugars have been extensively studied. It was reported that acyl sugars show great properties such as anti ovipositional, antifeedant, antioxidant, insecticidal, and toxic properties [15,53–56]. It is well documented that acyl sugars act as a direct defense in the Solanaceae family plant against herbivores and provide protection against a wide range of insets [22]. However, Weinhold et al., 2011 [27] have reported that acyl sugars were the first meal of lepidopteran herbivores on *Nicotiana attenuate* providing nutrients rather than toxic chemicals for them. Leckie et al., 2016 [55] have shown that acyl sugars in *S. pennellii* have the ability to alter the distribution of whitefly oviposition and suppress oviposition on materials treated with acyl sugars. Apart from those activities, amphipathic acyl sugars can reduce the surface tension of water droplets on its leaves, which enables plants to keep hydrated [12,45]. It is also used as antibiotics, anti-inflammatory drugs, food additives, and compounds in cosmetics products which added a great value to industrial applications [3,57–59].

1.4. *Solanum pennellii* plant

Tomato is an extensively cultivated and one of the important flowering crops worldwide. It is a very popular and important vegetable that provides a valuable source of nutrients such as amino acids, antioxidants, vitamins, fiber, and lycopene [60,61]. Tomato has several types of varieties and its popular cultivated species is the *S. lycopersicum* [62].

S. pennellii (Figure 4), which is endemic to South America, is a representative of wild-type tomato [63]. It belongs to the Solanaceae family [3]. Its full genomic information was studied and reported in the 100 Tomato Genome sequencing Consortium in 2014 [64]. Additionally, its introgression lines have been fully established [65,66]. Through

the various biochemical and biotechnological studies, its primary and secondary metabolites, soluble sold contents, volatile components, and biosynthesis have been extensively studied [66].

Figure 4. *Solanum pennellii* plant

As shown in Figure 4, *S. pennellii* has tiny hair-like sticky epidermal structures. Those are called trichomes. Based on the morphology studies, eight different types of trichomes can be found in plants, in which four characteristics of trichomes (type I, IV, VI, and VII) are considered as glandular capitate trichomes [2,3,67] and other four (type II, III, V, and VIII) are considered as non-glandular trichomes [2,3,67]. Particularly, in *S. pennellii*, type IV and VI trichomes can be found (Figure 5) [2,3,68,69]. These trichomes produce a diversity of secondary metabolites. Typically, those are terpenes [5], flavonoids [7,8], acyl sugars [4], phenylpropenes [6], and alkaloids [9] which add

numerical properties and protection to plants such as toxic and insecticidal effects, and antioxidant and antiinflammation properties. Several studies have reported that jasmonic acid (JA), a plant hormone, is an essential component of the defenses in trichomes [67].

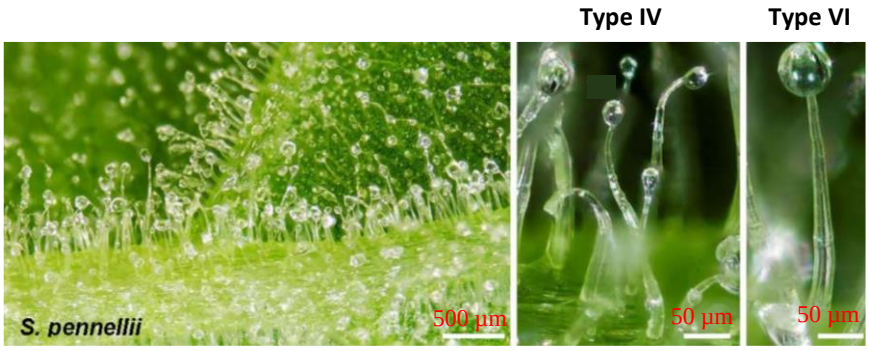

Figure 5. Types of trichomes in *S. pennellii* (Glas et al., 2012 [3])

1.5. Aims and objectives

There are numerous acyl glucoses in *S. pennellii* that had not been isolated and identified yet. Identification and elucidation of new structures are important tasks since those data support understanding the biosynthesis pathway of acyl sugars and evaluation of their biological activities. Therefore, in this dissertation, the main aim is to identify new acyl glucoses and investigate their biological activities. To achieve the goals, isolation of new acyl glucoses and elucidation of their chemical structures were carried out. In order to investigate further testing such as their biological activities, identified acyl glucoses were synthesized. Then, to clarify their biological activities, synthesized compounds were used as standards. To quantify the amount of acyl glucoses in plants, liquid chromatography time-of-flight mass spectroscopy (LC-TOF-MS) was used.

CHAPTER 2

ISOLATION, IDENTIFICATION, AND STRUCTURE DETERMINATION OF ACYL GLUCOSES FROM *Solanum pennellii*

2.1. Introduction

The outermost layer of plants is the first and strongest barrier that pathogens, viruses, and herbivores meet when they reach plants [70]. It provides the greatest protection against those harmful infections. The defense present in the outermost layer is always active. When pathogens or herbivores overcome this barrier, then the induced defense system is activated upon requirement. In order to provide active and strong protection, the plant's outer layer contains specific structures such as trichomes. Components present in trichomes and their density are the key factors of the plant's first defense against herbivores [71,72]. The defense system due to the components within trichomes is potent in different ways such as entrapping herbivores in sticky and toxic exudates, attracting predators [73], protecting against UV, temperature regulation, and tolerance to water stress [3]. These protections are provided through the synthesis of secondary metabolites such as the production of acyl sugars [20], polyphenols [6], and flavonoids [7].

Acyl sugars are a group of secondary metabolites that secrete and store in the granular trichomes in several plant families like Solanaceae, Martyniaceae, Rosaceae, Geraniaceae, Caryophyllaceae, and Brassicaceae [14,39]. These compounds are considered as valuable compounds for agriculture, medicine, and the food industry. Considering their valuable biological activities such as insecticidal effects [55], antioxidant [60], and anti-inflammation properties [58], the identification of acyl sugars has been paid attention recently. Although there are some acyl sugars have been

identified, many unidentified compounds remained due to their complexity and diversity. Therefore, isolation and identification of new acyl glucoses would be beneficial for future studies and commercial applications.

S. pennellii is a wild-type tomato plant that has been paid attention by scientists widely due to its availability, morphology, and applications. Its full genomic information has been investigated [64] which opened a path for biotechnological approaches for future developments. It is considered as a useful plant for the agricultural industry since this plant can be used to breed with other tomato species to produce desired characteristics such as having tolerance to abiotic and biotic stresses, salt and drought [63,74,75] resistance to disease [76], and production of high yield [77]. *S. pennellii* produces acyl sugars in its trichomes, generally, it is nearly 20% of its dry leaf weight [25].

Sugar molecules usually undergo anomerizaton at the anomeric carbon (C-1 position) of the pyranose ring. Figure 6 shows the anomerization mechanism of acyl glucose. Due to the anomerization, the isolation of acyl sugars becomes challenging.

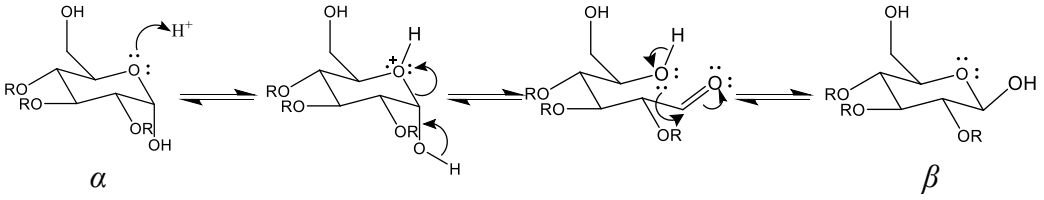

Figure 6. Mechanism of α and β anomerization of acyl glucoses

In this chapter, the difficulties arising from the anomerization were overcome by the *O*-benzylation of free hydroxyl groups present in the pyranose ring to isolate new acyl glucoses. Benzylation of acyl glucoses fixes the glucose into either one of the anomers.

In a previous study, Yamada et al., 2012 [78] have reported a method for making benzyl ethers utilizing a reagent called 2,4,6-tris(benzyloxy)-1,3,5-triazine (TriBOT). Thus, TriBOT can be used to prevent the anomerization that occurs in C-1 of the acyl glucoses (Scheme 1). Using this strategy, previously three acyl glucoses, pennelliisides A-C were isolated and their structures were elucidated by NMR spectroscopy [28]. With the continuing interest, in this study, a new acyl glucose was isolated and its structure was elucidated using 1D and 2D NMR together with field desorption (FD) mass analysis.

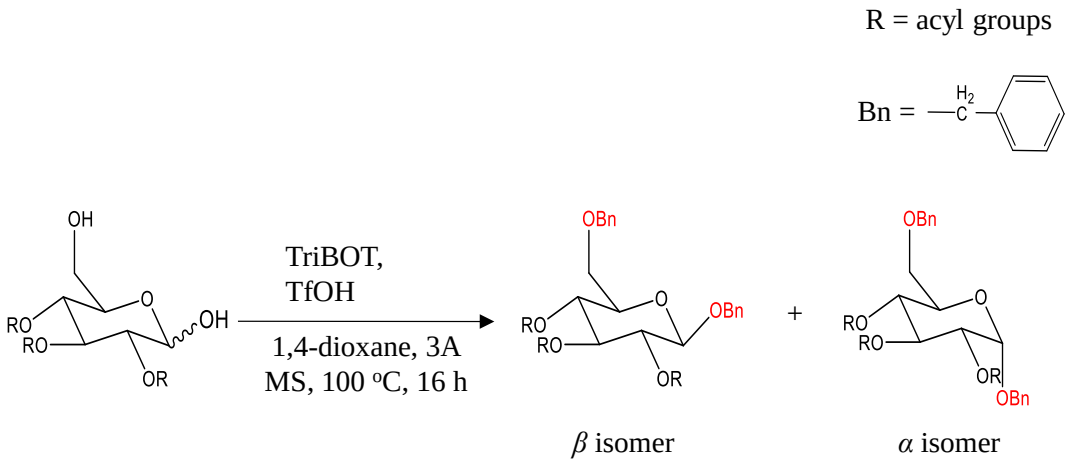

Scheme 1. Reaction of acyl glucose with TriBOT

2.2. Objective

The objective of this chapter is to isolate new acyl glucoses from *S. pennellii* and elucidate their chemical structures.

2.3. Experimental procedures

2.3.1. Plant materials

In this chapter, *S. pennellii* plants were used to isolate acyl glucoses. Seeds of *S. pennellii* were collected from the National Bioresource Project (NBRP, Tsukuba). Seeds were germinated in a plant growing chamber at 25 °C under 16 h of white luminescent light and 8 h of dark photoperiod for 30 days. Then plants were transferred to a greenhouse and grown for another 50 days at 25 °C at the Faculty of Agriculture, Hokkaido University, Hokkaido, Japan.

2.3.2. Extraction and isolation

Aerial parts of the *S. pennellii* plants (1.7 kg) were used to extract acyl sugars. Pieces of plants were roughly divided into five groups. Then, each group of plants was dipped in 1 L of EtOH and shaken for 30 s at room temperature to extract epicuticular lipophilic wax. All the EtOH fractions were combined together (collectively 5 L) and concentrated using a rotary evaporator. The obtained crude material was subjected to liquid-liquid extraction with EtOAc (500 mL) and sat. $NaHCO_3$ (500 mL). Then, the organic layer was dried with Na_2SO_4, and concentrated to obtain a crude sample. The crude material was then partially separated using silica gel column chromatography (MeOH-$CHCl_3$-CH_3COOH, 5:95:0.1).

In order to prevent the anomerization at C-1 in the pyranose ring, the crude sample containing acyl glucoses was treated with TriBOT as previously reported [28,78]. Simply the crude sample which included acyl glucoses was stirred with 100 mL of 1,4-dioxane under anhydrous conditions. Then 300 mg of TriBOT and 35 μL of trifluoromethanesulfonic acid were added to the reaction solution at room temperature.

The reaction mixture was stirred at room temperature for 16 h, and the organic solvent was evaporated using a rotary evaporator to yield an oily sample. Next, the sample was separated using silica gel column chromatography (EtOAc-*n*-hexane-CH_3COOH, 20:80:0.1). Two fractions were obtained. The second fraction, Fr 2 was further separated using high-performance liquid chromatography (HPLC) (InertSustain C_{18}, 10 × 250 mm, 2.5 mL/min, A_{210} nm, MeOH−H_2O−CH_3COOH, 91:9:0.1) to obtain the subfraction, Fr 2-1 (67.7 mg). It was again separated using another two consecutive HPLC separations (Shisheido Capcell park C_{18}, 4.6 × 250 nm, 5 μm, 2 mL/min, CH_3CN-H_2O, 80:20; Cadenza CK-C_{18}, 6 × 250 nm, 3 μm, 2 mL/min, MeOH-H_2O, 80:20) to yield colorless oil, **2** (19 mg). Its chemical structure was determined using ^{1}H NMR, ^{13}C NMR, and 2D NMR. The molecular weight of **2** was measured using high-resolution field desorption mass spectrometry (HRFD-MS). After obtaining the chemical structure, the specific rotation of **2** was measured using a polarimeter at room temperature with the concentration of 6 mg mL^{-1} of **2**.

2.4. Results and discussion

2.4.1. Isolation and structure determination of dibenzyl pennelliiside D

In the present study, new acyl glucose was isolated and its chemical structure was determined based on 1D and 2D NMR spectroscopy. The aerial parts of 80-day-old *S. pennellii* (1.7 kg) were dipped in EtOH for 30 s, and an extract of epicuticular lipophilic wax was obtained by evaporating the organic solvent under reduced pressure. The extract was partitioned between EtOAc and sat. $NaHCO_3$. The extract obtained from the EtOAc layer was roughly purified using silica gel column chromatography to give acyl glucoses.

In order to prevent the anomerization occurring at the C-1 position in the pyranose ring of acyl glucose, *O*-benzylation was carried out for the plant extract. Although some methods such as benzyl alcohol or benzyl bromide have been reported for benzylation of sugars [79,80], those methods result in a low yield or impurities. As reported by Yamada et al., 2012 [78], *O*-benzylation using TriBOT has given a relatively high yield. Thus, this method was adapted to protect the free hydroxyl groups (at C-1 and C-6) present at the glucose moiety of acyl glucoses (Scheme 1). After this step, isolation and structure determination were conducted for the dibenzylated compound. At last, the removal of benzyl groups was conducted to obtain the natural acyl glucose.

Using the above-mentioned strategy, new acyl glucose, dibenzyl pennelliiside D (**2**) was isolated (Figure 7B). Compound **2** was obtained as a colorless oil (19 mg). Its chemical structure is shown in Figure 7. Molecular formula and molecular weight of **2** were confirmed with HRFD-MS data that indicated the molecular weight as *m/z* 584.2992 $[M]^+$ (cal. *m/z* 584.2985 $[M]^+$), and molecular formula as $C_{33}H_{44}O_9$ (Figure S1, Appendix I). Thus, these results suggested that **2** has 12 degrees of unsaturation.

Next, the structure of **2** was elucidated with 1D and 2D NMR spectroscopy. By analyzing ^{1}H NMR, ^{13}C NMR together with COSY, HSQC, HMBC, and NOESY spectra, the structure of **2** was established as shown in Figure 7B. Table 1 shows summarized ^{1}H and ^{13}C NMR data of **2**. According to the ^{1}H NMR spectrum, peaks appeared at δ_H 4.38 (d, J = 7.6 Hz, 1H, H-1), 5.46 (m, 1H, H-2), 5.48 (m, 1H, H-3), 5.30 (dd, J = 10.7, 9.5 Hz, 1H, H-4), 3.42 (m, 1H, H-5), and 3.47 (m, 2H, H-6) confirmed the presence of glucopyranose (Figure S21, Appendix II). It was further confirmed by COSY correlations between the signals at H-1/H-2, H-2/H-3, H-3/H-4, and H-4/H-5 (Figure 8A, and Figure S23, Appendix II) and their corresponding coupling constants (Table 1). As shown in Figure 8B, NOESY interactions were observed between cross-peaks of H-2/H-4 and H-1/H-3/H-5 (Figure S26, Appendix II). The peak observed at δ_C 100.3 corresponded to the C-1 in ^{13}C NMR (Table 1 and Figure S22, Appendix II), and the coupling constant, J = 7.6 Hz in the ^{1}H NMR represents β anomeric structure of the glucose moiety. Next, ten shielded methine groups at δ_H 7.26 (t, J = 7.4 Hz, 4H, H-3', H-7', H-3'', H-7''), 7.12–7.19 (m, 4H, H-4', H-6', H-4'', H-6''), and 7.08 (t, J = 7.3 Hz, 2H, H-5', H-5'') (Table 1, and Figure S21, Appendix II), were identified as peaks corresponding to two benzene rings. Additionally, when comparing HMBC correlations, signals appeared at δ_H 4.75 (d, J = 12.2 Hz, 1H, H-1'), 4.45 (d, J = 12.2 Hz, 1H, H-1'), and 4.33 (d, J = 5.5 Hz, 2H, H-1'') in ^{1}H NMR were identified as protons corresponding to benzylidene attached to the C-1 and C-6 positions respectively (Figure 8A, and S25, Appendix II). The presence of two isobutyryl ester moieties was determined according to the ^{1}H and ^{13}C NMR spectra, and COSY and HMBC correlations (Figures S21 – S25, Appendix II). Signals appeared at δ_H 2.41 (m, 1H, H-B2), 2.31 (m, 1H, H-C2), 1.08 (d, J = 7.0 Hz, 6H, H-B3, B4), 1.02 (d, J = 7.0 Hz, 3H, H-C3), and 0.98 (d, J = 7.0 Hz, 3H, H-C4) in ^{1}H NMR confirmed the presence of

isobutyryl ester moieties. As shown in Figure 8A, these moieties have attached to C-3 and C-4 positions in the glucose moiety. In a similar way, the structure of 2-methylbutyryl fatty acid moiety was identified. Signals showed at δ_H 2.28 (m, 1H, H-A2), 1.69 (m, 1H, H-A4), 1.32 (m, 1H, H-A4), 1.08 (d, J = 7.0 Hz, 3H, H-A3), and 0.81 (t, J = 7.4 Hz, 3H, H-A2) in 1H NMR, and COSY and HMBC correlations expressed the presence of 2-methylbutyryl fatty moiety. It was attached to C-2 in the glucose moiety as shown in Figure 8A. Thus, the comprehensive analysis of NMR data elucidated the structure of **2**, and its IUPAC name was confirmed as 1,6-*O*-dibenzyl-3,4-*O*-diisobutyryl-2-*O*-(2-methylbutyryl)-*β*-D-glucose (Figure 7B). Then in order to understand the optical activity of **2**, specific rotation was measured. The optical activity of **2** was revealed to be $[\alpha]^{25}_D$ = -10.5 (c 0.6, MeOH).

It has been reported that the presence of 2-methylbutyryl in other natural compounds, and it is mostly in the (*S*) configuration [81,82]. Although some studies have reported the availability of 2-methylbutytryl fatty acid moiety in acyl sugar found in tomatoes [15,18], its configuration at the A2 position is still unknown. However, in this study, its absolute configuration could not be identified by using only NMR spectroscopy. It can be detected by comparing the NMR spectra of natural compounds with synthesized (*S*) and (*R*) isomers of **2** or by conducting HPLC analysis with natural fatty acid moiety and standard compounds of (*S*) and (*R*) configured fatty acids.

2.4.2. Debenzylation

In order to get the acyl glucose in its natural form, debenzylation was carried out. Pennelliiside D (**1**) was obtained by debenzylation of **2**. Debenzylation was carried out by reacting **2** with palladium carbon under a hydrogen gas atmosphere (Scheme 2). Compound **1** was obtained as a colorless oil (6 mg, 65%). FD mass analysis of **1**

revealed molecular formula and molecular weight to be $C_{19}H_{32}O_9$ and *m/z* 405.2133 $[M+H]^+$ (cal. *m/z* 405.2125 $[M+H]^+$), respectively (Figure S2, Appendix I). Thus, it indicated having four degrees of unsaturation. After the debenzylation, both anomers of α and β appeared in the sample. Therefore, its ^1H and ^{13}C NMR were quite complex due to the interference of both anomers. However, partial assignments of Hs and Cs corresponding to each anomer were done, and given in Table 2 and Figure S30, Appendix II. Then α and β anomers were identified separately based on signals that appeared in ^{13}C NMR and its coupling constant values in ^1H NMR. Precisely, the peak appeared at δ_C 96.1 in ^{13}C NMR was identified as the peak corresponding to the C-1 of β anomer since its corresponding H showed a coupling constant value as J = 6.9 Hz. In contrast, the peak appeared at δ_C 90.4 in ^{13}C NMR was specified as the peak corresponding to the C-1 of α anomer since its H showed a coupling constant value as J = 3.6 Hz. By analyzing other ^1H and ^{13}C NMR, and COSY, HSQC, and HMBC correlations, the chemical structure of **1** was revealed as 3,4-*O*-diisobutyryl-2-*O*-(2-methylbutyryl)-D-glucose (Figure 7A).

In this study, it was possible to isolate and determine its structure using the strategy of benzylation of free hydroxyl groups present in the pyranose ring. However, this method may not be possible to use to isolate compounds that have unsaturation fatty acid moieties since they react with palladium/carbon when the debenzylation is carried out. Up to date, some fatty acid moieties have been identified, although their exact position of the glucose or sucrose moiety was unclear yet. In this study, the chemical structure of new acyl glucose was fully discovered. So far, it was reported that the length of fatty acids in *S. pennellii* are ranging from C2 to C12 [21], which are straight or branched chains [45]. For example, in *S. pennellii* branched-chain fatty acids are 2-methylpropanoic acid, 3-methylbutanoic acid, 2-methylbutanoic acid, and

8-methylnonanoic acid, and straight-chain fatty acids are decanoic acid, and dodecanoic acid [19,45]. Nevertheless, it has not been reported any unsaturated fatty acid moiety in acyl glucoses or acyl sucroses so far.

A) B)

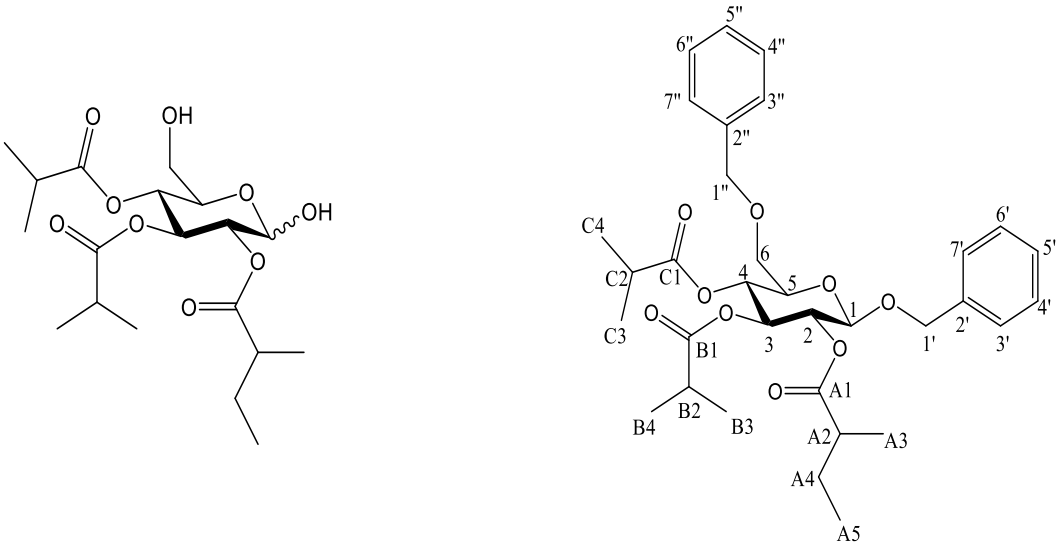

Pennelliiside D (**1**) Dibenzyl Pennelliiside D (**2**)

Figure 7. Structures of pennelliiside D and its benzylated derivative

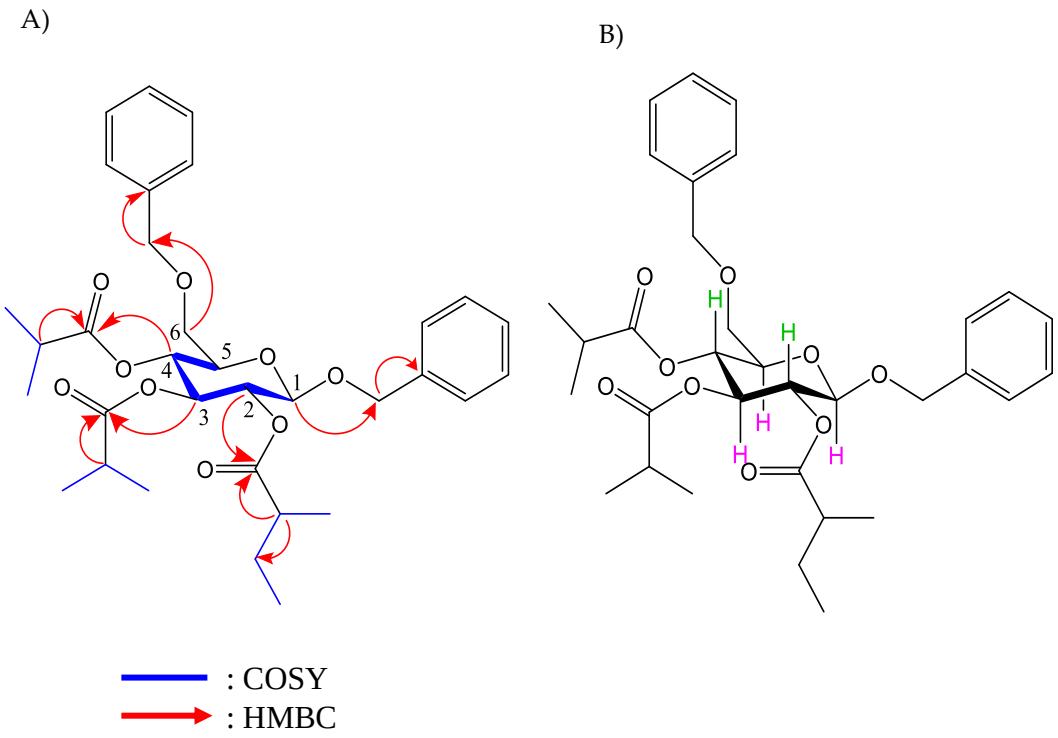

Figure 8. Important resonances of compound **2**; (A) Key ^{1}H-^{1}H COSY and HMBC correlations; (B) Key NOESY interactions observed between protons shown in same color (pink and green)

Table 1. ^{1}H NMR (500 MHz) and ^{13}C NMR (126 MHz) spectroscopic data of natural dibenzyl pennelliiside D (**2**) in C_6D_6 (δ in ppm, J in Hz)

Position	**Type**	**Natural dibenzyl pennelliiside D (2)**	
		δ_C	δ_H (J in Hz)
1	CH	100.3	4.38, d (7.6)
2	CH	71.9	5.46, m
3	CH	73.5	5.48, m
4	CH	70.1	5.30, dd (10.7, 9.5)
5	CH	74.3	3.42, m
6	CH_2	69.9	3.47, m
1a'	CH_2	70.7	4.75, d (12.2)
1b'			4.45, d (12.2)
2'	C	138.0	
3'	CH	128.1–128.6	7.26, t (7.4)
4'	CH	128.1–128.6	7.12–7.19, m
5'	CH	128.1–128.6	7.08, t (7.3)
6'	CH	128.1–128.6	7.12–7.19, m
7'	CH	128.1–128.6	7.26, t (7.4)
A1	C	174.7	
A2	CH	41.9	2.28, m
A3	CH_3	17.2	1.08, d (7.0)
A4	CH_2	27.2	1.32, 1.69, m, m
A5	CH_3	12.2	0.81, t (7.4)
B1	C	176.2	
B2	CH	34.6	2.41, m
B3	CH_3	19.2–19.5	1.08, d (7.0)
B4	CH_3	19.2–19.5	1.08, d (7.0)
C1	C	175.3	
C2	CH	34.5	2.31, m
C3	CH_3	19.2–19.5	1.02, d (7.0)
C4	CH_3	19.2–19.5	0.98, d (7.0)
1a"	CH_2	73.9	4.33, d (5.5)
1b"			4.33, d (5.5)
2"	C	139.0	
3"	CH	128.1–128.7	7.26, t (7.4)
4"	CH	128.1–128.7	7.12–7.19, m
5"	CH	128.1–128.7	7.08, t (7.3)
6"	CH	128.1–128.7	7.12–7.19, m
7"	CH	128.1–128.7	7.26, t (7.4)

Table 2. ^{1}H NMR (500 MHz) and ^{13}C NMR (126 MHz) spectroscopic data of natural pennelliiside D (**1**) in $CDCl_3$ (δ in ppm, J in Hz)

Position	**Type**	***α* Anomer**		***β* Anomer**	
		δ_C	δ_H (J in Hz)	δ_C	δ_H (J in Hz)
1	CH	90.4	5.48, d (3.6)	96.1	4.2 dd (9.8, 9.2))
2	CH	71.4	4.85, dd (6.8, 3.6)	73.5	4.91, dd (7.7, 6.9)
3	CH	69.0	5.65, dd (10.9, 9.9)	71.4	5.41, dd (10.4, 9.6)
4	CH	68.8	5.01, dd (10.9, 9.7)	68.8	5.09, dd (10.4, 8.1)
5	CH	69.7	4.06, m	74.7	3.59, m
6	CH_2	61.3	3.71, 3.55, m	61.3	3.75, 3.59, m
A1	C	176.6		176.6	
A2	CH	41.1	2.38, m	41.1	2.42, m
A3	CH_3	16.4–19.4	1.03–1.17, m	16.4–19.4	1.07-1.21, m
A4	CH_2	26.7	1.41, 1.62, m	26.7	1.45, 1.66, m
A5	CH_3	11.7	0.85, m	11.7	0.90, m
B1	C	176.0		176.0	
B2	CH	34.2	2.50, m	34.2	2.50, m
B3	CH_3	16.4–19.4	1.03–1.17, m	16.4–19.4	1.07–1.21, m
B4	CH_3	16.4–19.4	1.03–1.17, m	16.4–19.4	1.07–1.21, m
C1	C	176.9		176.9	
C2	CH	34.2	2.56, m	34.2	2.56, m
C3	CH_3	16.4–19.4	1.03–1.17, m	16.4–19.4	1.07–1.21, m
C4	CH_3	16.4–19.4	1.03–1.17, m	16.4–19.4	1.07–1.21, m

Scheme 2. Removal of benzyl ether

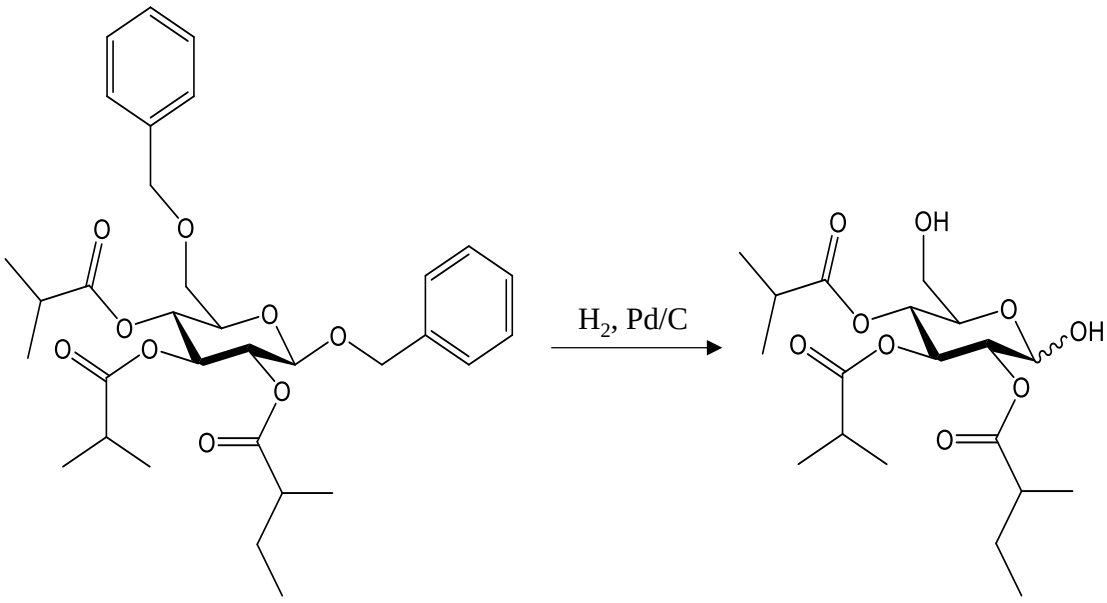

Dibenzyl pennelliiside D (**2**) Pennelliiside D (**1**)

2.5. Conclusions

In the present study, a new acyl glucose, pennelliiside D was isolated, and its chemical structure was elucidated. Isolation was carried out via *O*-benzylation with TriBOT to obtain dibenzyl pennelliside D, 1,6-*O*-dibenzyl-3,4-*O*-diisobutyryl-2-*O*-(2-methylbutyryl)-*β*-D-glucose. After determining its chemical structure using NMR spectroscopy, debenzylation was carried out to yield desired acyl glucose pennelliiside D. Its structure was revealed as 3,4-*O*-diisobutyryl-2-*O*-(2-methylbutyryl)-D-glucose.

CHAPTER 3

CHEMICAL SYNTHESIS OF ACYL GLUCOSES

3.1. Introduction

Chemical synthesis of compounds brings more advantageous applications such as modification of itself into drug molecules to develop new medicines, and new chemicals to apply in agriculture and the food industry [83]. It also helps to verify the structure of compounds isolated from a natural resource. In recent years, structural elucidation of natural products through total synthesis has been widely conducted [84]. In such cases, the chemical structures of the natural products are complex that are not able to be fully determined by NMR spectroscopy [85–87]. Total synthesis was started in the nineteen century by synthesizing urea [88]. Today it becomes a wide research area and shows dramatic technical development. Synthesis of chemical compounds is remarkable which makes the bridge to make different enantiomers, isomers that give different properties to the parent compound. One good example is the discovery of penicillins, a group of antibacterial drugs that inhibit most bacteria, by Alexander Fleming in 1928 [89]. Today penicillin came as an antibiotic drug, via modification of its structures to have desired activity by total and semisynthesis [90], which has helped to save millions of lives. Likewise, many other drug molecules such as vitamin A, morphine, cortisone, and chlorophyll came out to the market as the results of challenging multi-stepped chemical synthesis studies [91]. Chemical synthesis became more sharpened with the finding of organic synthesis reactions like the Diels-Alder reaction [91], the Wittig reaction [92], various palladium-catalyzed coupling reactions [93], and acid-catalysts reactions, together with developing protecting groups [94].

In this study, the chemical synthesis of acyl glucoses was conducted. Pennelliiside D (**1**), 3,4-*O*-diisobutyryl-2-*O*-(2-methylbutyryl)-D-glucose, is a acyl glucose isolated from *S. pennellii* that has been explained in Chapter 1. In order to fully discover its structure, identification of the correct configuration of the fatty acid moiety of 2-methylbytyryl is necessary. Although the availability of 2-methylbutyryl fatty acid in acyl sugars was reported, its absolute configuration was unrevealed yet. Therefore, in this chapter total synthesis was carried out for pennelliiside D to identify the absolute configuration of 2-methylbutyryl fatty acid moiety.

In a previous study, a commonly known tri acylated acyl glucose, 2,3,4-*O*-triisobutyryl-D-glucose (pennelliiside A), another two new acyl glucoses, 3-*O*-(8-methylnonanoyl)-2,4-*O*-diisobutyryl-D-glucose (pennelliiside B), and 3-*O*-decanoyl-2,4-*O*-diisobutyryl-D-glucose (pennelliiside C) were isolated, and their chemical structures were elucidated using 1D and 2D NMR spectroscopy [28]. Isolation was carried out via *O*-benzylation with TriBOT similar to the method explained in Chapter 1. In that study, it was found that some fatty acid moieties of isolated compounds contribute to the allelopathic properties in *Arabidopsis thaliana.* Thus, in the present study, dibenzylated pennelliisides A and B (Figure 9) were also synthesized which may allow for investigating their biological activities in future studies.

A)

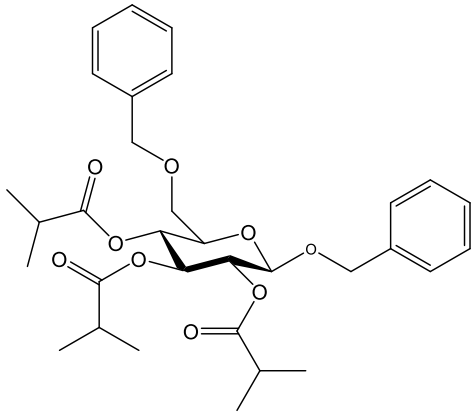

Dibenzyl Pennelliiside A (**14a**)

B)

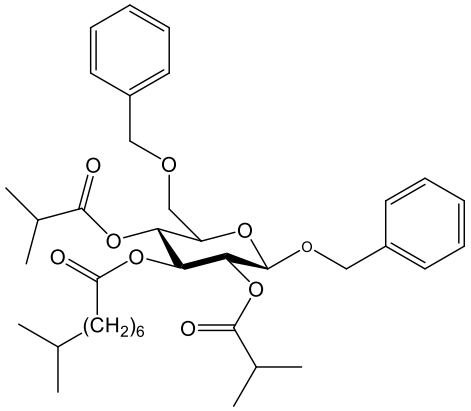

Dibenzyl Pennelliiside B (**14b**)

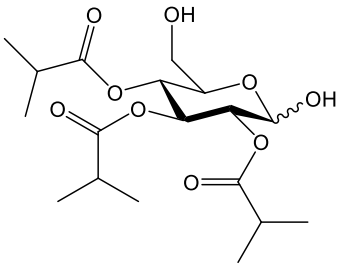

Pennelliiside A

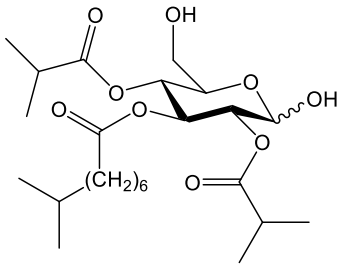

Pennelliiside B

Figure 9. Structures of pennelliisides A and B, and their benzylated derivatives

3.2. Objectives

The objectives of this study are to synthesize pennelliiside D to clarify the correct configuration of the fatty acid moiety, 2-methylbutyryl, and synthesize other known acyl sugars pennelliisides A and B, to carry out further studies. Synthesis of all compounds was started with a commercially available compound.

3.3. Experimental procedures

3.3.1. Total synthesis of (*S*) and (*R*) isomers of pennelliiside D

Total synthesis of pennelliiside D was commenced with a commercially available compound, *β*-D-glucose pentaacetate (**3**). Synthesis of compounds **4**, **5**, **6**, and **9** was conducted according to a reported method [95].

3.3.1.1. Synthesis of 1-*O*-benzyl-2,3,4,6-*O*-tetraacetyl-*β*-D-glucose (**4**)

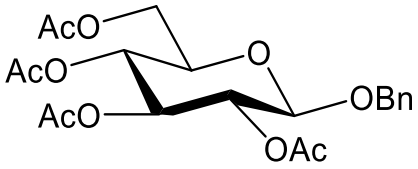

To a mixture of *β*-D-glucose pentaacetate (**3**, 20.00 g, 51.24 mmol) in 200 mL of anhydrous CH_2CH_2, benzyl alcohol (11.16 mL, 102.47 mmol) and $BF_3{\cdot}Et_2O$ (8.20 mL, 66.6 mmol) were added. The reaction mixture was stirred for 24 h at room temperature. The resulting solution was partitioned between sat. $NaHCO_3$ (200 mL × 3) and CH_2CH_2. The organic layer was washed with water (200 mL × 3) and dried over Na_2SO_4 followed by evaporation of the organic solvent to result in a crude product. The crude material was purified using silica gel column chromatography (EtOAc-*n*-hexane, 30:70) to yield a colorless oil, **4** (8.8 g, 19.98 mmol, 39%). ^{1}H NMR (270 MHz, $CDCl_3$, Figure S33, Appendix II): δ_H 7.15–7.32 (m, 5H, Ar-H), 4.92–5.12 (m, 3H, H-2, H-3, H-4), 4.54 (d, *J* = 12.3 Hz, 1H, H-7), 4.46 (d, *J* = 7.6 Hz, 1H, H-7), 4.46 (d, *J* = 7.6 Hz, 1H, H-1), 4.19 (dd, *J* = 11.9, 4.7 Hz, 1H, H-6), 4.08 (dd, *J* = 12.7, 2.5 Hz, 1H, H-6), 3.59 (m, 1H, H-5), 2.02 (s, 3H, CH_3), 1.93 (s, 3H, CH_3), 1.92 (s, 3H, CH_3), 1.91 (s, 3H, CH_3); ^{13}C NMR (126 MHz, $CDCl_3$, Figure S34, Appendix II): δ_C 170.7, 170.3, 169.4, 169.3, 136.6, 128.7–128.5, 99.3, 72.9, 71.9, 71.3, 70.8, 68.4, 62.0, 20.7, 20.6; HRFD-MS *m/z* 438.1516 $[M]^+$ (calcd for $C_{21}H_{26}O_{10}$ *m/z* 438.1526 $[M]^+$) (Figure S3, Appendix I).

3.3.1.2. Synthesis of 1-*O*-benzyl-*β*-D-glucose (**5**)

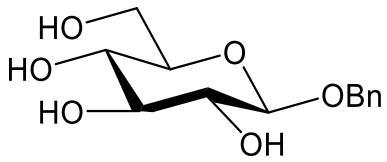

Triethylamine (15.9 mL) and H_2O (15.9 mL) were added to the reaction mixture containing **4** (8.8 g, 19.98 mmol) dissolved in MeOH (128 mL). The reaction mixture was stirred at room temperature for 3 h and concentrated using a rotary evaporator. The resulting residue was purified using silica gel column chromatography (MeOH-CH_2Cl_2, 20:80) to give white powder, **5** (5.3 g, 19.58 mmol, 98%). ^{1}H NMR (270 MHz, CD_3OD, Figure S35, Appendix II): δ_H 7.15–7.43 (m, 5H, Ar-H), 4.89 (d, *J* = 11.8 Hz, 1H, H-7), 4.62 (d, *J* = 11.8 Hz, 1H, H-7), 4.3 (d, *J* = 7.8 Hz, 1H, H-1), 3.85 (dd, *J* = 11.8, 2.0 Hz, 1H, H-6), 3.64 (dd, *J* = 12.1, 5.4 Hz, 1H, H-6), 3.14–3.33 (m, 4H, H-2, H-3, H-4, H-5); ^{13}C NMR (126 MHz, CD_3OD, Figure S36, Appendix II): δ_C 137.7, 127.9, 127.8, 127.3, 101.9, 76.7, 76.6, 73.8, 70.4, 70.3, 61.4; HRFD-MS *m/z* 271.1177 $[M + H]^+$ (calcd for $C_{13}H_{18}O_6$ *m/z* 271.1182 $[M + H]^+$) (Figure S4, Appendix I).

3.3.1.3. Synthesis of 1-*O*-benzyl-4,6-*O*-benzylidine-*β*-D-glucose (**6**)

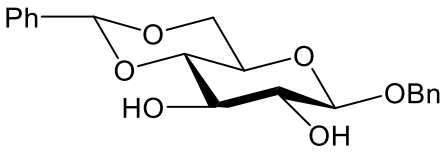

To a mixture of **5** (5.3 g, 19.58 mmol) and benzaldehyde dimethyl acetal ($PhCH(OMe)_2$) (3.5 mL, 23.50 mmol), *p*-toluenesulfonic acid ($TsOH \cdot H_2O$) (928.9 mg, 4.90 mmol) dissolved in dimethylformamide (DMF) (52 mL) was added. The reaction mixture was stirred for 5 min at room temperature, heated to 80 °C, and stirred for 4 h at 80 ºC. Then, it was allowed to cool to room temperature and evaporated using a rotary evaporator. The obtained residue was subjected to liquid-liquid extraction with CH_2Cl_2

(200 mL) and sat. $NaHCO_3$ (200 mL × 3). The organic layers were collected, dried over Na_2SO_4, and evaporated. The obtained crude material was purified using silica gel column chromatography (EtOAc-*n*-hexane, 50:50) to give an oil, **6** (3.6 g, 9.99 mmol, 51%). ^{1}H NMR (500 MHz, $CDCl_3$, Figure S37, Appendix II): δ_H 7.47–7.54 (m, 2H, Ar-H), 7.27–7.40 (m, 8H, Ar-H), 5.51 (s, 1H, H-7), 4.91 (d, J = 11.6 Hz, 1H, H-1′), 4.61 (d, J = 11.6 Hz, 1H, H-1′), 4.47 (d, J = 7.8 Hz, 1H, H-1), 4.34 (dd, J = 10.9, 5.0 Hz, 1H, H-6), 3.73–3.82 (m, 2H, H-3, H-6), 3.50–3.57 (m, 2H, H-2, H-4), 3.39–3.46 (m, 1H, H-5); ^{13}C NMR (126 MHz, $CDCl_3$, Figure S38, Appendix II): δ_C 136.9, 136.7, 125.9–129.6, 102.1, 101.9, 80.5, 74.5, 73.1, 71.5, 68.6, 66.4; COSY, HSQC, and HMBC data are shown in Figures S39 – S41, Appendix II; HRFD-MS *m/z* 358.1408 $[M]^+$ (calcd for $C_{20}H_{22}O_6$ *m/z* 358.1416 $[M]^+$) (Figure S5, Appendix I).

3.3.1.4. Synthesis of 1-*O*-benzyl-4,6-*O*-benzylidine-3-*O*-isobutyryl-*β*-D-glucose (**7**)

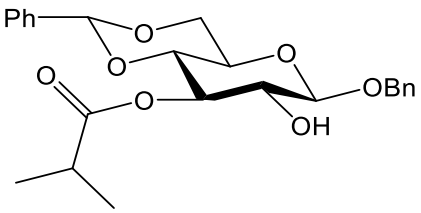

To **6** (2.0 g, 5.58 mmol) dissolved in anhydrous pyridine (200 mL) at 0 °C, isobutyryl chloride (0.6 mL, 0.59 mmol) was added. The reaction mixture was stirred for 24 h, neutralized with 1 M HCl, and evaporated using a rotary evaporator. The obtained crude material was partitioned between EtOAc (200 mL) and 1 M HCl (200 mL × 2) and between EtOAc (200 mL) and sat. $NaHCO_3$ (200 mL × 2). The organic layer was washed with H_2O (200 mL), dried over Na_2SO_4, and evaporated to give an oil, which was subjected to silica gel column chromatography (EtOAc-*n*-hexane, 25:75) to yield **7** (836.9 mg, 1.95 mmol, 35%). ^{1}H NMR (270 MHz, C_6D_6, Figure S42, Appendix II): δ_H 7.41–7.53 (m, 2H, Ar-H), 6.90–7.21 (m, 8H, Ar-H), 5.34

(dd, *J* = 10.5, 9.5 Hz, 1H, H-3), 5.07 (s, 1H, H-7), 4.64 (d, *J* = 11.8 Hz, 1H, H-1′), 4.25 (d, *J* = 11.8 Hz, 1H, H-1′), 4.12 (d, *J* = 7.6 Hz, 1H, H-1), 4.01 (dd, *J* = 10.3, 4.8 Hz, 1H, H-6), 3.55 (m, 1H, H-6), 3.25–3.42 (m, 2H, H-2, H-4), 2.88–3.20 (m, H, H-5), 2.51 (m, H, H-B2), 0.98 (d, *J* = 4.8 Hz, 3H, CH_3), 0.95 (d, *J* = 4.5 Hz, 3H, CH_3); ^{13}C NMR (126 MHz, C_6D_6, Figure S43, Appendix II): δ_C 176.5, 137.7, 137.5, 126.1–128.5, 102.9, 101.1, 78.8, 73.5, 71.1, 68.5, 66.1, 34.0, 18.9, 18.7; HRFD-MS *m/z* 429.1904 $[M + H]^+$ (calcd for $C_{24}H_{28}O_7$ *m/z* 429.1913 $[M + H]^+$) (Figure S6, Appendix I).

3.3.1.5. Synthesis of 1-*O*-benzyl-4,6-*O*-benzylidine-3-*O*-isobutyryl-2-*O*-((*S*)-2-methylbutyryl)-*β*-D-glucose [**8(*S*)**], and 1-*O*-benzyl-4,6-*O*-benzylidine-3-*O*-isobutyryl-2-*O*-((*R*)-2-methylbutyryl)-*β*-D-glucose [**8(*R*)**]

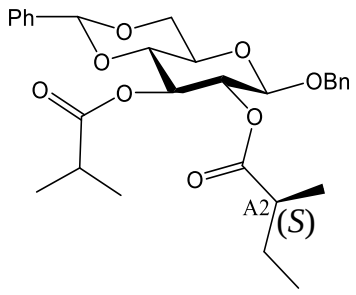

8(*S*): Dicyclohexylcarbodiimide (DCC) (294.3 mg, 1.40 mmol) and 4-dimethylaminopyridine (DMAP) (64.7 mg, 0.52 mmol) were added to **7** (149.7 mg, 0.35 mmol). A mixture of (*S*)-2-methylbutanoic acid (0.2 mL, 1.40 mmol) in anhydrous CH_2Cl_2 (35 mL) was added to the above mixture, and the reaction mixture was stirred for 24 h at room temperature. After evaporating volatile components in the reaction mixture, the obtained crude material was subjected to liquid-liquid extraction with CH_2Cl_2 (50 mL) and sat. $NaHCO_3$ (50 mL × 2), followed by washing the organic layer with 1 M HCl (50 mL × 2) and H_2O (50 mL × 2). After drying with Na_2SO_4 and evaporating, purification was performed using silica gel column chromatography (EtOAc-*n*-hexane, 30:70) to yield a pale green oil, **8(*S*)** (128.9 mg, 0.25 mmol, 72%).

^{1}H NMR (500 MHz, C_6D_6, Figure S44, Appendix II): δ_H 7.56–7.61 (m, 2H, Ar-H), 7.21–7.27 (m, 2H, Ar-H), 7.12–7.18 (m, 4H, Ar-H), 7.06–7.12 (m, 2H, Ar-H), 5.57 (dd, *J* = 10.4, 9.6 Hz, 1H, H-3), 5.47 (dd, *J* = 8.5, 8.0 Hz, 1H, H-2), 5.17 (s, 1H, H-7), 4.74 (d, *J* = 12.1 Hz, 1H, H-1′), 4.37 (d, *J* = 6.6 Hz, 1H, H-1′), 4.35 (d, *J* = 6.9 Hz, 1H, H-1), 4.12 (dd, *J* = 10.0, 5.0 Hz, 1H, H-6), 3.44 (dd, *J* = 12.8, 10.2 Hz, 1H, H-6), 3.38 (dd, *J* = 10.2, 9.4 Hz, 1H, H-4), 3.10 (m, 1H, H-5), 2.47 (m, 1H, H-B2), 2.34 (m, 1H, H-A2), 1.73 (m, 1H, H-A4), 1.34 (m, 1H, H-A4), 1.07–1.15 (m, 9H, H-A3, H-B3, H-B4), 0.84 (t, *J* = 7.4 Hz, 3H, A5); ^{13}C NMR (126 MHz, C_6D_6, Figure S45, Appendix II): δ_C 176.1, 175.0, 139.0, 138.3, 126.5–129.8, 101.8, 101.3, 79.3, 72.4, 72.1, 71.3, 69.0, 66.8, 41.8, 34.6, 27.3, 16.9–19.7, 12.2; COSY, HSQC, HMBC, and NOESY data are shown in Figures S46 – S49, Appendix II; HRFD-MS *m/z* 511.2338 $[M-H]^+$ (calcd for $C_{29}H_{36}O_8$ *m/z* 511.2332 $[M-H]^+$) (Figure S7, Appendix I).

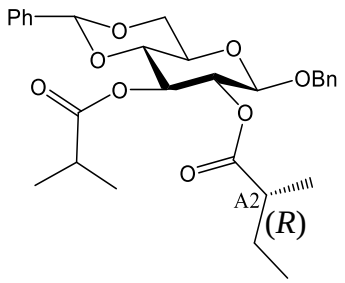

8(*R*): DCC (983.2 mg, 4.67 mmol) and DMAP (216.0 mg, 1.75 mmol) were added to **7** (500.0 mg, 1.17 mmol). A mixture of (*R*)-2-methylbutanoic acid (0.6 mL, 4.67 mmol) in anhydrous CH_2Cl_2 (100 mL) was added to the above mixture, and it was stirred for 24 h at room temperature. After evaporating volatile components in the reaction mixture, the obtained crude material was subjected to liquid-liquid extraction with CH_2Cl_2 (100 mL) and sat. $NaHCO_3$ (100 mL × 2), followed by washing the organic layer with 1 M HCl (100 mL × 2) and H_2O (100 mL × 2). After drying over Na_2SO_4 and evaporating, the resulting material was subjected to purification using silica gel

column chromatography (EtOAc-*n*-hexane, 20:80) to yield pale green oil, **8(*R*)** (251.5 mg, 0.49 mmol, 44%). ^{1}H NMR (500 MHz, C_6D_6, Figure S50, Appendix II): δ_H 7.58 (d, *J* = 12.2 Hz, 2H, Ar-H), 7.25 (dd, *J* = 9.4, 7.6 Hz, 2H, Ar-H), 7.13–7.20 (m, 4H, Ar-H), 7.09 (dd, *J* = 7.2, 7.6 Hz, 2H, Ar-H), 5.57 (dd, *J* = 9.6, 9.2 Hz, 1H, H-3), 5.47 (dd, *J* = 7.9, 7.9 Hz, 1H, H-2), 5.18 (s, 1H, H-7), 4.74 (d, *J* = 12.1 Hz, 1H, H-1'), 4.38 (d, *J* = 4.1 Hz, 1H, H-1'), 4.36 (d, *J* = 7.9 Hz, 1H, H-1), 4.11 (dd, *J* = 6.5, 5.0 Hz, 1H, H-6), 3.44 (dd, *J* = 10.2, 10.2 Hz, 1H, H-6), 3.40 (dd, *J* = 9.6, 9.6 Hz, 1H, H-4), 3.10 (m, 1H, H-5), 2.47 (m, 1H, H-B2), 2.35 (m, 1H, H-A2), 1.71 (m, 1H, H-A4), 1.36 (m, 1H, H-A4), 1.08–1.14 (m, 9H, H-A3, B3, B4), 0.83 (t, *J* = 7.4 Hz, 3H, H-A3) ; ^{13}C NMR (126 MHz, C_6D_6, Figure S51, Appendix II): δ_C 176.2, 175.2, 137.9, 128.1–129.5, 126.9, 101.8, 101.2, 79.2, 72.5, 72.3, 71.3, 67.0, 66.8, 41.7, 34.6, 27.3, 19.5, 19.4, 17.3, 12.1; COSY, HSQC, and HMBC data are shown in Figures S52 – S54, Appendix II; HRFD-MS *m/z* 513.2471 $[M+H]^+$ (calcd for $C_{29}H_{36}O_8$ *m/z* 513.2488 $[M+H]^+$) (Figure S8, Appendix I).

3.3.1.6. Synthesis of 1,6-*O*-dibenzyl-3-*O*-isobutyryl-2-*O*-((*S*)-2-methylbutyryl)-*β*-D-glucose [**9(*S*)**] and 1,6-*O*-dibenzyl-3-*O*-isobutyryl-2-*O*-((*R*)-2-methylbutyryl)-*β*-D-glucose [**9(*R*)**]

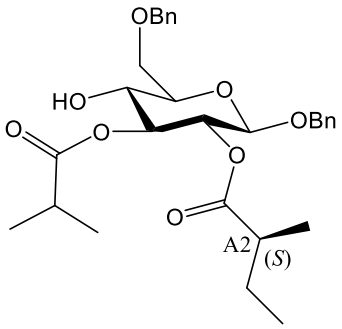

9(*S*): To **8(*S*)** (129.0 mg, 0.25 mmol) in anhydrous CH_2Cl_2 (10 mL) at 0 °C, trifluoroacetic acid (TFA) (25. 3 μL, 0.76 mmol) and triethylsilane (Et_3SiH) (121.7 μL,

0.76 mmol) were added. The reaction was carried out at room temperature overnight. The reaction mixture was diluted by adding EtOAc (20 mL) and subjected to liquid-liquid extraction with EtOAc (20 mL) and sat. $NaHCO_3$ (30 mL × 2), followed by washing the organic layer with 1 M HCl (30 mL) and H_2O (30 mL). The obtained organic layer was dried over Na_2SO_4 and evaporated under reduced pressure. Next, purification was performed by silica gel column chromatography (EtOAc-*n*-hexane, 30:70) to yield an oil, **9(*S*)** (63.4 mg, 0.12 mmol, 49%). ^{1}H NMR (500 MHz, C_6D_6, Figure S55, Appendix II):): δ_H 7.04–7.28 (m, 10H, Ar-H), 5.43 (dd, *J* = 10.3, 9.4 Hz, 1H, H-2), 5.23 (dd, *J* = 10.5, 9.2 Hz, 1H, H-3), 4.78 (d, *J* = 12.5 Hz, 1H, H-1′), 4.45 (d, *J* = 12.2 Hz, 1H, H-1′), 4.37 (d, *J* = 8.0 Hz, 1H, H-1), 4.33 (d, *J* = 5.1 Hz, 2H, H-1″), 3.61 (m, 3H, H-4, 2H-6), 3.23 (m, 1H, H-5), 2.44 (m, 1H, H-B2), 2.31 (m, 1H, H-A2), 1.70 (m, 1H, H-A4), 1.34 (m, 1H, H-A4), 1.06–1.12 (m, 9H, H-A3, H-B3, H-B4), 0.83 (t, *J* = 7.4 Hz, 3H, A5); ^{13}C NMR (126 MHz, C_6D_6, Figure S56, Appendix II): δ_C 177.5, 174.9, 138.9, 138.1, 128.1–129.1, 100.5, 76.4, 75.4, 74.0, 71.7, 71.6, 70.8, 70.7, 41.9, 34.6, 27.2, 19.4, 17.2, 12.2; COSY, HSQC, HMBC, and NOESY data are shown in Figures S57 – S60, Appendix II; HRFD-MS *m/z* 513.2483 $[M-H]^+$ (calcd for $C_{29}H_{38}O_8$ *m/z* 513.2488 $[M-H]^+$) (Figure S9, Appendix I).

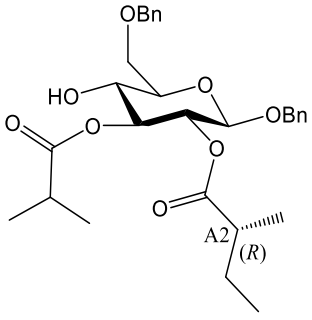

9(*R*): To **8(*R*)** (251.5 mg, 0.49 mmol) in anhydrous CH_2Cl_2 (10 mL) at 0 °C, TFA (49. 3 μL, 1.47 mmol) and Et_3SiH (237.5 μL, 1.47 mmol) were added. The reaction was carried out at room temperature overnight. The reaction mixture was diluted by

adding EtOAc (20 mL) and subjected to liquid-liquid extraction with EtOAc (20 mL) and sat. $NaHCO_3$ (30 mL × 2), followed by washing the organic layer with 1 M HCl (30 mL) and H_2O (30 mL). The obtained organic layer was dried over Na_2SO_4 and evaporated under reduced pressure. Next, purification was performed by silica gel column chromatography (EtOAc-*n*-hexane, 30:70) to yield an oil, **9(*R*)** (60.6 mg, 0.12 mmol, 24%). ^{1}H NMR (270 MHz, C_6D_6, Figure S61, Appendix II): δ_H 7.04–7.30 (m, 10H, Ar-H), 5.42 (dd, *J* = 8.0, 8.0 Hz, 1H, H-2), 5.23 (dd, *J* = 9.4, 9.4 Hz, 1H, H-3), 4.79 (d, *J* = 12.1 Hz, 1H, H-1'), 4.45 (d, *J* = 12.1 Hz, 1H, H-1'), 4.38 (d, *J* = 7.2 Hz, 1H, H-1), 4.33 (s, 2H, H-1''), 3.65 (dd, *J* = 4.8, 4.7 Hz, 1H, H-4), 3.60 (m, 2H, H-6), 3.23 (m, 1H, H-5), 2.44 (m, 1H, H-B2), 2.31 (m, 1H, H-A2), 1.69 (m, 1H, H-A4), 1.35 (m, 1H, H-A4), 1.05–1.13 (m, 9H, H-A3, H-B3, H-B4), 0.83 (t, *J* = 7.4 Hz, 3H, A5); ^{13}C NMR (126 MHz, C_6D_6, Figure S62, Appendix II): δ_C 177.1, 174.7, 138.5, 137.7, 127.8–128.7, 100.0, 76.1, 74.9, 73.6, 71.4, 71.2, 70.5, 70.3, 41.2, 34.3, 27.0, 19.0, 16.8, 11.7; HRFD-MS *m/z* 514.2584 $[M]^+$ (calcd for $C_{29}H_{38}O_8$ *m/z* 514.2567 $[M]^+$) (Figure S10, Appendix I).

3.3.1.7. Synthesis of 1,6-*O*-dibenzyl-3,4-*O*-diisobutyryl-2-*O*-((*S*)-2-methylbutyryl)-*β*-D-glucose (**2(*S*)**) and synthesis of 1,6-*O*-dibenzyl-3,4-*O*-diisobutyryl-2-*O*-((*R*)-2-methylbutyryl)-*β*-D-glucose (**2(*R*)**)

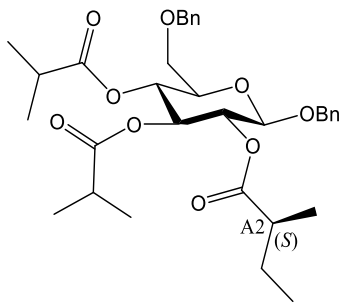

2(*S*): To **9(*S*)** (63.4 mg, 0.12 mmol) dissolved in anhydrous pyridine (10 mL) at 0 °C, isobutyryl chloride (64.7 *μ*L, 0.62 mmol) was added. The reaction mixture was

stirred for 24 h, neutralized with 1 M HCl, and evaporated using a rotary evaporator. The obtained crude material was partitioned between EtOAc (30 mL) and 1 M HCl (30 mL × 2), and between EtOAc (30 mL) and sat. $NaHCO_3$ (30 mL × 2). The organic layer was washed with H_2O (30 mL), dried over Na_2SO_4, and evaporated to give an oil, which was subjected to silica gel column chromatography (EtOAc-*n*-hexane, 20:80) to yield **2(*S*)** (37.5 mg, 0.06 mmol, 52%). For ^1H NMR and ^{13}C NMR, see Table 3, Figures S63 – S64, Appendix II and for COSY, HSQC, HMBC, and NOESY data, see Figures S65 – S68, Appendix II); HRFD-MS *m/z* 584.2995 $[M]^+$ (calcd for $C_{33}H_{44}O_9$ *m/z* 584.2985 $[M]^+$) (Figure S11, Appendix I).

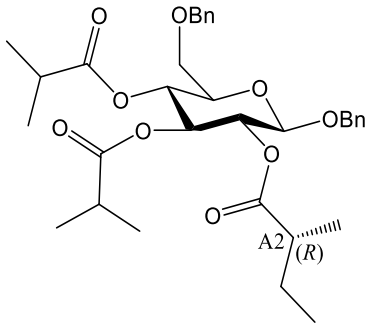

2(*R*): To **9(*R*)** (60.6 mg, 0.12 mmol) dissolved in anhydrous pyridine (5 mL) at 0 °C, isobutyryl chloride (123.7 µL, 1.18 mmol) was added. The reaction mixture was stirred for 24 h, neutralized with 1 M HCl, and evaporated using a rotary evaporator. The obtained crude material was partitioned between EtOAc (30 mL) and 1 M HCl (30 mL × 2), and between EtOAc (30 mL) and sat. $NaHCO_3$ (30 mL × 2). The organic layer was washed with H_2O (30 mL), dried over Na_2SO_4, and evaporated to give an oil, which was subjected to silica gel column chromatography (EtOAc-*n*-hexane, 30:70) to give an oil of **2(*R*)** (64.0 mg, 0.11 mmol, 93%). For ^1H NMR and ^{13}C NMR, see Table 3, Figures S69 – S70, Appendix II and for COSY, HSQC, HMBC, and NOESY data, see Figures S71 – S74, Appendix II); HRFD-MS *m/z* 584.2968 $[M]^+$ (calcd for $C_{33}H_{44}O_9$ *m/z* 584.2985 $[M]^+$) (Figure S12, Appendix I).

3.3.1.8. Removal of benzyl ether

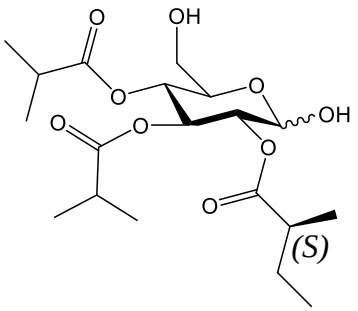

To a solution of **2(*S*)** (35.0 mg, 0.06 mmol) in 2 mL of EtOAc, 4 mg of palladium black was added. The reaction mixture was stirred for 5 h at room temperature under a hydrogen gas atmosphere. Then, it was filtered using celite, and volatile components were evaporated under reduced pressure. The obtained crude material was purified using silica gel column chromatography (EtOAc-*n*-hexane, 60:40) to yield colorless oil, synthesized **1** (13.0 mg, 0.03 mmol, 54%).

3.3.2. Synthesis of dibenzyl pennelliisides A and B

Synthesis of dibenzyl pennelliisides A and B was started with the previously obtained compound, **6**.

3.3.2.1. Synthesis of 1-*O*-benzyl-4,6-*O*-benzylidine-2,3-*O*-diisobutyryl-*β*-D-glucose (**10**)

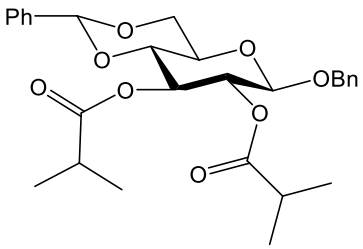

To **6** (123.8 mg, 0.35 mmol) dissolved in anhydrous pyridine (5 mL) at 0 °C, isobutyryl chloride (368.0 μL, 3.50 mmol) was added. The reaction mixture was stirred for 24 h, neutralized with 1 M HCl, and evaporated using a rotary evaporator. The

obtained crude material was partitioned between EtOAc (30 mL) and 1 M HCl (30 mL × 2), and between EtOAc (30 mL) and sat. $NaHCO_3$ (30 mL × 2). The organic layer was washed with H_2O (30 mL), dried over Na_2SO_4, and evaporated to give an oil, which was subjected to silica gel column chromatography (EtOAc-*n*-hexane, 15:85) to yield **10** (129.0 mg, 0.26 mmol, 75%). ^{1}H NMR (500 MHz, C_6D_6, Figure S81, Appendix II): δ_H 7.57 (d, *J* = 7.2 Hz, 2H, Ar-H), 7.23 (d, *J* = 7.5 Hz, 2H, Ar-H), 7.15 (m, 4H, Ar-H), 7.10 (m, 2H, Ar-H), 5.55 (dd, *J* = 9.6, 9.6 Hz, 1H, H-3), 5.45 (dd, *J* = 7.9, 7.9 Hz, 1H, H-2), 5.17 (s, 1H, H-7), 4.73 (d, *J* = 12.3 Hz, 1H, H-1′), 4.36 (d, *J* = 12.5 Hz, 1H, H-1′), 4.43 (d, *J* = 7.9 Hz, 1H, H-1), 4.10 (dd, *J* = 5.0, 5.0 Hz, 1H, H-6), 3.43 (dd, *J* = 10.2 Hz, 1H, H-6), 3.37 (dd, *J* = 9.6, 9.6 Hz, 1H, H-4), 3.07 (m, 1H, H-5), 2.46 (m, 2H, H-A2, B2), 1.04–1.14 (m, 12H, H-A3, A4, B3, B4); ^{13}C NMR (126 MHz, C_6D_6, Figure S82, Appendix II): δ_C 175.5, 174.8, 137.6, 137.3, 126.1–128.3, 101.1, 100.5, 78.5, 72.0, 71.5, 70.6, 68.3, 66.1, 33.9, 18.8, 18.7; COSY, HSQC, and HMBC data are shown in Figures S83 – S85, Appendix II; HRFD-MS *m/z* 499.2317 $[M + H]^+$ (calcd for $C_{24}H_{28}O_7$ *m/z* 499.2332 $[M + H]^+$) (Figure S14, Appendix I).

3.3.2.2. Synthesis of 1-*O*-benzyl-4,6-*O*-benzylidine-3-*O*-(8-methylnonanoyl)-*β*-D-glucose (**11**)

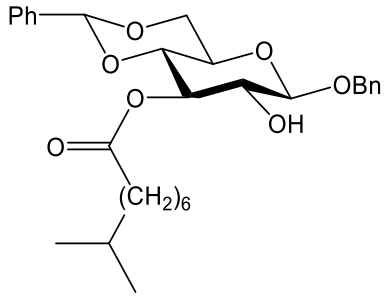

To a mixture of DCC (58.8 mg, 0.28 mmol) and DMAP (8.7 mg, 0.07 mmol) and **6** (100.0 mg, 0.28 mmol), 8-methylnonanoic acid (17.5 μL, 0.14 mmol) in anhydrous CH_2Cl_2 (10 mL) was added. The mixture was stirred for 24 h at room temperature. After

evaporating volatile components in the reaction mixture, the obtained crude material was subjected to liquid-liquid extraction with CH_2Cl_2 (50 mL) and sat. $NaHCO_3$ (50 mL × 2), followed by washing the organic layer with 1 M HCl (50 mL × 2) and H_2O (50 mL × 2). After drying over Na_2SO_4 and evaporating, purification was performed using silica gel column chromatography (EtOAc-*n*-hexane, 30:70) followed by a preparative TLC ($CHCl_3$, 100%) to yield a colorless oil, **11** (48.6 mg, 0.09 mmol, 34%). ^{1}H NMR (500 MHz, $CDCl_3$, Figure S86, Appendix II): δ_H 7.46 (m, 2H, Ar-H), 7.27–7.41 (m, 8H, Ar-H), 5.53 (s, 1H, H-7), 5.23 (dd, *J* = 9.4, 9.4 Hz, 1H, H-3), 4.97 (d, *J* = 11.6 Hz, 1H, H-1′), 4.69 (d, *J* = 11.6 Hz, 1H, H-1′), 4.60 (d, *J* = 7.6 Hz, 1H, H-1), 4.41 (dd, *J* = 5.0, 5.0 Hz, 1H, H-6), 3.84 (dd, *J* = 10.2, 10.2 Hz, 1H, H-6), 3.70 (d, *J* = 9.5 Hz, 1H, H-4), 3.66 (dd, *J* = 8.3, 3.9 Hz, 1H, H-2), 3.55 (m, 1H, H-5), 2.53 (s, 1H, H-2OH), 2.40 (t, *J* = 7.4 Hz, 2H, H-B2), 1.65 (m, 2H, H-B3), 1.50 (m, 1H, H-B8), 1.32 (m, 2H, H-B4), 1.29 (m, 2H, H-B5), 1.23 (m, 2H, B6), 1.13 (m, 2H, H-B7), 0.86 (d, *J* = 6.6 Hz, 6H, H-B9, B10); ^{13}C NMR (126 MHz, C_6D_6, Figure S87, Appendix II): δ_C 173.9, 136.9, 136.6, 128.0–129.2, 102.5, 101.5, 78.5, 73.5, 73.3, 71.7, 68.7, 66.6, 38.9, 34.4, 29.5, 29.0, 27.9, 27.2, 25.1, 22.6; COSY, HSQC, and HMBC data are shown in Figures S88 – S90, Appendix II; HRFD-MS *m/z* 513.2862 $[M-H]^+$ (calcd for $C_{30}H_{40}O_7$ *m/z* 513.2852 $[M-H]^+$) (Figure S15, Appendix I).

3.3.2.3. Synthesis of 1-*O*-benzyl-4,6-*O*-benzylidine-2-*O*-isobutyryl-3-*O*-(8-methylnonanoyl)-*β*-D-glucose (**12**)

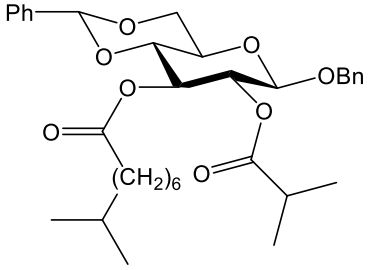

To **11** (48.6 mg, 0.09 mmol) dissolved in anhydrous pyridine (5 mL) at 0 °C, isobutyryl chloride (50.0 μL, 0.47 mmol) was added, and the reaction mixture was stirred for 24 h. Then it was neutralized with 1 M HCl and evaporated using a rotary evaporator. The obtained crude material was partitioned between EtOAc (30 mL) and 1 M HCl (30 mL × 2), and between EtOAc (30 mL) and sat. $NaHCO_3$ (30 mL × 2). The organic layer was washed with H_2O (30 mL), dried over Na_2SO_4 and evaporated to give an oil, which was subjected to silica gel column chromatography (EtOAc-*n*-hexane, 15:85) to yield colorless oil, **12** (43.1 mg, 0.07 mmol, 78%). ^{1}H NMR (500 MHz, C_6D_6, Figure S91, Appendix II): δ_H 7.58 (m, 2H, Ar-H), 7.05–7.25 (m, 8H, Ar-H), 5.60 (dd, *J* = 9.6, 9.6 Hz, 1H, H-3), 5.46 (dd, *J* = 7.9, 7.9 Hz, 1H, H-2), 5.20 (s, 1H, H-7), 4.74 (d, *J* = 12.3 Hz, 1H, H-1′), 4.38 (d, *J* = 12.3 Hz, 1H, H-1′), 4.37 (d, *J* = 7.9 Hz, 1H, H-1), 4.10 (dd, *J* = 4.9, 5.0 Hz, 1H, H-6), 3.45 (dd, *J* = 4.1, 4.6 Hz, 1H, H-6), 3.42 (d, *J* = 6.1 Hz, 1H-4), 3.12 (m, 1H, H-5), 2.50 (m, 1H, H-A2), 2.23 (m, 2H, H-B2) 1.58 (m, 2H, H-B3) 1.44 (m, 1H, H-B8) 1.10–1.16 (m, 12H, H-B4, B5, B6, A3, A4) 1.07 (m, 2H, H-B7) 0.86 (d, *J* = 6.6 Hz, 6H, H-B9, B10); ^{13}C NMR (126 MHz, C_6D_6, Figure S92, Appendix II): δ_C 174.9, 172.2, 137.5, 137.3, 126.2–128.8, 101.3, 100.5, 78.5, 72.1, 71.6, 70.6, 68.3, 66.2, 38.9, 34.0, 29.5, 29.0, 27.9, 27.2, 24.9, 22.5, 18.8, 18.7; COSY, HSQC, and HMBC data are shown in Figures S93 – S95, Appendix II; HRFD-MS *m/z* 583.3283 $[M + H]^+$ (calcd for $C_{34}H_{46}O_8$ *m/z* 583.3271 $[M + H]^+$) (Figure S16, Appendix I).

3.3.2.4. Synthesis of **13a** and **b**

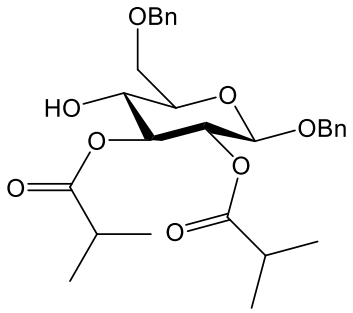

13a, 1,6-*O*-dibenzyl-2,3-*O*-diisobutyryl-*β*-D-glucose; To **10** (129.0 mg, 0.27 mmol) in anhydrous CH_2Cl_2 (10 mL) at 0 °C, TFA (26.1 μL, 0.78 mmol) and Et_3SiH (125.7 μL, 0.78 mmol) were added. The reaction mixture was stirred for 1 h at room temperature. The reaction mixture was diluted by adding EtOAc (20 mL) and subjected to liquid-liquid extraction with EtOAc (20 mL) and sat. $NaHCO_3$ (30 mL × 2), followed by washing the organic layer with 1 M HCl (30 mL) and H_2O (30 mL). The obtained organic layer was dried over Na_2SO_4 and evaporated under reduced pressure. Next, purification was performed by silica gel column chromatography (EtOAc-*n*-hexane, 30:70) to yield an oil, **13a** (61.8 mg, 0.12 mmol, 48%), colorless oil, ^{1}H NMR (500 MHz, C_6D_6, Figure S96, Appendix II): δ_H 7.04–7.29 (m, 10H, Ar-H), 5.41 (dd, *J* = 8.1, 8.0 Hz, 1H, H-2), 5.22 (dd, *J* = 9.6, 9.6 Hz, 1H, H-3), 5.53 (s, 1H, H-7), 4.77 (d, *J* = 12.4 Hz, 1H, H-1′), 4.46 (d, *J* = 12.4 Hz, 1H, H-1′), 4.37 (d, *J* = 7.8 Hz, 1H, H-1), 4.33 (d, *J* = 4.8 Hz, 1H, H-7), 3.63 (m, 1H, H-4), 3.61 (m, 2H, H-6), 3.22 (m, 1H, H-5), 2.38–2.50 (m, 2H, H-A2, B2), 1.06–1.12 (m, 12H, H-A3, A4, B3, B4); ^{13}C NMR (126 MHz, C_6D_6, Figure S97, Appendix II): δ_C 177.1, 175.1, 138.5, 137.8, 127.7–128.7, 100.0, 76.0, 75.0, 73.6, 71.5, 70.5, 70.3, 34.3, 19.1; COSY, HSQC, and HMBC data are shown in Figures S98 – S100, Appendix II; HRFD-MS *m/z* 500.2400 $[M]^+$ (calcd for $C_{28}H_{36}O_8$ *m/z* 500.2410 $[M]^+$) (Figure S17, Appendix I).

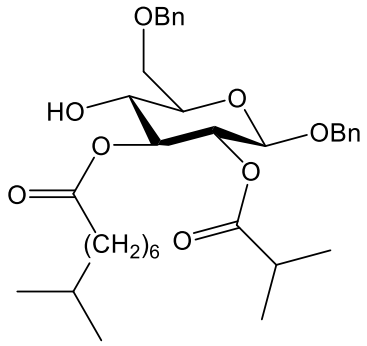

13b, 1,6-*O*-dibenzyl-2-*O*-isobutyryl-3-*O*-(8-methylnonanoyl)-*β*-D-glucose; To **12** (43.1 mg, 0.07 mmol) in anhydrous CH_2Cl_2 (5 mL) at 0 °C, TFA (7.4 μL, 0.22 mmol) and Et_3SiH (35.8 μL, 0.22 mmol) were added. The reaction mixture was shaken for 1 h at room temperature. The reaction mixture was diluted by adding EtOAc (25 mL) and subjected to liquid-liquid extraction with EtOAc (25 mL) and sat. $NaHCO_3$ (30 mL × 2), followed by washing the organic layer with 1 M HCl (30 mL) and H_2O (30 mL). The obtained organic layer was dried over Na_2SO_4 and evaporated under reduced pressure. Purification was performed by silica gel column chromatography (EtOAc-*n*-hexane, 20:80) to yield an colorless oil, **13b** (22.5 mg, 0.04 mmol, 52%), ^{1}H NMR (500 MHz, C_6D_6, Figure S101, Appendix II) δ_H 7.25 (m, 4H, Ar-H), 7.05–7.18 (m, 6H, Ar-H), 5.42 (dd, *J* = 7.9, 8.0 Hz, 1H, H-2), 5.25 (dd, *J* = 9.5, 9.3 Hz, 1H, H-3), 4.77 (d, *J* = 12.2 Hz, 1H, H-8), 4.46 (d, *J* = 12.3 Hz, 1H, H-8), 4.38 (d, *J* = 8.0 Hz, 1H, H-1), 4.31 (d, *J* = 5.2 Hz, 2H, H-1″), 3.64 (dd, *J* = 9.5, 9.5 Hz, 1H, H-4), 3.59 (dd, *J* = 4.7, 1.6 Hz, 2H, H-6), 3.21 (m, 1H, H-5), 2.57 (s, 1H, H-4OH) 2.49 (m, 1H, H-A2), 2.23 (m, 2H, H-B2), 1.60 (m, 2H, H-B3), 1.46 (m, 1H, H-B8), 1.18 (m, 2H, H-B4), 1.10–1.14 (m, 12H, H-B5, B6, B7, A3, A4), 0.87 (d, *J* = 6.6 Hz, 6H, H-B9, B10); ^{13}C NMR (126 MHz, C_6D_6, Figure S102, Appendix II): δ_C 174.8, 173.5, 138.1, 137.5, 127.2–128.4, 99.7, 75.8, 74.6, 73.3, 71.3, 70.8, 70.1, 70.0, 38.9, 34.1, 29.5, 29.1, 27.9, 27.2, 24.9, 22.5, 18.8, 18.7; COSY, HSQC, and HMBC data are shown in Figures S103 –

S105, Appendix II; HRFD-MS *m/z* 585.3368 $[M + H]^+$ (calcd for $C_{34}H_{48}O_8$ *m/z* 584.3349 $[M + H]^+$) (Figure S18, Appendix I).

3.3.2.5. Synthesis of **14a** and **b**

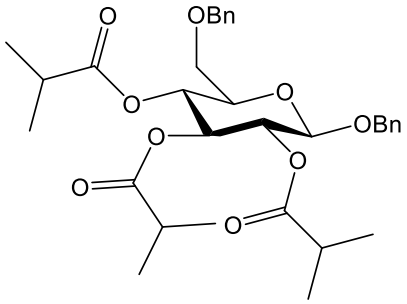

14a, dibenzyl pennelliiside A, 1,6-*O*-dibenzyl-2,3,4-*O*-triisobutyryl-*β*-D-glucose; To **13a** (61.8 mg, 0.12 mmol) dissolved in anhydrous pyridine (5 mL) at 0 °C, isobutyryl chloride (63.2 *μ*L, 0.60 mmol) was added. The reaction mixture was stirred for 24 h, neutralized with 1 M HCl, and evaporated using a rotary evaporator. The obtained crude material was partitioned between EtOAc (30 mL) and 1 M HCl (30 mL × 2), and between EtOAc (30 mL) and sat. $NaHCO_3$ (30 mL × 2). The organic layer was washed with H_2O (30 mL), dried over Na_2SO_4, and evaporated to give an oil, which was subjected to silica gel column chromatography (EtOAc-*n*-hexane, 20:80) to yield a yellow oil **14a** (28.7 mg, 0.05 mmol, 41%). $[\alpha]^{25}_D$ = +29.1 (c 0.5, $CHCl_3$), ^{1}H NMR (500 MHz, C_6D_6, Figure S106, Appendix II) δ_H 7.21–7.28 (m, 4H, Ar-H), 7.11–7.19 (m, 4H, Ar-H), 7.07 (t, *J* = 7.2 Hz, 2H, Ar-H), 5.44 (dd, *J* = 8.5, 6.2 Hz, 1H, H-2), 5.43 (dd, *J* = 9.0, 8.4 Hz, 1H, H-3), 5.29 (dd, *J* = 10.0, 9.8 Hz, 1H, H-4), 4.74 (d, *J* = 12.7 Hz, 1H, H-8), 4.44 (d, *J* = 12.4 Hz, 1H, H-8), 4.36 (d, *J* = 7.1 Hz, 1H, H-1), 4.32 (d, *J* = 12.2 Hz, 2H, H-1″), 3.47 (m, 2H, H-6), 3.39 (m, 1H, H-5), 2.41 (m, 1H, H-A2), 2.39 (m, 2H, H-B2, C2), 1.07 (d, *J* = 6.8 Hz, 6H, H-A3, A4), 1.06 (d, *J* = 7.1 Hz, 6H, H-B3, B4), 1.01 (d, *J* = 7.0 Hz, 3H, H-C3), 0.97 (d, *J* = 7.0 Hz, 3H, H-C4); ^{13}C NMR (126 MHz, C_6D_6, Figure S107, Appendix II): δ_C 175.5, 174.6, 174.5, 138.3, 137.4,

127.2–128.4, 99.5, 73.5, 73.2, 72.9, 71.3, 70.0, 69.2, 33.9, 18.4–18.9; COSY, HSQC, and HMBC data are shown in Figures S108 – S110, Appendix II; HRFD-MS *m/z* 570.2818 $[M]^+$) (calcd for $C_{32}H_{42}O_9$ *m/z* 570.2829 $[M]^+$ (Figure S19, Appendix I).

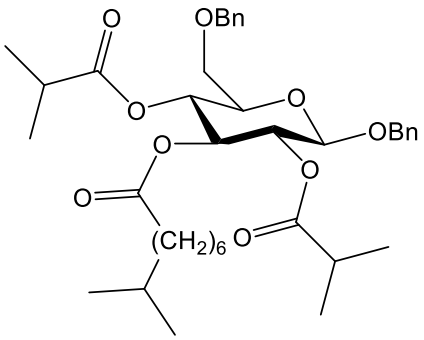

14b; dibenzyl pennelliiside B, 1,6-*O*-dibenzyl-2,4-*O*-diisobutyryl-3-*O*-(8-methylnonanoyl)-*β*-D-glucose; To **13b** (22.5 mg, 0.04 mmol) dissolved in anhydrous pyridine (5 mL) at 0 °C, isobutyryl chloride (20.3 μL, 0.19 mmol) was added. The reaction mixture was stirred for 24 h, neutralized with 1 M HCl, and evaporated using a rotary evaporator. The obtained crude material was partitioned between EtOAc (30 mL) and 1 M HCl (30 mL × 2), and between EtOAc (30 mL) and sat. $NaHCO_3$ (30 mL × 2). The organic layer was washed with H_2O (30 mL), dried over Na_2SO_4, and evaporated to give an oil, which was subjected to silica gel column chromatography (EtOAc-*n*-hexane, 20:80) to yield colorless oil, **14b** (12.3 mg, 0.02 mmol, 49%), $[\alpha]^{25}_D$ = −13.3 (c 0.6, $CHCl_3$), ^{1}H NMR (500 MHz, C_6D_6, Figure S111, Appendix II) δ_H 7.23–7.28 (m, 4H, Ar-H), 7.12–7.18 (m, 4H, Ar-H), 7.07 (t, *J* = 7.6 Hz, 2H, Ar-H), 5.49 (dd, *J* = 9.6, 8.2 Hz, 1H, H-3), 5.46 (dd, *J* = 8.8, 8.5 Hz, 1H, H-2), 5.31 (dd, *J* = 9.5, 8.8 Hz, 1H, H-4), 4.75 (d, *J* = 12.2 Hz, 1H, H-8), 4.45 (d, *J* = 12.3 Hz, 1H, H-8), 4.39 (d, *J* = 7.7 Hz, 1H, H-1), 4.33 (d, *J* = 12.3 Hz, 2H, H-1″), 3.48 (m, 2H, H-6), 3.42 (m, 1H, H-5), 2.46 (m, 1H, H-A2), 2.34 (m, 1H, H-C2), 2.22 (t, *J* = 7.5 Hz, 2H, H-B2), 1.59 (m,

2H, H-B3), 1.47 (m, 1H, H-B8), 1.13–1.23 (m, 6H, 1H-B4, B5, B6), 1.07–1.13 (m, 6H, H-A3, A4), 1.05 (d, J = 7.0 Hz, 3H, H-C3), 1.00 (d, J = 7.0 Hz, 3H, H-C4), 0.88 (d, J = 6.6 Hz, 6H, H-B9, B10); ^{13}C NMR (126 MHz, C_6D_6, Figure S112, Appendix II): δ_C 175.0, 174.9, 172.7, 138.6, 137.7, 127.7–128.6, 99.8, 73.9, 73.6, 73.3, 71.7, 70.3, 69.7, 69.6, 39.3, 34.3, 34,3, 34.2, 29.9, 29.4, 28.3, 27.5, 25.2, 22.8, 19.0, 18.8; COSY, HSQC, and HMBC data are shown in Figures S113 – S115, Appendix II; HRFD-MS *m/z* 654.3774 $[M]^+$) (calcd for $C_{38}H_{54}O_9$ *m/z* 654.3769 $[M]^+$ (Figure S20, Appendix I).

3.4. Results and discussion

3.4.1. Total synthesis of pennelliiside D

Pennelliiside D (**1**) was newly isolated from *S. pennellii* via its benzylated derivative, 1,6-*O*-dibenzyl-3,4-*O*-diisobutyryl-2-*O*-(2-methylbutyryl)-*β*-D-glucose (Figure 7) as explained in Chapter 2. Its planar chemical structure was revealed as 3,4-*O*-diisobutyryl-2-*O*-(2-methylbutyryl)-D-glucose using ^{1}H NMR, ^{13}C NMR, and COSY, HSQC, HMBC, and NOESY correlations. However, the absolute configuration of the fatty acid moiety, 2-methylbutyryl attached to C-2 in the glucose moiety was unknown. In order to identify its absolute configuration, in this chapter syntheses of two possible isomers of (*S*) and (*R*) dibenzyl pennelliiside D were performed.

Total synthesis of **2** was initiated with commercially available *β*-D-glucose pentaacetate (**3)** as reported by Degenstein et al., 2015 [95] (Scheme 3). At first, the benzyl group was substituted with the acetate group present at C-1 position in **3** with benzyl alcohol and boron trifluoride etherate. Compound **5** was obtained by removing all other acetate groups in **4**. Next, protection of C-4 and C-6 carbons in **5** with benzaldehyde dimethyl acetal and *p*-toluenesulfonic acid was done to afford **6**. Isobutyryl chloride was selectively esterified at the C-3 position by reacting **6** with isobutyryl chloride at 0 ºC. Then, condensation of **7** with (*S*)-2-methylbutanoic acid was conducted under a nitrogen gas atmosphere, which gave the desired compound **8(*S*)**. Cleavage of 4,6-*O*-benzylidine moiety of **8(*S*)** using Et_3SiH and TFA was done to yield **9(*S*)**, which was followed by esterification with isobutyryl chloride to give preferred dibenzyl pennelliiside D, **2(*S*)**. (Table 3, Figures S3 – S11, Appendix I, and S33 – S49, S55 – 60, and S63 – S68, Appendix II). The molecular formula and molecular weight of **2(*S*)** were similar to those of the natural **2**, which were $C_{33}H_{44}O_9$ and *m/z* 584.2995 $[M]^+$

(calcd *m/z* 584.2995 $[M]^+$), according to HRFD-MS data (Figure S11, Appendix I), respectively. Similarly, synthesis of (*R*) configured compound, **2(*R*)** was done starting from **7**, which was conjugated with (*R*)-2-methylbutanoic acid to yield **8(*R*)** as shown in Scheme 3. Cleavage of 4,6-*O*-benzylidine moiety in **8(*R*)** was done which was then esterified with isobutyryl chloride to yield desired (*R*) configured compound, **2(*R*)**. The molecular formula and molecular weight of **2(*R*)** were similar to those of the natural **2** and synthesized **2(*S*)**, which were $C_{33}H_{44}O_9$ and *m/z* 584.2968 $[M]^+$ (calcd *m/z* 584.2985 $[M]^+$), respectively, using HRFD-MS data (Figure S12, Appendix I). Structures of all synthesized compounds were elucidated using ^{1}H NMR, ^{13}C NMR (Table 3), and COSY, HSQC, and HMBC correlations together with FD mass analysis (Figures S10, S12, Appendix I, and Figures S50 – S54, S61– S62, S69 – S74, Appendix II).

The comparison of ^{1}H NMR and ^{13}C NMR data of natural and synthesized compounds (*S*/*R*), showed good accordance between natural and synthesized (*S*) isomer of dibenzyl pennelliiside D (**2(*S*),** Table 1 and 3). In the ^{1}H NMR, the differences between synthesized (*S*/*R*) with the natural compound were found in the resonances around δ 1.65 and δ 1.32 as shown in Figure 10. Furthermore, a significant difference was shown when comparing specific rotation values with **2(*R*)**, while natural **2** and synthesized **2(*S*)** showed almost the same value. The specific rotation values measured for natural **2** and synthesized **2(*S*)**, and **2(*R*)** were $[\alpha]^{25}_D$ = -10.5, -10.7, and -21.3 (c 0.6, MeOH), respectively. Based on the above observations, it was confirmed that the absolute configuration of the 2-methylbutyryl fatty acid moiety in natural **2** was (*S*), and its structure as 1,6-*O*-dibenzyl-3,4-*O*-diisobutyryl-2-*O*-((*S*)-2-methylbutyryl)-β-D-glucose (Figure 11).

In order to further confirm the structure, debenzylation was carried out for **2(*S*)**. By debenzylation of synthesized **2(*S*)** with palladium black under a hydrogen gas atmosphere (Scheme 3), synthesized **1** (5.9 mg) was obtained as a colorless oil. The molecular formula and molecular weight were similar to those of the natural **1**, which were $C_{19}H_{32}O_9$ and *m/z* 405.2133 $[M+H]^+$ (calcd *m/z* 405.2125 $[M+H]^+$), using HRFD-MS data (Figure S13, Appendix I). Summarized ^{1}H NMR and ^{13}C NMR data of synthesized **1** are shown in Table 4. ^{1}H NMR, ^{13}C NMR, COSY, HSQC, and HMBC data are shown in Figures S75 – S80 in Appendix II. Similar to the natural **1**, partial assignment of H and C corresponding to the α and β anomers of D-glucose for synthesized **1** is shown in Figure S78 in Appendix II. Comparison of ^{1}H NMR and ^{13}C NMR spectra of the natural and synthesized **1** also showed similar data (Tables 2 and 4, and Figures S27 – S32 and S75 – S76, Appendix II) and revealed the chemical structure of **1** to be 3,4-*O*-diisobutyryl-2-*O*-((*S*)-2-methylbutyryl)-D-glucose (Figure 11).

3.4.2. Synthesis of the benzylated derivative of pennelliisides A and B

Previously pennelliisides A and B were isolated and identified from *S. pennellii* (Figure 9) [28]. Their chemical structures were revealed as 2,3,4-*O*-triisobutyryl-D-glucose and 3-*O*-(8-methylnonanoyl)-2,4-*O*-diisobutyryl-D-glucose by analyzing 1D and 2D NMR spectroscopy, respectively. Since chemical synthesis brings more advantages to agriculture, medicine, and the food industry, in this chapter, chemical syntheses of their benzylated derivates were conducted.

Synthesis of dibenzyl pennelliiside A was begun with previously synthesized intermediate, **6** (Scheme 3). Compound **6** was subjected to the esterification with

isobutyryl chloride to attach the fatty acid moiety to both C-2 and C-3 positions. Cleavage of 4,6-*O*-benzylidine present at C-4 and C-5 in **10** was done with Et_3SiH and TFA followed by another esterification with isobutyryl chloride to yield dibenzyl pennelliiside A (**14a**). The molecular formula and molecular weight were obtained as $C_{32}H_{42}O_9$ and *m/z* 570.2818 $[M]^+$ (calcd *m/z* 570.2829 $[M]^+$), respectively, using HRFD-MS data (Figure S19, Appendix I) which showed the similar values reported for those of the natural dibenzyl pennelliiside A. Additionally, optical rotation of the dibenzyl pennelliiside A was measured to be $[\alpha]^{25}_D$ = +29.1 (c 0.5, $CHCl_3$) which showed a good correspondence with reported dibenzyl pennelliiside A [28].

Similarly, the synthesis of dibenzyl pennelliiside B (**14b**) was commenced with selective esterification at C-3 by reacting **6** with 8-methylnonanoic acid to yield **11**. Next, **11** was reacted with isobutyryl chloride to get **12**. As same as the previous synthesis, cleavage of 4,6-*O*-benzylidine present at C-4 and C-5 in **12** was done followed by esterification with isobutyryl chloride to yield desired dibenzyl pennelliiside B (**14b**). HRFD-MS analysis revealed the molecular formula and molecular weight as $C_{38}H_{54}O_9$ and *m/z* 654.3774 $[M]^+$ (calcd *m/z* 654.3769 $[M]^+$), (Figure S20, Appendix I) which showed the same data as reported dibenzyl pennelliiside B. Chemical structures of all synthesized compounds were confirmed with ^1H NMR, ^{13}C NMR, and COSY, HSQC, HMBC, and NOESY correlations (Figures S111 – S115, Appendix II). The optical rotation of dibenzyl pennelliiside B was measured to be $[\alpha]^{25}_D$ = -13.3 (c 0.6, $CHCl_3$) which showed relevant values to those previously reported values [28].

It has been already proven that the removal of benzyl groups can be accomplished as Scheme 1 to obtain pennelliisides A and B. Based on the above, it is possible to mention that formal total syntheses were accomplished.

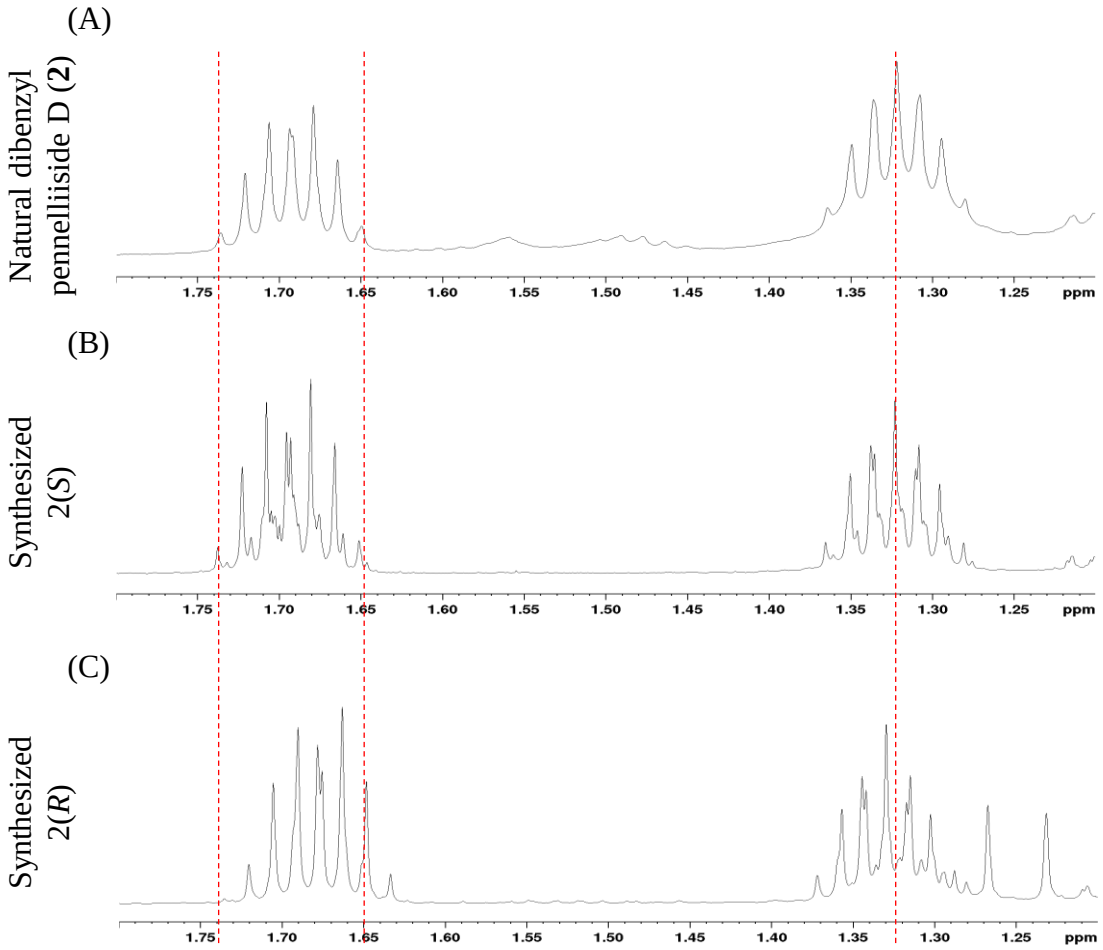

Figure 10. Expanded key ^{1}H-NMR spectrum for the H-A4 resonances of natural dibenzyl pennelliiside D (**2**) and its synthesized isomers (*S*/*R*). (A) ^{1}H-NMR spectrum of natural dibenzyl pennelliiside D (500 MHz, C_6D_6); (B) ^{1}H-NMR spectrum of the synthesized isomer (*S*) (500 MHz, C_6D_6); (C) ^{1}H-NMR spectrum of the synthesized isomer (*R*) (500 MHz, C_6D_6).

(A)

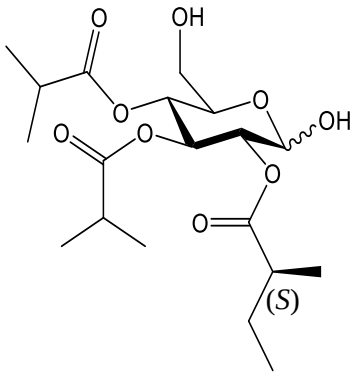

Pennelliiside D (**1**)

(B)

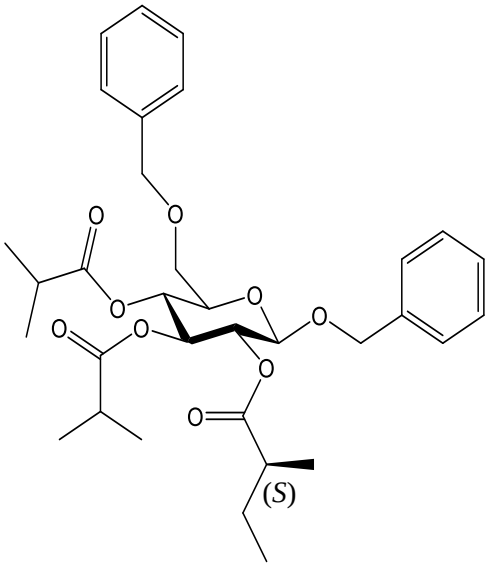

Dibenzyl pennelliiside D (**2**)

Figure 11. The absolute configuration of pennelliiside D and its benzylated derivative.

Table 3. ^{1}H NMR (500 MHz) and ^{13}C NMR (126 MHz) spectroscopic data of synthesized (*S*) and (*R*) isomers of dibenzyl pennelliiside D (**2**) in C_6D_6 (δ in ppm, *J* in Hz).

Position	Type	Synthesized (*S*) isomer of dibenzyl pennelliiside D (2)		Synthesized (*R*) isomer of dibenzyl pennelliiside D (2)	
		δ_C	δ_H (*J* in Hz)	δ_C	δ_H (*J* in Hz)
1	CH	100.3	4.38, d (7.6)	100.2	4.38, d (7.9)
2	CH	71.8	5.46, m	71.9	5.45, m
3	CH	73.5	5.48, m	73.6	5.47, m
4	CH	70.1	5.30, dd (9.6, 9.5)	70.0	5.30, dd (9.8, 9.5)
5	CH	74.3	3.42, m	74.3	3.42, m
6	CH_2	69.9	3.47, m	69.9	3.47, m
1a'	CH_2	70.7	4.75, d (12.2)	70.7	4.75, d (12.2)
1b'			4.45, d (12.2)		4.45, d (12.2)
2'	C	138.0		138.0	
3'	CH	128.1–128.6	7.26, t (7.3)	128.1–128.7	7.26, t (7.3)
4'	CH	128.1–128.6	7.12–7.19, m	128.1–128.7	7.12–7.19, m
5'	CH	128.1–128.6	7.08, t (7.3)	128.1–128.7	7.08, t (7.0)
6'	CH	128.1–128.6	7.12-7.19, m	128.1–128.7	7.12–7.19, m
7'	CH	128.1–128.6	7.26, t (7.3)	128.1–128.7	7.26, t (7.3)
A1	C	174.7		174.9	
A2	CH	41.9	2.28 m	41.6	2.29, m
A3	CH_3	17.2	1.08, d (7.1)	17.1-19.6	1.07, d (7.1)
A4	CH_2	27.2	1.32, 1.69, m, m	27.3	1.33, 1.68, m, m
A5	CH_3	12.2	0.81, t (7.4)	12.1	0.81, t (7.4)
B1	C	176.2		175.3	
B2	CH	34.6	2.41, m	34.5	2.41, m
B3	CH_3	19.2–19.5	1.08, d (7.0)	17.1–19.6	1.07, d (7.1)
B4	CH_3	19.2–19.5	1.08, d (7.0)	17.1–19.6	1.07, d (7.1)
C1	C	175.3		175.3	
C2	CH	34.5	2.31, m	34.5	2.30, m
C3	CH_3	19.2–19.5	1.02, d (7.0)	17.1–19.6	1.02, d (7.0)
C4	CH_3	19.2–19.5	0.98, d (7.0)	17.1–19.6	0.98, d (7.0)
1a"	CH_2	73.9	4.33, d (5.5)	73.9	4.33, d (5.4)
1b"			4.33, d (5.5)		4.33, d (5.4)
2"	C	139.0		139.0	
3"	CH	128.1–128.7	7.26, t (7.3)	128.1–128.7	7.26, t (7.3)
4"	CH	128.1–128.7	7.12–7.19, m	128.1–128.7	7.12–7.19, m
5"	CH	128.1–128.7	7.08, t (7.3)	128.1–128.7	7.08, t (7.0)
6"	CH	128.1–128.7	7.12–7.19, m	128.1–128.7	7.12–7.19, m
7"	CH	128.1–128.7	7.26, t (7.3)	128.1–128.7	7.26, t (7.3)

Table 4. ^{1}H NMR (500 MHz) and ^{13}C NMR (126 MHz) spectroscopic data of synthesized (*S*) isomer of pennelliiside D (**1**) in $CDCl_3$ (δ in ppm, *J* in Hz).

Position	**Type**	***α* Anomer**		***β* Anomer**	
		δ_C	δ_H (*J* in Hz)	δ_C	δ_H (*J* in Hz)
1	CH	90.4	5.48, d (3.6)	96.1	4.72, dd (7.1, 6.1)
2	CH	71.4	4.85, dd (6.8, 3.6)	73.5	4.87, dd (7.7, 6.9)
3	CH	69.0	5.65, dd (10.9, 9.9)	71.4	5.37, dd (10.4, 9.6)
4	CH	68.8	5.01, dd (10.9, 9.7)	68.8	5.05, dd (10.4, 8.1)
5	CH	69.7	4.06, m	74.7	3.55, m
6	CH_2	61.3	3.71, 3.55, m	61.3	3.71, 3.55, m
A1	C	176.6		176.6	
A2	CH	41.1	2.24–2.42, m	41.1	2.24–2.42, m
A3	CH_3	16.4–19.4	1.03–1.17, m	16.4–19.4	1.03–1.17, m
A4	CH_2	26.7	1.41, 1.62, m	26.7	1.41, 1.62, m
A5	CH_3	11.7	0.85, m	11.7	0.85, m
B1	C	176.0		176.0	
B2	CH	34.2	2.50, m	34.2	2.50, m
B3	CH_3	16.4–19.4	1.03–1.17, m	16.4–19.4	1.03–1.17, m
B4	CH_3	16.4–19.4	1.03–1.17, m	16.4–19.4	1.03–1.17, m
C1	C	176.9		176.9	
C2	CH	34.2	2.56, m	34.2	2.52, m
C3	CH_3	16.4–19.4	1.03–1.17, m	16.4–19.4	1.03–1.17, m
C4	CH_3	16.4–19.4	1.03–1.17, m	16.4–19.4	1.03–1.17, m

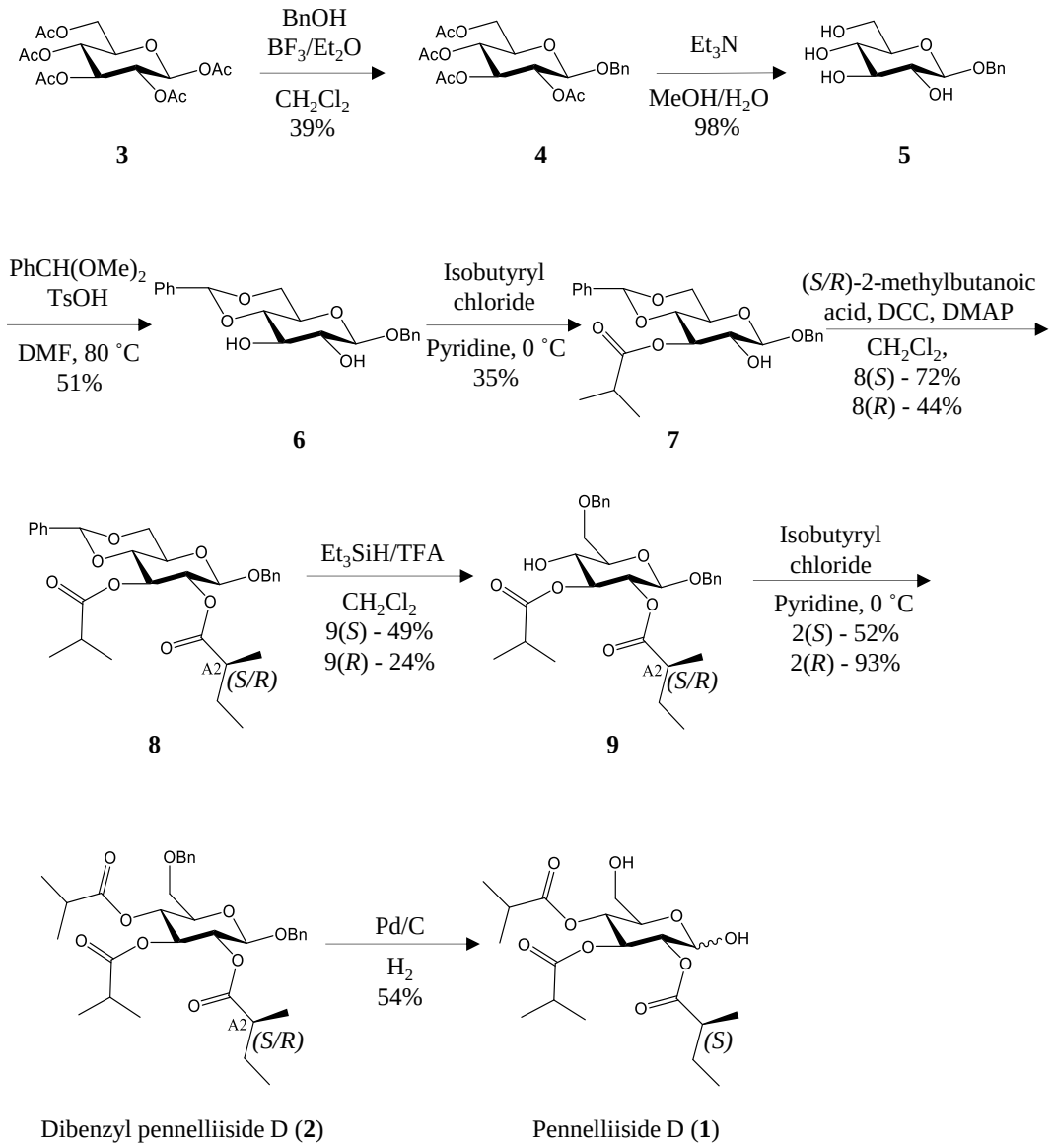

Scheme 3. Total synthesis of dibenzyl pennelliiside D

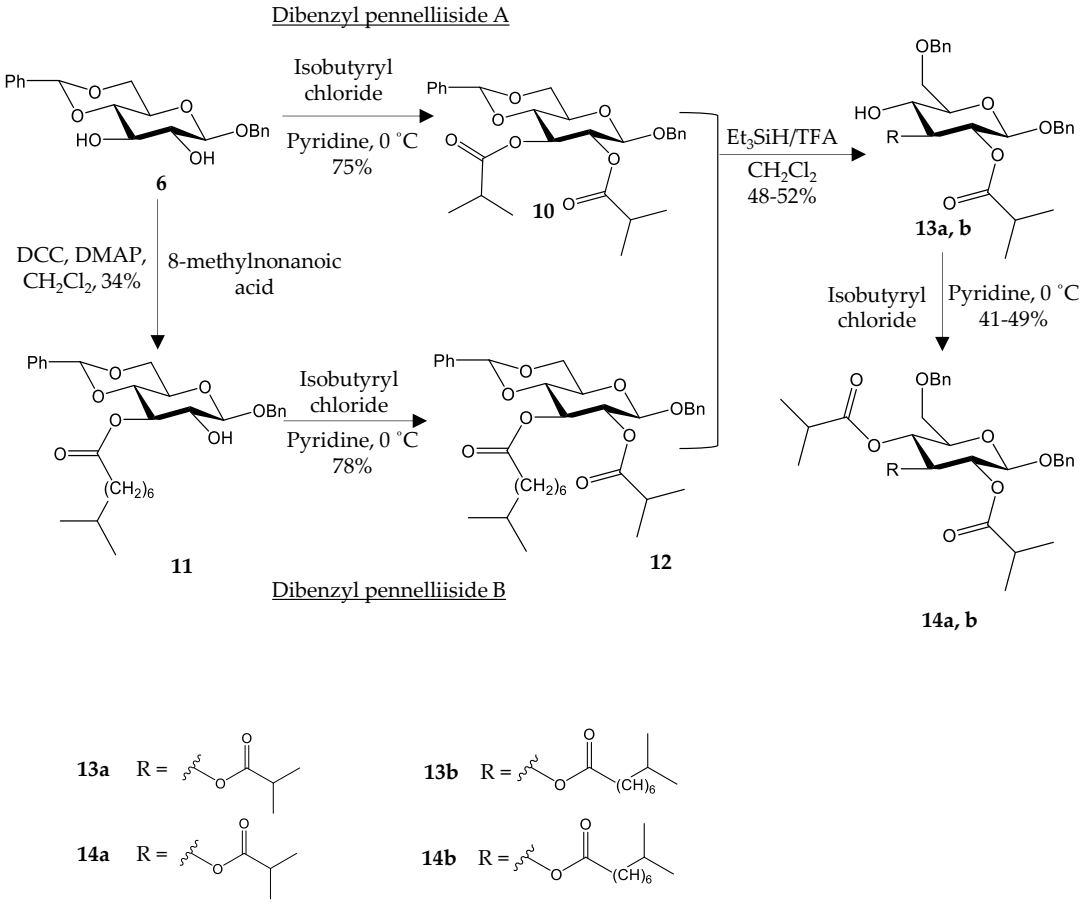

Scheme 4. Synthesis of dibenzyl pennelliisides A and B.

3.5. Conclusions

In the present study, the chemical synthesis of pennelliisides was aimed. In order to identify the correct absolute configuration of the fatty acid moiety of 2-methylbutyryl present at C-2 in pennelliiside D, total synthesis of its (*S*) and (*R*) isomers of dibenzyl pennelliiside D were conducted with *β*-D-glucose pentaacetate as the starting material. By comparing ^{1}H NMR and ^{13}C NMR of both (*S*) and (*R*) isomers together with the comparison of specific rotation values of the compounds, the absolute configuration of the fatty acid moiety, 2-methylbutyryl was found to be (*S*) configuration. Thus, its chemical name was assigned as 1,6-*O*-dibenzyl-3,4-*O*-diisobutyryl-2-*O*-((*S*)-2-methylbutyryl)-*β*-D-glucose.

Additionally, in this study, the chemical syntheses of benzyl derivatives of previously reported pennelliisides A and B were presented. Their chemical syntheses were started from 1-*O*-benzyl-4,6-*O*-benzylidine-*β*-D-glucose, which was the key intermediate compound used for the synthesis of pennelliiside D.

CHAPTER 4

BIOLOGICAL ACTIVITIES OF ACYL GLUCOSES

4.1. Introduction

Plants have been used extensively for many years for enriching human life. For example, medicinal plants have been used to treat various diseases since ancient times. With the civilization and the development of science and technology, studying the biological activities of plants and identifying new compounds became more important research areas. Today numerous types of medicines, and compounds for agriculture and the food industry have been invented through studying the biological activities of compounds in plants.

Acyl sugars show various biological activities. Apart from its agricultural and medicinal applications, it has been reported that acyl sucrose showed a root-growth inhibitory effect on velvetleaf [96]. Thus, in the chapter, the root-growth inhibitory activity of the pennelliiside D and its constituent fatty acid was investigated.

Moreover, it is well known that *S. pennellii* responds to drought (dehydration) and water stress thus, it is used as a model tomato plant for breeding purposes [97]. Ziaf et al., 2011 [98] have reported *SpERD15* gene from *S. pennellii* that gradually increases the mRNA accumulation by drought, salinity, cold, ABA, gibberellic acid, and ethylene treatments. Egea et al., 2018 [97] have shown the ability of *S. pennellii* leaves to avoid water loss and oxidative damage by studying physiological and molecular mechanics. However, no reports have been reported on how the endogenous amounts of acyl glucoses are changed by water or drought stresses.

Trichomes in plants are important parts of the plants since they defend the plant against pathogen or herbivore attacks. Some studies have shown that jasmonic acid (JA), a plant hormone correlates with trichome density and plant defenses [99]. JA is a naturally occurring phytohormone that ubiquitously exists in seed plant species [100]. Many studies demonstrate that JA is a modulator of numerous plant physiological processes that are related to development and defense responses [100–102]. Wounding, herbivores, or pathogen attacks activate the JA biosynthesis pathway [101]. It has been reported that herbivore feeding and JA treatment induce trichome density in newly formed leaves [103]. Additionally, it has been reported that the application of methyl jasmonate (MeJA) also induces trichome density in new leaves, and increases acyl sugar content [104]. Thus, it was suggested that JA is an essential component to control trichome defenses.

Similarly, salicylic acid (SA) is known as a plant hormone that shows several physiological and biochemical effects. These include flowering induction, inhibition of phosphate and potassium uptake, plant growth and development, vegetative growth, thermogenesis, photosynthesis, and defense responses [105,106]. Methyl salicylate (MeSA), a volatile organic compound, is an inactive form of SA, which plays a critical role in plant defense signaling [107], and is known as a long-distance phloem signaling molecule [105]. It has been reported that MeSA provides volatile signals to the neighboring plant upon pathogen infections [108]. Although some studies have been reported on the increment of acyl sugar amounts and changes in trichome content with JA treatment, there are no reports on changes in acyl sugars or trichome density with SA or MeSA treatments.

In the present study, in order to understand the biological effects of pennelliisides, a root-growth inhibitory for pennelliiside D and its constituent fatty acid, and changes in pennelliisides accumulation on water stress and plant hormone treatment such MeJA and MeSA were conducted.

4.2. Objective

The objective of this study is to investigate the biological activities of pennelliisides A-D by conducting the root-growth inhibitory test, giving water stress, and treating with airborne MeSA and MeJA.

4.3. Experimental procedure

4.3.1. Rooth-growth inhibitory test

In order to investigate the root-growth inhibitory effects of pennelliiside D and its constituent fatty acids, *A. thaliana* seeds were used. The seeds were sterilized with 1% tween and sodium hypochlorite for 30 min and washed with water to remove damaged and decolorized seeds. MS medium was prepared with 1/20 strength, and it was adjusted to pH 6.3 with 0.2 mM potassium hydroxide. Ten solutions were prepared, and gellan gum (1.5%) was added to each MS medium. All mediums were autoclaved at 120 ºC for 15 min. Next, 0.2 M stock solutions of natural and synthesized **1**, and (*S*)-2-methylbutanoic acid were prepared separately. Then another two concentrations of 0.1 M and 0.02 M solutions of the compounds were prepared from their stock solutions. In order to reach the final concentrations of 10 μM, 50 μM, and 100 μM of each compound in the plates, 10 μL of each compound was added to the MS medium from above prepared 0.2 M, 0.1 M, and 0.02 M solutions separately. Immediately, the mediums were poured into plates and allowed to cool to room temperature. As the control, *A, thaliana* seeds were germinated on the MS medium without adding any compound. The seeds were planted on each medium, and the plates were placed vertically and left in a 16 h light and 8 h dark photoperiod at 23 ºC. The root length of each seed was measured after 13 days.

4.3.2. Water stress treatment

S. pennellii plants were used for the experiment. Seeds were germinated in a plant growing chamber at 25 °C under 16 h of light and 8 h of dark photoperiod for 30 days. Six plants were kept in a container, and they were irrigated with 300 mL of water every two days. The water level was always 3 – 4 cm in height (Figure 12). As the control,

six plants were irrigated with 200 mL of water every four days. The stress was given for 10 days. Then, the shoots of the plants were harvested, crushed with liquid nitrogen, and extracted with EtOH. The extract was filtered, and the filtrate was concentrated under reduced pressure. Samples were re-extracted with 6 mL (2 mL×3) of 80% MeOH and loaded into a cartridge column of Bond Elut C18 (Varian, CA, U.S.A). The elute was evaporated to complete dryness under reduced pressure. Finally, samples were prepared by dissolving the residue in 300 μL of 80% MeOH. Principal component analysis was performed by LC-TOF-MS system in positive mode. Conditions applied for the LC-TOF-MS analysis were shown in Table 5.

Control Water stress treated plants

Figure 12. Plants treated with water stress

4.3.3. Treatment of airborne MeSA and MeJA

Plants of the *S. pennellii* were grown in a chamber at 23 ºC with 16 h light and 8 h dark photoperiod for 30 days. Six plants were kept in a closed chamber with three glass bottles that were turned upside down. Then, a piece of filter paper containing 1 mg of MeSA in MeOH was placed on top of the glass bottles as an airborne signal as shown in Figure 13. This treatment was kept for 24 h. MeOH was used instead of MeSA for control samples. The same procedure was followed for airborne MeJA treatment.

Shoots of the plants treated with airborne MeSA, MeJA, and without treatment were harvested, weighed, immediately crushed with liquid nitrogen, and extracted with EtOH. Then the extract was filtered, and the filtrate was concentrated under reduced pressure. Samples were re-extracted with 6 mL (2 mL×3) of 80% MeOH and loaded into a cartridge column of Bond Elut C18 (Varian, CA, U.S.A). The elute was evaporated to complete dryness under reduced pressure. Finally, samples were prepared by dissolving the residue in 300 μL of 80% MeOH. Principal component analysis was performed by LC-TOF-MS system in positive mode. Conditions applied for the LC-TOF-MS analysis were shown in Table 5.

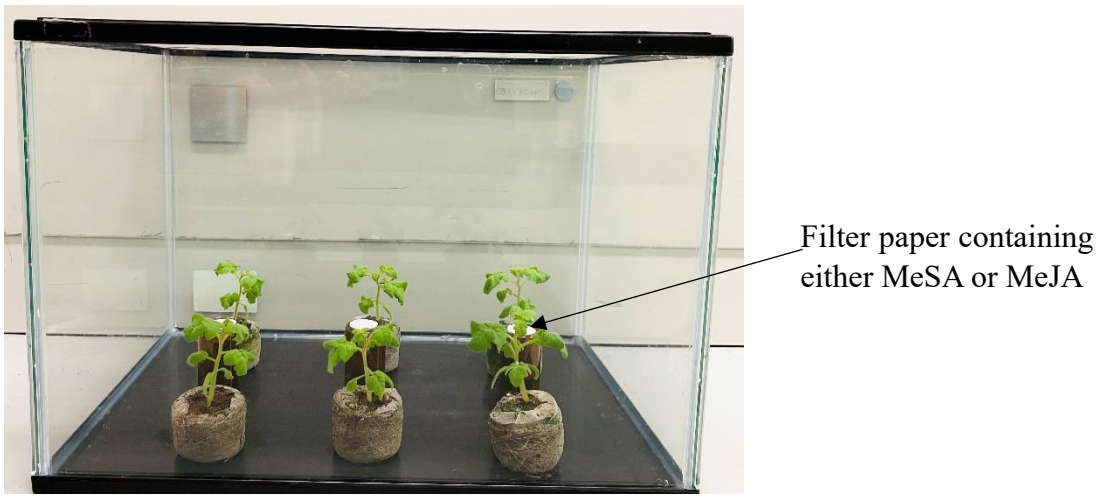

Figure 13. Experimental setup for the airborne MeSA/MeJA treatment

4.4. Results and discussion

4.4.1. Root-growth inhibitory effect

According to the experiment conducted by Nakashima et al., 2020 [28], the constituent fatty acids of pennelliisides, 8-methylnonanoic acid, and isobutyric acid showed root-growth inhibition activity in *A. thaliana*. Therefore, in this study, root growth-inhibitory activity against natural derived, synthesized **1** and its constituent fatty acid, (*S*)-2-methylbutanoic acid, was assessed. *A. thaliana* seeds and 10 μM, 50 μM, and 100 μM concentrations of compounds were used in this experiment. As the control, *A. thaliana* seeds were germinated in the MS medium without adding any compound. The data revealed that neither compound showed root growth-inhibitory activity at any tested concentration (Figure 14). Figure 15 shows the photographs of *A. thaliana* plants grown in MS medium after 13 days. Nakashima et al., 2020 [28] have reported similar results that pennelliisides A, B, and C did not show any root-growth inhibition activity. Collectively, the results may well support that longer chain carbon fatty acids of acyl sugars show a root-growth-inhibitory effect.

4.4.2. Responses to water stress

Wild plants often face various environmental stresses such as water stress and drought stress. Although it is known that acyl sugars provide broad protection against insects, there is a lack of knowledge regarding how acyl sugar profiles vary with water stress. Therefore, *S. pennellii* plants were subjected to water stress for 10 days, and the accumulation of pennelliisides A-D was explored. Based on LC-TOF-MS analysis, compounds did not show any significant difference compared to those of control (Figure 16). Since pennelliisides B and C show similar retention times (14.124, 13.786 min, and 14.366, 13.554 min, respectively), it was hard to determine the relative

abundance corresponding to pennelliisides B and C exactly. However, overall results suggest that water stress to *S. pennellii* plants may not affect to the endogenous amount of pennelliisides.

4.4.3. Responses to airborne MeSA and MeJA

MeSA and MeJA are known as airborne signals in plants. In order to understand the effect of airborne MeSA and MeJA on acyl sugar profile, accumulation of pennelliisides A-D was observed upon exposure of *S. pennellii* plant to airborne MeSA and MeJA. Interestingly, based on LC-TOF-MS analysis, Pennelliiside D showed a significantly higher relative abundance upon exposure to airborne MeJA and MeSA compared to those of control (Figure 17). Neither pennelliisides A-C were detected upon airborne MeSA or MeJA treatment. These results suggest that pennelliiside D may accumulate upon airborne MeSA and MeJA signals. However, further testing is required to understand the metabolism of pennelliiside D upon airborne MeSA and MeJA treatments, as well as the relationship with SA and JA signaling.

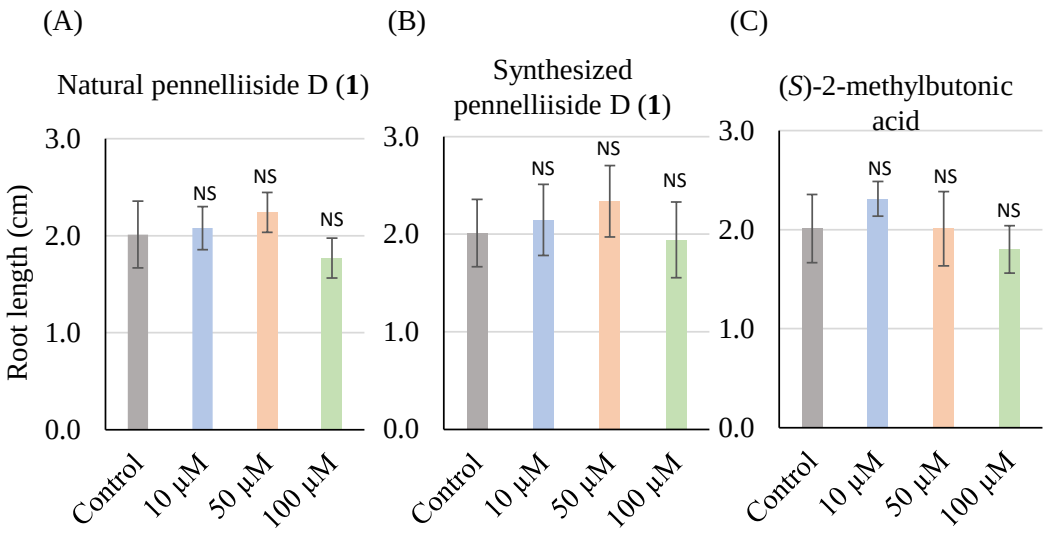

Figure 14. Root growth inhibitory effect of pennelliiside D (**1**) and its constituent fatty acids. (A) and (B) root length of natural and synthesized pennelliiside D (**1**), and (C) root length of (*S*)-2-methylbutonic acid. Error bars indicate ± SE (n = 12; results are from one representative experiment); Welch's t-test, NS: Not significant.

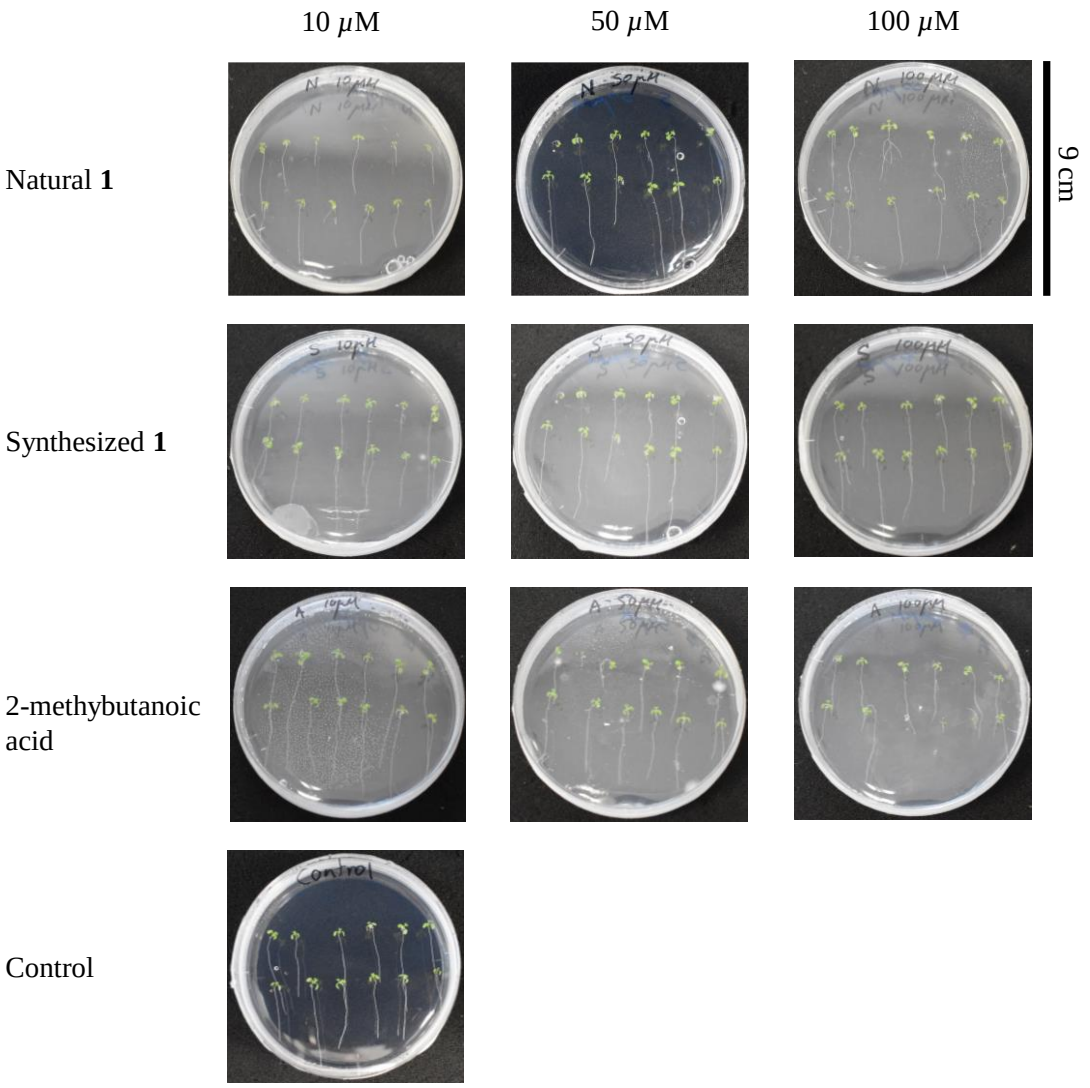

Figure 15. Photographs of root growth inhibitory effect of pennelliiside D (**1**) and 2-methylbutanoic acid.

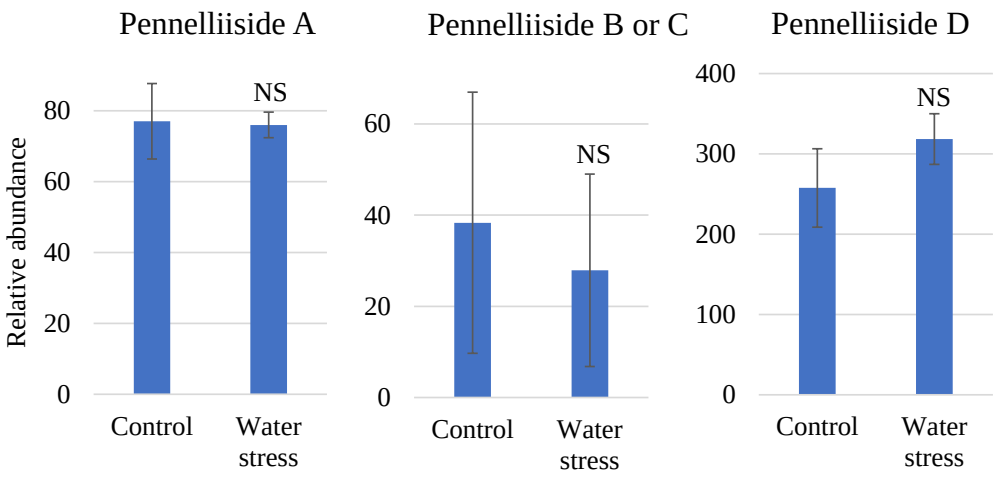

Figure 16. Evaluation of pennelliisides A-D in *S. pennellii* upon water stress. Plants were given water stress for 10 days. The upper part of the plants was harvested and extracted with EtOH. Samples were analyzed using LC-TOF-MS. Each value is represented as the mean ± SD of six independent replicates. Results are from one representative experiment. Welch`s test, NS: Not significant.

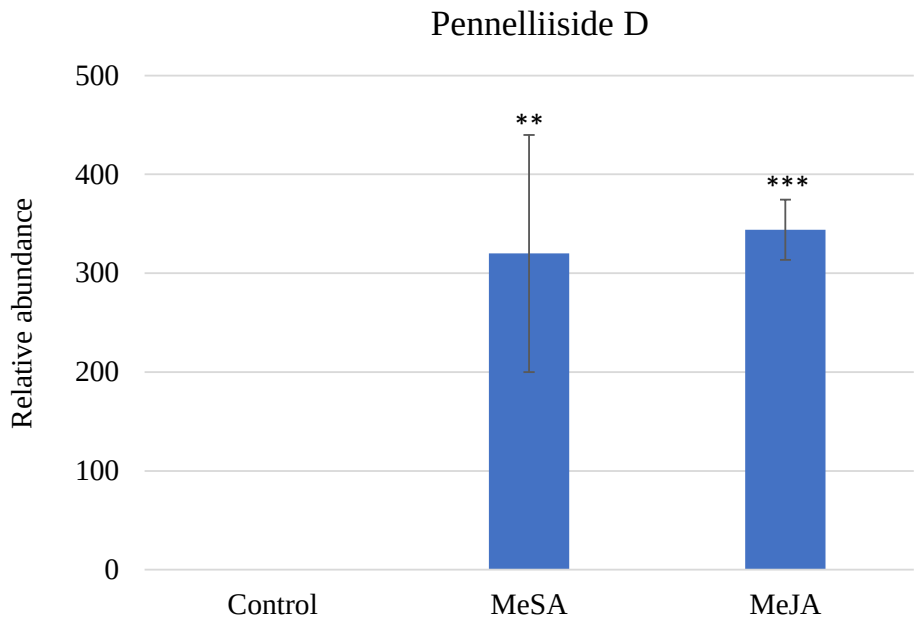

Figure 17. Evaluation of pennelliiside D in *S. pennellii* upon airborne MeSA and MeJA. Plants were exposed to airborne MeSA and MeJA for 24 h separately. The upper part of the plants was harvested and extracted with EtOH. Samples were analyzed using LC-TOF-MS. Each value is represented as the mean ± SD of six independent replicates. Results are from one representative experiment. Welch`s test, **: $p < 0.01$, ***: $p < 0.001$.

4.5. Conclusions

In the present study, the biological activities of pennelliisides A-D were investigated. Based on the root-growth inhibitory activity test results, pennelliiside D and its constituent fatty acid, 2-methylbutanoic acid did not show any root elongation activity. With reference to the previously reported root-growth inhibitory activity of pennelliisides A-C, the results provide evidence that longer chain fatty acids of acyl sugars show root-growth inhibitory effects. Water stress was given to *S. pennellii* to investigate whether the regulation of pennelliisides has a relationship with water stress. None of the compounds showed a significant difference in relative abundance compared to those of controls, which implies that there may not be a relationship with water stress tolerance. Additionally, pennelliiside D showed a higher relative abundance upon airborne MeSA and MeJA which suggests that pennelliiside D correlates with SA and JA signaling. However, further testing is required to confirm these results more.

CHAPTER 5

CONCLUSIONS

In this thesis, isolation, identification, and structural elucidation of acyl glucoses from *S. pennellii* were studied. In order to identify the correct absolute configuration of the identified compound, total synthesis was carried out. Apart from that, other previously identified acyl glucoses, pennelliisides A and B were synthesized. Finally, the biological activity of the isolated compound and its synthesized compounds was evaluated.

Because of the availability of a wide diversity of acyl sugars, their chemical structures are complex and diverse. Thus, isolation and identification of acyl sugars were carried out in this study. Since acyl glucoses undergo anomerization at C-1 in the glucose moiety, the isolation and identification of acyl sugars are difficult. In the present research, a new acyl sugar, pennelliiside D was isolated using a strategy to prevent the anomerization into either one of the isomers. Anomerization in acyl sugars was fixed into either one of the isomers by treating the ethanol extract of *S. pennellii* with TriBOT to attach the benzyl groups with free hydroxyl groups present at the glucose moiety. Then separation was done by silica gel column chromatography followed by HPLC separation to yield a new benzylated derivative of pennelliiside D. The structural determination of dibenzyl pennelliiside D was conducted by 1D and 2D NMR spectroscopy, and it was revealed that the chemical structure of dibenzyl pennelliiside D was to be 1,6-*O*-dibenzyl-3,4-*O*-diisobutyryl-2-*O*-(2-methylbutyryl)-*β*-D-glucose. Then, benzyl groups were removed under a hydrogen gas atmosphere with palladium/carbon to yield pennelliiside D. Its structure was confirmed as 3,4-*O*-

diisobutyryl-2-*O*-(2-methylbutyryl)-D-glucose based on the analysis of 1D and 2D NMR spectroscopy.

Although the planner structure of pennelliiside D was determined as above, it was not performed to determine the absolute configuration of the 2-methylbutyryl fatty acid moiety in pennelliiside D. Thus, the total syntheses of two possible isomers of (*R*) and (*S*) of 2-methylbutyryl fatty acid moiety in pennelliiside D were carried out starting from *β*-D-glucose pentaacetate. By comparing the spectroscopic data and the specific rotation values of natural dibenzyl pennelliiside D with those of synthesized dibenzyl pennelliiside D, the absolute configuration of the acyl moiety in pennelliiside D was identified to be (*S*). Then, deprotection of benzyloxy groups was carried out to yield pennelliiside D, 3,4-*O*-diisobutyryl-2-*O*-((*S*)-2-methylbutyryl)-D-glucose. Additionally, in this study, benzylated derivatives of two identified acyl sugars, dibenzyl pennelliisides A and B, were synthesized. Their chemical synthesis was started from 1-*O*-benzyl-4,6-*O*-benzylidine-*β*-D-glucose, which was the intermediate compound used for the synthesis of pennelliiside D.

The root-growth activity of pennelliiside D and its constituent fatty acid moieties were examined using *A. thaliana,* which revealed that neither the compound nor the fatty acid moieties showed root-growth-inhibitory activity at any tested concentration. These results were reported in Masimbula et al., 2022 [109].

Since, it has been reported that the ability of airborne MeSA and MeJA to induce the endogenous amount of other secondary metabolites [108], there is a possibility to induce the accumulation of pennelliisides upon airborne MeSA or MeJA in tomatoes. Thus, to investigate the biological activities of pennelliisides, the accumulation of pennelliisides upon contact with airborne MeSA and MeJA was examined.

Interestingly, pennelliiside D showed a higher relative abundance upon contact with both airborne MeSA and MeJA, which suggest the possibility of positive regulation of the endogenous amount of pennelliiside D upon treatments of airborne MeSA and MeJA. In order to investigate the endogenous amount of accumulated pennelliisides using UPLC-MS/MS, the synthesis of deuterium-labeled pennelliisides can be conducted using the synthetic schemes developed in this study.

Additionally, water stress was given to *S. pennellii* plants to investigate whether the endogenous amounts of pennelliisides have a correlation with water stress tolerance. Neither compound showed a significant difference in accumulation compared to their controls which suggest that there may not be a correlation between pennelliisides A-D with water stress.

CHAPTER 6

GENERAL EXPERIMENTAL PROCEDURES

6.1. Equipment and their conditions

Optical rotations were obtained with a JASCO P-2200 polarimeter. NMR spectra were recorded in C_6D_6, CD_3OD, and $CDCl_3$ using a JNM-EX 270 FT-NMR spectrometer (JEOL, ^{1}H NMR: 270 MHz) and AMX 500 Bruker system (^{1}H NMR: 500 MHz, ^{13}C NMR: 126 MHz). Assignment of ^{1}H and ^{13}C was performed by examining the data of ^{1}H NMR, ^{13}C NMR (referenced for C_6D_6, CD_3OD and $CDCl_3$ at δ_H 7.16, 3.31 and 7.24, and δ_C 128.4, 49.2 and 77.2, respectively), COSY, HSQC, HMBC, and NOESY spectra. FD-MS analysis was performed on a JMS-T100GCV (JEOL) instrument. Chromatographic analysis was performed using an HPLC system (InertSustain, A_{210max} nm) equipped with a Shisheido Capcell park C18 column (4.6 × 250 nm, 5 μm, 2 mL/min, MeOH-H_2O, 80:20) and a Cadenza CK-C18 column (6 × 250 nm, 3 μm, 2 mL/min, MeOH-H_2O, 80:20). LC-TOF-MS analysis was performed using Waters ACQUITY UPLC BEH C18 1.7 μm column (2.1 × 100 mm; Waters, Milford, MA, USA) and Waters Micromass LCT Premier XE Mass Spectrometer (Waters, Milford, MA, USA).

All moisture-sensitive reactions were performed under a nitrogen gas atmosphere. All chemicals used in the study were of analytical grade and purchased from Sigma–Aldrich, Tokyo, Japan, Kanto Chemical Co., Inc, Tokyo, Japan, and Cayman Chemical, Michigan, United States.

6.2. LC-TOF-MS analysis condition for airborne MeSA and MeJA, and water stress treatments

Table 5. LC-TOF-MS analysis condition

(A) MS configuration

Cone voltage (V)	35
Aperture voltage (V)	0
Frequency (scans)	5
Mass (*m*/*z*)	100 – 1000
Time (min)	0 – 18.5

(B) Conditions of LC

Column temperature	40˚C
Sample temperature	20˚C

Time (min)	Flow rate (mL/min)	%A	%B	Curve
0.2	0.25	90.0	10.0	6
15.50	0.25	0.0	100.0	6
18.80	0.25	0.0	100.0	6
19.00	0.25	90.0	10.0	6
20.00	0.25	90.0	10.0	6

A: 20% aq. MeOH + 0.05% AcOH

B: 100% MeOH + 0.05% AcOH

(C) Pseud molecular ions for pennelliisides A-D and their retention times in the analysis of LC-TOF-MS in positive mode

Compound	$[M-H_2O]^+$ (*m*/*z*)	Retention time (min)
Pennelliiside A	373.2302	9.645
Pennelliiside B	457.2955	14.124
		13.786
Pennelliiside C	457.3134	14.366
		13.554
Pennelliiside D	387.2457	10.254
		8.998

REFERENCES

1. Wurtzel, E.T.; Kutchan, T.M. Plant Metabolism, the Diverse Chemistry Set of the Future. *Science.* **2016**, *353*, 1232–1236, doi:10.1126/science.aad2062.

2. Schuurink, R.; Tissier, A. Glandular Trichomes: Micro-Organs with Model Status? *New Phytol.* **2020**, *225*, 2251–2266, doi:10.1111/nph.16283.

3. Glas, J.J.; Schimmel, B.C.J.; Alba, J.M.; Escobar-Bravo, R.; Schuurink, R.C.; Kant, M.R. Plant Glandular Trichomes as Targets for Breeding or Engineering of Resistance to Herbivores. *Int. J. Mol. Sci.* **2012**, *13*, 17077–17103, doi:10.3390/ijms131217077.

4. Schilmiller, A.L.; Last, R.L.; Pichersky, E. Harnessing Plant Trichome Biochemistry for the Production of Useful Compounds. *Plant J.* **2008**, *54*, 702–711, doi:10.1111/j.1365-313X.2008.03432.x.

5. Turner, G.W.; Gershenzon, J.; Croteau, R.B. Distribution of Peltate Glandular Trichomes on Developing Leaves of Peppermint. *Plant Physiol.* **2000**, *124*, 655–663, doi:10.1104/pp.124.2.655.

6. Gang, D.R.; Wang, J.; Dudareva, N.; Nam, K.H.; Simon, J.E.; Lewinsohn, E.; Pichersky, E. An Investigation of the Storage and Biosynthesis of Phenylpropenes in Sweet Basil. *Plant Physiol.* **2001**, *125*, 539–555, doi:10.1104/pp.125.2.539.

7. Jia, P.; Liu, H.; Gao, T.; Xin, H. Glandular Trichomes and Essential Oil of *Thymus quinquecostatus*. *Sci. World J.* **2013**, *2013*, 1–8, doi:10.1155/2013/387952.

8. Kim, J.; Matsuba, Y.; Ning, J.; Schilmiller, A.L.; Hammar, D.; Jones, A.D.; Pichersky, E.; Last, R.L. Analysis of Natural and Induced Variation in Tomato Glandular Trichome Flavonoids Identifies a Gene Not Present in the Reference Genome. *Plant Cell* **2014**, *26*, 3272–3285, doi:10.1105/tpc.114.129460.

9. Jing, H.; Liu, J.; Liu, H.; Xin, H. Histochemical Investigation and Kinds of Alkaloids in Leaves of Different Developmental Stages in *Thymus quinquecostatus*. *Sci. World J.* **2014**, *2014*, doi:10.1155/2014/839548.

10. Aharoni, A.; Jongsma, M.A.; Kim, T.Y.; Ri, M.B.; Giri, A.P.; Verstappen, F.W.A.; Schwab, W.; Bouwmeester, H.J. Metabolic Engineering of Terpenoid Biosynthesis in Plants. *Phytochem. Rev.* **2006**, *5*, 49–58, doi:10.1007/s11101-005-3747-3.

11. Bleeker, P.M.; Mirabella, R.; Diergaarde, P.J.; VanDoorn, A.; Tissier, A.; Kant, M.R.; Prins, M.; De Vos, M.; Haring, M.A.; Schuurink, R.C. Improved Herbivore Resistance in Cultivated Tomato with the Sesquiterpene Biosynthetic Pathway from a Wild Relative. *Proc. Natl. Acad. Sci. U. S. A.* **2012**, *109*, 20124–20129, doi:10.1073/pnas.1208756109.

12. Fobes, J.F.; Mudd, J.B.; Marsden, M.P.F. Epicuticular Lipid Accumulation on the Leaves of *Lycopersicon pennellii* (Corr.) D'Arcy and *Lycopersicon esculentum* Mill. *Plant Physiol.* **1985**, *77*, 567–570, doi:10.1104/pp.77.3.567.

13. Wagner, G.J.; Wang, E.; Shepherd, R.W. New Approaches for Studying and Exploiting an Old Protuberance, the Plant Trichome. *Ann. Bot.* **2004**, *93*, 3–11, doi:10.1093/aob/mch011.

14. Pengxiang, F.; J., L.B.; L., L.R. Tip of the Trichome: Evolution of Acylsugar Metabolic Diversity in Solanaceae. *Curr. Opin. Plant Biol.* **2019**, *49*, 8–16, doi:10.1016/j.pbi.2019.03.005.

15. Kroumova, A.B.M.; Zaitlin, D.; Wagner, G.J. Natural Variability in Acyl Moieties of Sugar Esters Produced by Certain Tobacco and Other Solanaceae Species. *Phytochemistry* **2016**, *130*, 218–227, doi:10.1016/j.phytochem.2016.05.008.

16. Fan, P.; Miller, A.M.; Liu, X.; Jones, A.D.; Last, R.L. Evolution of a Flipped Pathway Creates Metabolic Innovation in Tomato Trichomes through BAHD Enzyme Promiscuity. *Nat. Commun.* **2017**, *8*, 1–13, doi:10.1038/s41467-017-02045-7.

17. Liu, Y.; Jing, S.X.; Luo, S.H.; Li, S.H. Non-Volatile Natural Products in Plant Glandular Trichomes: Chemistry, Biological Activities and Biosynthesis. *Nat. Prod. Rep.* **2019**, *36*, 626–665, doi:10.1039/c8np00077h.

18. Leong, B.J.; Lybrand, D.B.; Lou, Y.R.; Fan, P.; Schilmiller, A.L.; Last, R.L. Evolution of Metabolic Novelty: A Trichome-Expressed Invertase Creates Specialized Metabolic Diversity in Wild Tomato. *Sci. Adv.* **2019**, *5*, 1–13, doi:10.1126/sciadv.aaw3754.

19. Slocombe, S.P.; Schauvinhold, I.; McQuinn, R.P.; Besser, K.; Welsby, N.A.; Harper, A.; Aziz, N.; Li, Y.; Larson, T.R.; Giovannoni, J.; et al. Transcriptomic and Reverse Genetic Analyses of Branched-Chain Fatty Acid and Acyl Sugar Production in *Solanum pennellii* and *Nicotiana benthamiana*. *Plant Physiol.* **2008**, *148*, 1830–1846, doi:10.1104/pp.108.129510.

20. Kroumova, A.B.; Wagner, G.J. Different Elongation Pathways in the Biosynthesis of Acyl Groups of Trichome Exudate Sugar Esters from Various Solanaceous Plants. *Planta* **2003**, *216*, 1013–1021, doi:10.1007/s00425-002-0954-7.

21. Lybrand, D.B.; Anthony, T.M.; Jones, A.D.; Last, R.L. An Integrated Analytical Approach Reveals Trichome Acylsugar Metabolite Diversity in the Wild Tomato *Solanum pennellii*. *Metabolites* **2020**, *10*, 1–25, doi:10.3390/metabo10100401.

22. Puterka, G.J.; Farone, W.; Palmer, T.; Barrington, A. Structure-Function Relationships Affecting the Insecticidal and Miticidal Activity of Sugar Esters. *Exotoxicology* **2003**, *96*, 636–644.

23. Schilmiller, A.L.; Charbonneau, A.L.; Last, R.L. Identification of a BAHD Acetyltransferase That Produces Protective Acyl Sugars in Tomato Trichomes. *Proc. Natl. Acad. Sci. U. S. A.* **2012**, *109*, 16377–16382, doi:10.1073/pnas.1207906109.

24. Schilmiller, A.L.; Moghe, G.D.; Fan, P.; Ghosh, B.; Ning, J.; Jones, A.D.; Last, R.L. Functionally Divergent Alleles and Duplicated Loci Encoding an

Acyltransferase Contribute to Acylsugar Metabolite Diversity in Solanum Trichomes. *Plant Cell* **2015**, *27*, 1002–1017, doi:10.1105/tpc.15.00087.

25. Kim, J.; Kang, K.; Gonzales-Vigil, E.; Shi, F.; Daniel Jones, A.; Barry, C.S.; Last, R.L. Striking Natural Diversity in Glandular Trichome Acylsugar Composition Is Shaped by Variation at the Acyltransferase2 Locus in the Wild Tomato *Solanum habrochaites*. *Plant Physiol.* **2012**, *160*, 1854–1870, doi:10.1104/pp.112.204735.

26. Ghosh, B.; Westbrook, T.C.; Jones, A.D. Comparative Structural Profiling of Trichome Specialized Metabolites in Tomato (*Solanum lycopersicum*) and *S. habrochaites*: Acylsugar Profiles Revealed by UHPLC/MS and NMR. *Metabolomics* **2014**, *10*, 496–507, doi:10.1007/s11306-013-0585-y.

27. Weinhold, A.; Baldwin, I.T. Trichome-Derived *O*-Acyl Sugars Are a First Meal for Caterpillars That Tags Them for Predation. *Proc. Natl. Acad. Sci. U. S. A.* **2011**, *108*, 7855–7859, doi:10.1073/pnas.1101306108.

28. Nakashima, T.; Nambu, Y.; Inoue, Y.; Masimbula, R.; Matsuura, H. Pennelliisides A-C, 2,3,4-Trisubstituted Acyl Glucoses Isolated from *Solanum pennellii*. *J. Nat. Prod.* **2020**, *83*, 2337–2346, doi:10.1021/acs.jnatprod.9b01234.

29. Fan, P.; Wang, P.; Lou, Y.R.; Leong, B.J.; Moore, B.M.; Schenck, C.A.; Combs, R.; Cao, P.; Brandizzi, F.; Shiu, S.H.; et al. Evolution of a Plant Gene Cluster in Solanaceae and Emergence of Metabolic Diversity. *Biochem. Chem. Biol.* **2020**, *9*, 1–26, doi:10.7554/eLife.56717.

30. Ning, J.; Moghe, G.D.; Leong, B.; Kim, J.; Ofner, I.; Wang, Z.; Adams, C.; Jones, A.D.; Zamir, D.; Last, R.L. A Feedback-Insensitive Isopropylmalate Synthase Affects Acylsugar Composition in Cultivated and Wild Tomato. *Plant Physiol.* **2015**, *169*, 1821–1835, doi:10.1104/pp.15.00474.

31. Schilmiller, A.L.; Gilgallon, K.; Ghosh, B.; Jones, A.D.; Last, R.L. Acylsugar Acylhydrolases: Carboxylesterase-Catalyzed Hydrolysis of Acylsugars in Tomato Trichomes. *Plant Physiol.* **2016**, *170*, 1331–1344, doi:10.1104/pp.15.01348.

32. Luu, V.T.; Weinhold, A.; Ullah, C.; Dressel, S.; Schoettner, M.; Gase, K.; Gaquerel, E.; Xu, S.; Baldwin, I.T. *O*-Acyl Sugars Protect a Wild Tobacco from Both Native Fungal Pathogens and a Specialist Herbivore. *Plant Physiol.* **2017**, *174*, 370–386, doi:10.1104/pp.16.01904.

33. Shapiro, J.A.; Steffens, J.C.; Mutschler, M.A. Acylsugars of the Wild Tomato *Lycopersicon pennellii* in Relation to Geographic Distribution of the Species. *Biochem. Syst. Ecol.* **1994**, *22*, 545–561, doi:10.1016/0305-1978(94)90067-1.

34. Severson, R.F.; Arrendale, R.F.; Chortyk, O.T.; Green, C.R.; Thome, F.A.; Stewart, J.L.; Johnson, A.W. Isolation and Characterization of the Sucrose Esters of the Cuticular Waxes of Green Tobacco Leaf. *J. Agric. Food Chem.* **1985**, *33*, 870–875, doi:10.1021/jf00065a026.

35. Arrendale, R.F.; Severson, R.F.; Sisson, V.A.; Costello, C.E.; Leary, J.A.; Himmelsbach, D.S.; van Halbeek, H.; Sisson, V.A.; Costello, C.E.; Leary, J.A.; et al. Characterization of the Sucrose Ester Fraction from *Nicotiana glutinosa*. *J. Agric. Food Chem.* **1990**, *38*, 75–85, doi:10.1021/jf00091a015.

36. Matsuzaki, T.; Shinozaki, Y.; Suhara, S.; Ninomiya, M.; Shigematsu, H.; Koiwai, A. Isolation of Glycolipids from the Surface Lipids of *Nicotiana bigelovii* and Their Distribution in Nicotiana Species. *Agric. Biol. Chem.* **1989**, *53*, 3079–3082, doi:10.1080/00021369.1989.10869779.

37. Ohya, I.; Sinozaki, Y.; Tobita, T.; Takahashi, H.; Matsuzaki, T.; Koiwai, A. Sucrose Esters from the Surface Lipids of *Nicotiana cavicola*. *Phytochemistry* **1994**, *37*, 143–145, doi:10.1016/0031-9422(94)85014-3.

38. Jia, C.; Wang, Y.; Zhu, Y.; Xu, C.; Mao, D. Preparative Isolation and Structural Characterization of Sucrose Ester Isomers from Oriental Tobacco. *Carbohydr. Res.* **2013**, *372*, 73–77, doi:10.1016/j.carres.2013.01.021.

39. Nadakuduti, S.S.; Uebler, J.B.; Liu, X.; Jones, A.D.; Barry, C.S. Characterization of Trichome-Expressed BAHD Acyltransferases in *Petunia axillaris* Reveals Distinct Acylsugar Assembly Mechanisms within the Solanaceae. *Plant Physiol.* **2017**, *175*, 36–50, doi:10.1104/pp.17.00538.

40. Schilmiller, A.; Shi, F.; Kim, J.; Charbonneau, A.L.; Holmes, D.; Daniel Jones, A.; Last, R.L. Mass Spectrometry Screening Reveals Widespread Diversity in Trichome Specialized Metabolites of Tomato Chromosomal Substitution Lines. *Plant J.* **2010**, *62*, 391–403, doi:10.1111/j.1365-313X.2010.04154.x.

41. A. Burke, B.; Goldsby, G.; Brian Mudd, J. Polar Epicuticular Lipids of *Lycopersicon pennellii*. *Phytochemistry* **1987**, *26*, 2567–2571, doi:10.1016/S0031-9422(00)83879-0.

42. Liu, X.; Enright, M.; Barry, C.S.; Jones, A.D. Profiling, Isolation and Structure Elucidation of Specialized Acylsucrose Metabolites Accumulating in Trichomes of Petunia Species. *Metabolomics* **2017**, *13*, 1–10, doi:10.1007/s11306-017-1224-9.

43. Roslund, M.U.; Tähtinen, P.; Niemitz, M.; Sjöholm, R. Complete Assignments of the ^{1}H and ^{13}C Chemical Shifts and JH,H Coupling Constants in NMR Spectra of d-Glucopyranose and All d-Glucopyranosyl-d-Glucopyranosides. *Carbohydr. Res.* **2008**, *343*, 101–112, doi:10.1016/J.CARRES.2007.10.008.

44. Kaufmann, M.; Mügge, C.; Kroh, L.W. NMR Analyses of Complex D-Glucose Anomerization. *Food Chem.* **2018**, *265*, 222–226, doi:10.1016/j.foodchem.2018.05.100.

45. Mandal, S.; Ji, W.; McKnight, T.D. Candidate Gene Networks for Acylsugar Metabolism and Plant Defense in Wild Tomato *Solanum pennellii*. *Plant Cell* **2020**, *32*, 81–99, doi:10.1105/tpc.19.00552.

46. Fan, P.; Miller, A.M.; Schilmiller, A.L.; Liu, X.; Ofner, I.; Jones, A.D.; Zamir, D. In Vitro Reconstruction and Analysis of Evolutionary Variation of the Tomato Acylsucrose Metabolic Network. *Proc. Natl. Acad. Sci.* **2015**, *113*, E239–E248, doi:10.1073/pnas.1517930113.

47. Article, L.B.; Peng, M.; Gao, Y.; Chen, W.; Wang, W.; Shen, S.; Shi, J.; Wang, C.; Zhang, Y.; Zou, L.; et al. Evolutionarily Distinct BAHD *N* -Acyltransferases Are Responsible for Natural Variation of Aromatic Amine Conjugates in Rice. *Plant Cell* **2016**, *28*, 1533–1550, doi:10.1105/tpc.16.00265.

48. Auria, J.C.D. Acyltransferases in Plants : A Good Time to Be BAHD. *Curr. Opin. Plant Biol.* **2006**, *9*, 331–340, doi:10.1016/j.pbi.2006.03.016.

49. Tuominen, L.K.; Johnson, V.E.; Tsai, C. Differential Phylogenetic Expansions in BAHD Acyltransferases across Five Angiosperm Taxa and Evidence of Divergent Expression among Populus Paralogues. *BMC Genomics* **2011**, *12*, 236.

50. St-Pierre, B.; Luca, V. De Evolution of Acyltransferase Genes: Origin and Diversification of the BAHD Superfamily of Acyltransferases Involved in Secondary Metabolism. *Recent Adv. Phytochem.* **2000**, *34*, 285–315, doi:10.1016/S0079-9920(00)80010-6.

51. Li, A.X.; Eannetta, N.; Ghangas, G.S.; Steffens, J.C. Glucose Polyester Biosynthesis. Purification and Characterization of a Glucose Acyltransferase. *Plant Physiol.* **1999**, *121*, 453–460, doi:10.1104/pp.121.2.453.

52. Walters, D.S.; Steffens, J.C. Branched Chain Amino Acid Metabolism in the Biosynthesis of *Lycopersicon pennellii* Glucose Esters. *Plant Physiol.* **1990**, *93*, 1544–1551, doi:10.1104/pp.93.4.1544.

53. Goffreda, J.C.; Mutschler, M.A.; Avé, D.A.; Tingey, W.M.; Steffens, J.C. Aphid Deterrence by Glucose Esters in Glandular Trichome Exudate of the Wild Tomato, *Lycopersicon pennellii*. *J. Chem. Ecol.* **1989**, *15*, 2135–2147, doi:10.1007/BF01207444.

54. Juvik, J.A.; Shapiro, J.A.; Young, T.E.; Mutschler, M.A. Acylglucoses from Wild Tomatoes Alter Behavior and Reduce Growth and Survival of *Helicoverpa zea* and *Spodoptera exigua* (Lepidoptera: Noctuidae). *J. Econ. Entomol.* **1994**, *87*, 482–492, doi:10.1093/jee/87.2.482.

55. Leckie, B.M.; D'Ambrosio, D.A.; Chappell, T.M.; Halitschke, R.; De Jong, D.M.; Kessler, A.; Kennedy, G.G.; Mutschler, M.A. Differential and Synergistic Functionality of Acylsugars in Suppressing Oviposition by Insect Herbivores. *PLoS One* **2016**, *11*, 1–19, doi:10.1371/journal.pone.0153345.

56. Chortyk, O.T.; Pomonis, J.G.; Johnson, A.W.; Carolina, S. Syntheses and

Characterizations of Insecticidal Sucrose Esters. *J. Agric. Food Chem.* **1996**, *44*, 1551–1557.

57. T Chortyk, O.; F Severson, R.; C Cultler, H.; A Sisson, V. Antibiotic Activities of Sugar Esters Isolated from Selected Nicotiana Species. *Biosci. Biotechnol. Biochem.* **1993**, *57*, 1355–1356.

58. Herrera-salgado, Y.; Va, L.; Rios, Y.; Alvarez, L. Myo -Inositol-Derived Glycolipids with Anti-Inflammatory Activity from *Solanum lanceolatum*. *J. Nat. Prod.* **2005**, *68*, 1031–1036, doi:https://doi.org/10.1021/np050054s.

59. Hill, K.; Rhode, O. Sugar-Based Surfactants for Consumer Products and Technical Applications. *Fett-Lipid* **1999**, *101*, 25–33, doi:10.1201/9781420051674.

60. Fanasca, S.; Colla, G.; Maiani, G.; Venneria, E.; Rouphael, Y.; Azzini, E.; Saccardo, F. Changes in Antioxidant Content of Tomato Fruits in Response to Cultivar and Nutrient Solution Composition. *J. Agric. Food Chem.* **2006**, *54*, 4319–4325.

61. Lall, R.; Thomas, G.; Singh, S.; Singh, A.; Wadhwa, G. Comparative Genome Analysis of *Solanum lycopersicum* and *Solanum tuberosum*. *Bioinformation* **2013**, *9*, 923–928, doi:10.6026 / 97320630009923.

62. Mcdowell, E.T.; Kapteyn, J.; Schmidt, A.; Li, C.; Kang, J.; Descour, A.; Shi, F.; Larson, M.; Schilmiller, A.; An, L.; et al. Comparative Functional Genomic Analysis of Solanum Glandular Trichome Types. *Plant Physiol.* **2011**, *155*, 524–539, doi:10.1104/pp.110.167114.

63. Bolger, A.; Scossa, F.; Bolger, M.E.; Lanz, C.; Maumus, F.; Tohge, T.; Quesneville, H.; Alseekh, S.; Sørensen, I.; Lichtenstein, G.; et al. The Genome of the Stress-Tolerant Wild Tomato Species *Solanum pennellii*. *Nat. Genet.* **2014**, *46*, 1034–1038, doi:10.1038/ng.3046.

64. Aflitos, S.; Schijlen, E.; De Jong, H.; De Ridder, D.; Smit, S.; Finkers, R.; Wang, J.; Zhang, G.; Li, N.; Mao, L.; et al. Exploring Genetic Variation in the Tomato

(*Solanum* Section l*ycopersicon*) Clade by Whole-Genome Sequencing; The 100 Tomato Genome Sequencing Consortium. *Plant J.* **2014**, *80*, 136–148, doi:10.1111/tpj.12616.

65. Chitwood, D.H.; Kumar, R.; Headland, L.R.; Ranjan, A.; Covington, M.F.; Ichihashi, Y.; Fulop, D.; Jiménez-Gómez, J.M.; Peng, J.; Maloof, J.N.; et al. A Quantitative Genetic Basis for Leaf Morphology in a Set of Precisely Defined Tomato Introgression Lines. *Plant Cell* **2013**, *25*, 2465–2481, doi:10.1105/tpc.113.112391.

66. Liu, Z.; Alseekh, S.; Brotman, Y.; Zheng, Y.; Fei, Z.; Tieman, D.M.; Giovannoni, J.J.; Fernie, A.R.; Klee, H.J. Identification of a *Solanum pennellii* Chromosome 4 Fruit Flavor and Nutritional Quality-Associated Metabolite QTL. *Front. Plant Sci.* **2016**, *7*, 1–15, doi:10.3389/fpls.2016.01671.

67. Channarayappa; Shivashankar, G.; Muniyappa, V.; Frist, R.H. Resistance of Lycopersicon Species to *Bemisia tabaci*, a Tomato Leaf Curl Virus Vector. *Can. J. Bot.* **1992**, *70*, 2193–2197.

68. Mirnezhad, M.; Romero-González, R.R.; Leiss, K.A.; Choi, Y.H.; Verpoorte, R.; Klinkhamera, P.G.L. Metabolomic Analysis of Host Plant Resistance to Thrips in Wild and Cultivated Tomatoes. *Phytochem. Anal.* **2010**, *21*, 110–117, doi:10.1002/pca.1182.

69. Vosman, B.; Kashaninia, A.; van't Westende, W.; Meijer-Dekens, F.; van Eekelen, H.; Visser, R.G.F.; de Vos, R.C.H.; Voorrips, R.E. QTL Mapping of Insect Resistance Components of *Solanum galapagense*. *Theor. Appl. Genet.* **2019**, *132*, 531–541, doi:10.1007/s00122-018-3239-7.

70. Fordyce, J.A.; Agrawalt, A.A. The Role of Plant Trichomes and Caterpillar Group Size on Growth and Defence of the Pipevine Swallowtail *Battus Philenor*. **2001**, *70*, 997–1005.

71. Simmons, A.T.; Gurr, G.M. Trichomes of Lycopersicon Species and Their Hybrids: Effects on Pests and Natural Enemies. *Agric. For. Entomol.* **2005**, *7*, 265–276, doi:10.1111/j.1461-9555.2005.00271.x.

72. Kennedy, G.G. Tomato, Pests, Parasitoids, and Predators: Tritrophic Interactions Involving the Genus Lycopersicon. *Annu. Rev. Entomol.* **2003**, *48*, 51–72, doi:10.1146/annurev.ento.48.091801.112733.

73. Johnson, H.B. Plant Pubescence: An Ecological Perspective. *Rev. Lit. Arts Am.* **1975**, *41*, 233–253.

74. Fernandez-Moreno, J.P.; Levy-Samoha, D.; Malitsky, S.; Monforte, A.J.; Orzaez, D.; Aharoni, A.; Granell, A. Uncovering Tomato Quantitative Trait Loci and Candidate Genes for Fruit Cuticular Lipid Composition Using the *Solanum pennellii* Introgression Line Population. *J. Exp. Bot.* **2017**, *68*, 2703–2716, doi:10.1093/jxb/erx134.

75. Pineda, B.; García-abellán, J.O.; Antón, T.; Pérez, F.; Moyano, E.; Sogo, B.G.; Campos, J.; Angosto, T.; Morales, B.; Capel, J.; et al. Tomato : Genomic Approaches for Salt and Drought Stress Tolerance. In Improve crop resistance to Abiotic stress; Tuteja, N., Gill, S.S., Tiburcia, A.F., Tuteja, R., Eds.; Wiley-VCH Verlag & Co. KGaA, 2012; pp. 1085–1120.

76. Sandbrink, J.M.; Van Ooijen, J.W.; Purimahua, C.C.; Vrielink, M.; Verkerk, R.; Zabel, P.; Lindhout, P. Localization of Genes for Bacterial Canker Resistance in *Lycopersicon peruvianum* Using *RFLPs*; Springer-Verlag, 1995;

77. Gur, A.; Semel, Y.; Osorio, S.; Friedmann, M.; Seekh, S.; Ghareeb, B.; Ayed, M.; Pleban, T.; Gera, G.; Fernie, A.R.; et al. Yield Quantitative Trait Loci from Wild Tomato Are Predominately Expressed by the Shoot. *Theor Appl Genet* **2011**, *122*, 405–420, doi:10.1007/s00122-010-1456-9.

78. Yamada, K.; Fujita, H.; Kunishima, M. A Novel Acid-Catalyzed *O*-Benzylating Reagent with the Smallest Unit of Imidate Structure. *Org. Lett.* **2012**, *14*, 5026–5029, doi:10.1021/ol302222p.

79. Finan, P.A.; Cassidy, J.N.; Reidy, J.P. Benzylation Studies on Sucrose. *Proc. R. Ir. Acad. B.* **1989**, *89B*, 157–166.

80. Kazushige Sogawa, and M.D.P. Benzylation of Carbohydrate Derivatives in

Dimethyl Sulfoxide. *Chem. Pharm. Bull.* **1967**, *15*, 1803–1806.

81. Corona-Castañeda, B.; Chérigo, L.; Fragoso-Serrano, M.; Gibbons, S.; Pereda-Miranda, R. Modulators of Antibiotic Activity from *Ipomoea murucoides*. *Phytochemistry* **2013**, *95*, 277–283, doi:10.1016/j.phytochem.2013.07.007.

82. Rosas-Ramírez, D.; Escalante-Sánchez, E.; Pereda-Miranda, R. Batatins III-VI, Glycolipid Ester-Type Dimers from *Ipomoea batatas*. *Phytochemistry* **2011**, *72*, 773–780, doi:10.1016/j.phytochem.2011.03.002.

83. Nicolaou, K.C.; Snyder, S.A. The Essence of Total Synthesis. *Proc. Natl. Acad. Sci.* **2004**, *101*, 11929–11936, doi:10.1073/pnas.0403799101.

84. Liu, J.; Liu, X.; Wu, J.; Li, C. Total Synthesis of Natural Products Containing a Bridgehead Double Bond. *Chem* **2020**, *6*, 579–615, doi:10.1016/j.chempr.2019.12.027.

85. Masimbula, R.; Yamada, A.; Takahashi, K.; Matsuura, H. Total Synthesis of (8*S*) and (8*R*) Methyl 8-*β*- D -Glucopyranosyl-Helianthenate B and Their Application for Other Derivatives. *Nat. Prod. Commun.* **2019**, doi:10.1177/1934578X19861013.

86. Nicolaou, K.C.; Hale, C.R.H.; Nilewski, C.; Ioannidou, H.A. Constructing Molecular Complexity and Diversity : Total Synthesis of Natural Products of Biological and Medicinal Importance. *Chem. Soc. Rev.* **2012**, *41*, 5017–5364, doi:10.1039/c2cs35116a.

87. Iwasaki, A.; Ohtomo, K.; Kurisawa, N.; Shiota, I.; Rahmawati, Y.; Jeelani, G.; Nozaki, T.; Suenaga, K. Isolation, Structure Determination, and Total Synthesis of Hoshinoamide C, an Antiparasitic Lipopeptide from the Marine Cyanobacterium *Caldora penicillata*. *J. Nat. Prod.* **2021**, *84*, 126–135, doi:10.1021/acs.jnatprod.0c01209.

88. Nicolaou, K.C.; Vourloumis, D.; Winssinger, N.; Baran, P.S. The Art and Science of Total Synthesis. *Angew. Chemie Int. Ed. English* **2000**, *39*, 44–122.

89. Fleming, A. On the Antibacterial Action of Cultures of a Penicillium , with Special Reference to Their Use in the Isolation of *B. influenzae*. *Br. J. Exp. Pathol.* **1929**, *10*, 226–236.

90. Sussman, G.L.; Davis, K.; Kohler, P.F. Penicillin Allergy : A Practical Approach to Management. *Can. Med. Assoc. J.* **1986**, *134*, 1353–1356.

91. Corey, E.J. The Logic of Chemical Synthesis : Multistep Synthesis of Complex Carbogenic Molecules. *Nobel Lect.* **1990**, 686–708.

92. Lao, Z.; Toy, P.H. Catalytic Wittig and Aza-Wittig Reactions. *Beilstein J. Org. Chem.* **2016**, 2577–2587, doi:10.3762/bjoc.12.253.

93. Wiley, V.J.T.; Chichester Palladium Reagents and Catalysts Innovations in Organic Synthesis. *Angew. Chemie Int. Ed. English* **1995**, *108*, 2291.

94. Schelhaas, M.; Waldmann, H. Protecting Group Strategies in Organic Synthesis. *Angew. Chemie Int. Ed. English* **1996**, *35*, 2056–2083.

95. Degenstein, J.C.; Murria, P.; Easton, M.; Sheng, H.; Hurt, M.; Dow, A.R.; Gao, J.; Nash, J.J.; Agrawal, R.; Delgass, W.N.; et al. Fast Pyrolysis of 13c-Labeled Cellobioses: Gaining Insights into the Mechanisms of Fast Pyrolysis of Carbohydrates. *J. Org. Chem.* **2015**, *80*, 1909–1914, doi:10.1021/jo5025255.

96. Peterson, J.K.; Harrison, H.F.; Chortyk, O.T. Effects of Various Synthetic Sucrose Esters on Weed Seed Germination and Crop Growth: Structure-Activity and Dose-Response Relationships. *J. Agric. Food Chem.* **1997**, *45*, 4833–4837, doi:10.1021/jf9703157.

97. Egea, I.; Albaladejo, I.; Meco, V.; Morales, B.; Sevilla, A.; Bolarin, M.C.; Flores, F.B. The Drought-Tolerant *Solanum pennellii* Regulates Leaf Water Loss and Induces Genes Involved in Amino Acid and Ethylene/Jasmonate Metabolism under Dehydration. *Sci. Rep.* **2018**, *8*, 1–14, doi:10.1038/s41598-018-21187-2.

98. Ziaf, K.; Loukehaich, R.; Gong, P.; Liu, H.; Han, Q.; Wang, T.; Li, H.; Ye, Z. A Multiple Stress-Responsive Gene ERD15 from *Solanum pennellii* Confers Stress

Tolerance in Tobacco. *Plant Cell Physiol.* **2011**, *52*, 1055–1067, doi:10.1093/pcp/pcr057.

99. Agrawal, A.A.; Conner, J.K.; Johnson, M.T.J.; Wallsgrove, R. Ecological Genetics of an Induced Plant Defense against Herbivores: Additive Genetic Variance and Costs of Phenotypic Plasticity. *Evolution (N. Y).* **2002**, *56*, 2206–2213.

100. Creelman, R.A.; Mullet, J.E. Biosynthesis and Action of Jasmmonates in Plants. *Annu. Rev. Plant Physiol. Plant Mol. Biol.* **1997**, *48*, 355–381.

101. Wasternack, C.; Hause, B. Jasmonates: Biosynthesis, Perception, Signal Transduction and Action in Plant Stress Response, Growth and Development. An Update to the 2007 Review in Annals of Botany. *Ann. Bot.* 2013.

102. Han, G.Z. Evolution of Jasmonate Biosynthesis and Signalling Mechanisms. *J. Exp. Bot.* **2017**, *68*, 1323–1331, doi:10.1093/jxb/erw470.

103. Tian, D.; Tooker, J.; Peiffer, M.; Chung, S.H.; Felton, G.W. Role of Trichomes in Defense against Herbivores: Comparison of Herbivore Response to Woolly and Hairless Trichome Mutants in Tomato (*Solanum lycopersicum*). *Planta* **2012**, *236*, 1053–1066, doi:10.1007/s00425-012-1651-9.

104. Boughton, A.J.; Hoover, K.; Felton, G.W. Rapid Communication of Methyl Jasmonate Application Induces Increased Densities of Glandular Trichomes on Tomato, *Lycopersicon esculentum*. *J. Chem. Ecol.* **2005**, *31*, doi:10.1007/s10886-005-6228-7.

105. Maruri-López, I.; Aviles-Baltazar, N.Y.; Buchala, A.; Serrano, M. Intra and Extracellular Journey of the Phytohormone Salicylic Acid. *Front. Plant Sci.* **2019**, *10*, 1–11, doi:10.3389/fpls.2019.00423.

106. Lee, H.; Leon, J.; Raskin, I. Biosynthesis and Metabolism of Salicylic Acid. *Proc. Natl. Acad. Sci.* **1995**, *92*, 493–496.

107. Dempsey, D.A.; Vlot, A.C.; Wildermuth, M.C.; Klessig, D.F. Salicylic Acid

Biosynthesis and Metabolism. *Arab. B.* **2011**, *9*, 2–24, doi:10.1199/tab.0156.

108. Masimbula, R.; Oki, K.; Takahashi, K.; Matsuura, H. Metabolism of Airborne Methyl Salicylate in Adjacent Plants. *Biosci. Biotechnol. Biochem.* **2020**, *00*, 1–8, doi:10.1080/09168451.2020.1769465.

109. Masimbula, R.; Kobayashi, H.; Nakashima, T.; Nambu, Y.; Kitaoka, N. Pennelliiside D , a New Acyl Glucose from *Solanum pennellii* and Chemical Synthesis of Pennelliisides. *Molecules* **2022**, *27*, 3728.

APPENDIX I: FD-MASS DATA

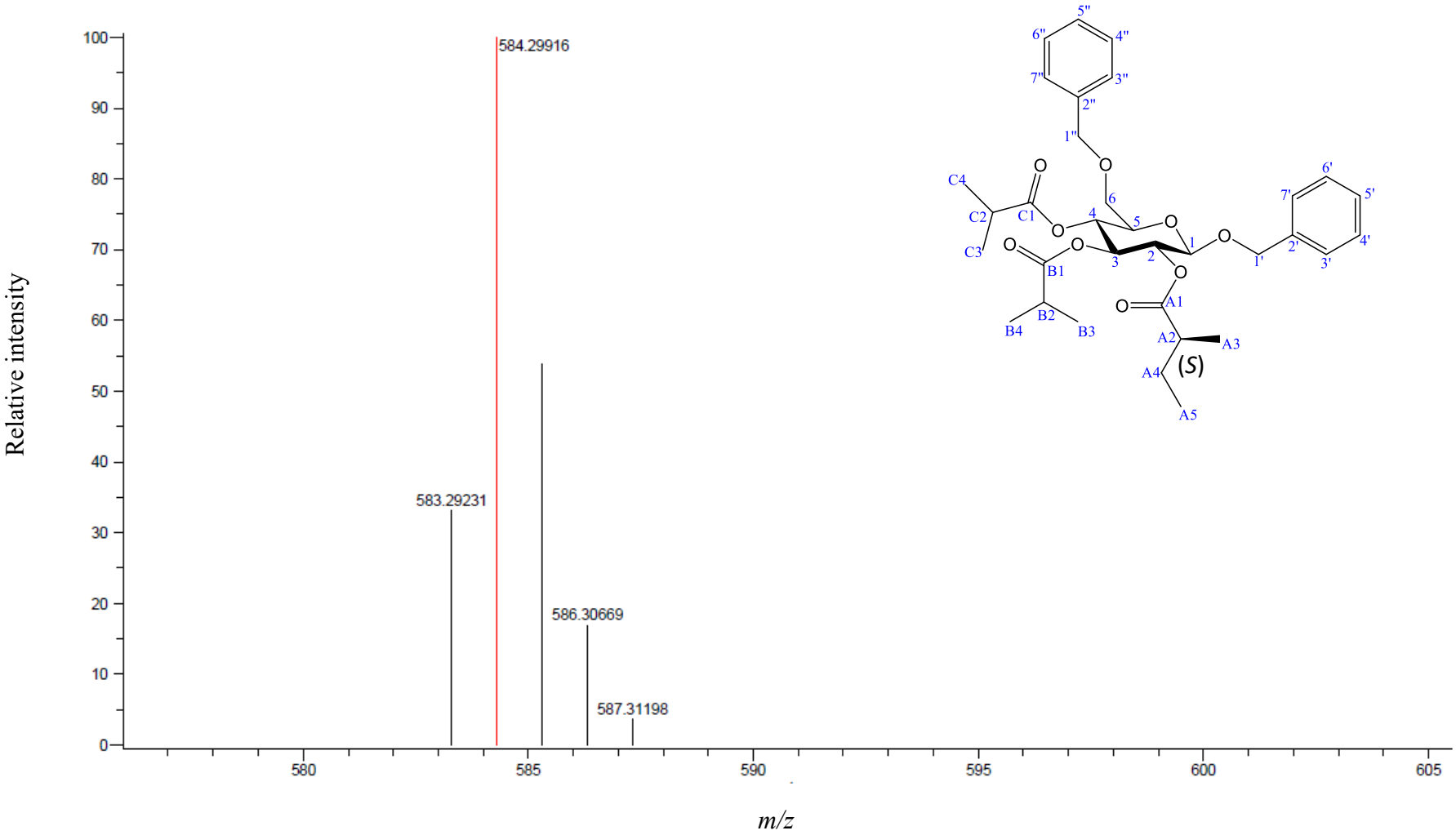

Figure S1: HRFD-MS spectrum of natural dibenzyl pennelliiside D (**2**).

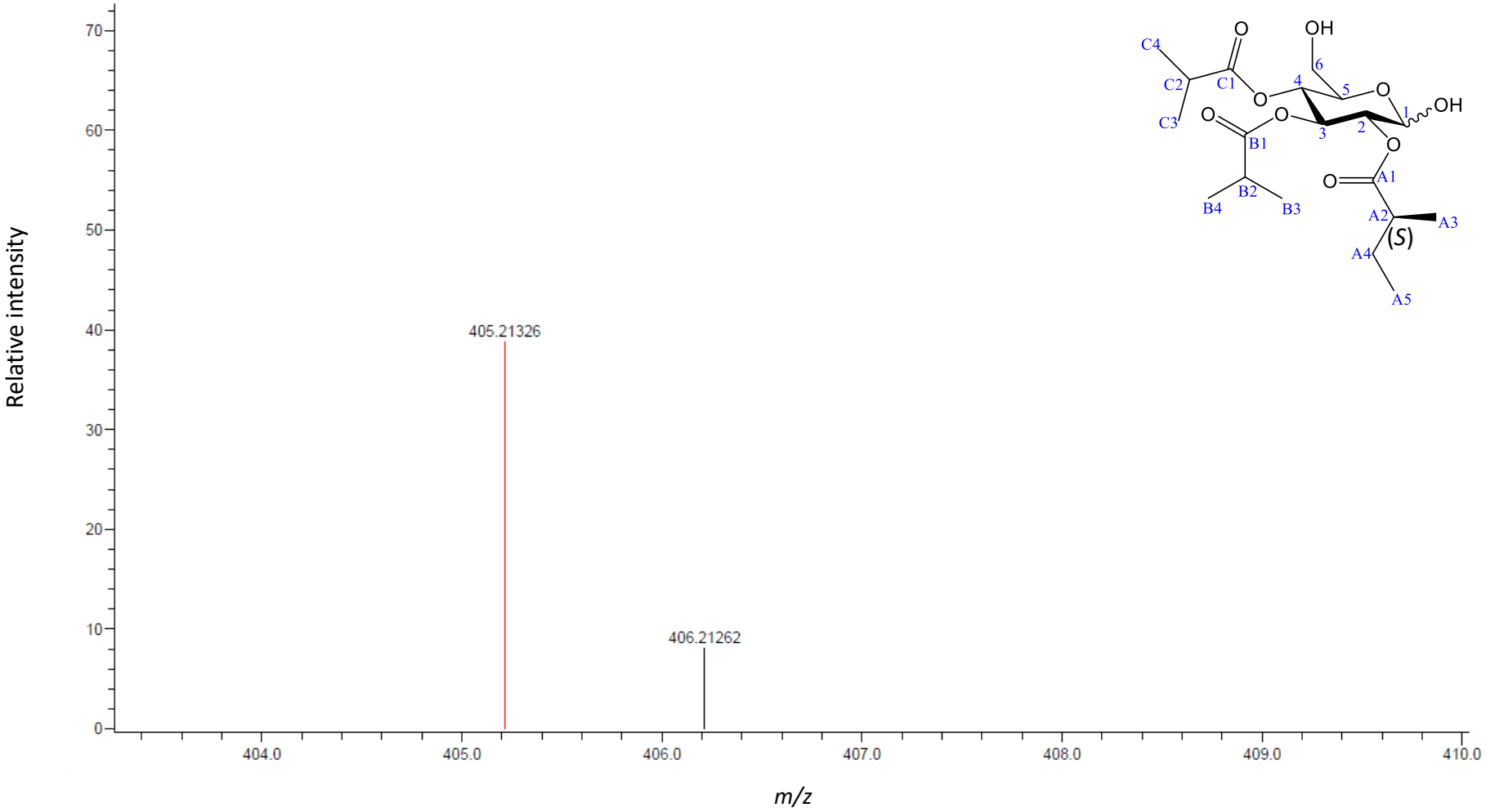

Figure S2: HRFD-MS spectrum of natural pennelliiside D (**1**).

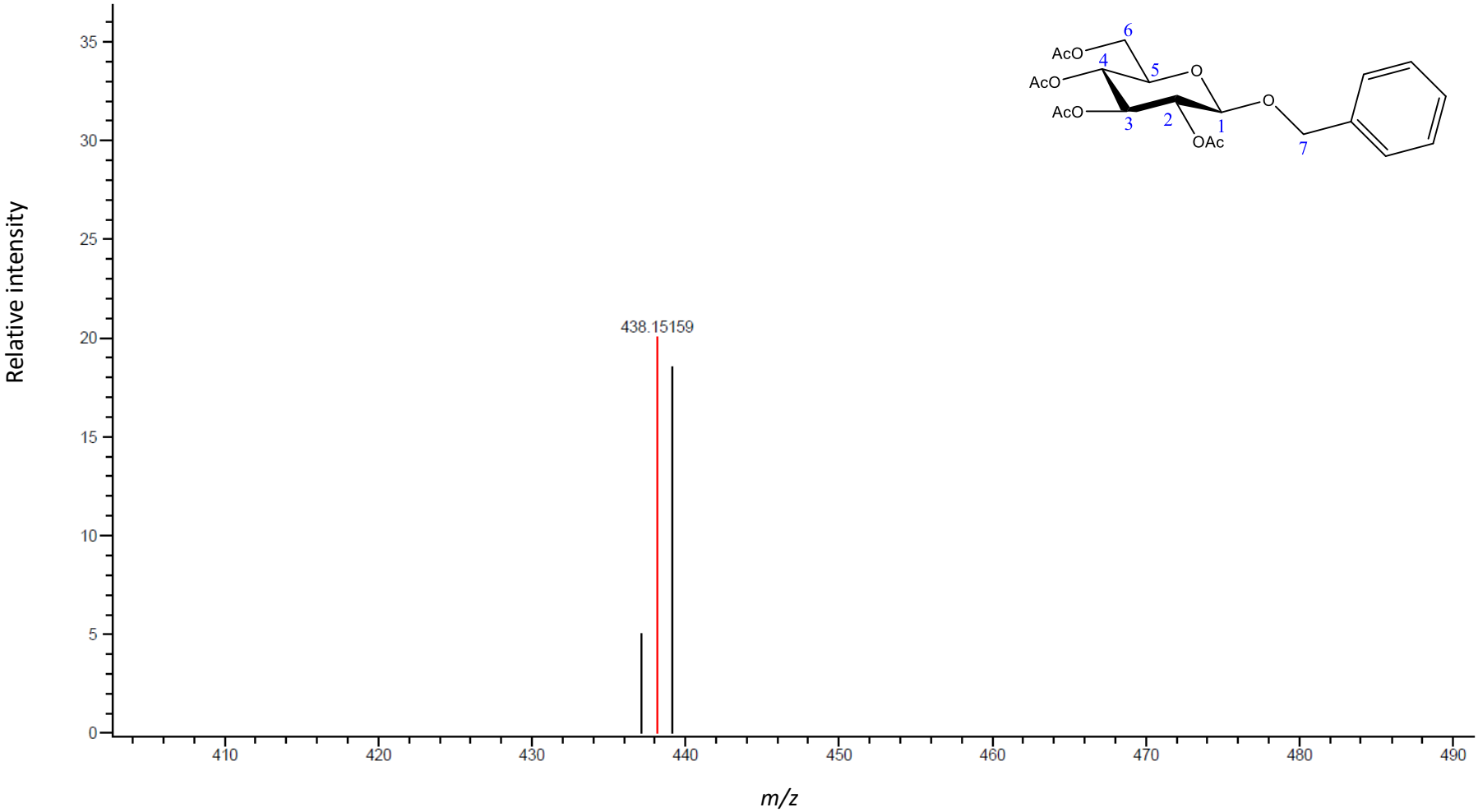

Figure S3: HRFD-MS spectrum of **4**.

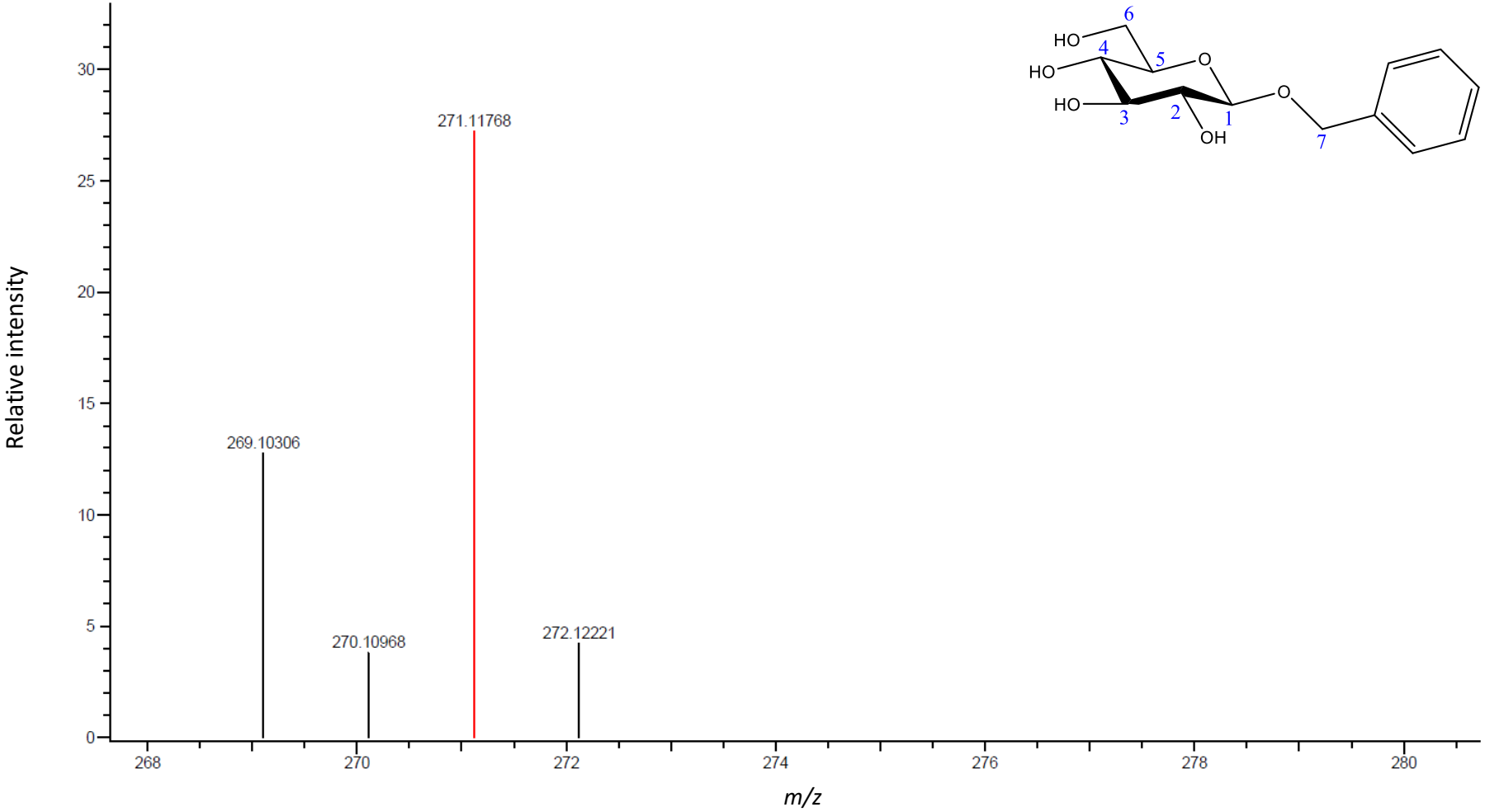

Figure S4: HRFD-MS spectrum of compound **5**.

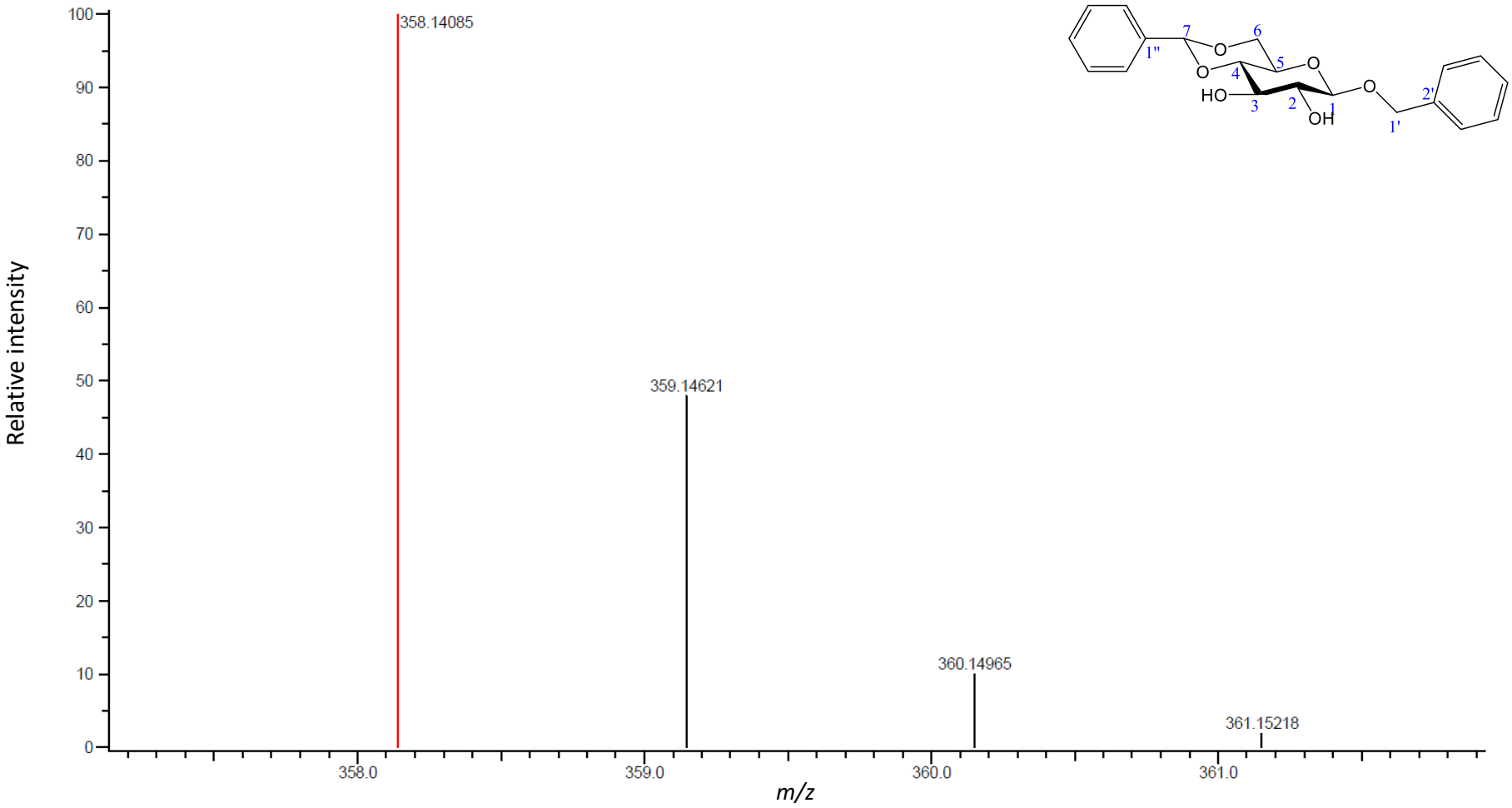

Figure S5: HRFD-MS spectrum of compound **6**.

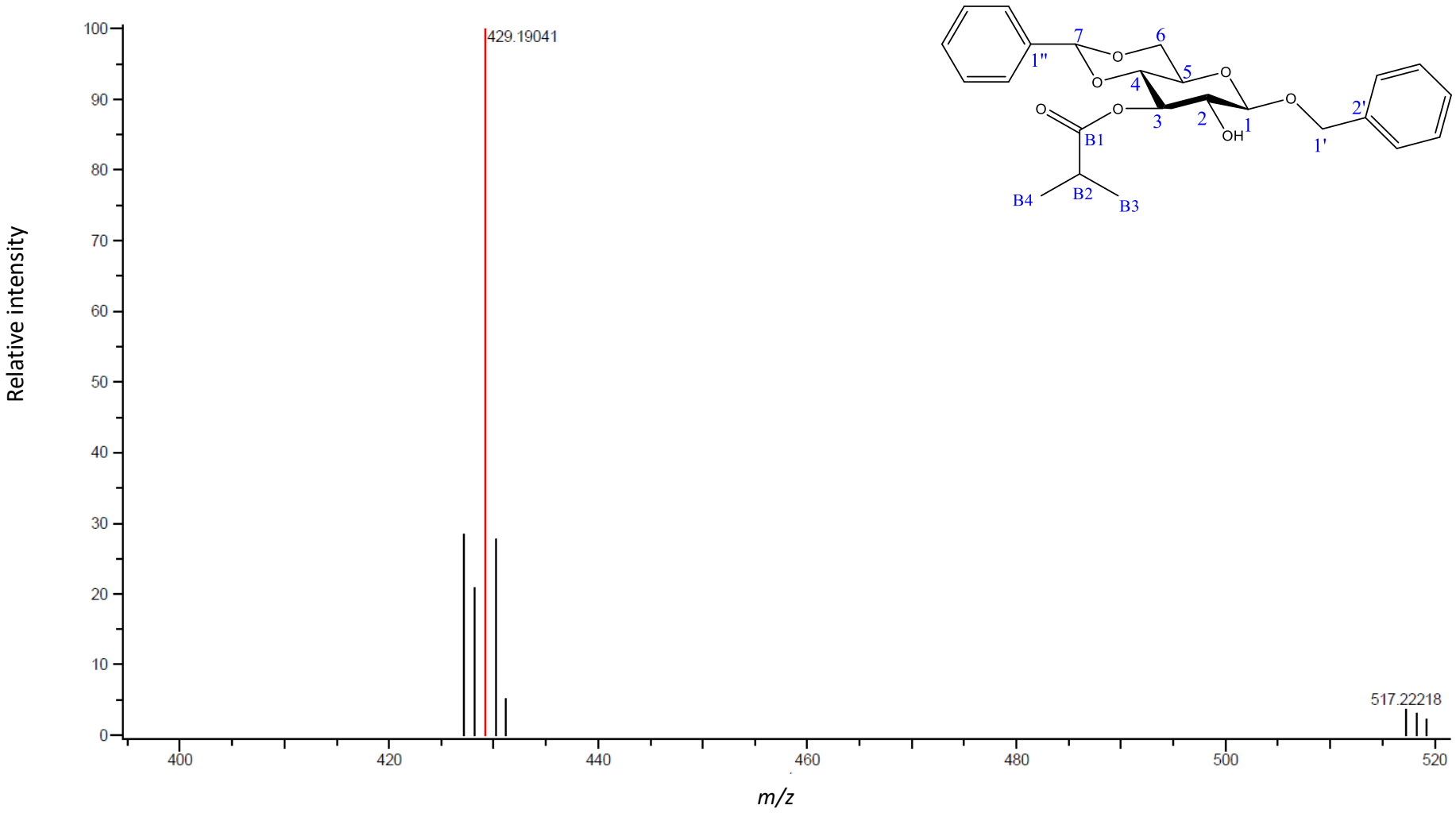

Figure S6: HRFD-MS spectrum of compound **7**.

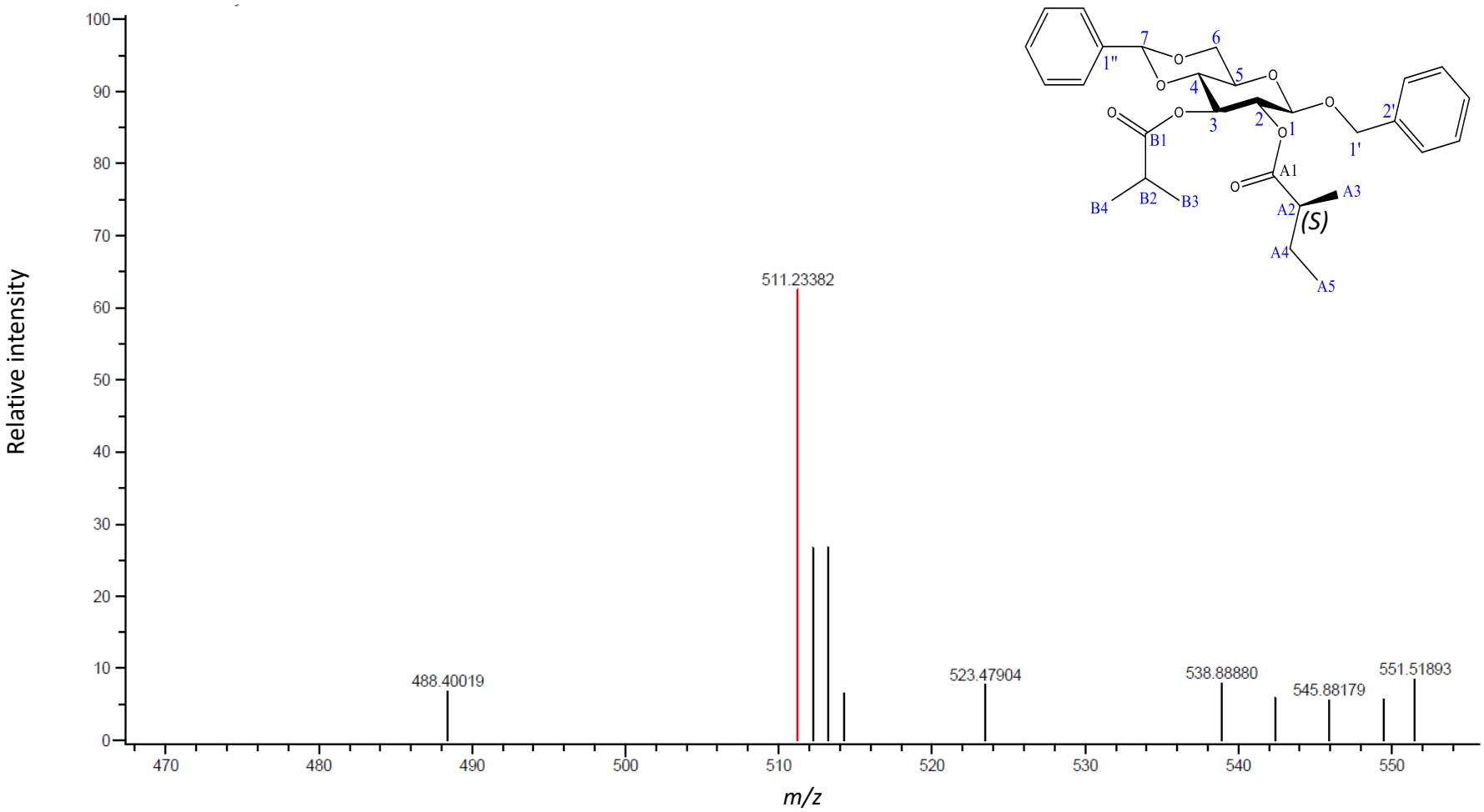

Figure S7: HRFD-MS spectrum of compound **8(*S*)**.

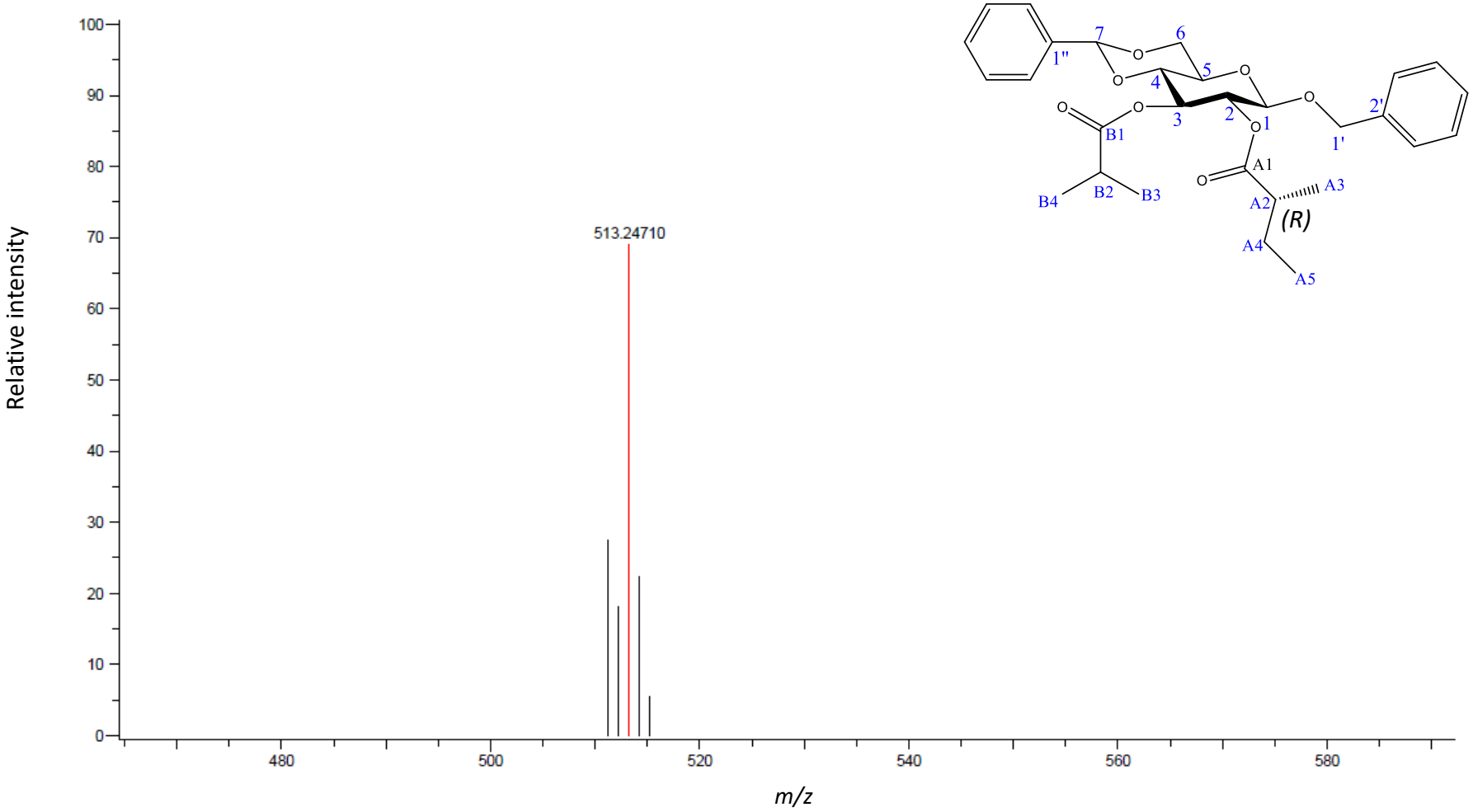

Figure S8: HRFD-MS spectrum of compound **8(*R*)**.

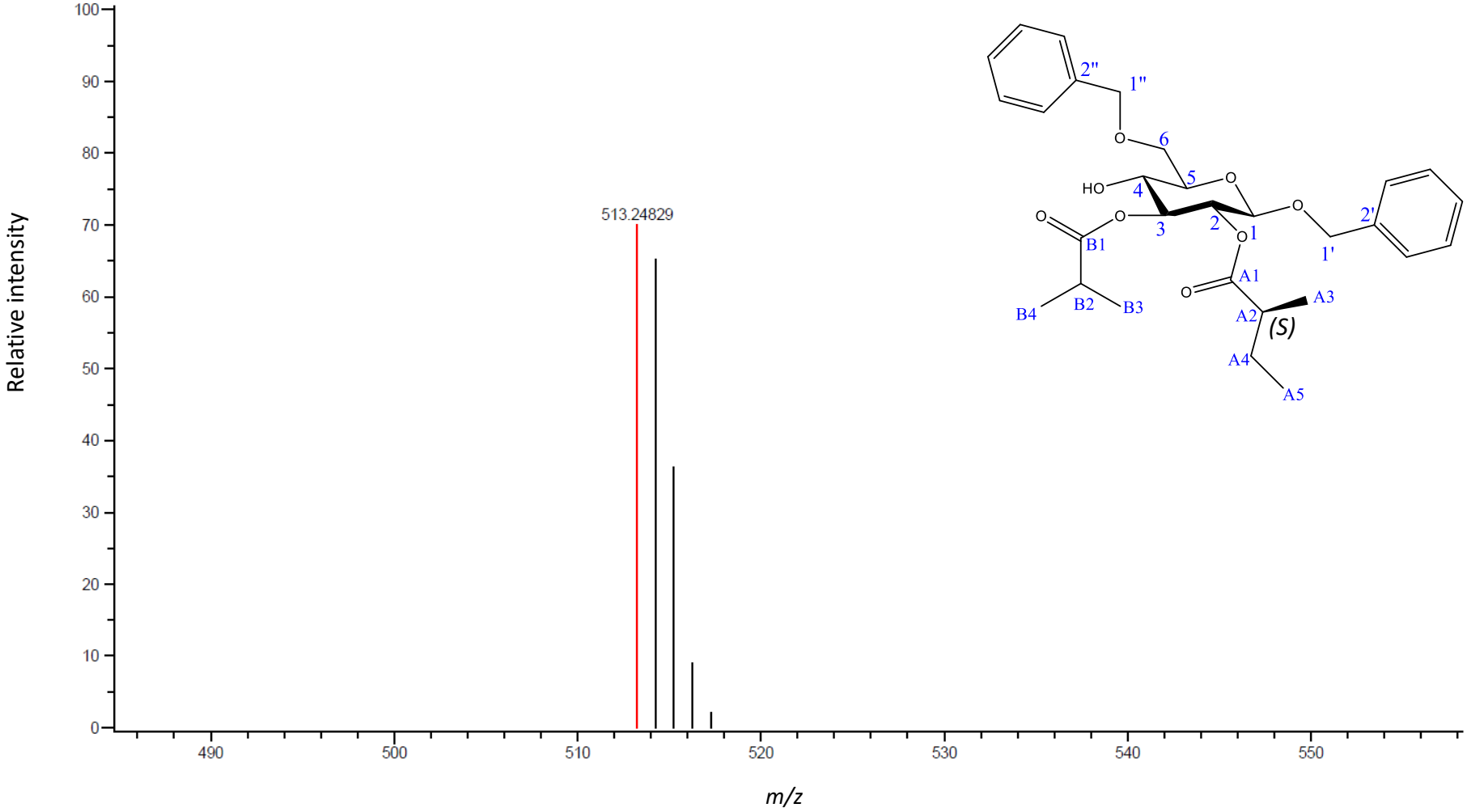

Figure S9: HRFD-MS spectrum of compound **9(*S*)**.

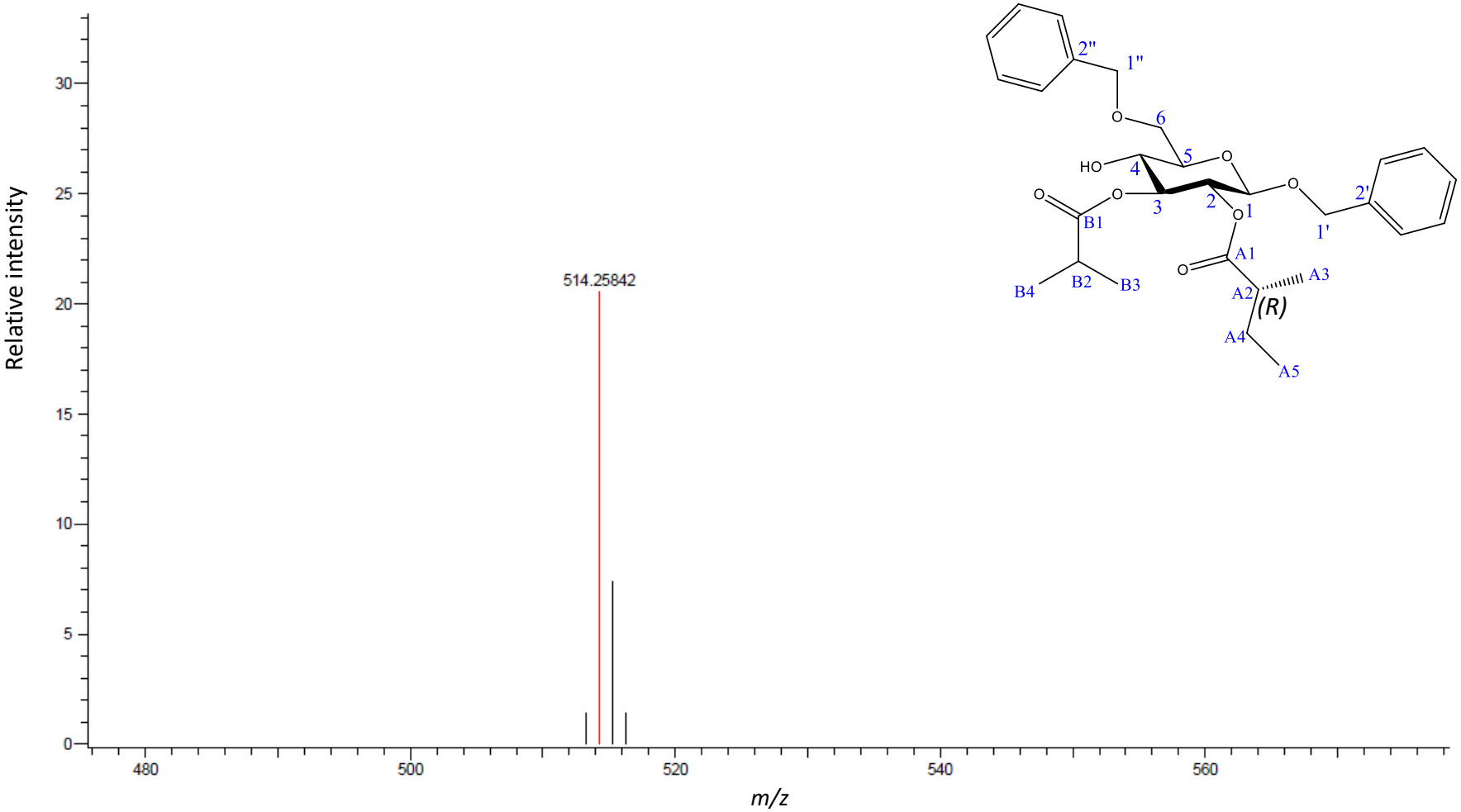

Figure S10: HRFD-MS spectrum of compound ***9(R)***.

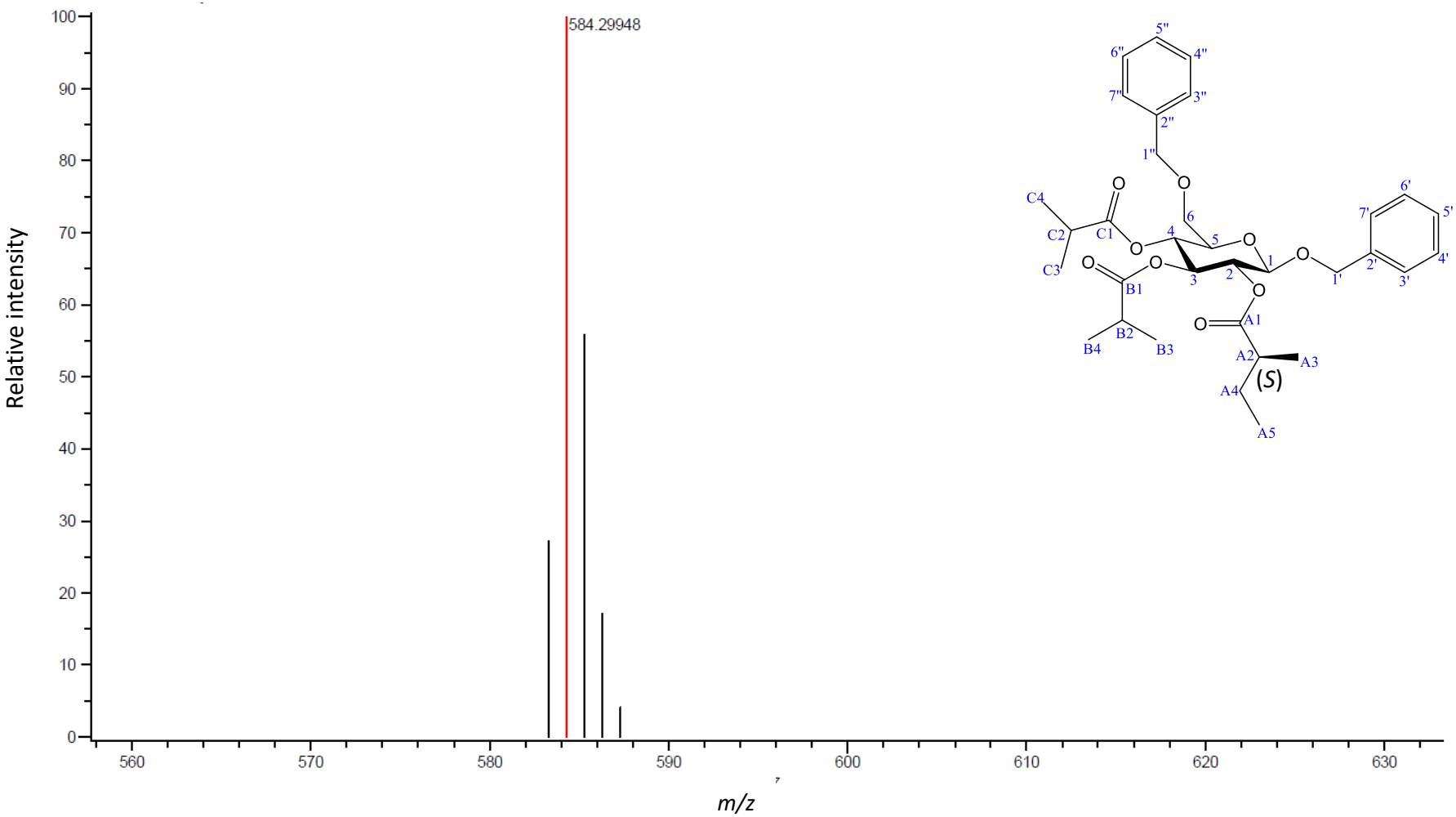

Figure S11: HRFD-MS spectrum of synthesized dibenzyl pennelliiside D [**2(*S*)**].

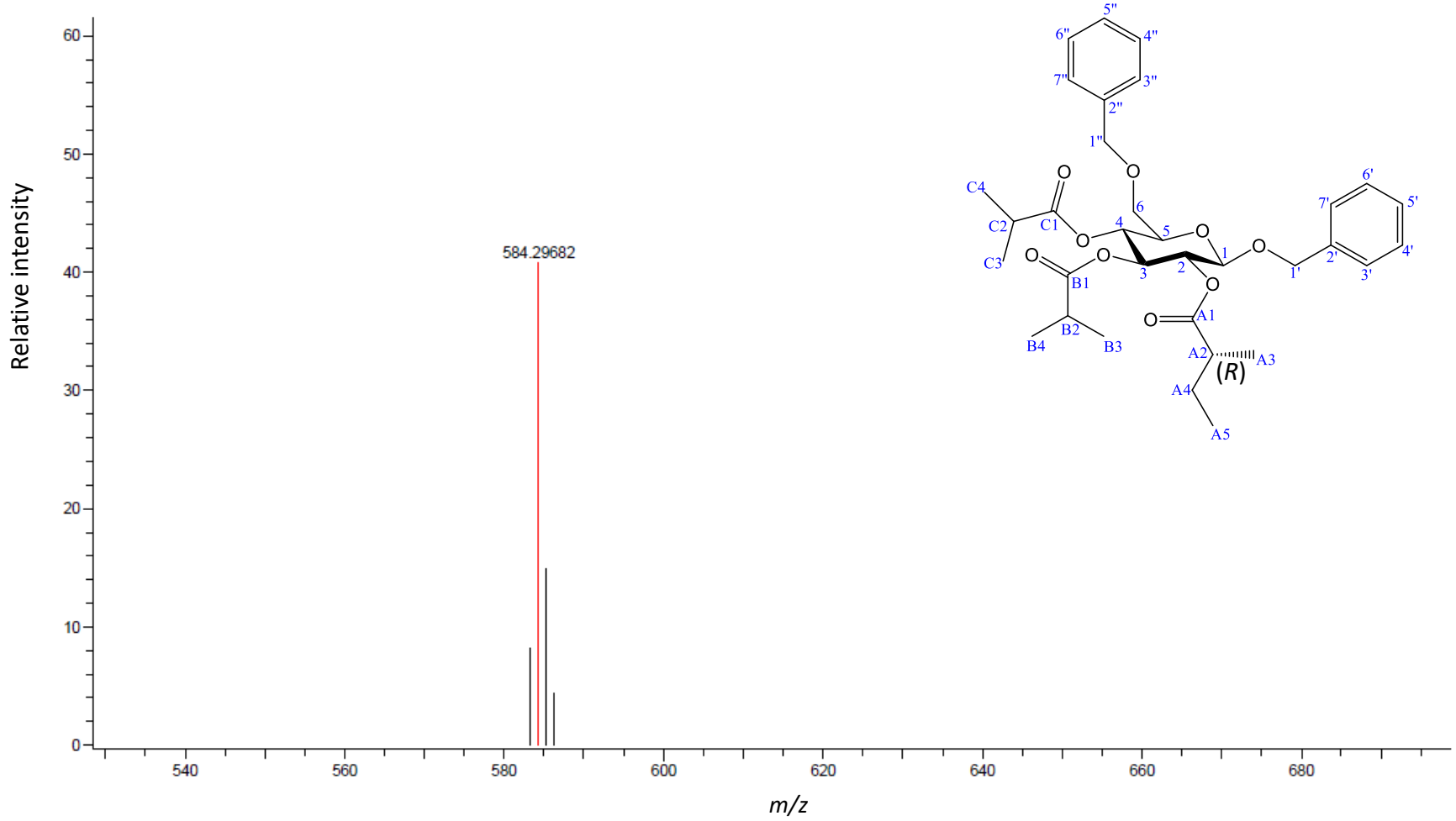

Figure S12: HRFD-MS spectrum of compound **2(*R*)**.

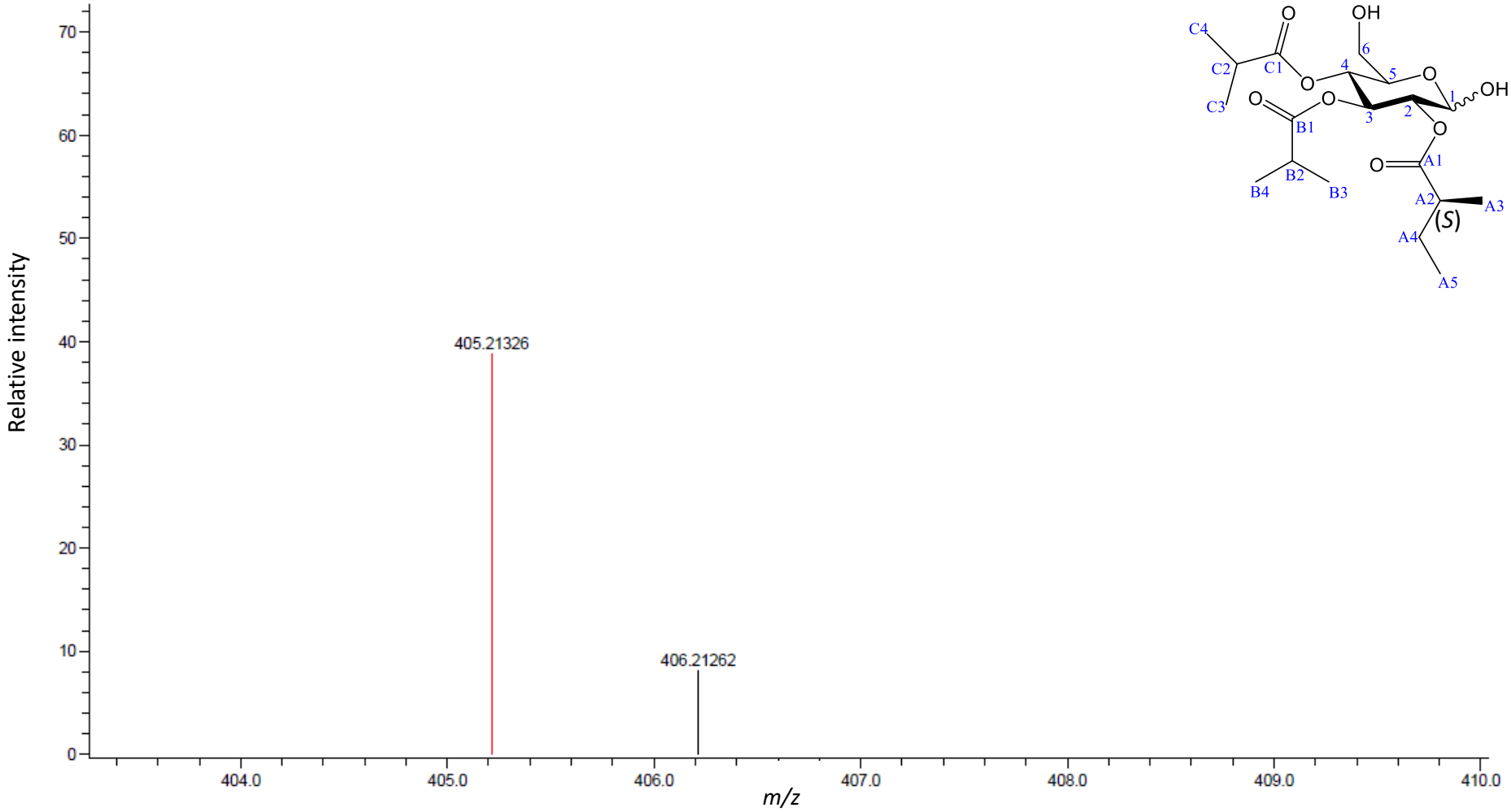

Figure S13: HRFD-MS spectrum of synthesized pennelliiside D (**1**).

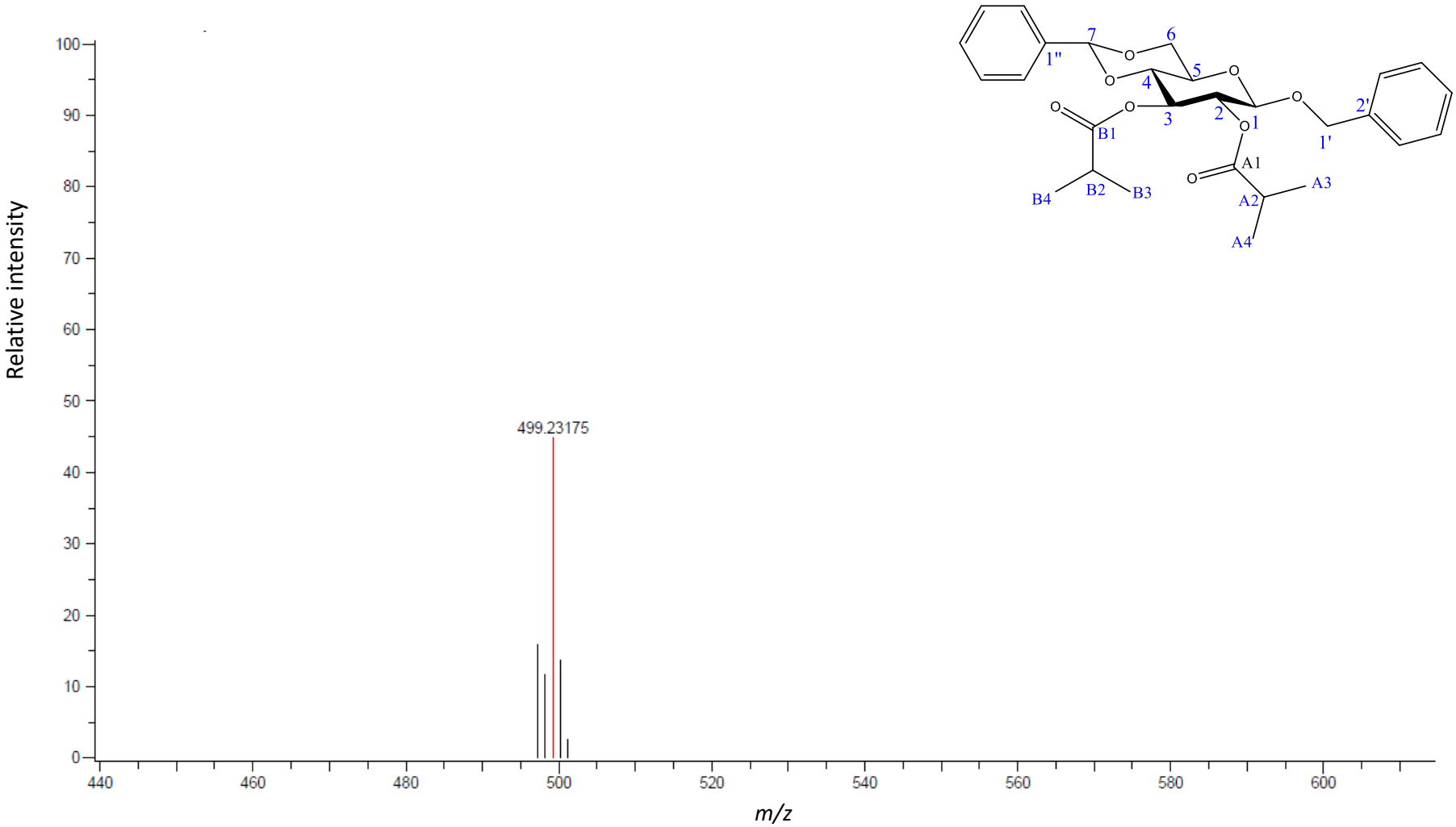

Figure S14. HRFD-MS spectrum of compound **10**.

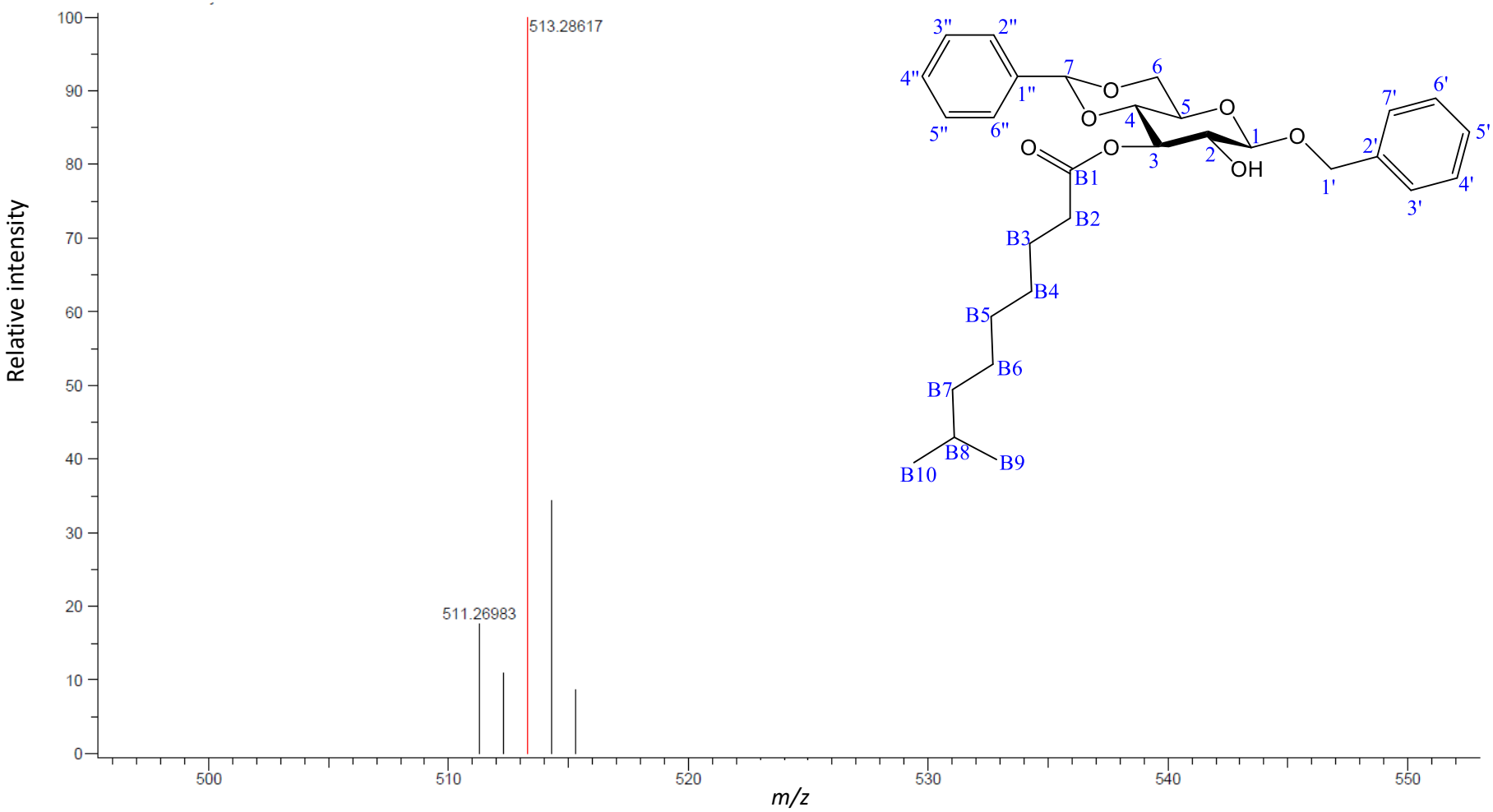

Figure S15. HRFD-MS spectrum of compound **11**.

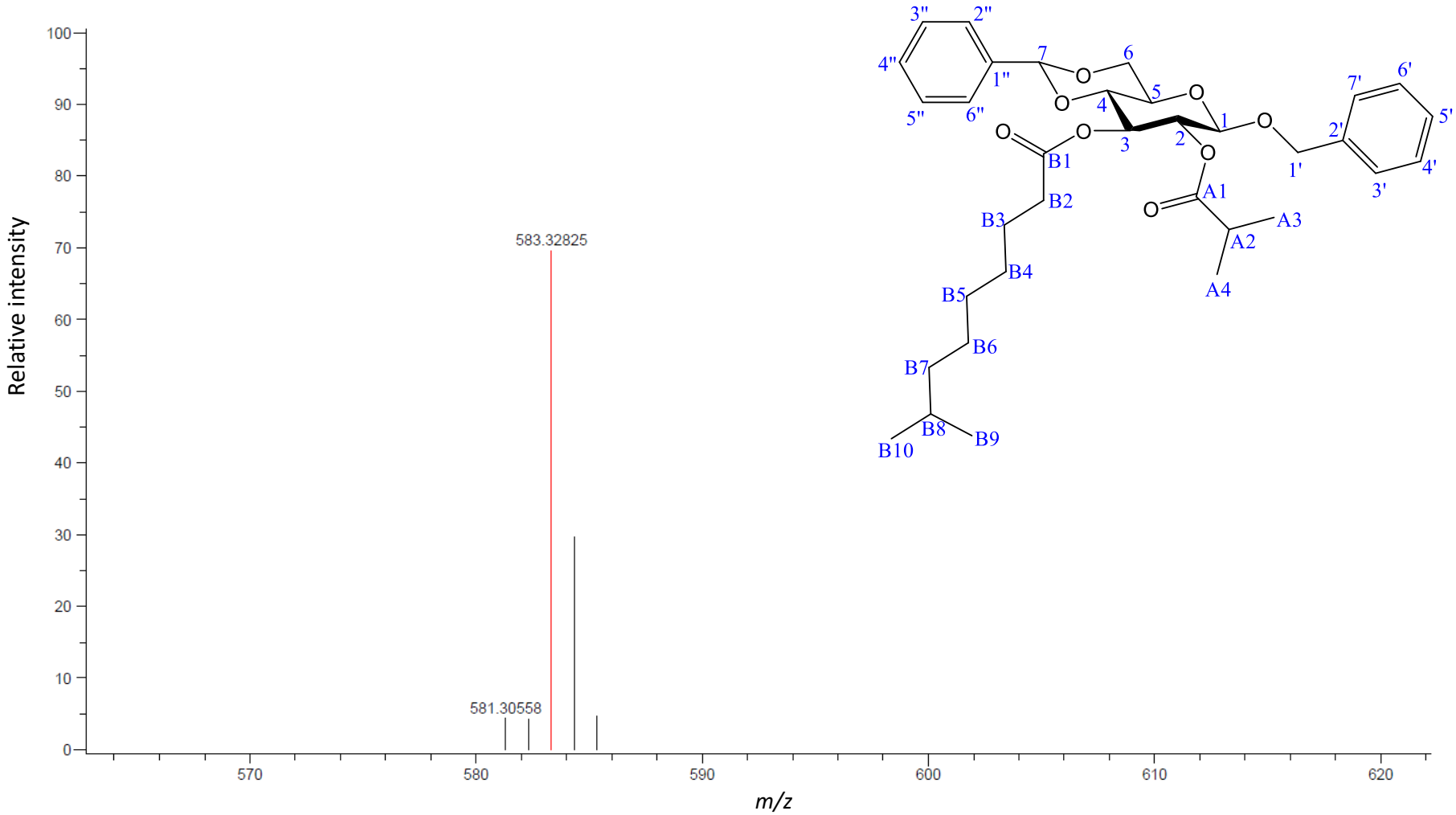

Figure S16. HRFD-MS spectrum of compound **12**.

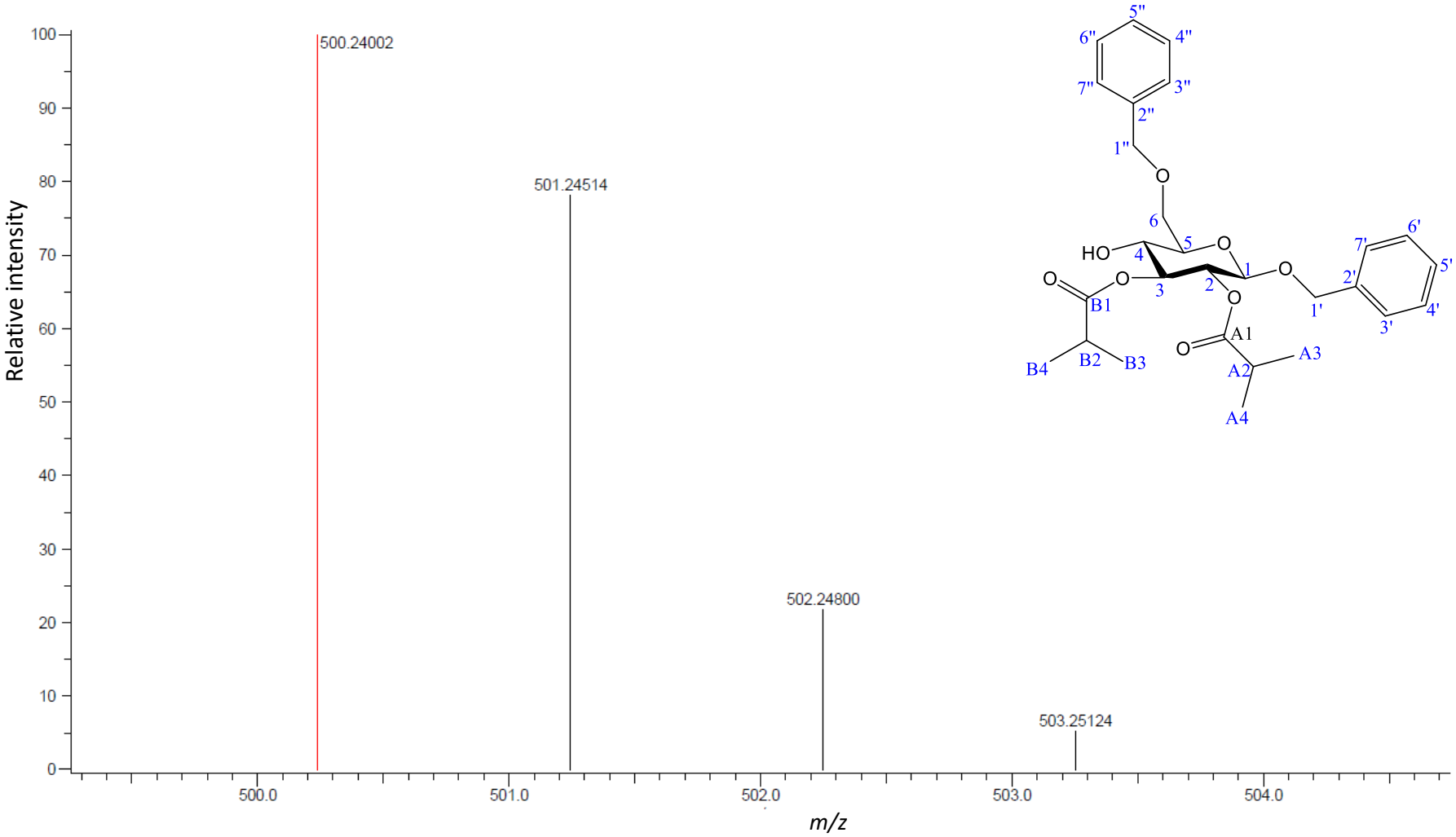

Figure S17. HRFD-MS spectrum of compound **13a**.

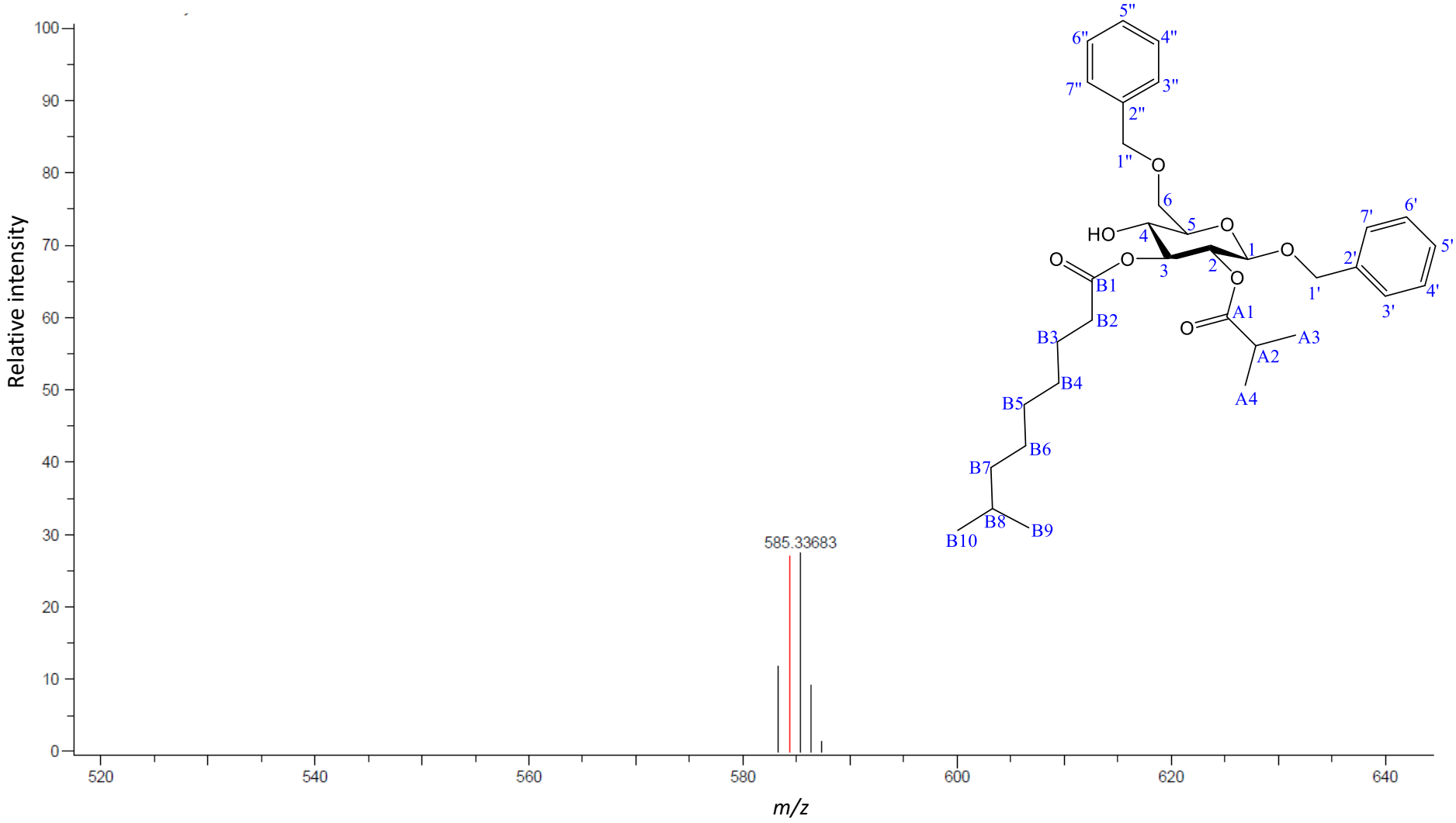

Figure S18. HRFD-MS spectrum of compound **13b**.

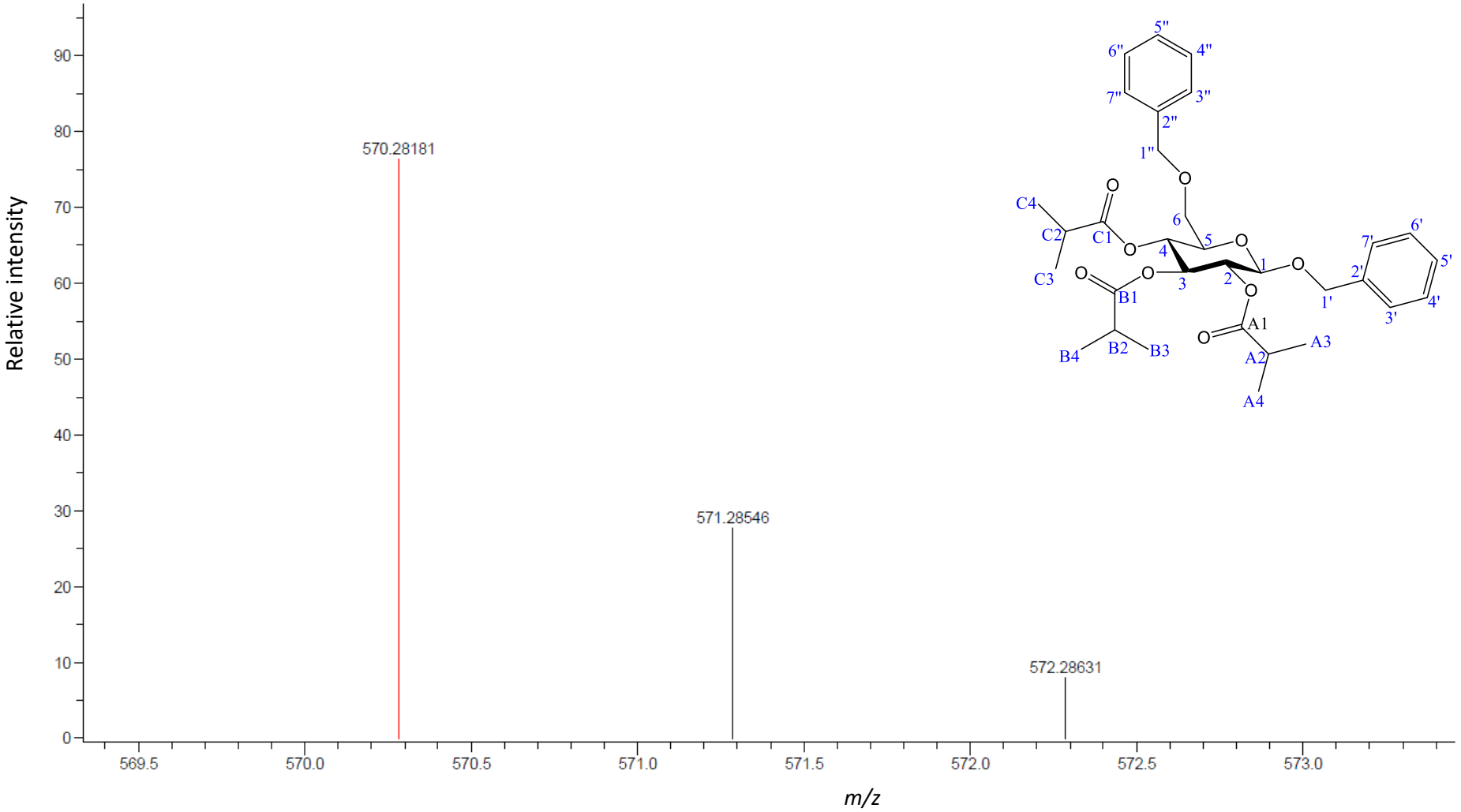

Figure S19. HRFD-MS spectrum of compound **14a**.

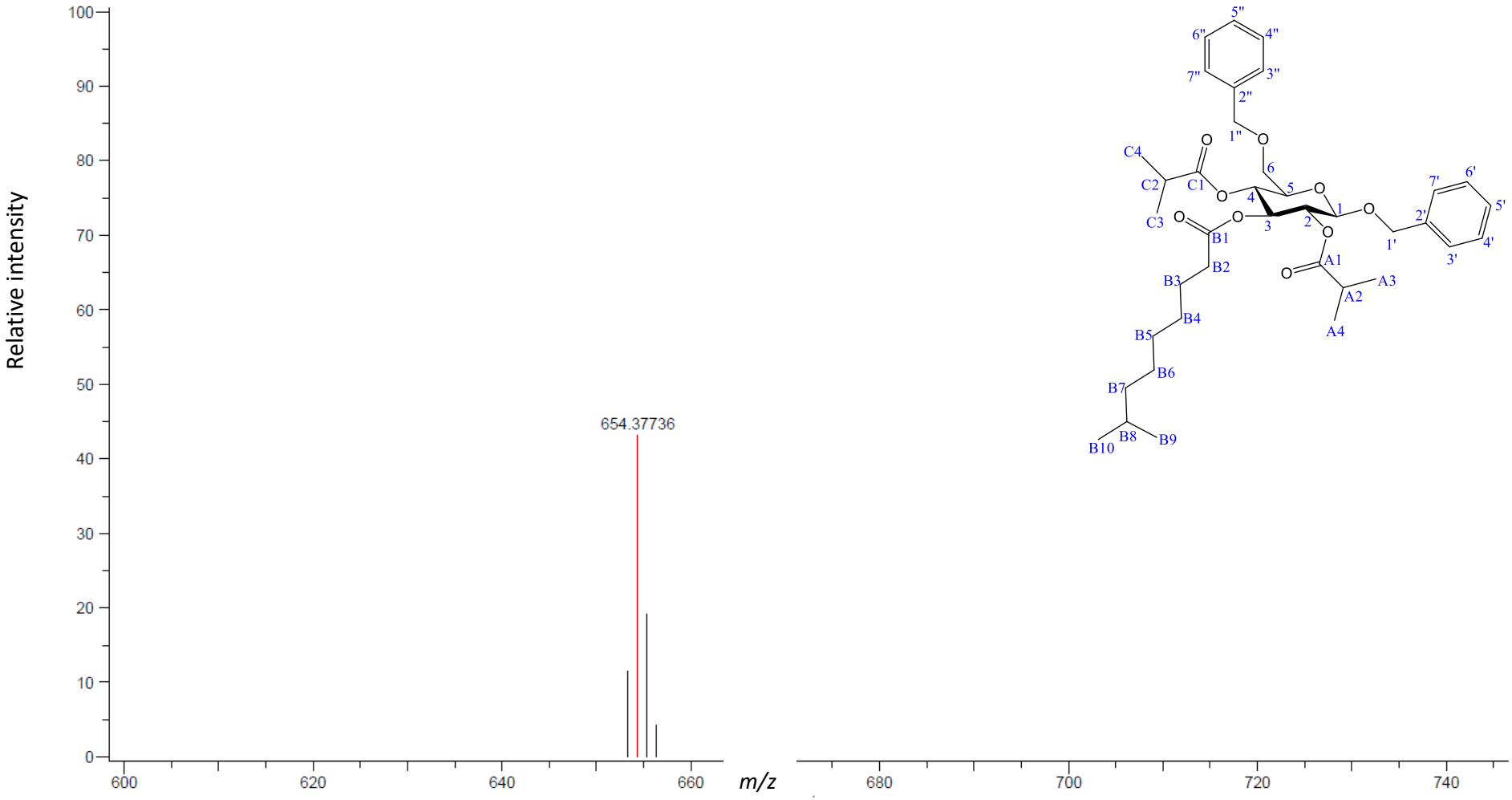

Figure S20. HRFD-MS spectrum of compound **14b**.

APPENDIX II: NMR SPECTRA

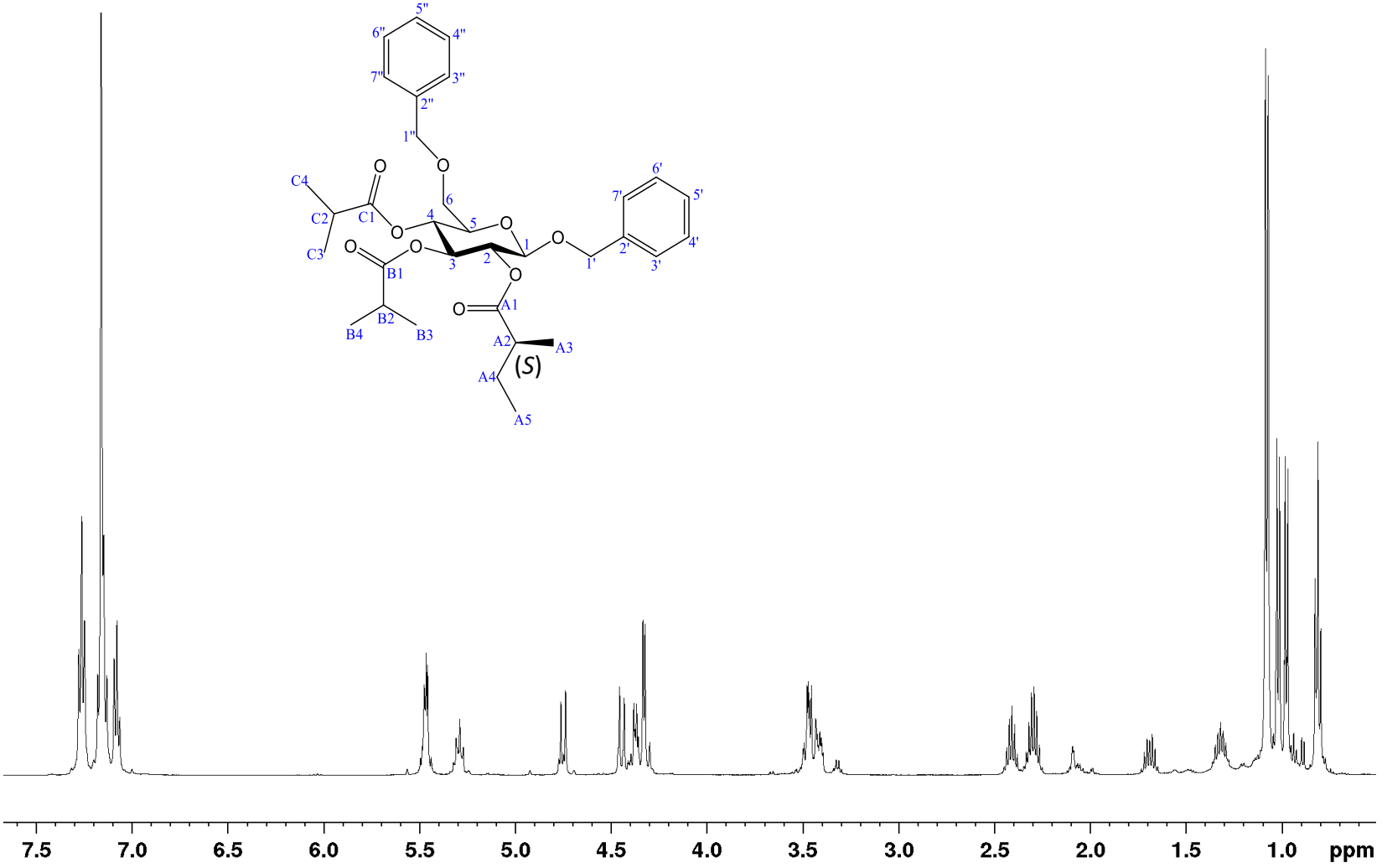

Figure S21: ^{1}H NMR spectrum of natural dibenzyl pennelliiside D (**2**) (500 MHz, C_6D_6).

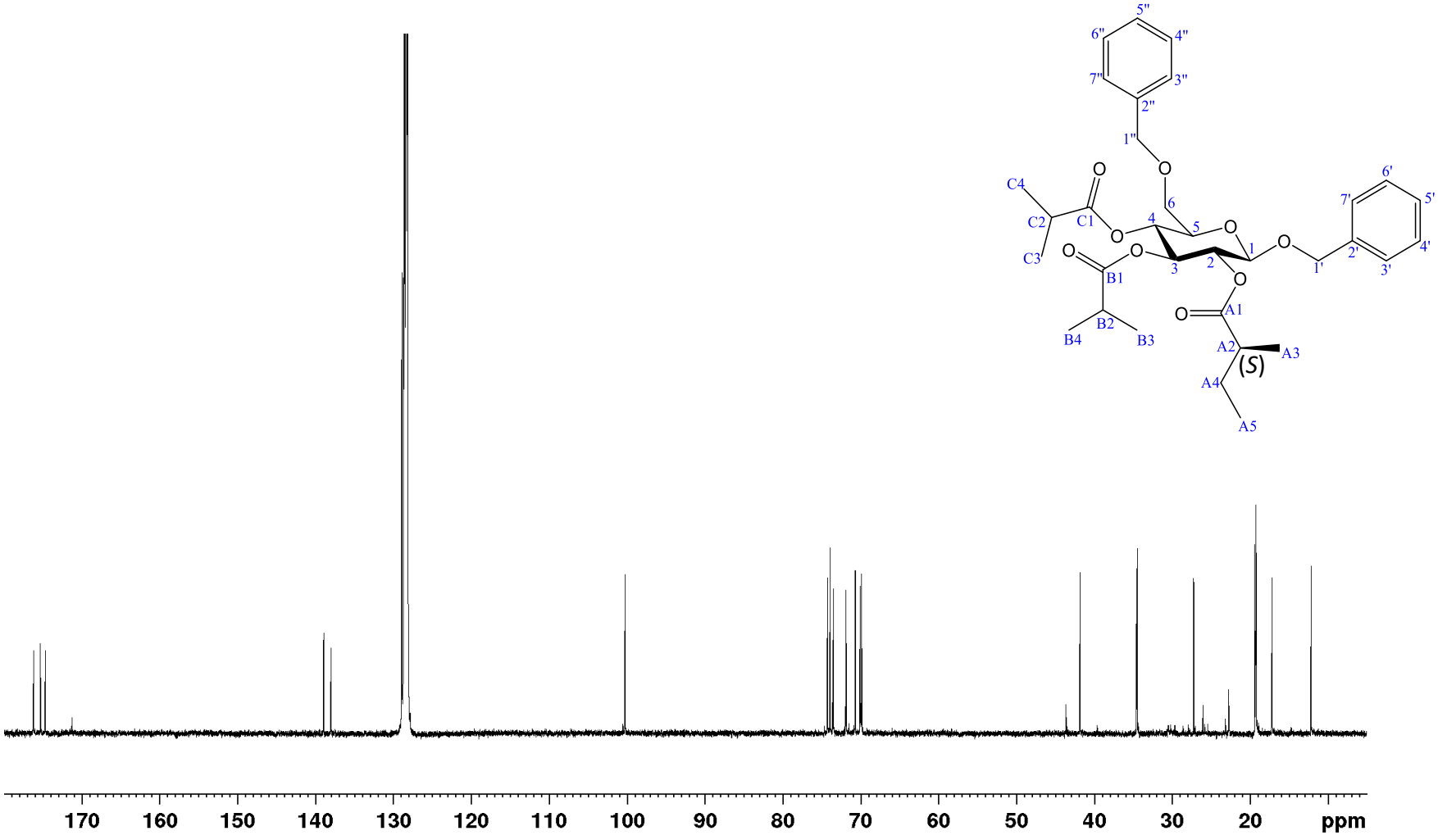

Figure S22: ^{13}C NMR spectrum of natural dibenzyl pennelliiside D (**2**) (126 MHz, C_6D_6).

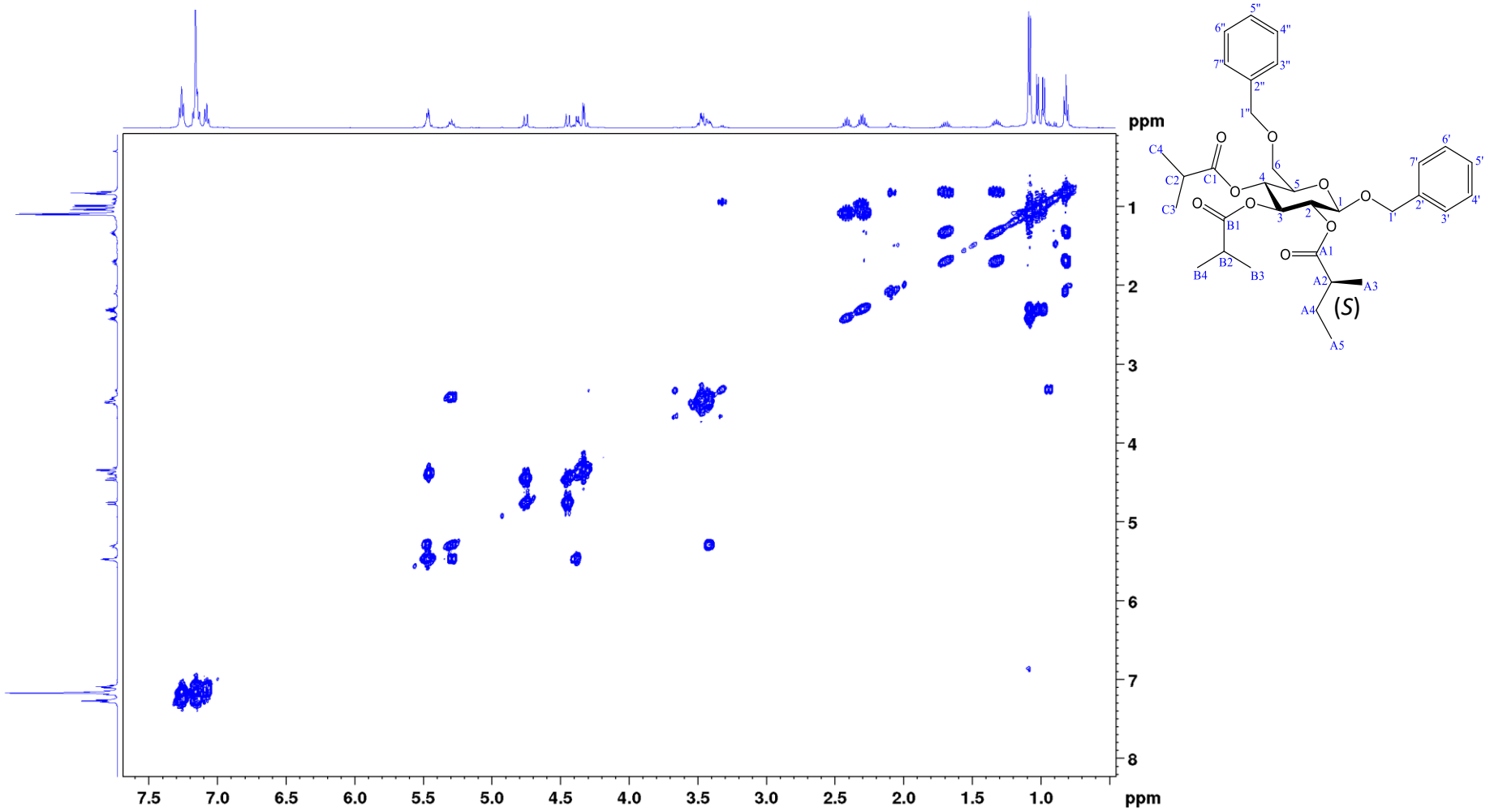

Figure S23: COSY spectrum of natural dibenzyl pennelliiside D (**2**) (500 MHz, C_6D_6).

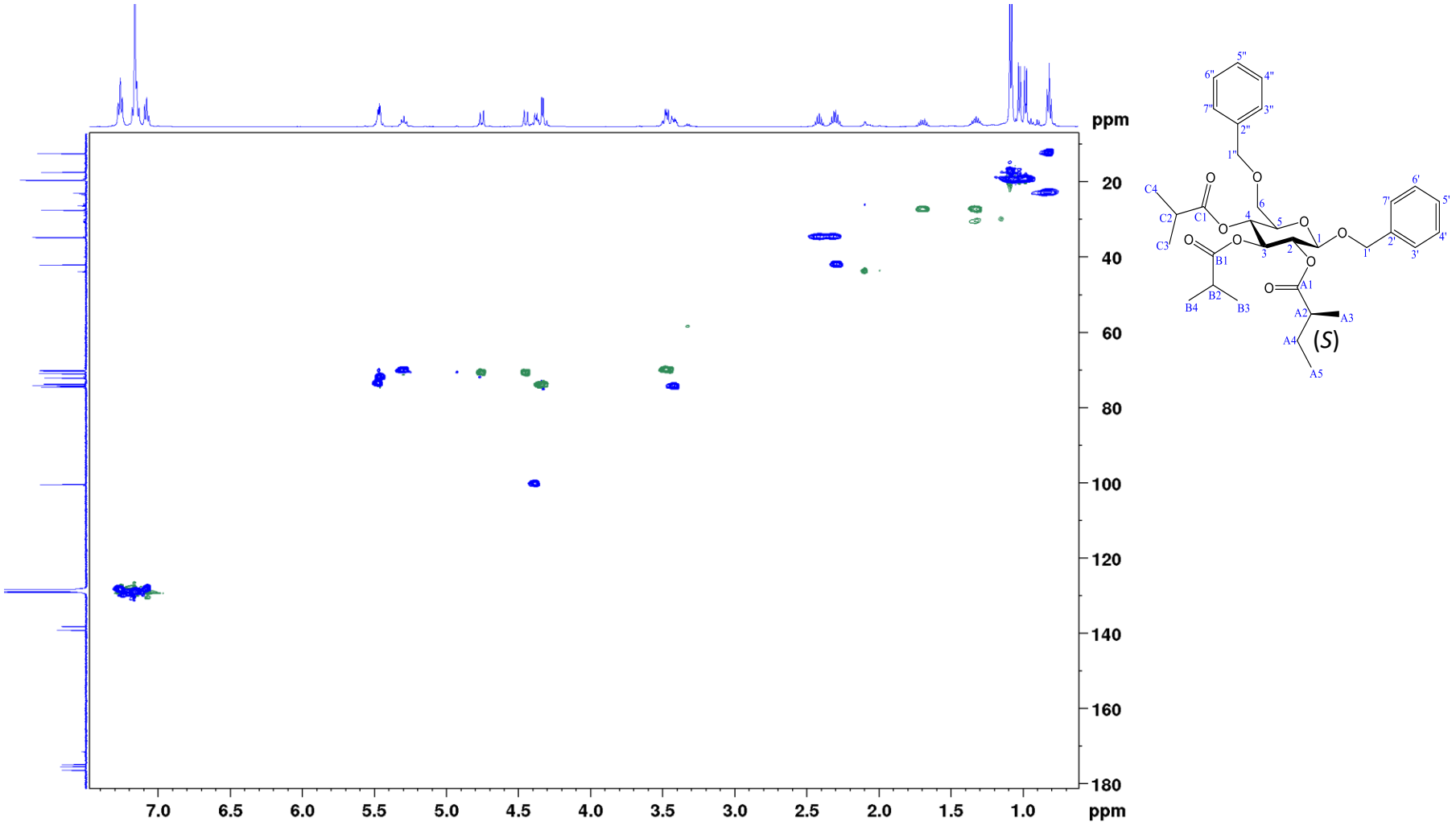

Figure S24: HSQC spectrum of natural dibenzyl pennelliiside D (**2**) (500 MHz, C_6D_6).

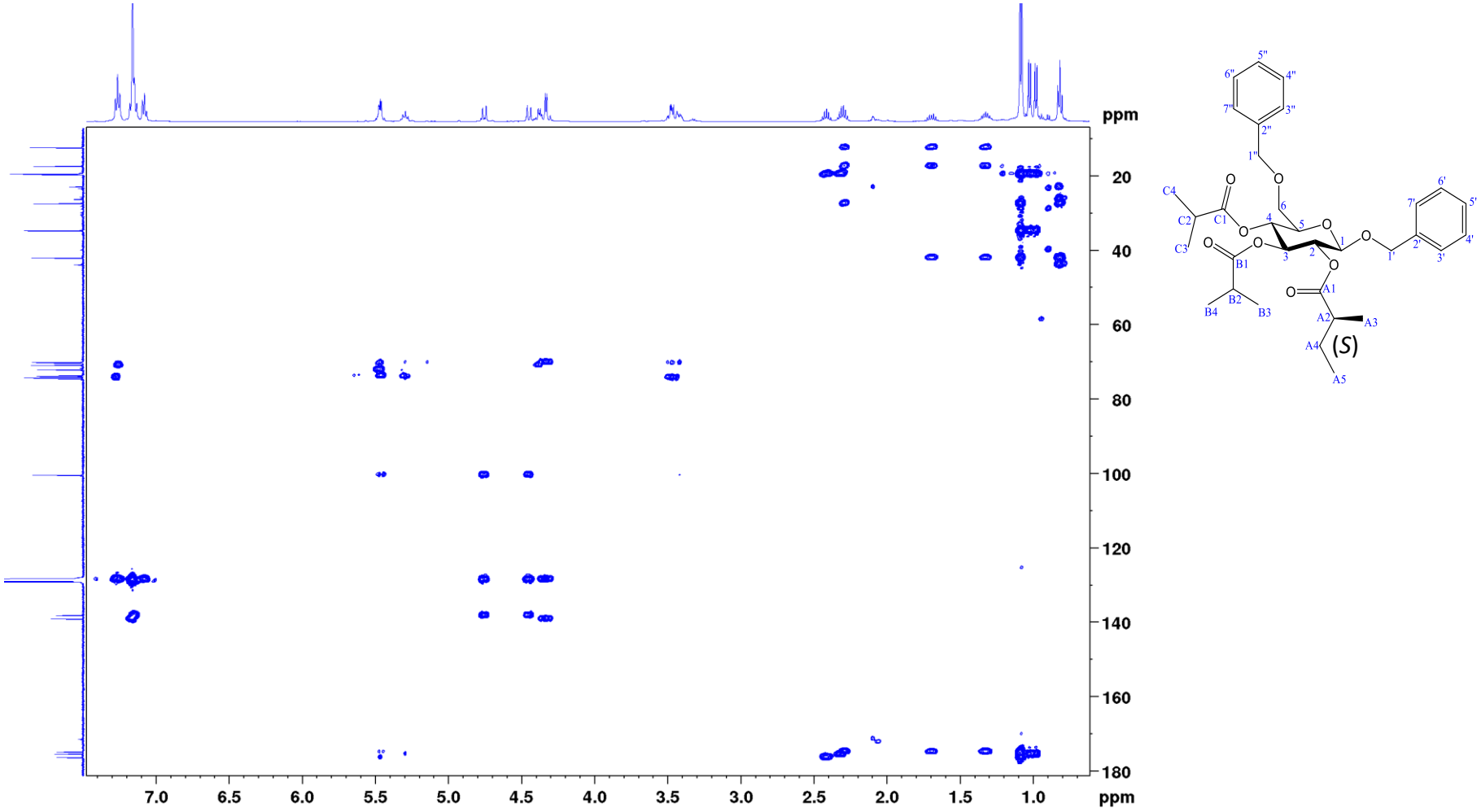

Figure S25: HMBC spectrum of natural dibenzyl pennelliiside D (**2**) (500 MHz, C_6D_6).

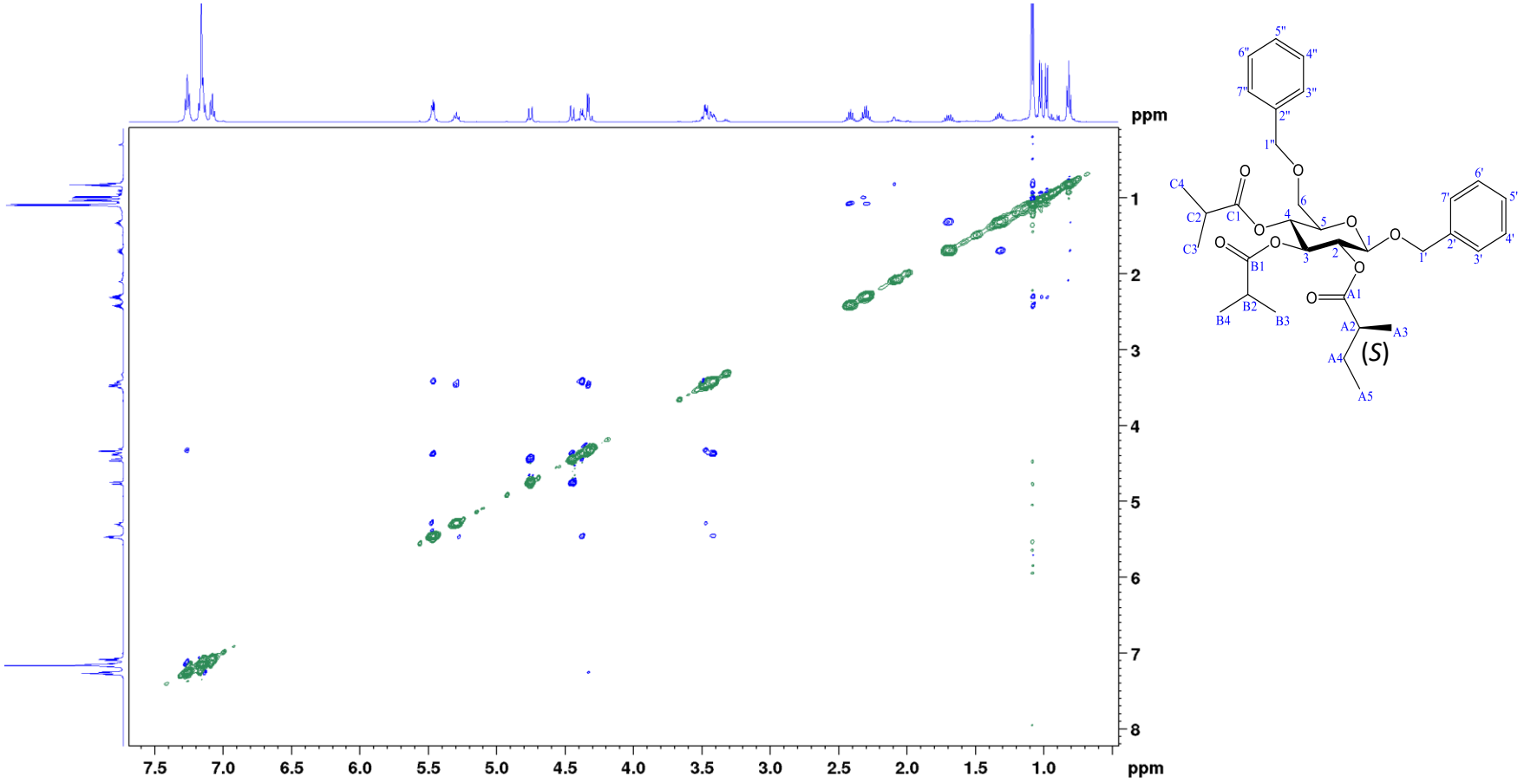

Figure S26: NOESY spectrum of natural dibenzyl pennelliiside D (**2**) (500 MHz, C_6D_6).

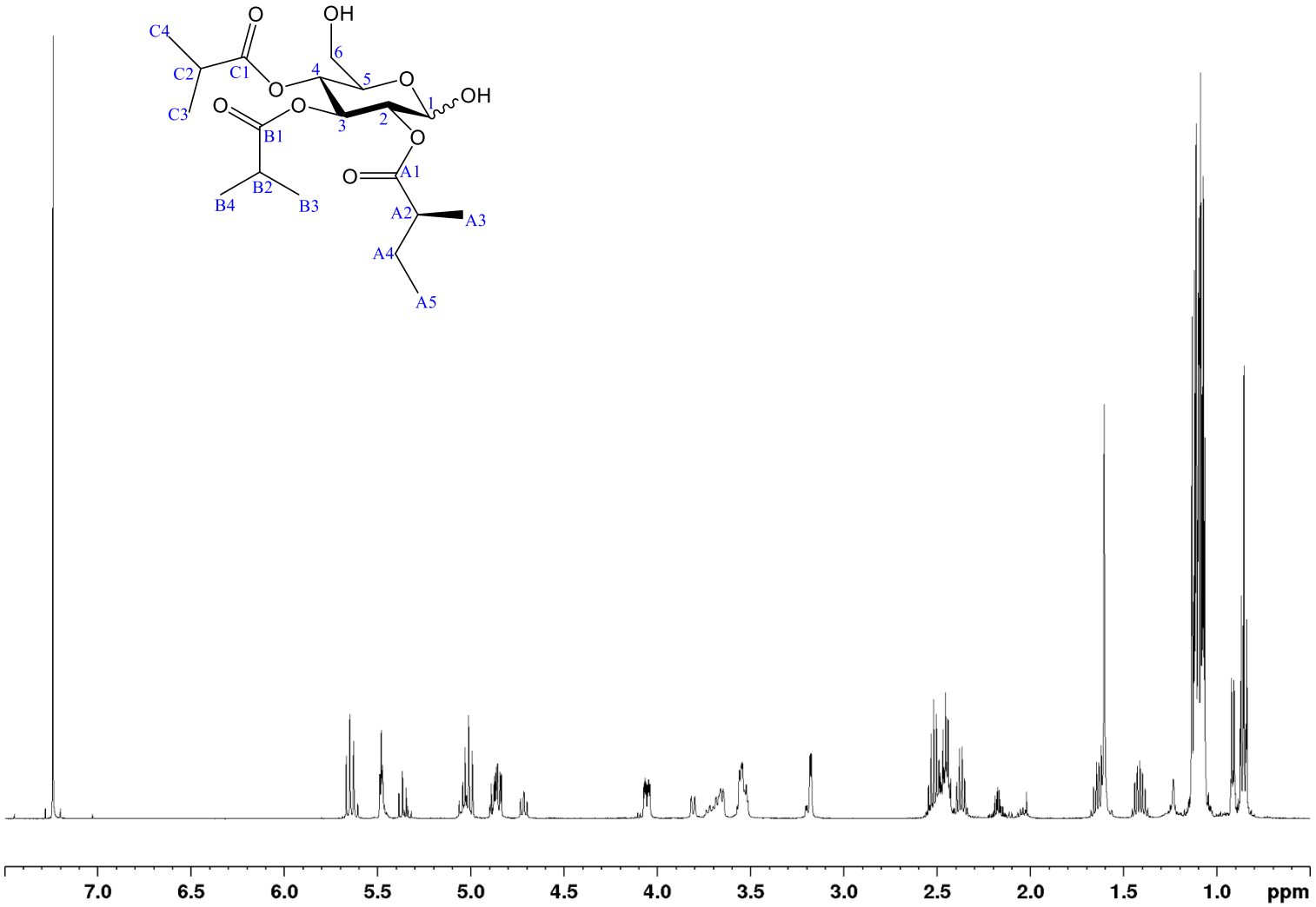

Figure S27: ^{1}H NMR spectrum of natural pennelliiside D (**1**) (500 MHz, $CDCl_3$).

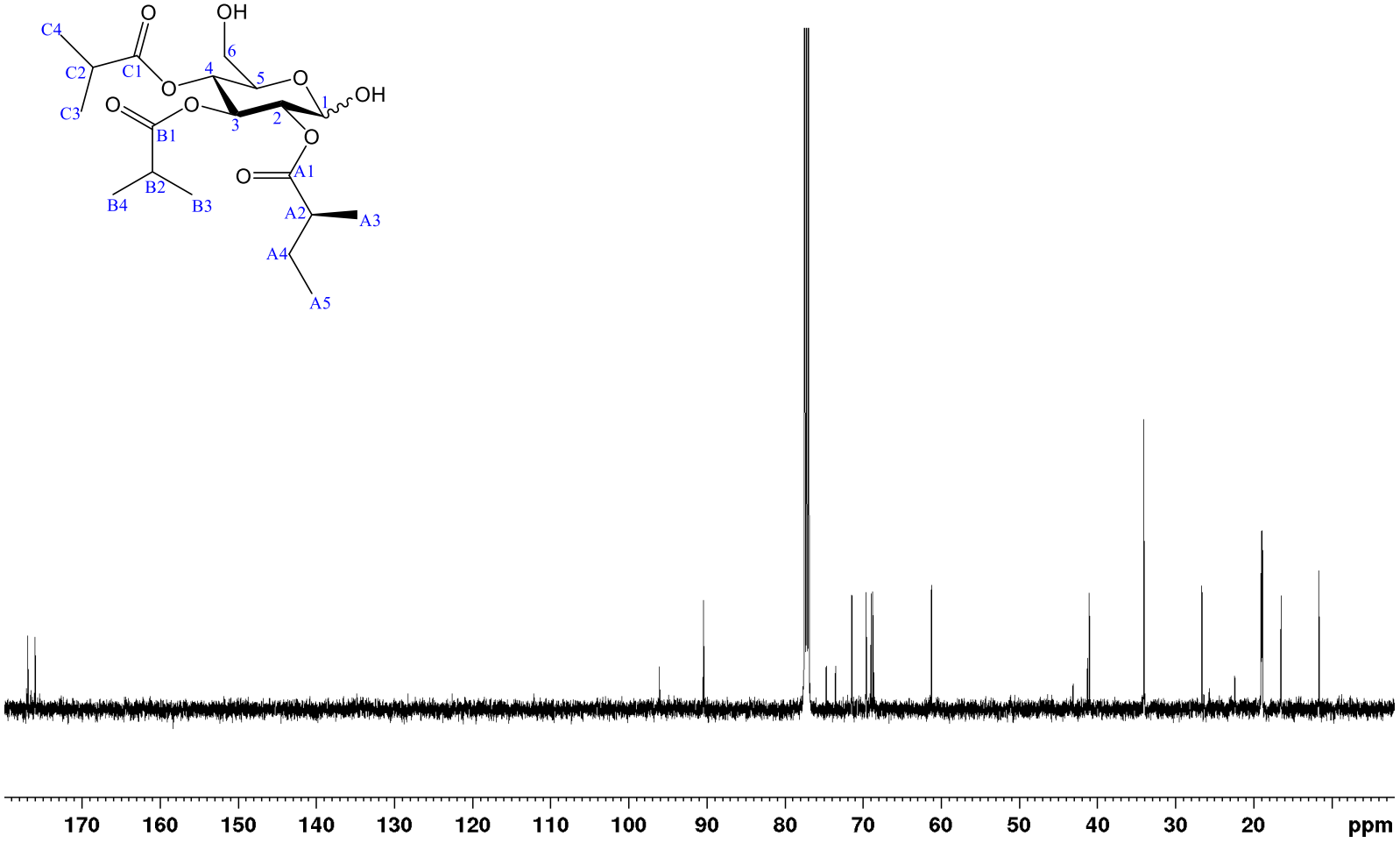

Figure S28: ^{13}C NMR spectrum of natural pennelliiside D (**1**) (126 MHz, $CDCl_3$).

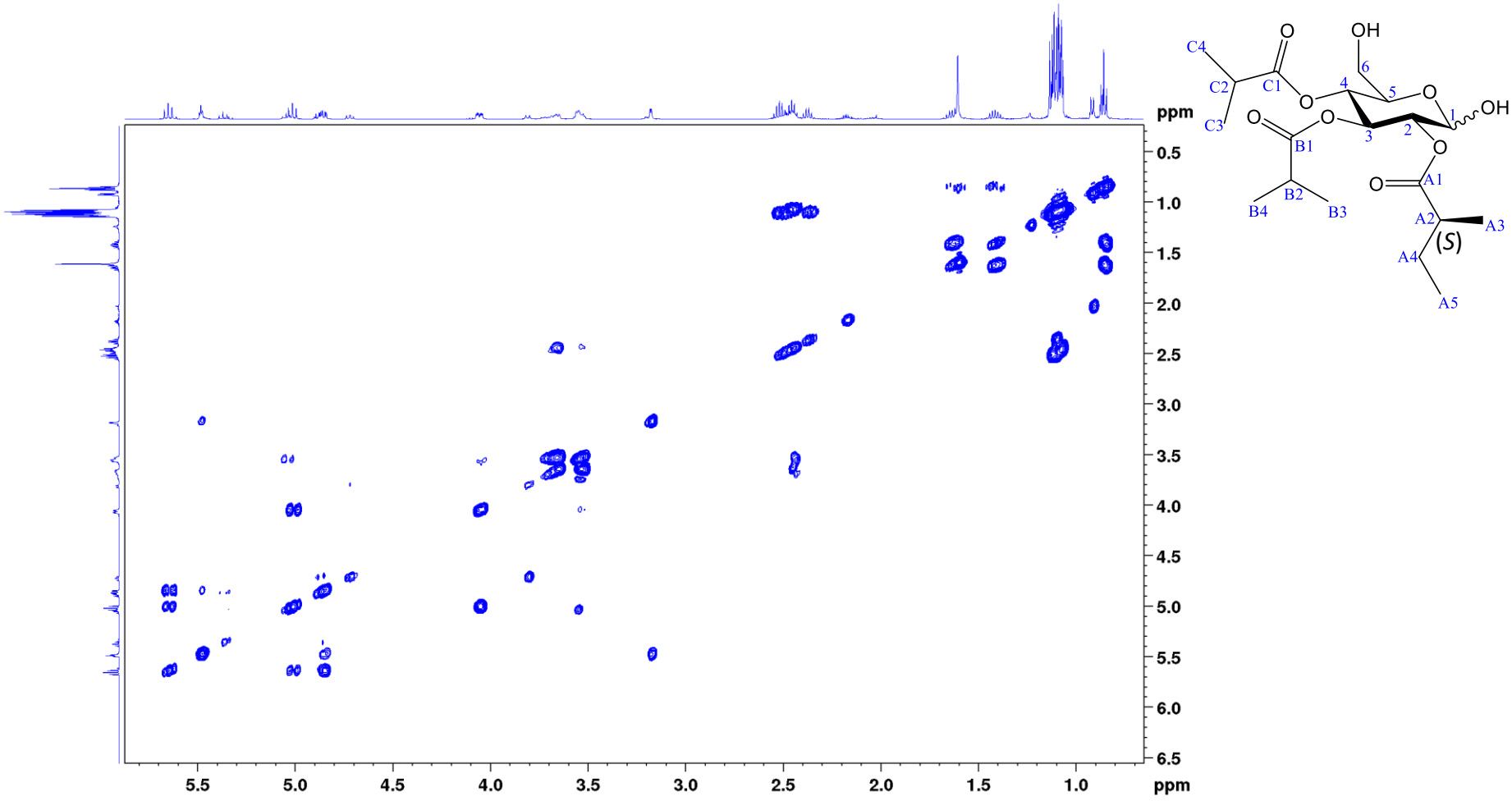

Figure S29: COSY spectrum of natural pennelliiside D (**1**) (500 MHz, $CDCl_3$).

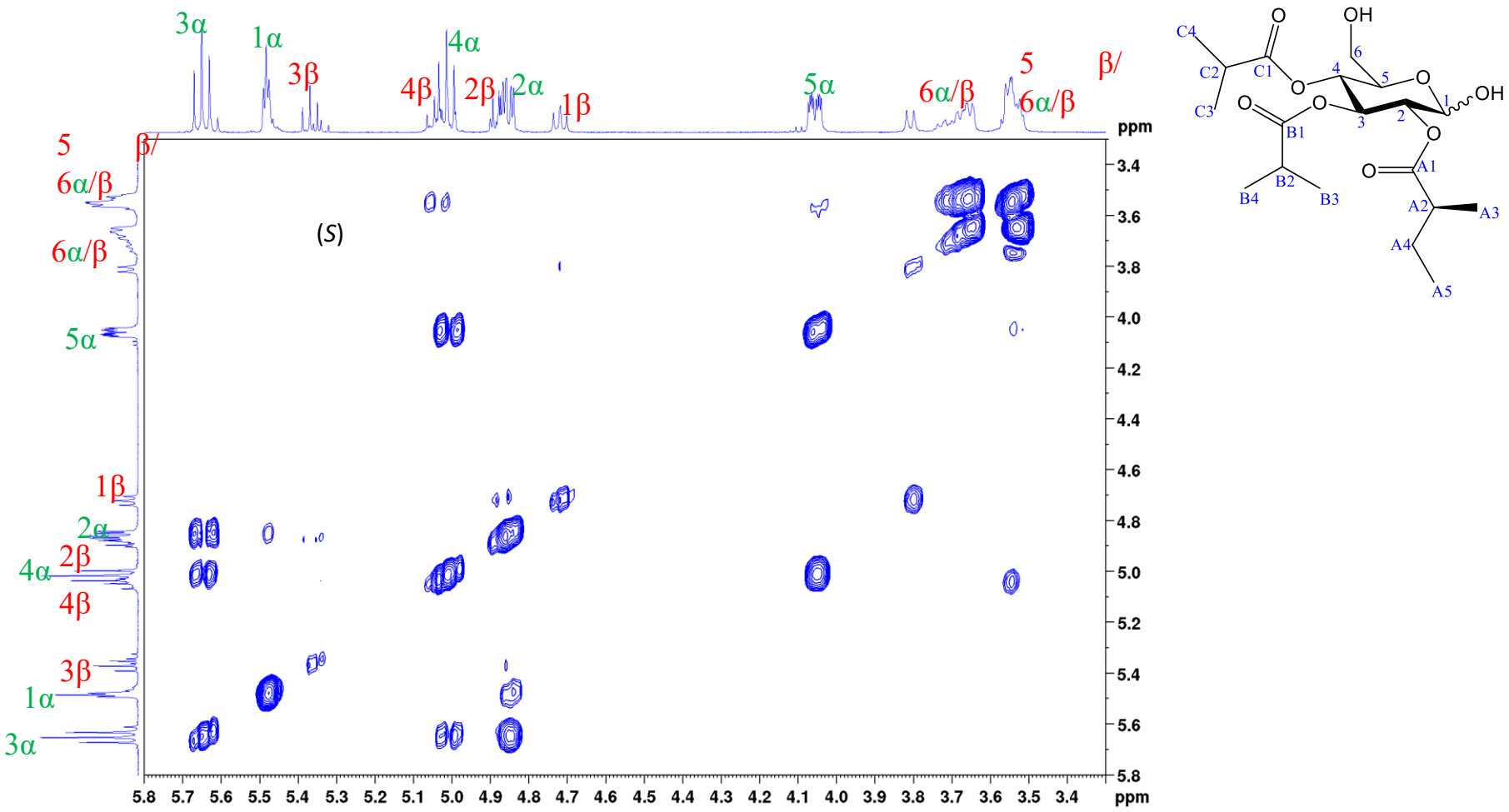

Figure S30: COSY spectrum of natural pennelliiside D (**1**) (500 MHz, $CDCl_3$).

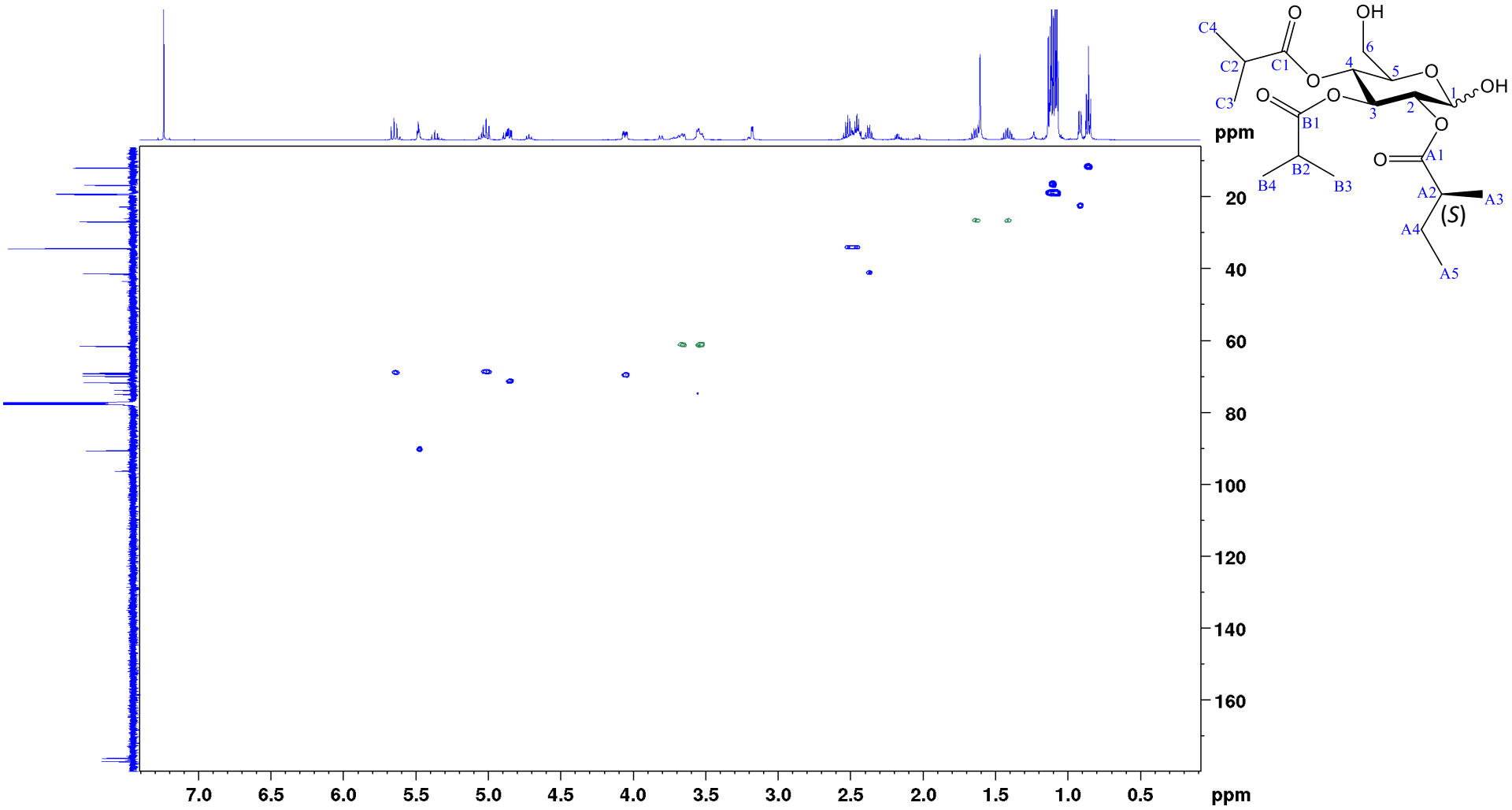

Figure S31: HSQC spectrum of natural pennelliiside D (**1**) (500 MHz, $CDCl_3$).

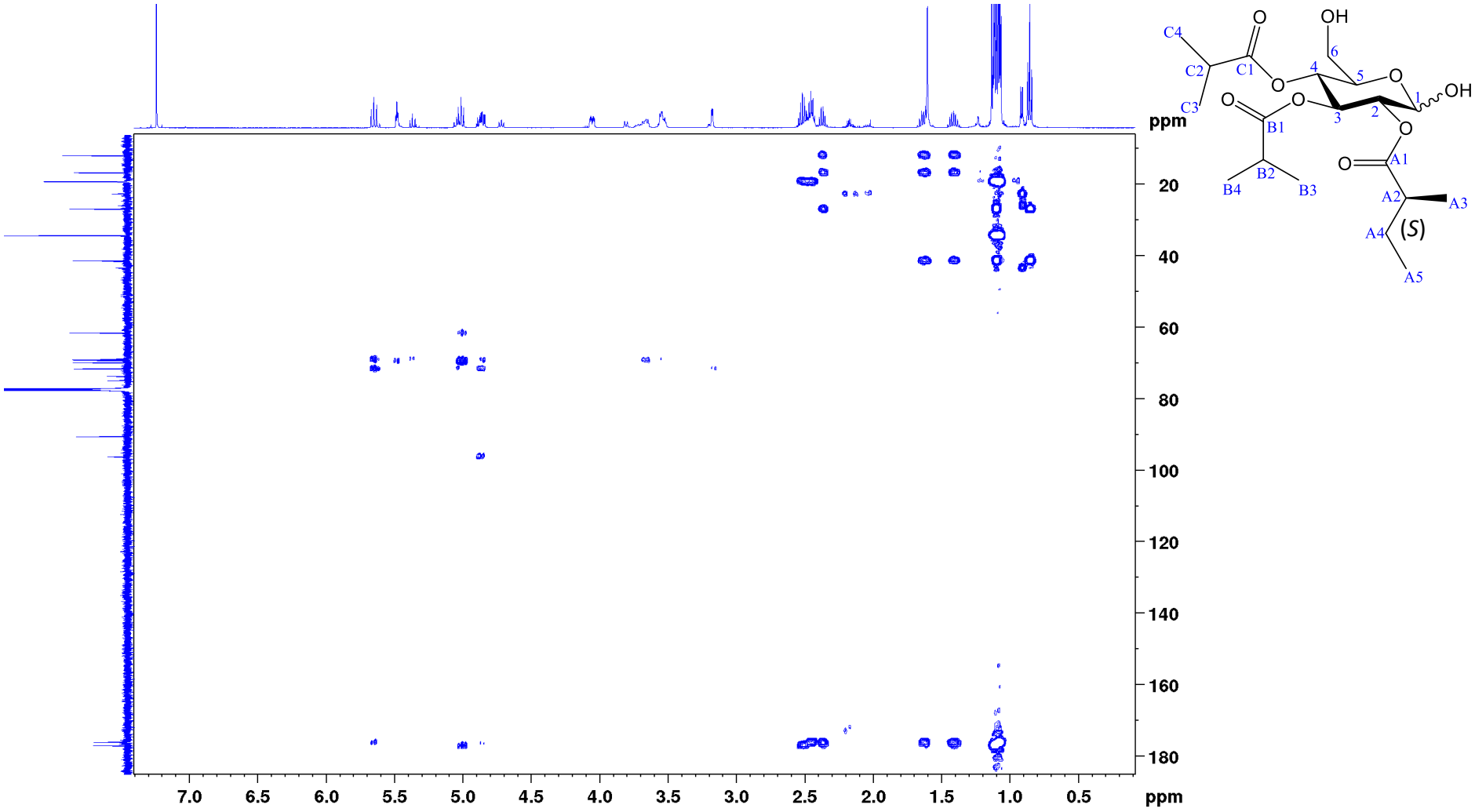

Figure S32: HMBC spectrum of natural pennelliiside D (**1**) (500 MHz, $CDCl_3$).

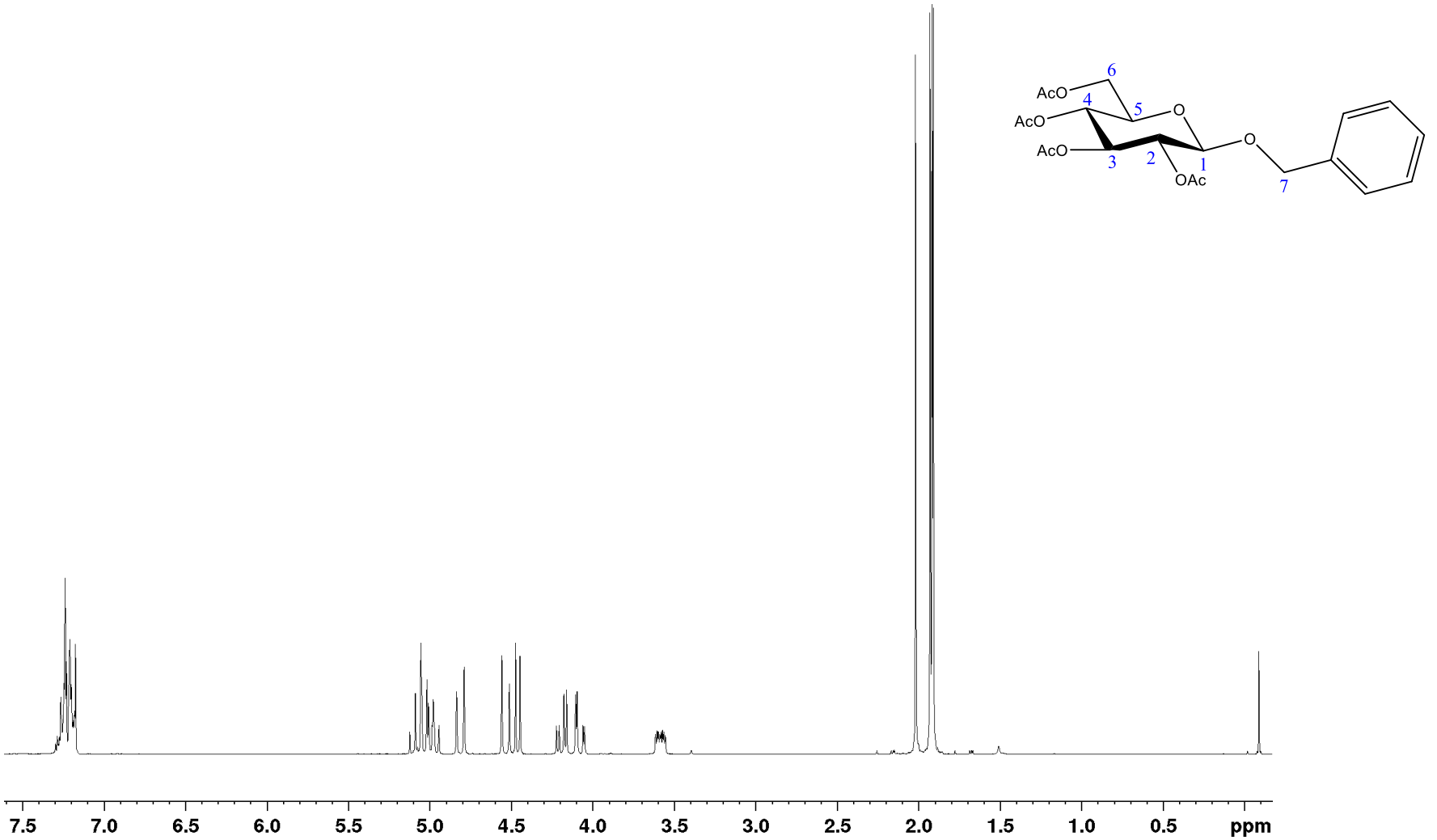

Figure S33: ^{1}H NMR spectrum of compound **4** (270 MHz, $CDCl_3$).

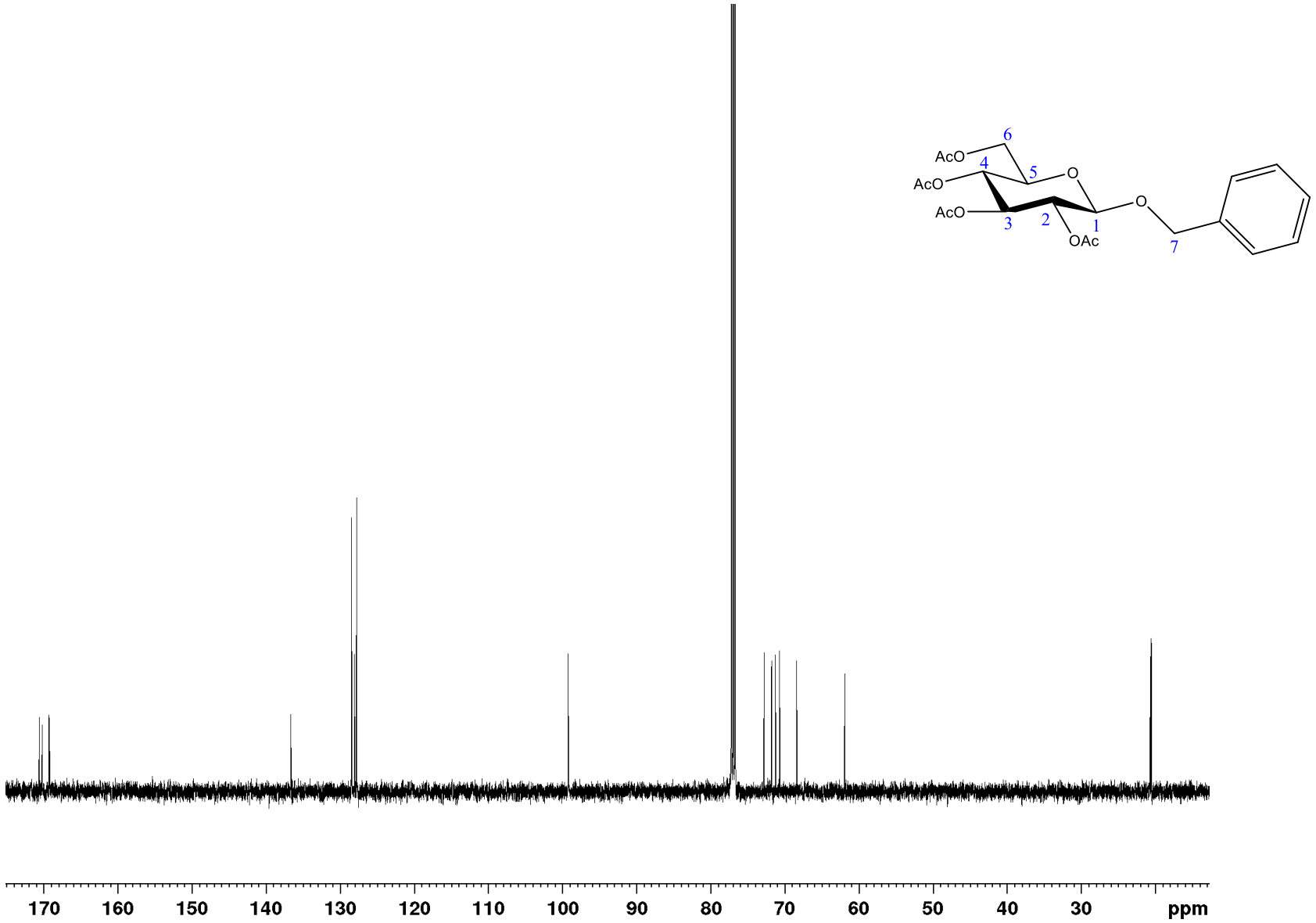

Figure S34: ^{13}C NMR spectrum of compound **4** (126 MHz, $CDCl_3$).

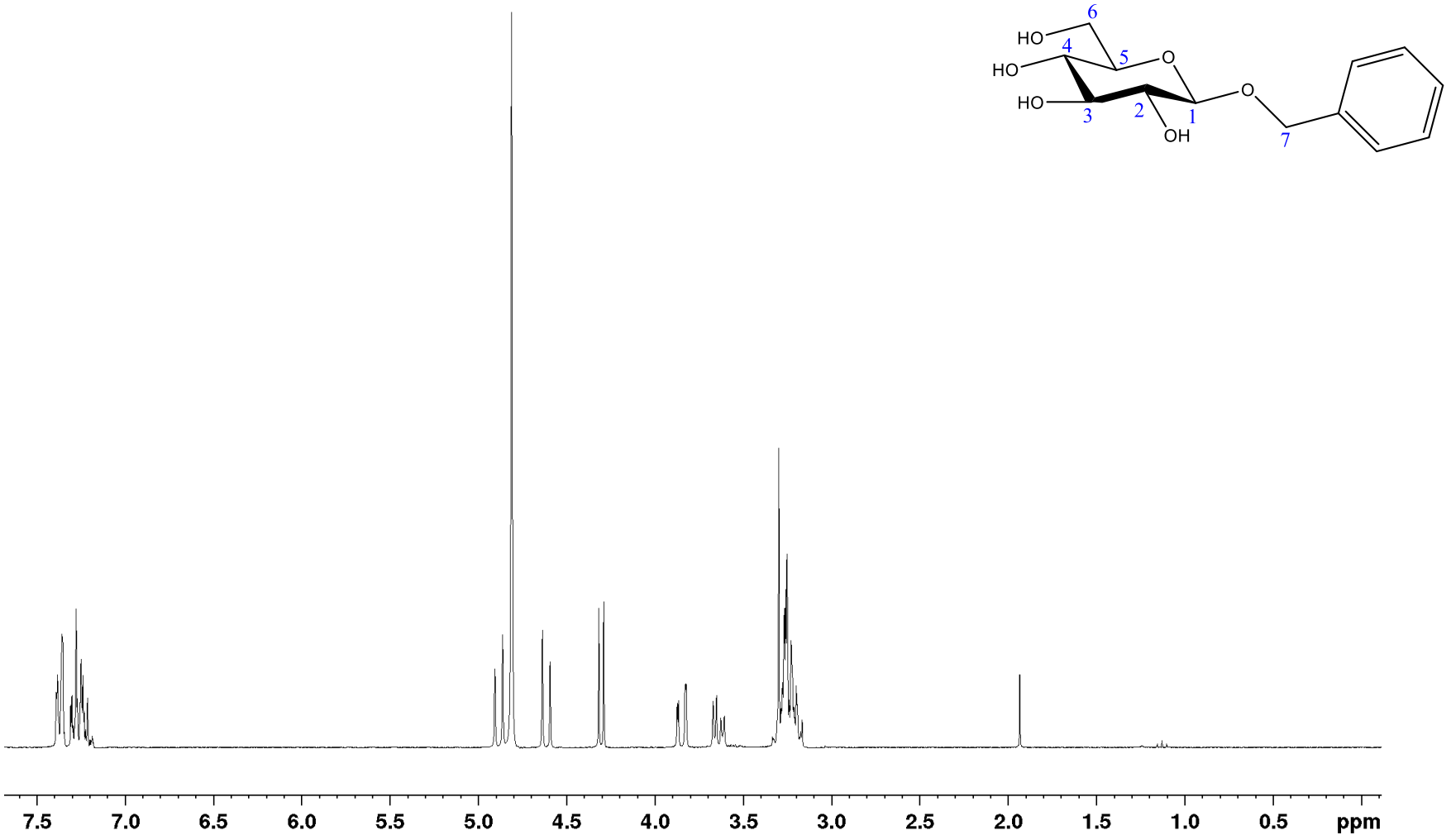

Figure S35: ^{1}H NMR spectrum of compound **5** (270 MHz, CD_3OD).

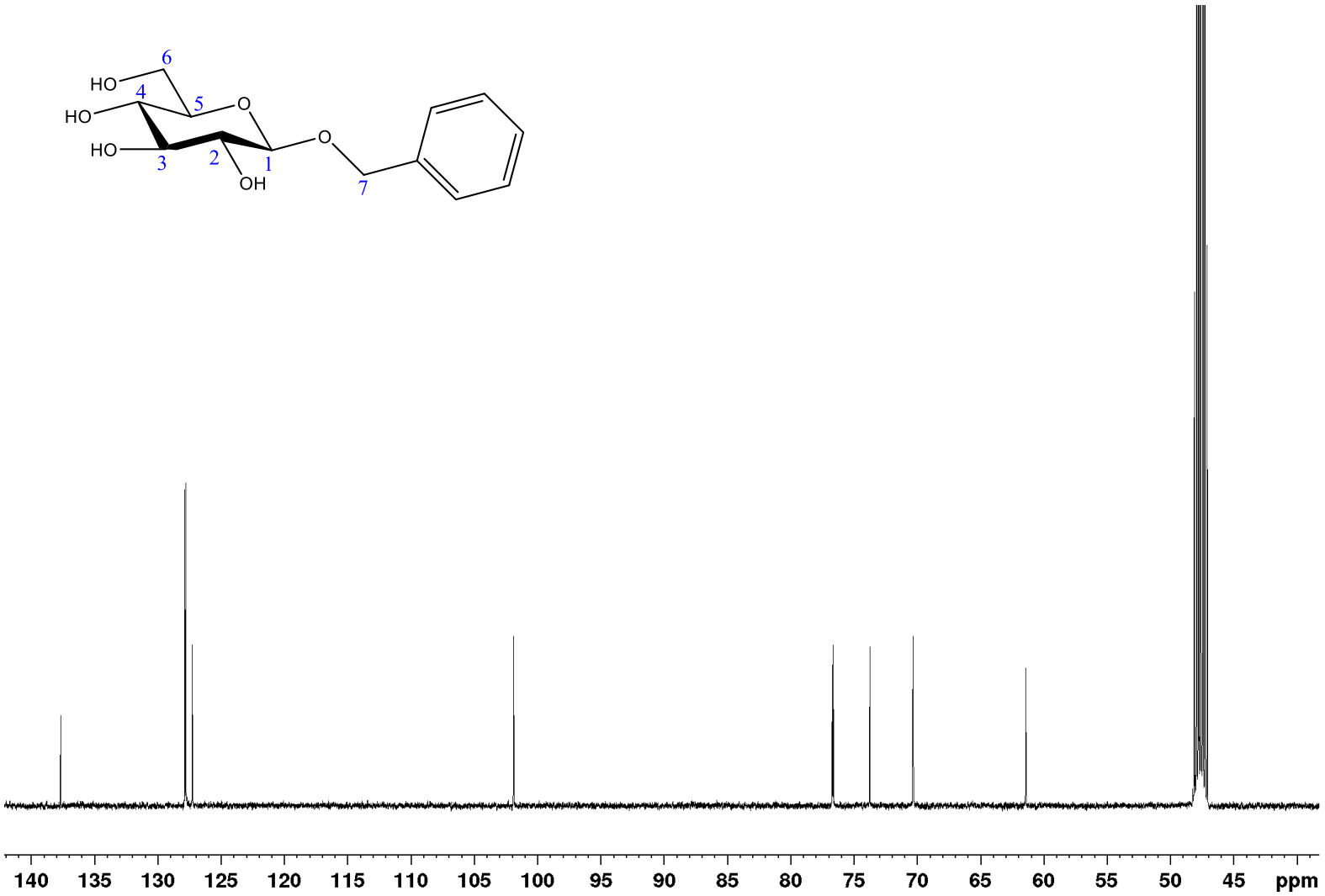

Figure S36: ^{13}C NMR spectrum of compound **5** (126 MHz, CD_3OD).

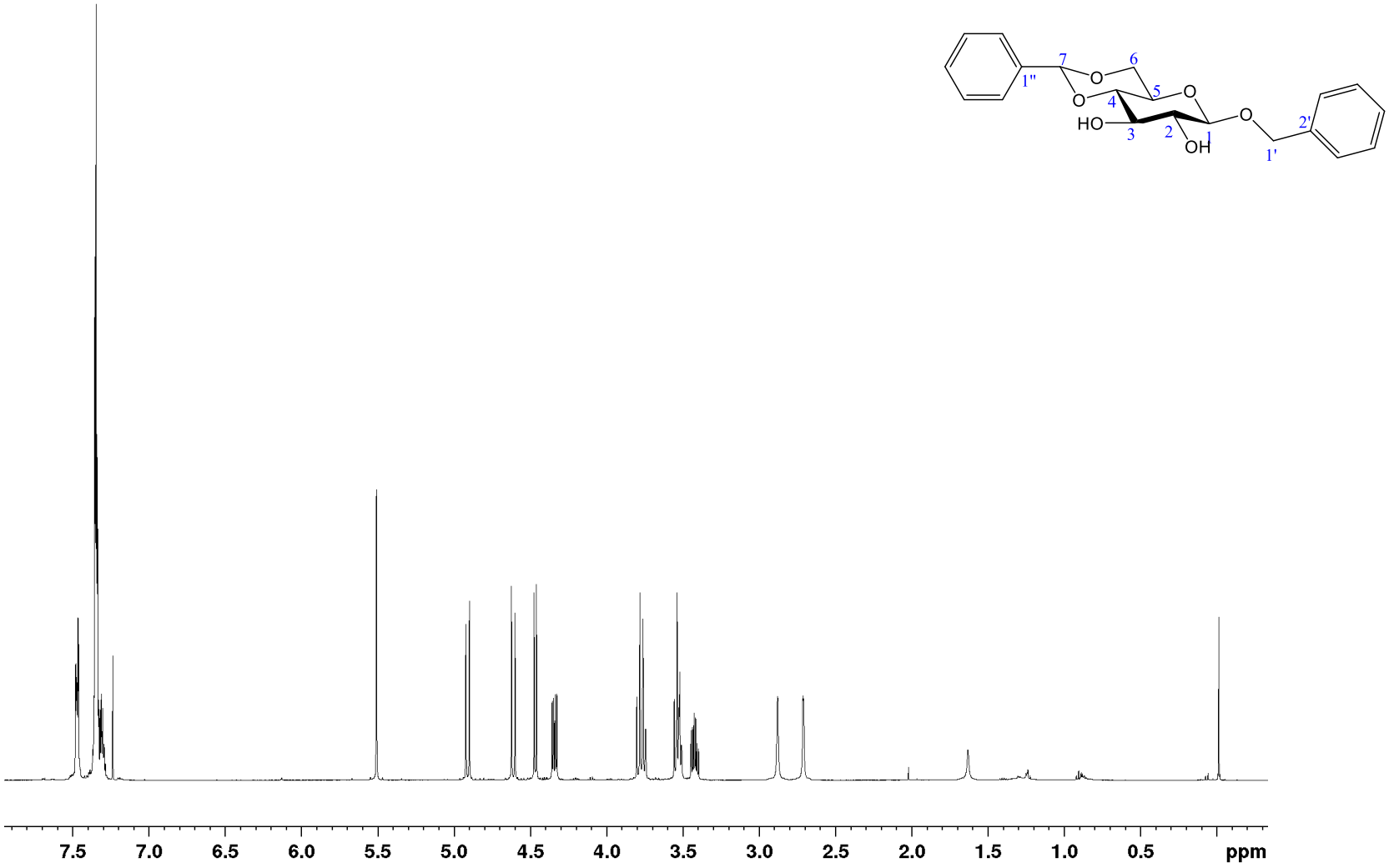

Figure S37: ^{1}H NMR spectrum of compound **6** (500 MHz, $CDCl_3$).

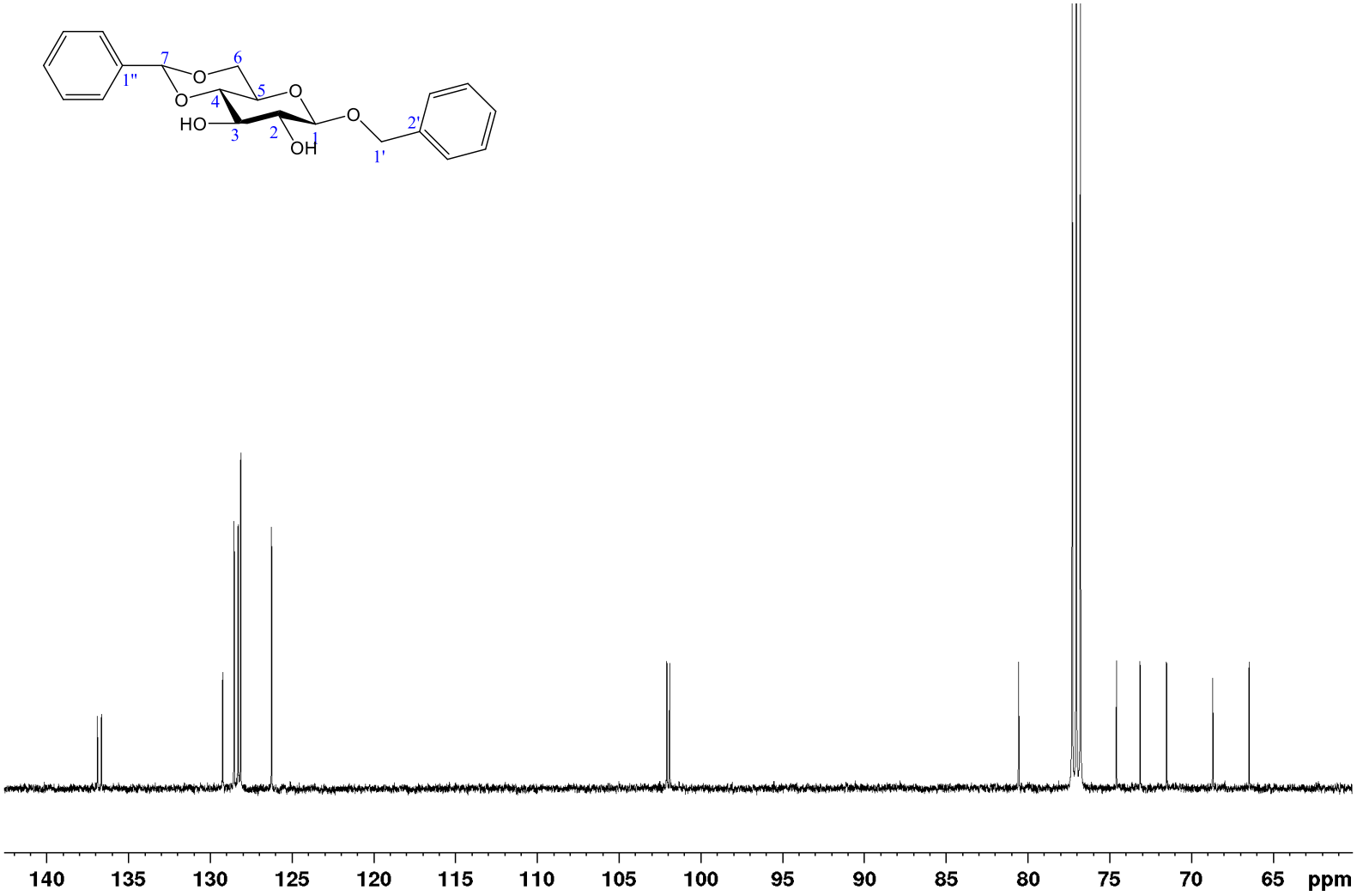

Figure S38: ^{13}C NMR spectrum of compound **6** (126 MHz, $CDCl_3$).

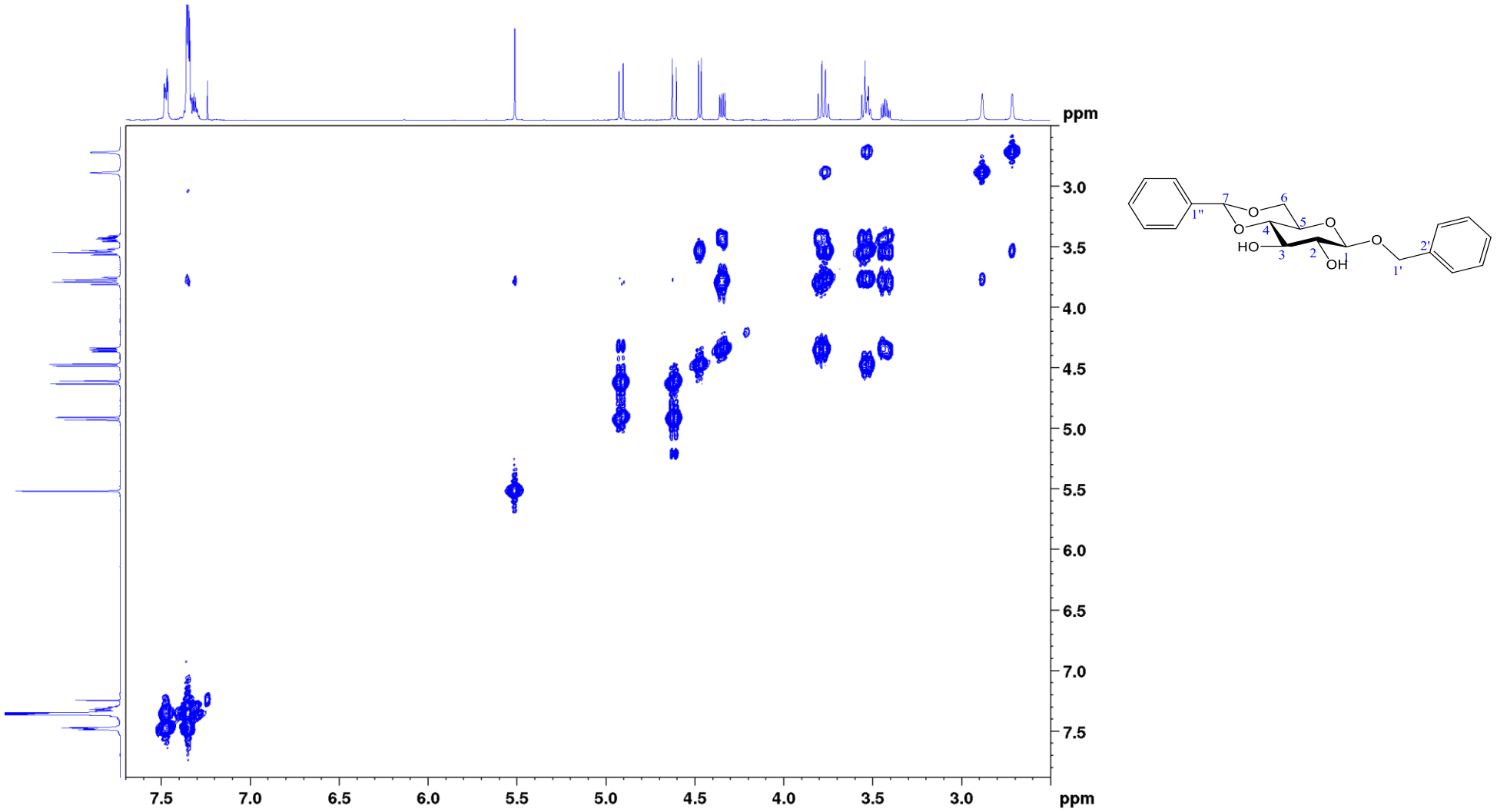

Figure S39: COSY spectrum of compound **6** (500 MHz, $CDCl_3$).

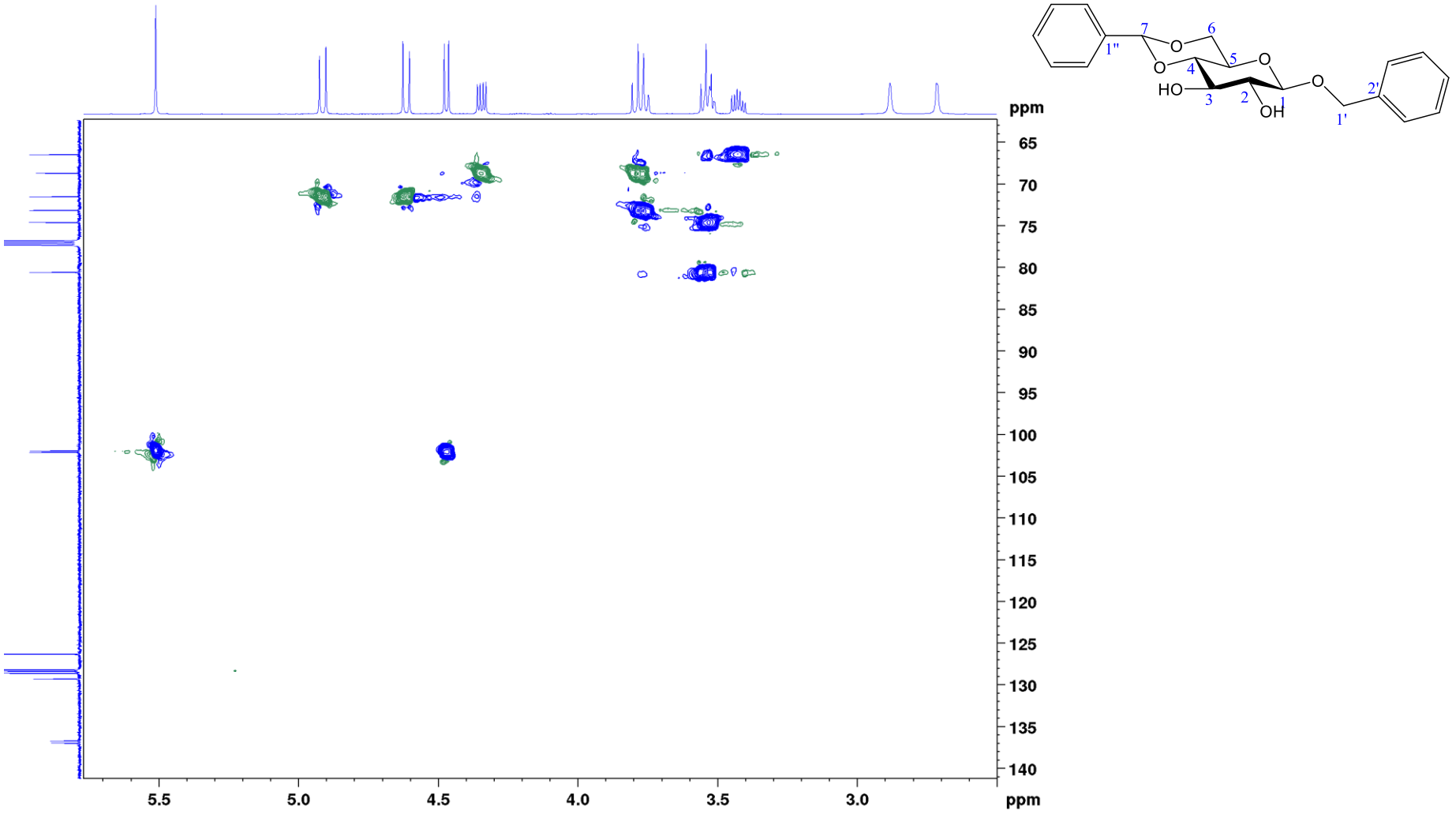

Figure S40: HSQC spectrum of compound **6** (500 MHz, $CDCl_3$).

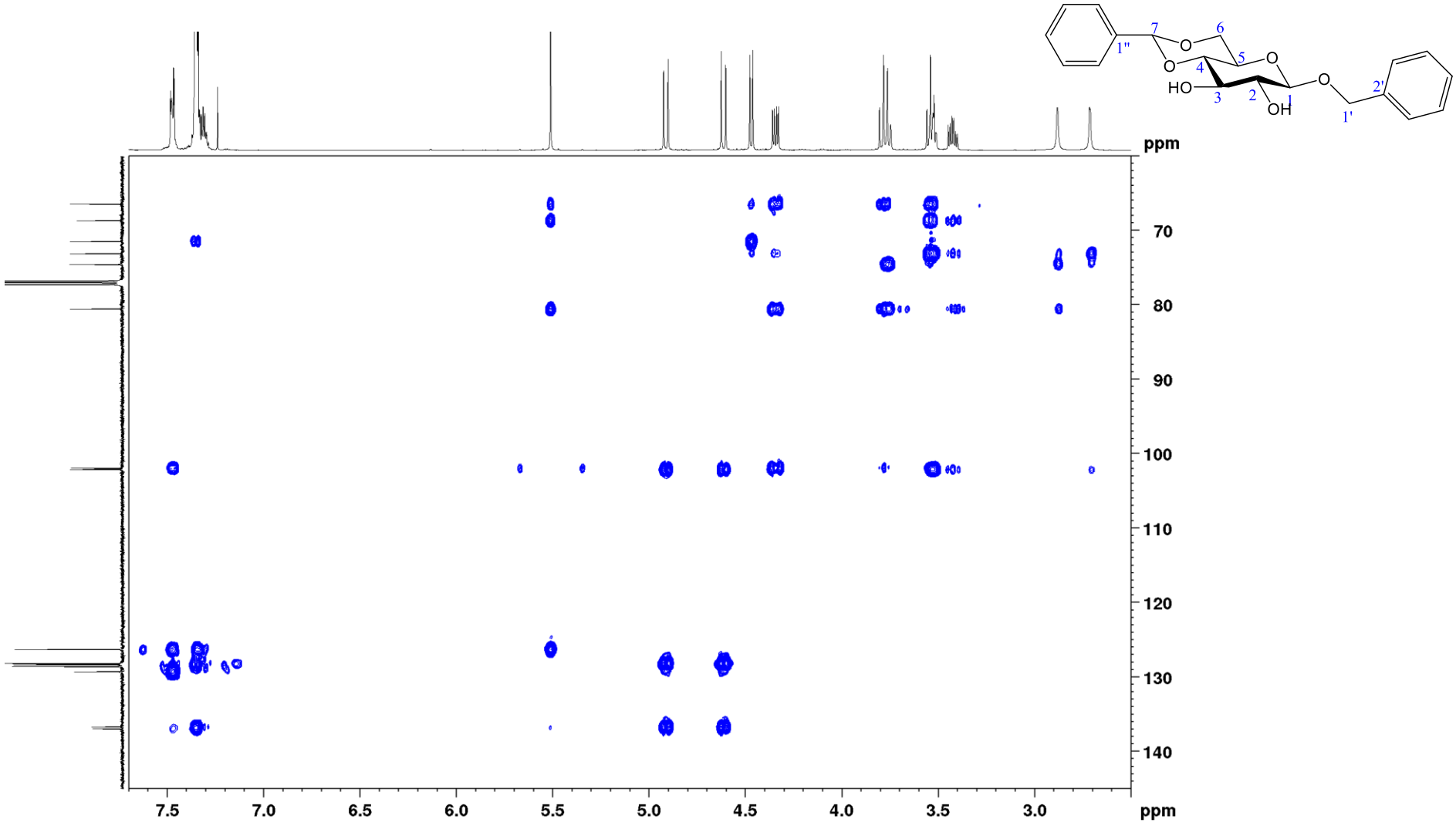

Figure S41: HMBC spectrum of compound **6** (500 MHz, $CDCl_3$).

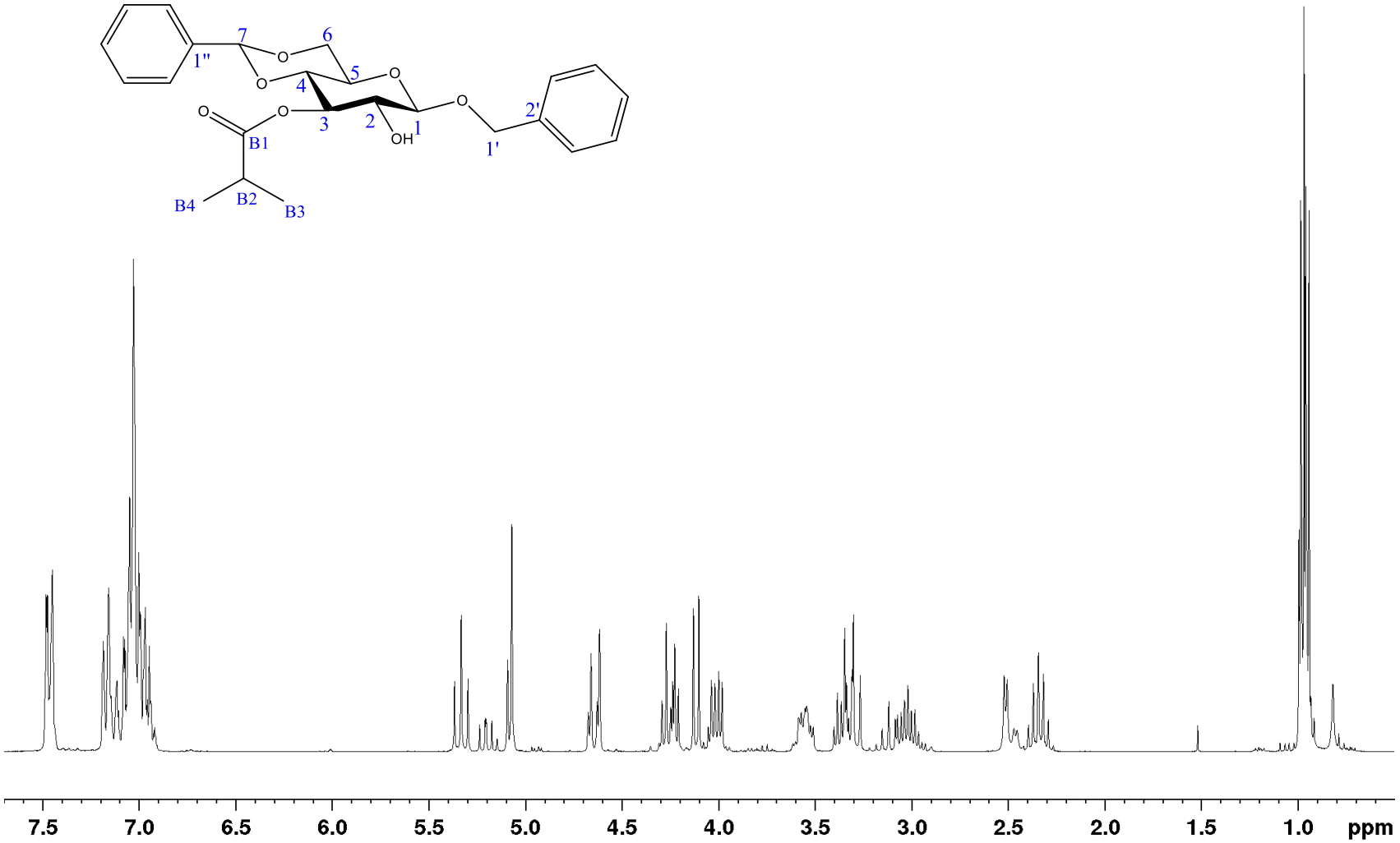

Figure S42: ^{1}H NMR spectrum of compound **7** (270 MHz, C_6D_6).

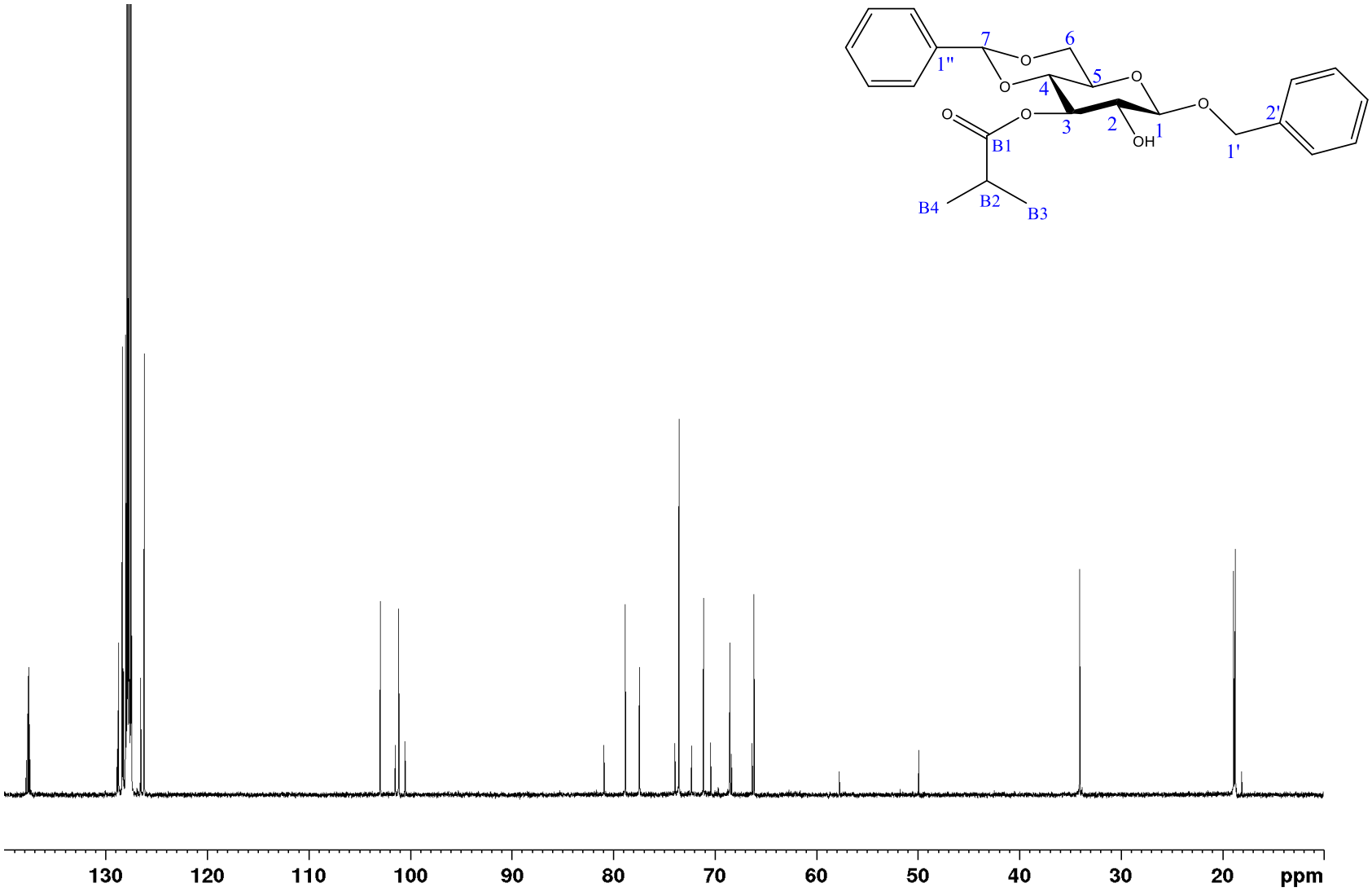

Figure S43: ^{13}C NMR spectrum of compound **7** (126 MHz, C_6D_6).

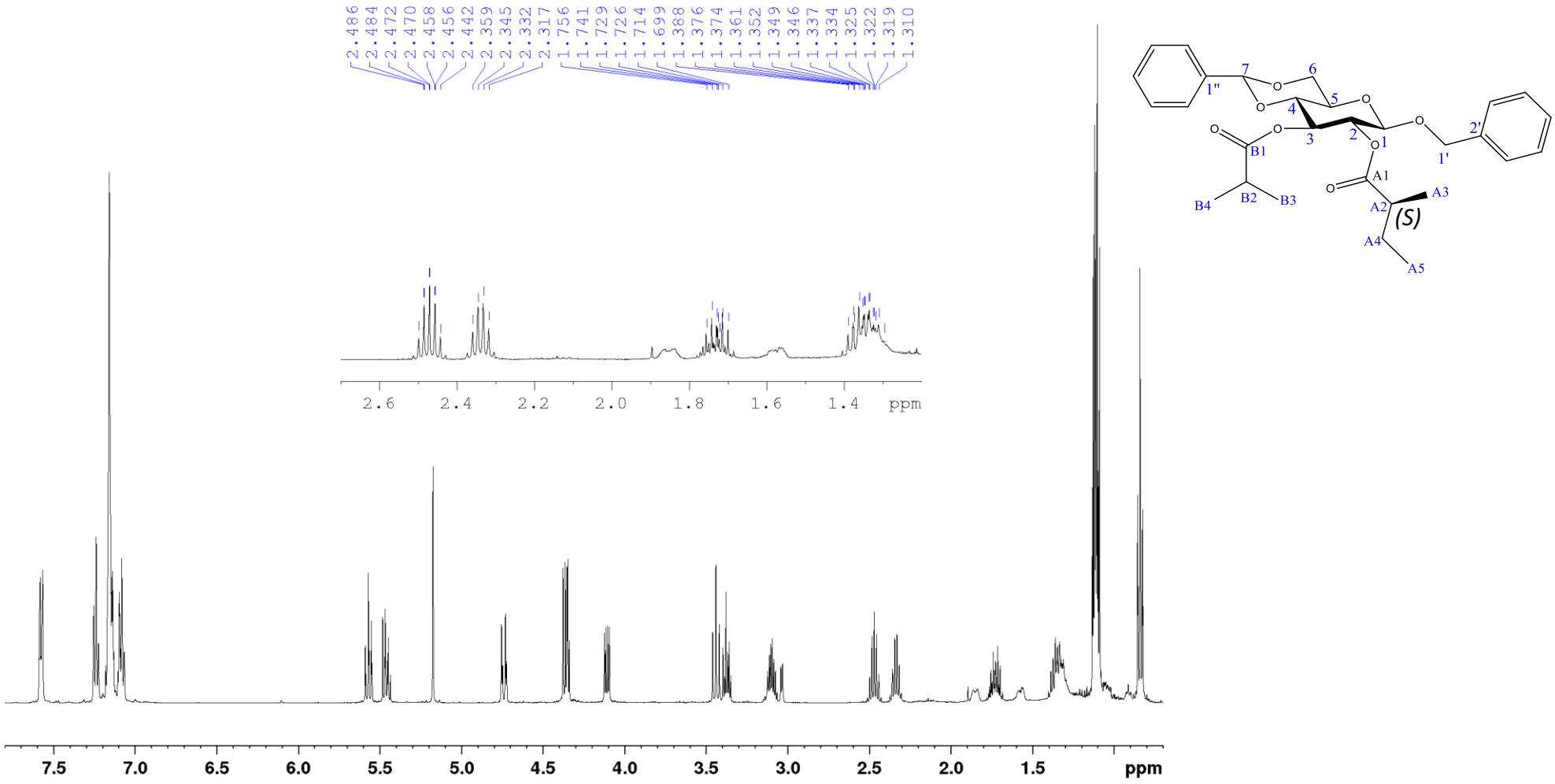

Figure S44: ^{1}H NMR spectrum of compound **8(*S*)** (500 MHz, C_6D_6).

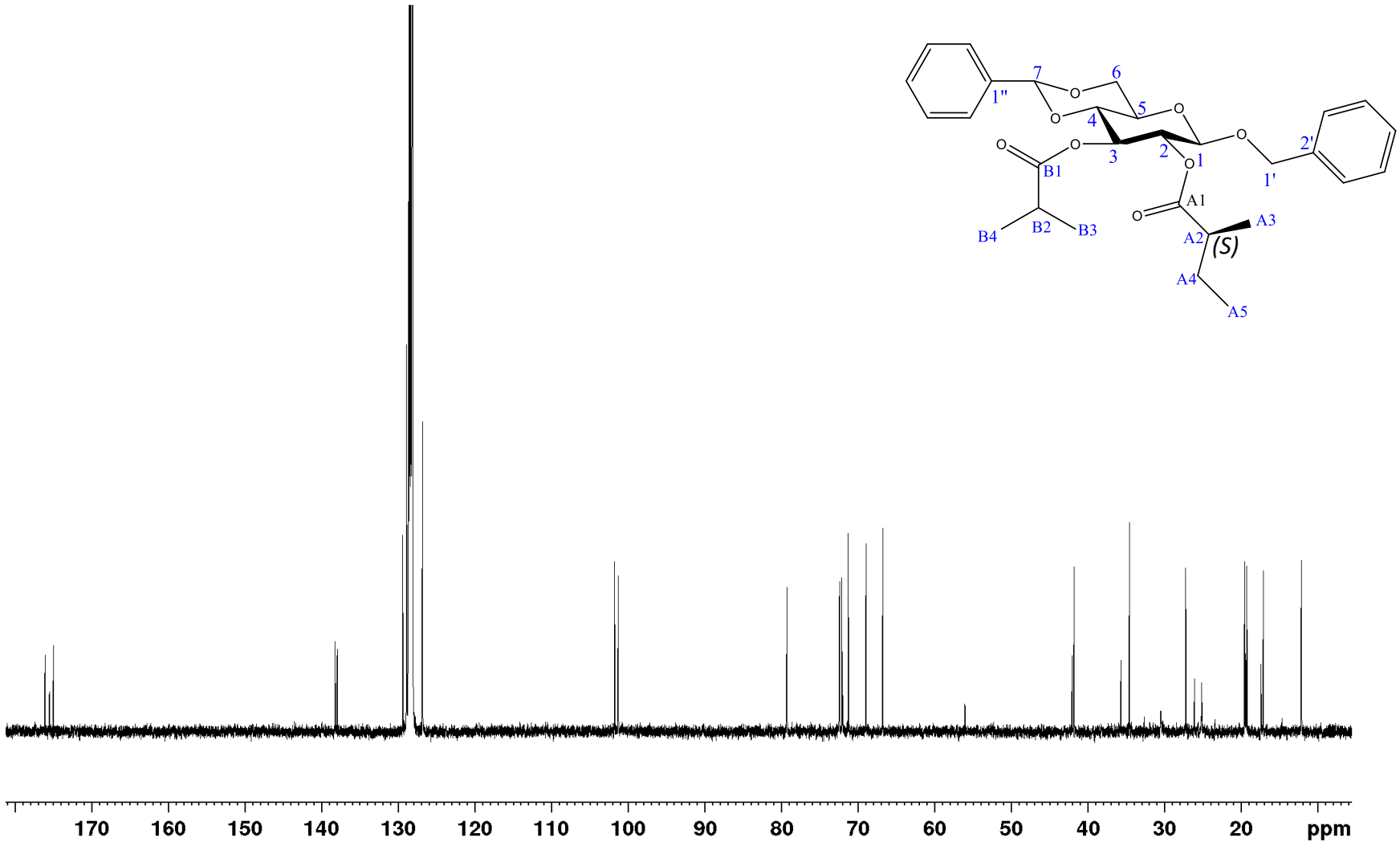

Figure S45: ^{13}C NMR spectrum of compound **8(*S*)** (126 MHz, C_6D_6).

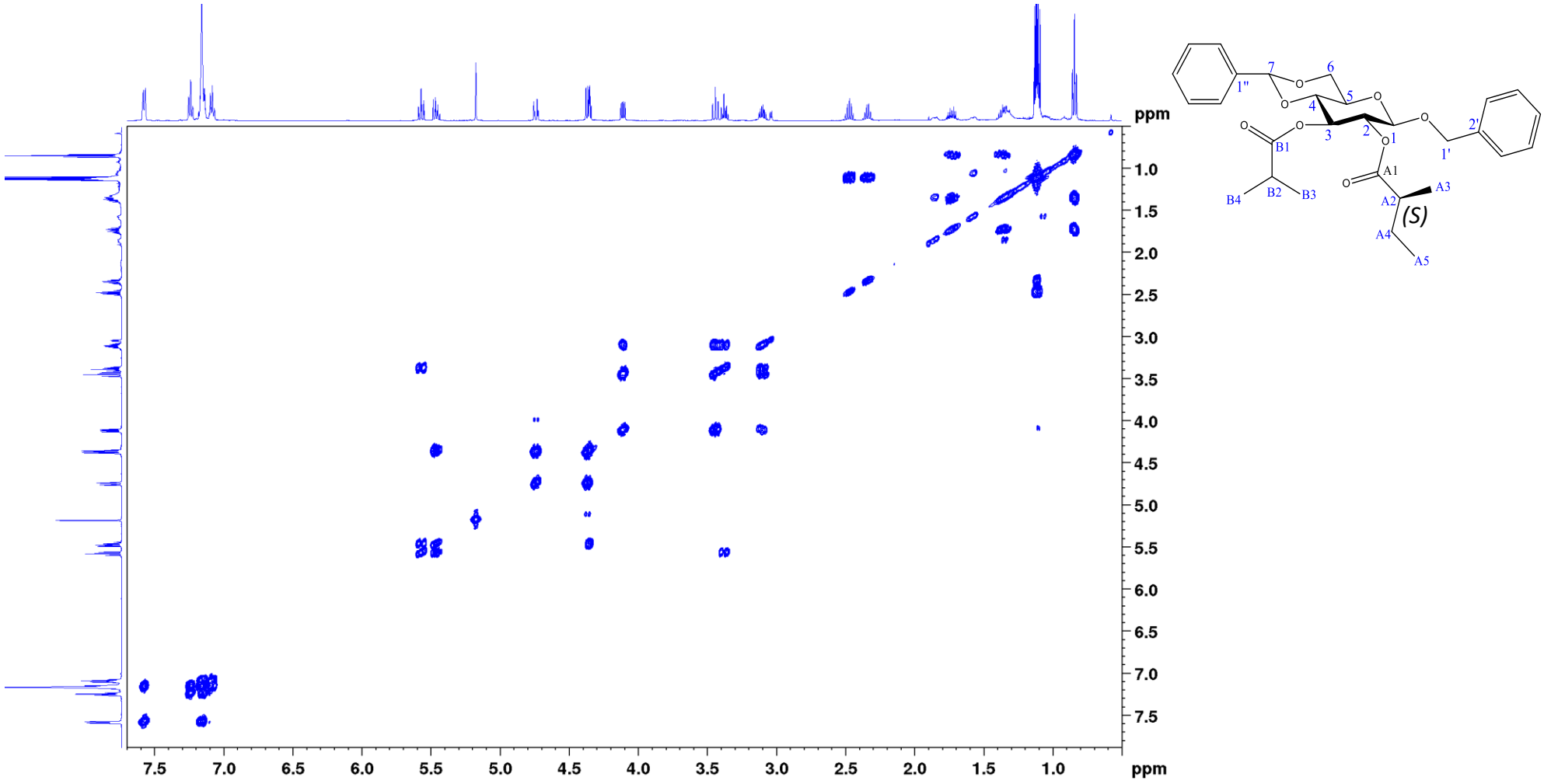

Figure S46: COSY spectrum of compound **8(*S*)** (500 MHz, C_6D_6).

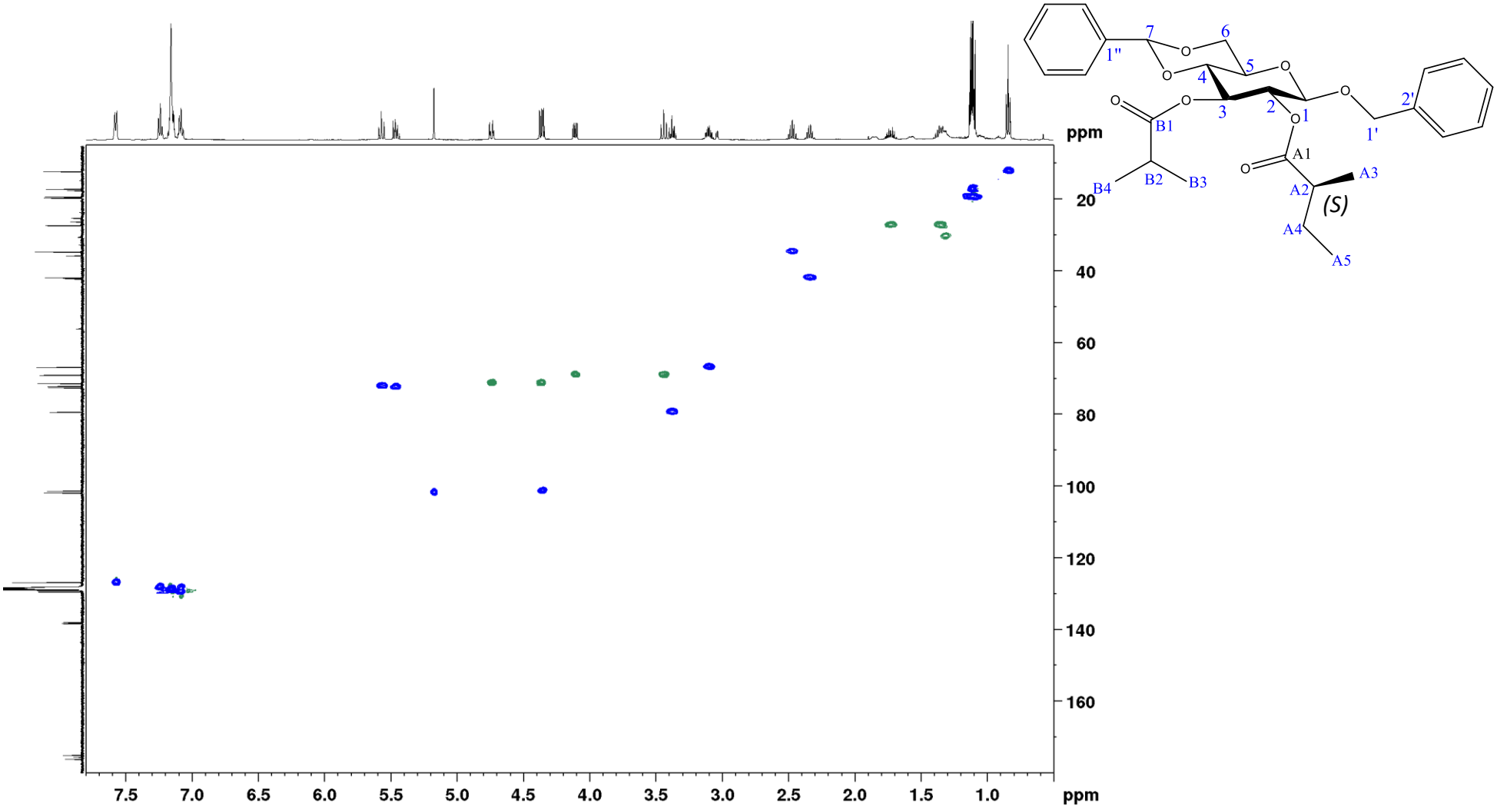

Figure S47: HSQC spectrum of compound **8**(*S*) (500 MHz, C_6D_6).

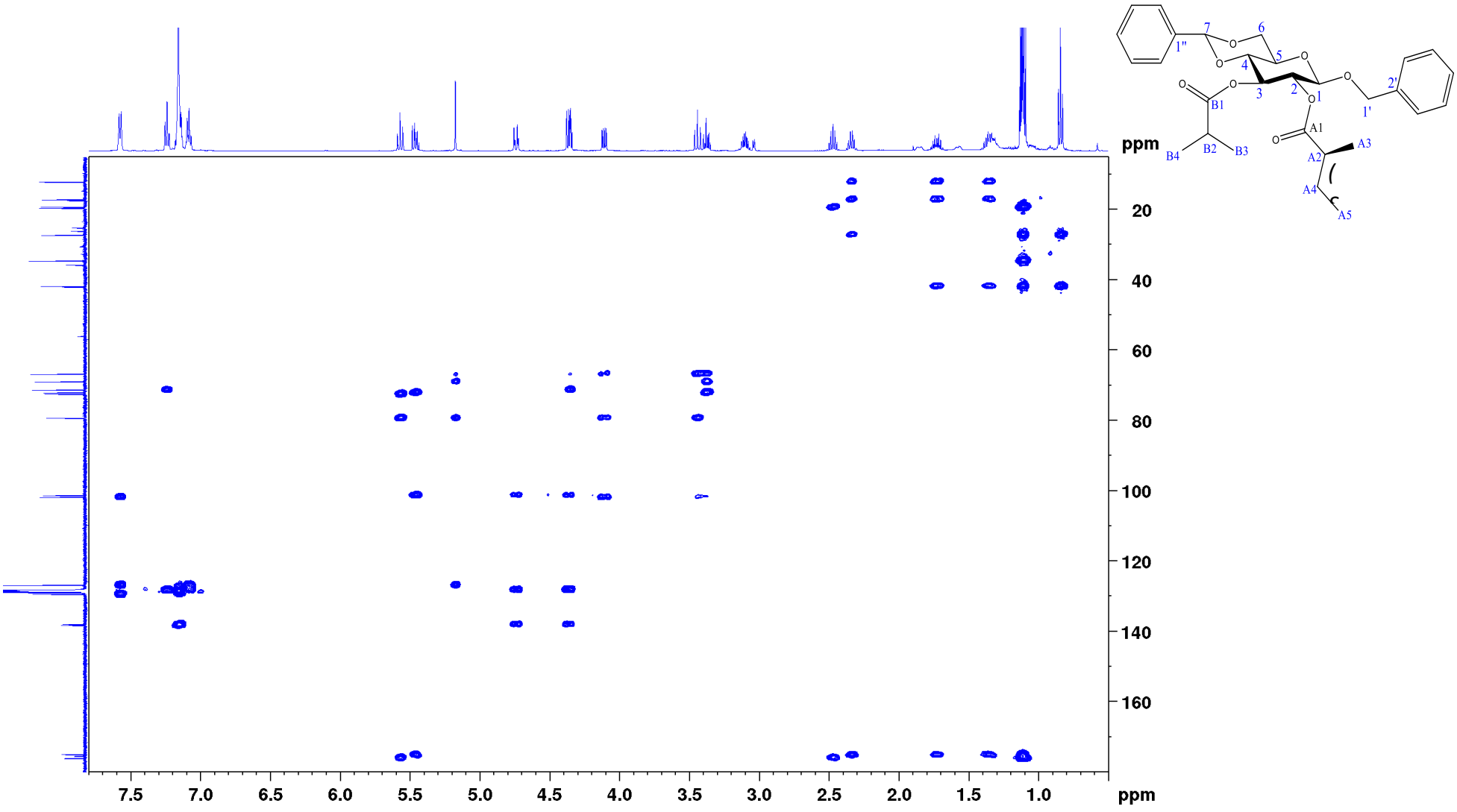

Figure S48: HMBC spectrum of compound **8(*S*)** (500 MHz, C_6D_6).

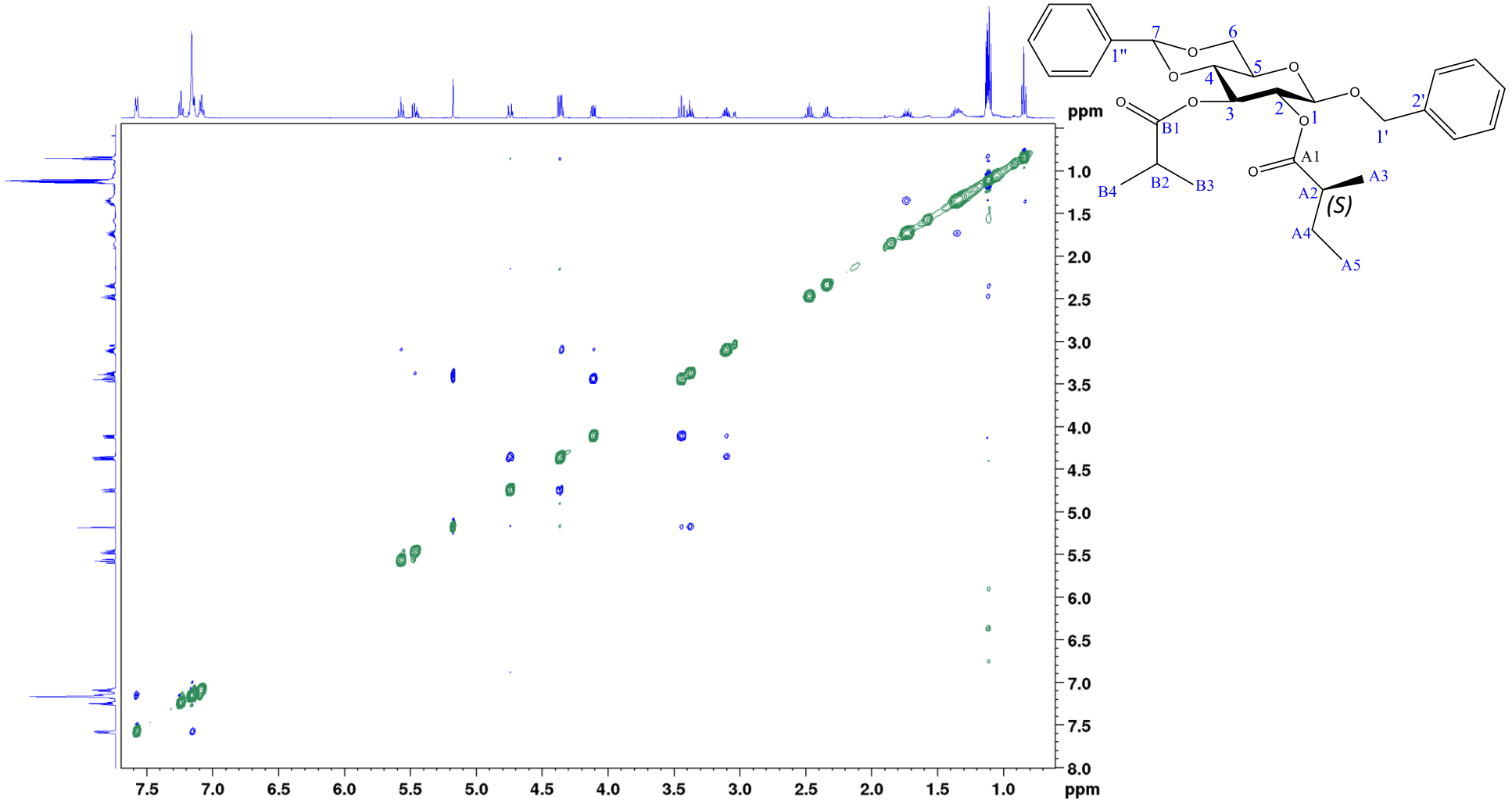

Figure S49: NOESY spectrum of compound **8(*S*)** (500 MHz, C_6D_6).

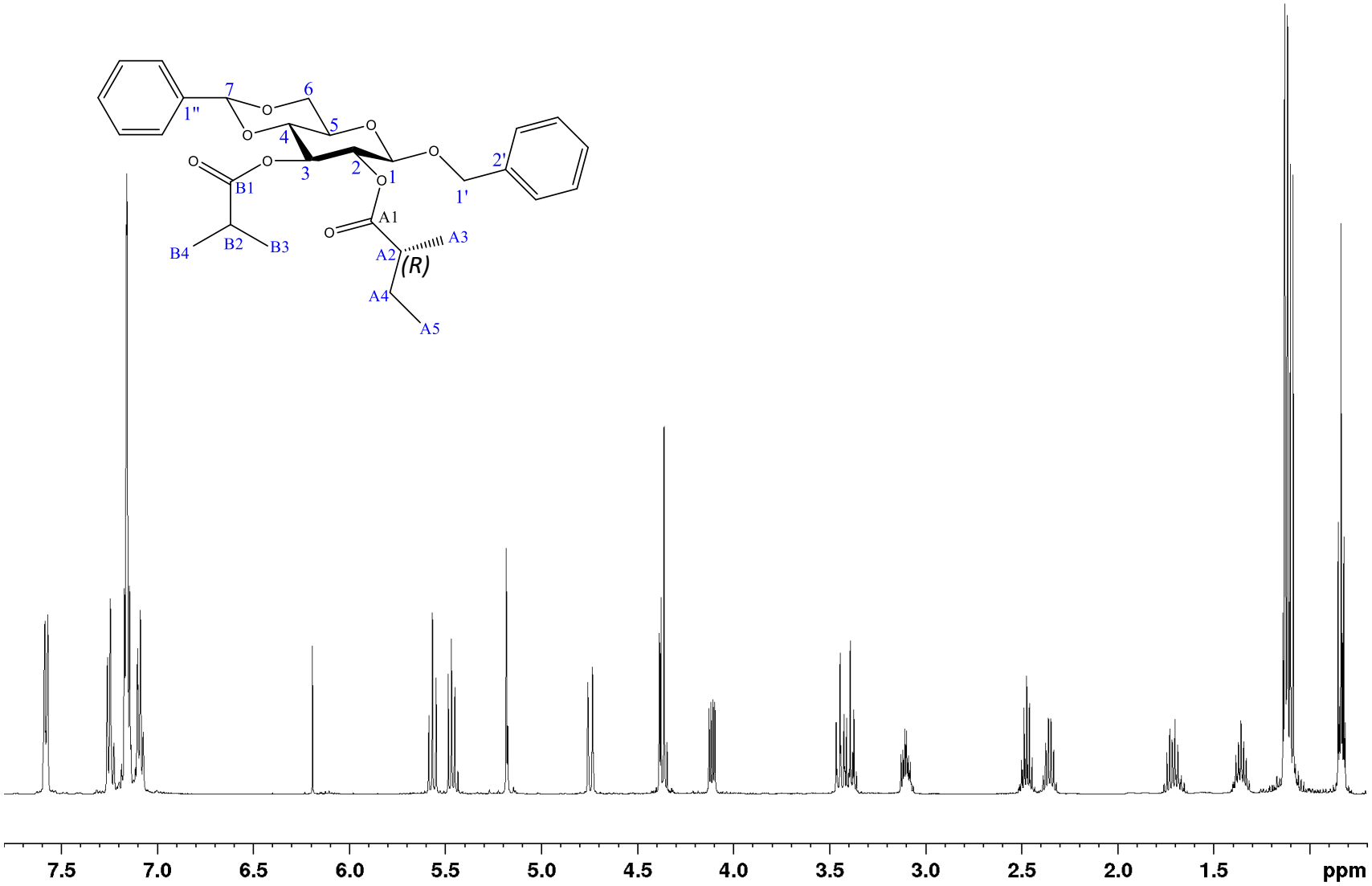

Figure S50: ^{1}H NMR spectrum of compound **8(*R*)** (500 MHz, C_6D_6).

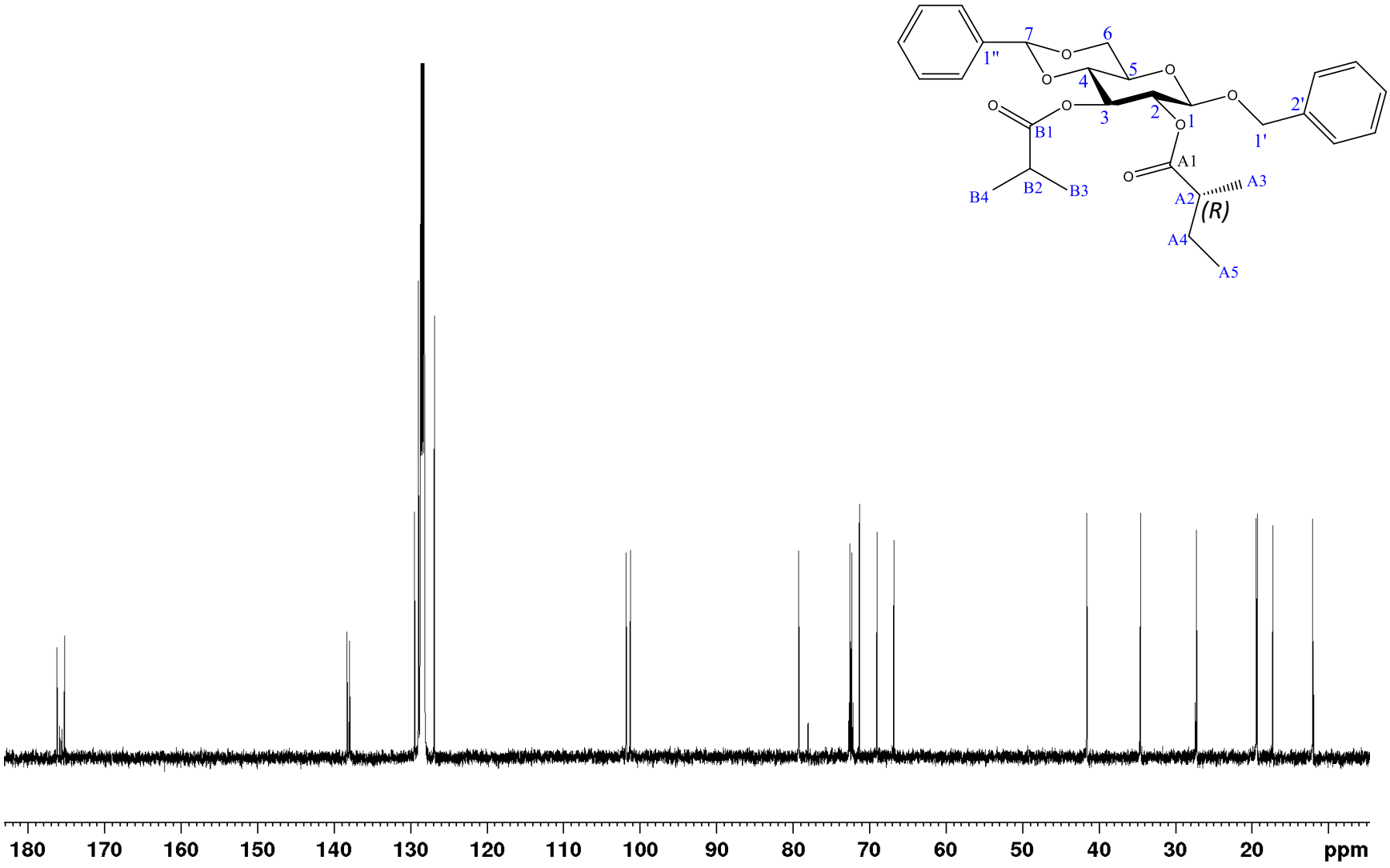

Figure S51: ^{13}C NMR spectrum of compound **8(*R*)** (126 MHz, C_6D_6).

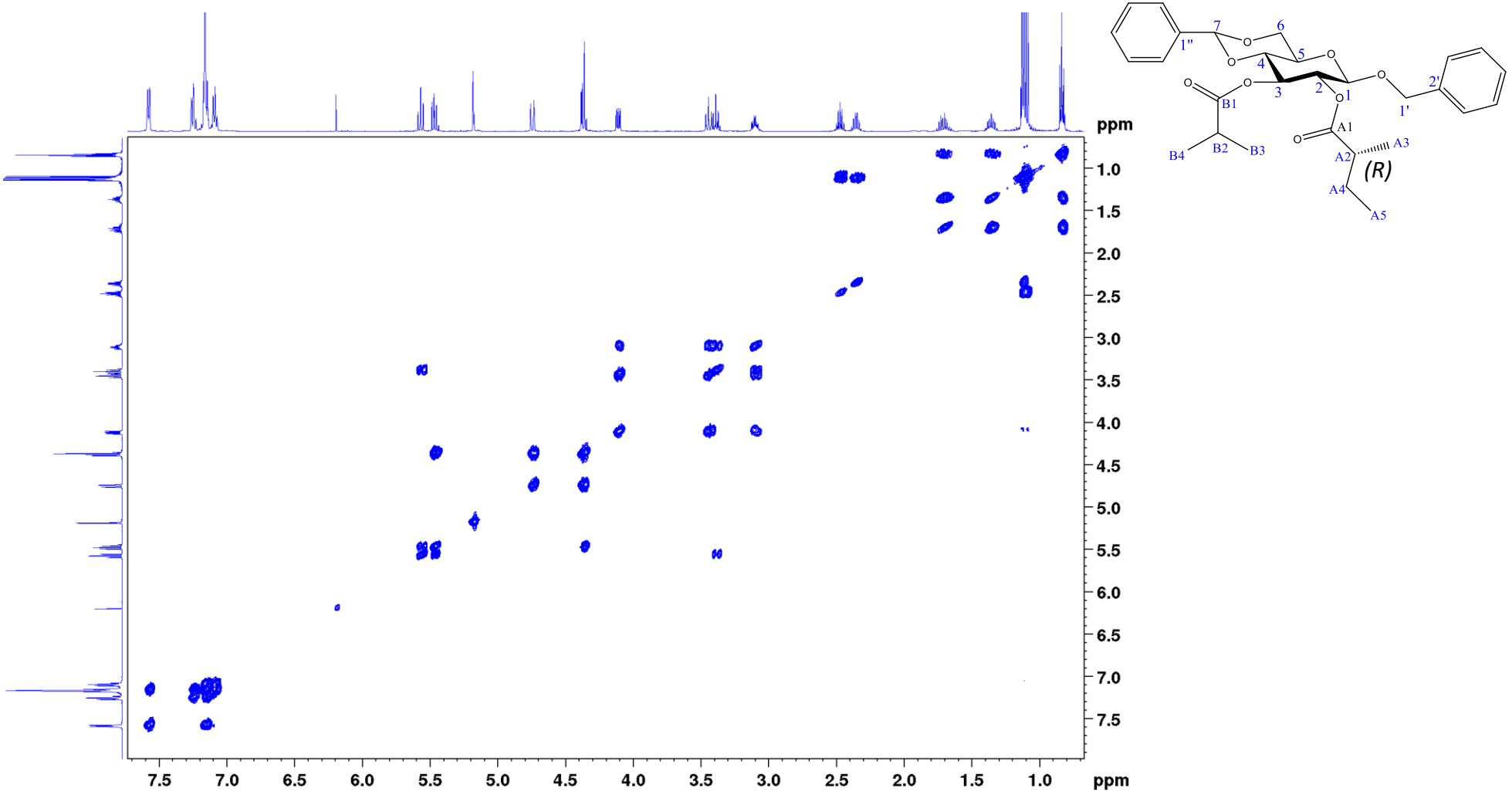

Figure S52: COSY spectrum of compound **8(*R*)** (500 MHz, C_6D_6).

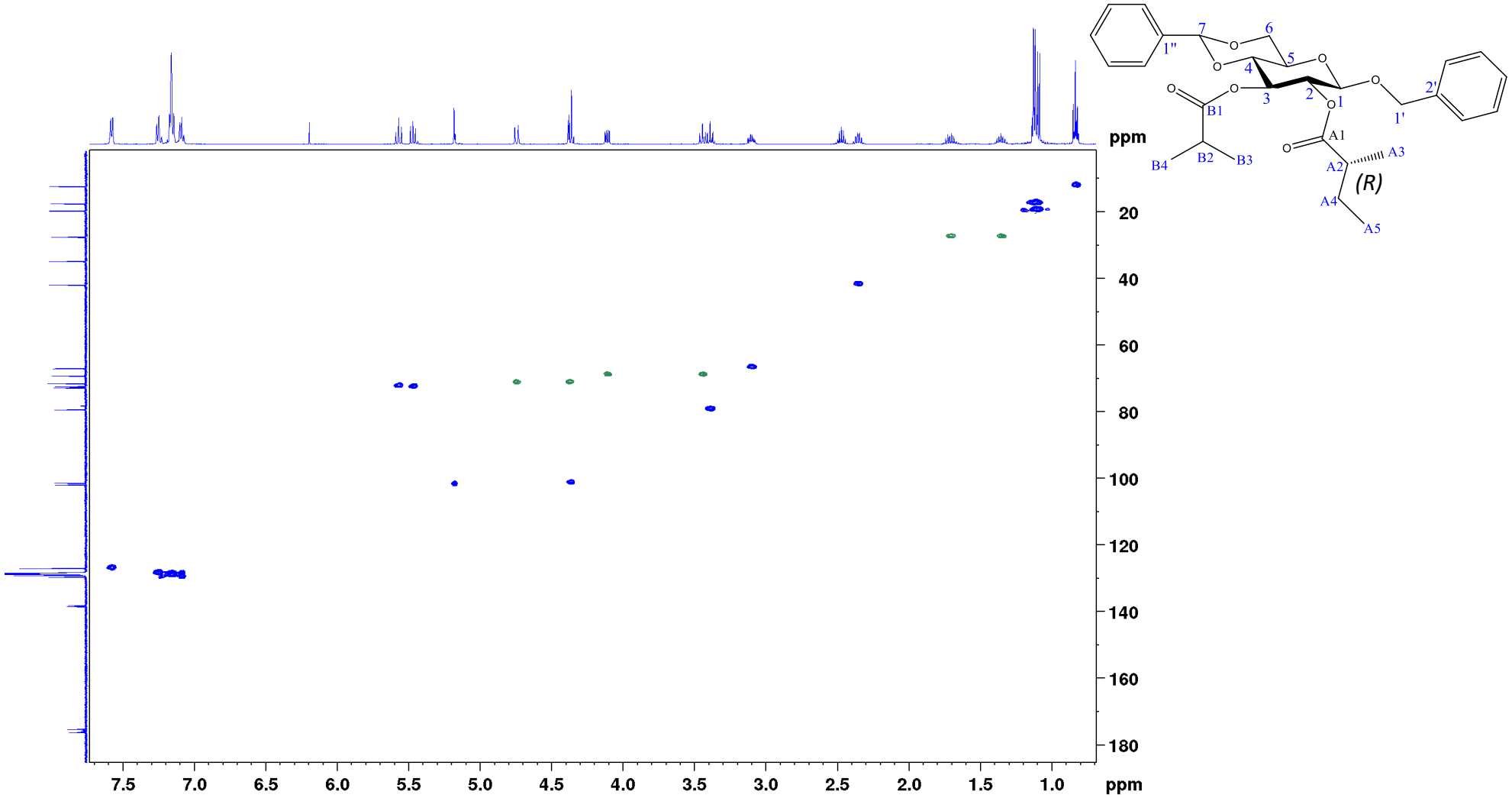

Figure S53: HSQC spectrum of compound **8(*R*)** (500 MHz, C_6D_6).

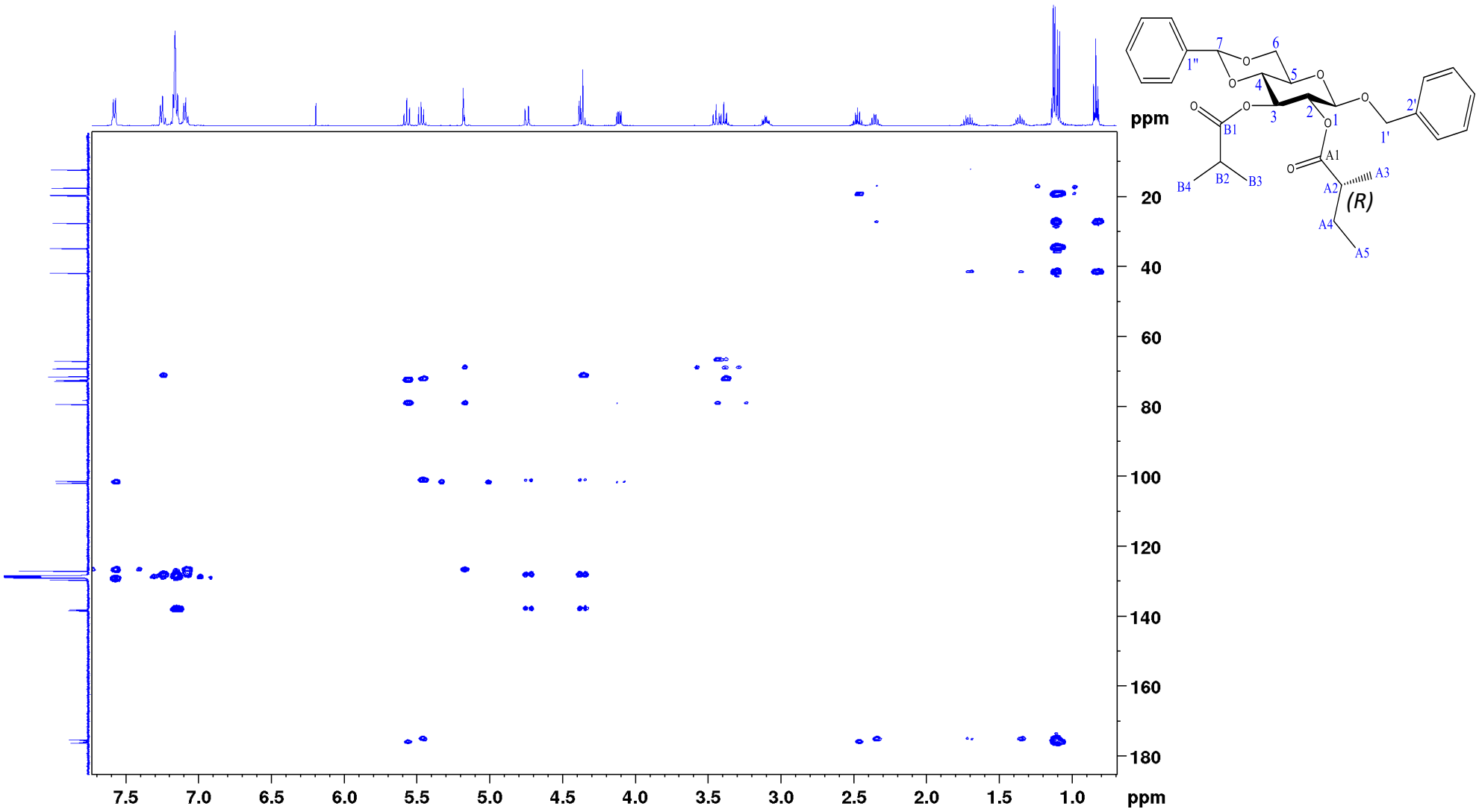

Figure S54: HMBC spectrum of compound **8(*R*)** (500 MHz, C_6D_6).

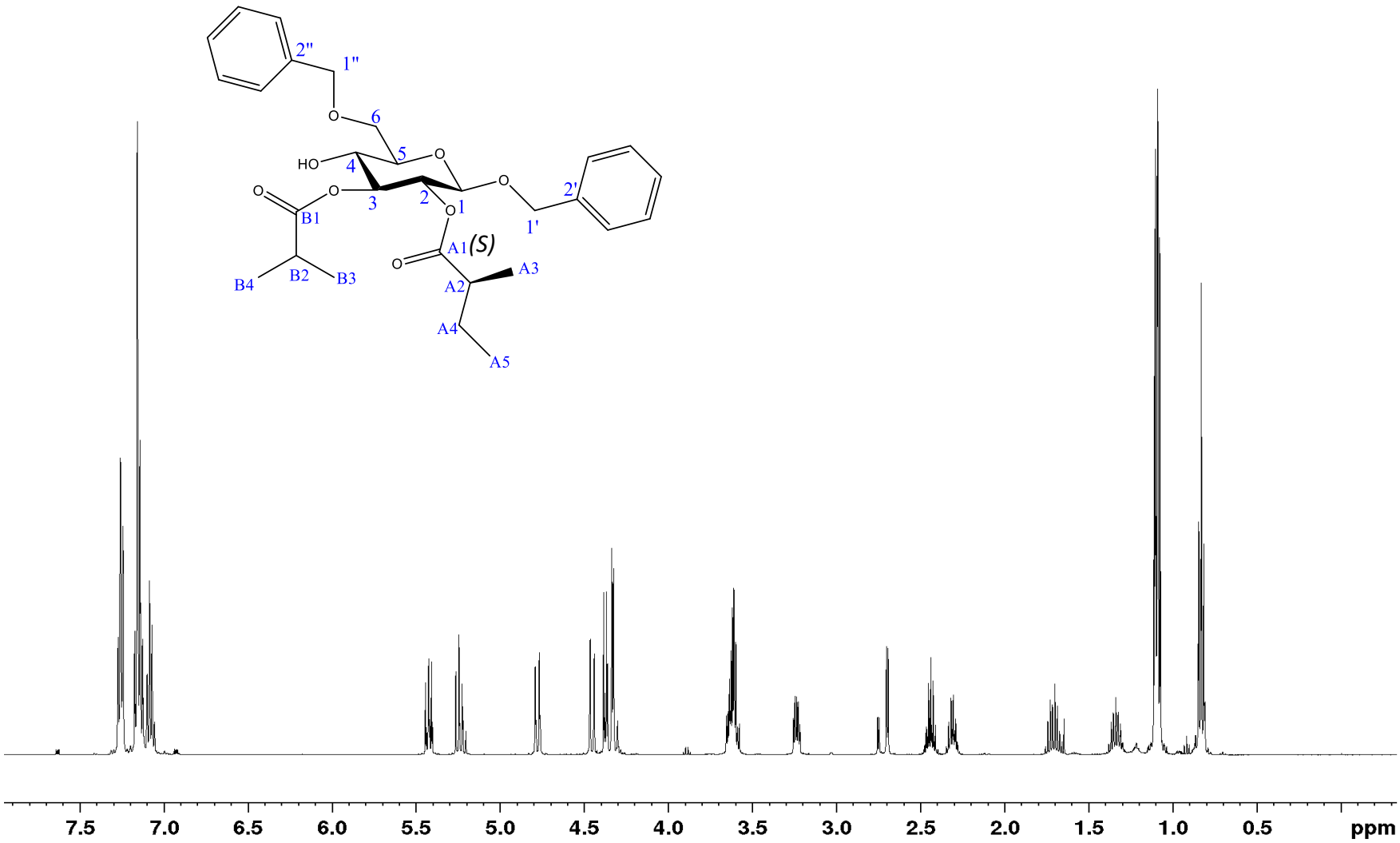

Figure S55: ^{1}H NMR spectrum of compound **9(*S*)** (500 MHz, C_6D_6).

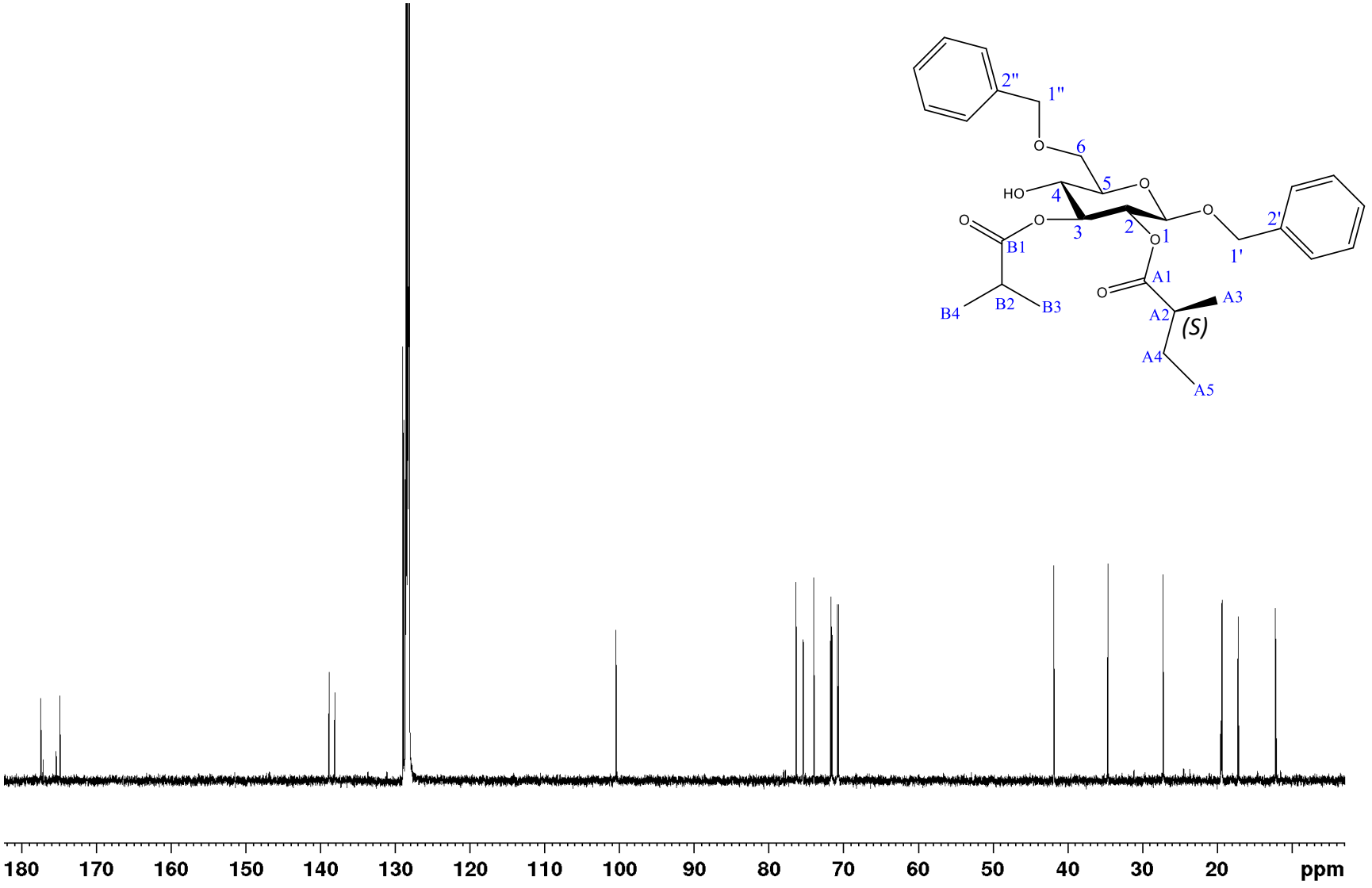

Figure S56: ^{13}C NMR spectrum of compound **9(*S*)** (126 MHz, C_6D_6).

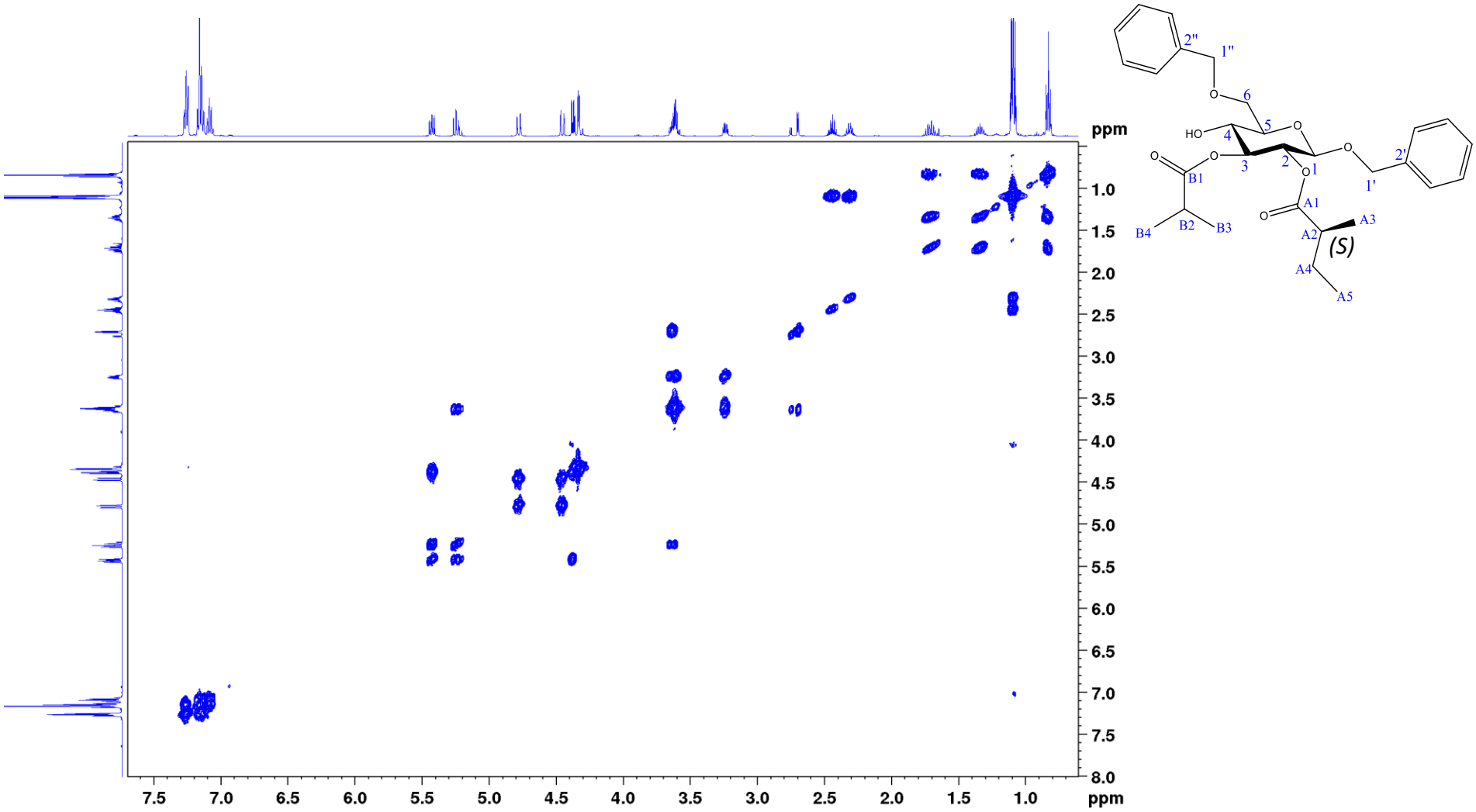

Figure S57: COSY spectrum of compound **9(*S*)** (500 MHz, C_6D_6).

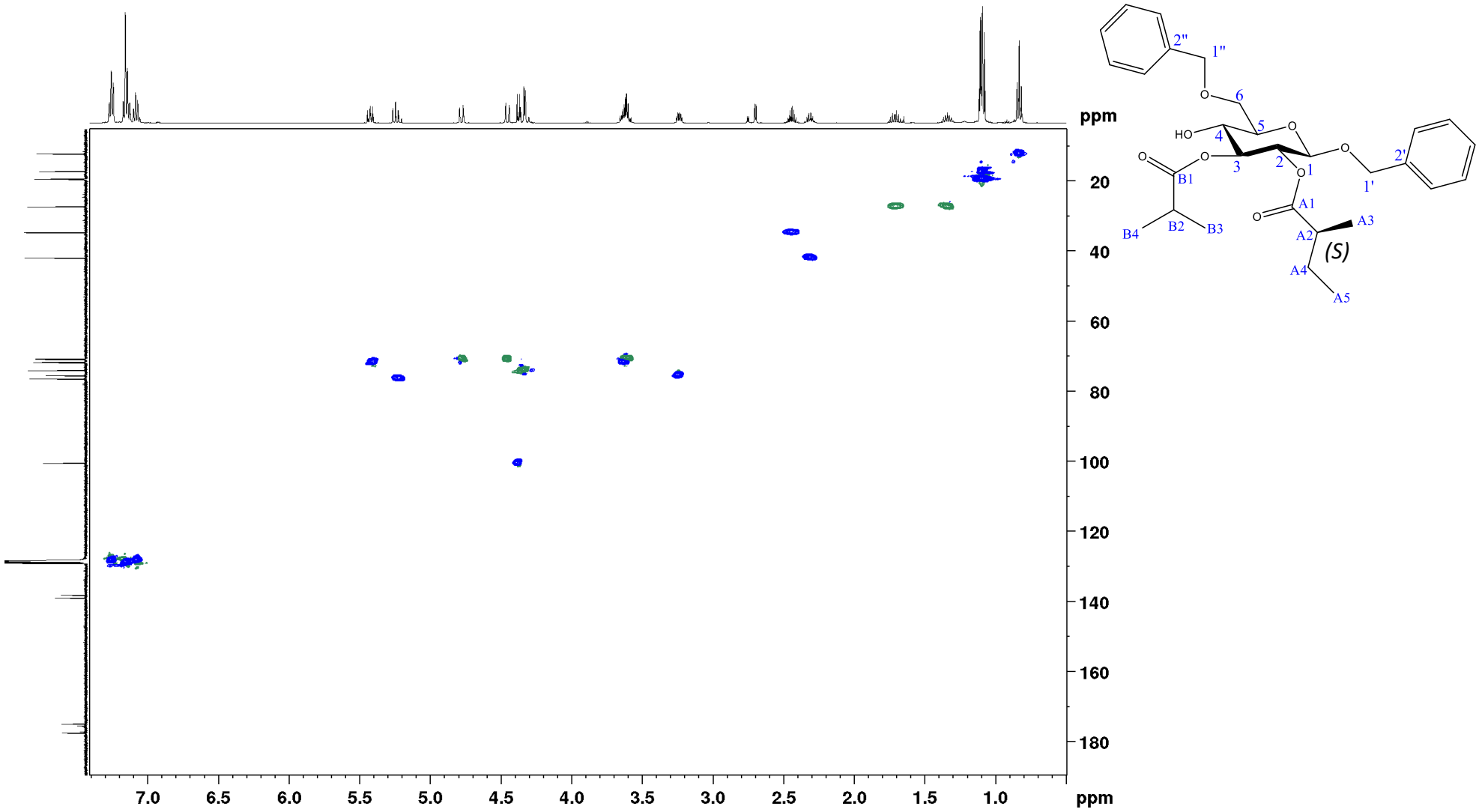

Figure S58: HSQC spectrum of compound **9(*S*)** (500 MHz, C_6D_6).

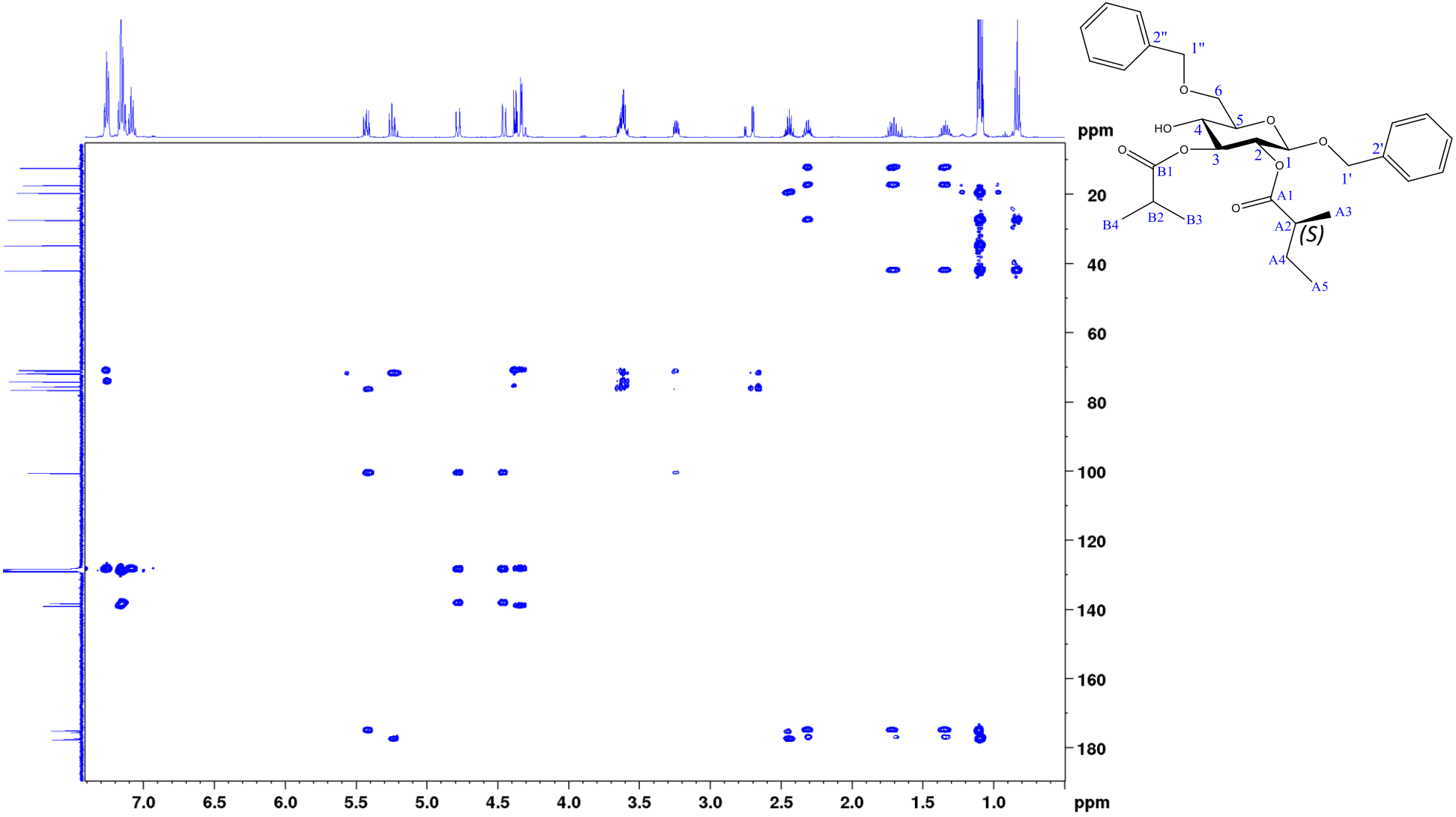

Figure S59: HMBC spectrum of compound **9(*S*)** (500 MHz, C_6D_6).

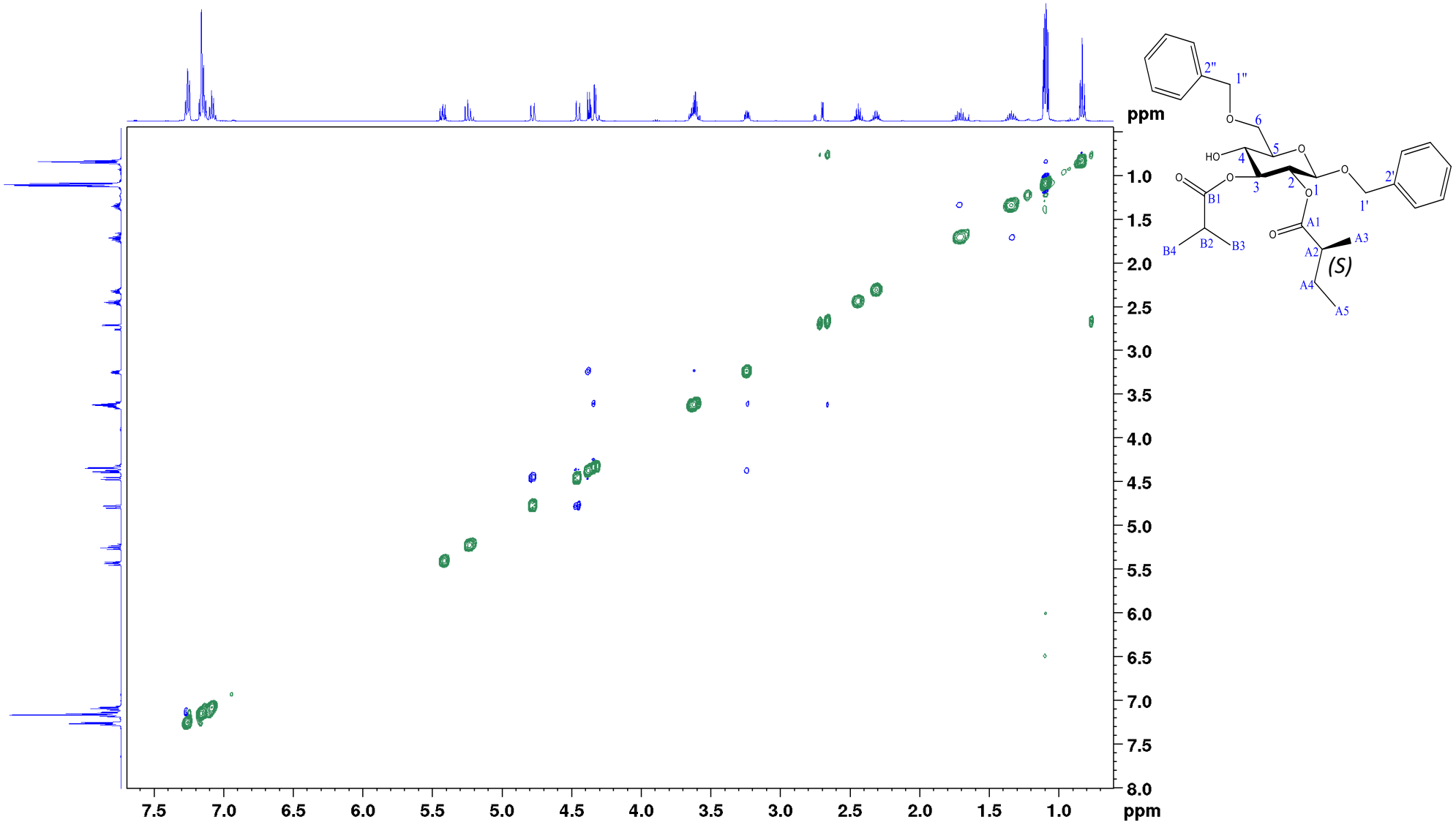

Figure S60: NOESY spectrum of compound **9***(S)* (500 MHz, C_6D_6).

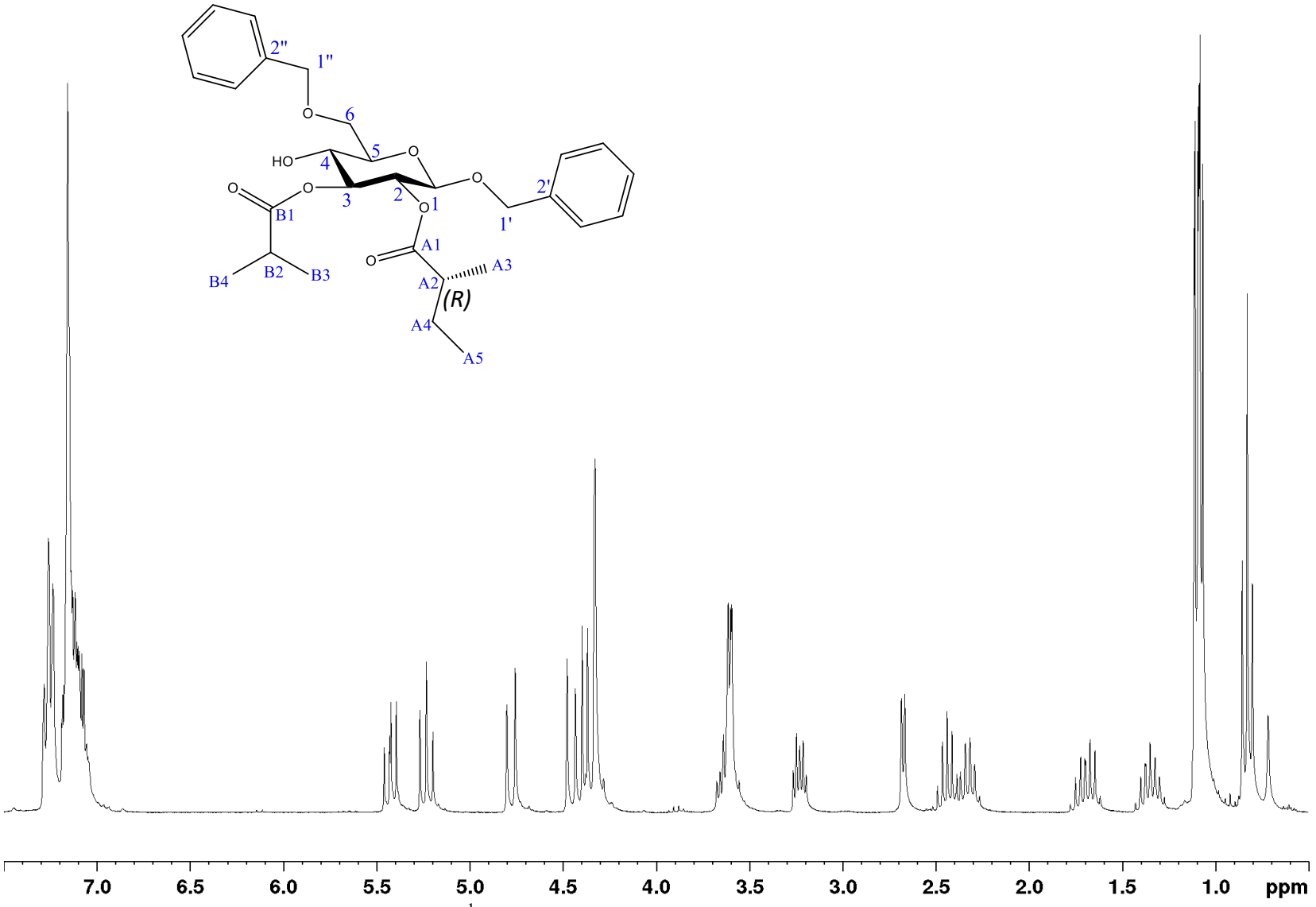

Figure S61: ^{1}H NMR spectrum of compound **9(*R*)** (270 MHz, C_6D_6).

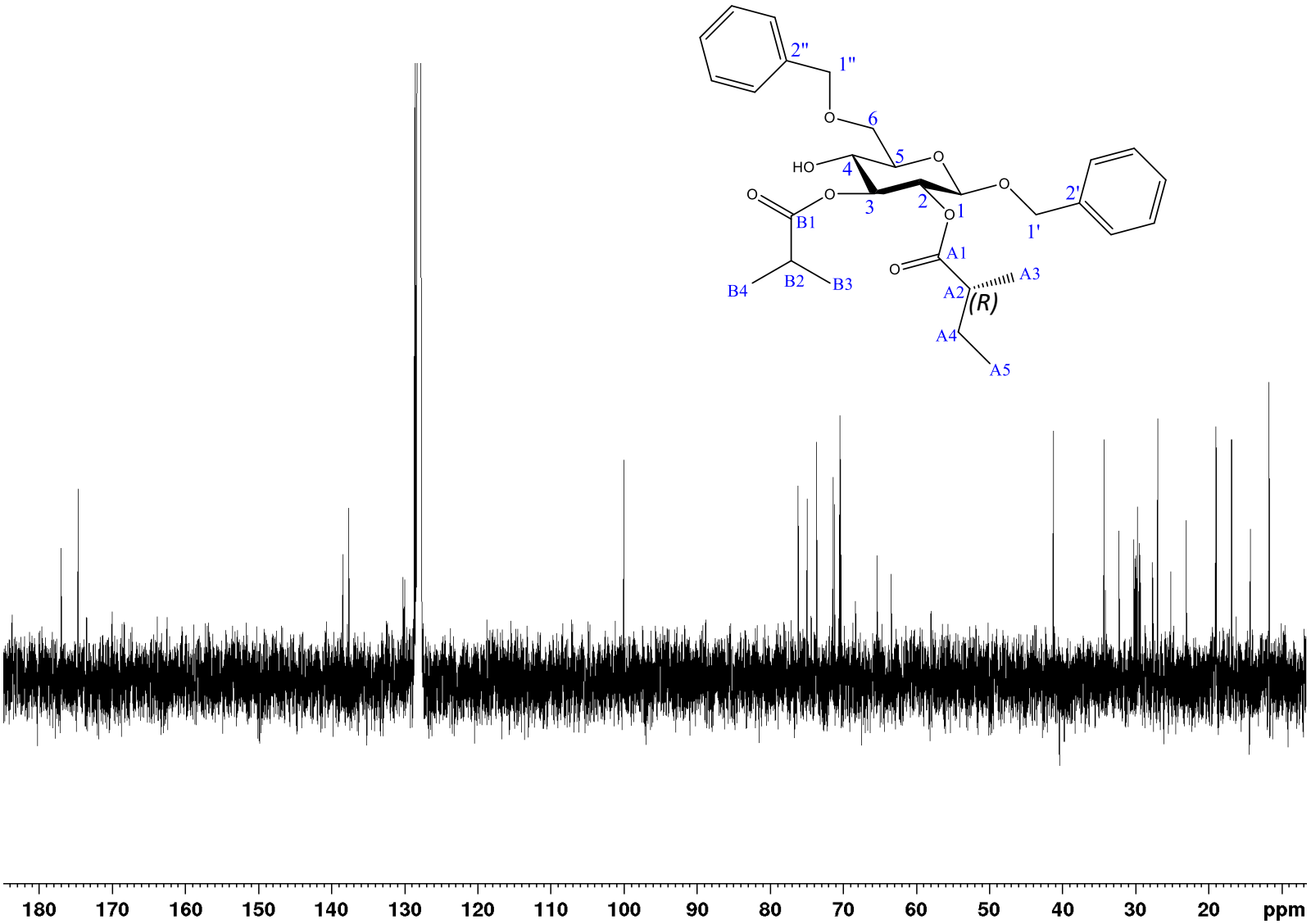

Figure S62: ^{13}C NMR spectrum of compound **9(*R*)** (126 MHz, C_6D_6).

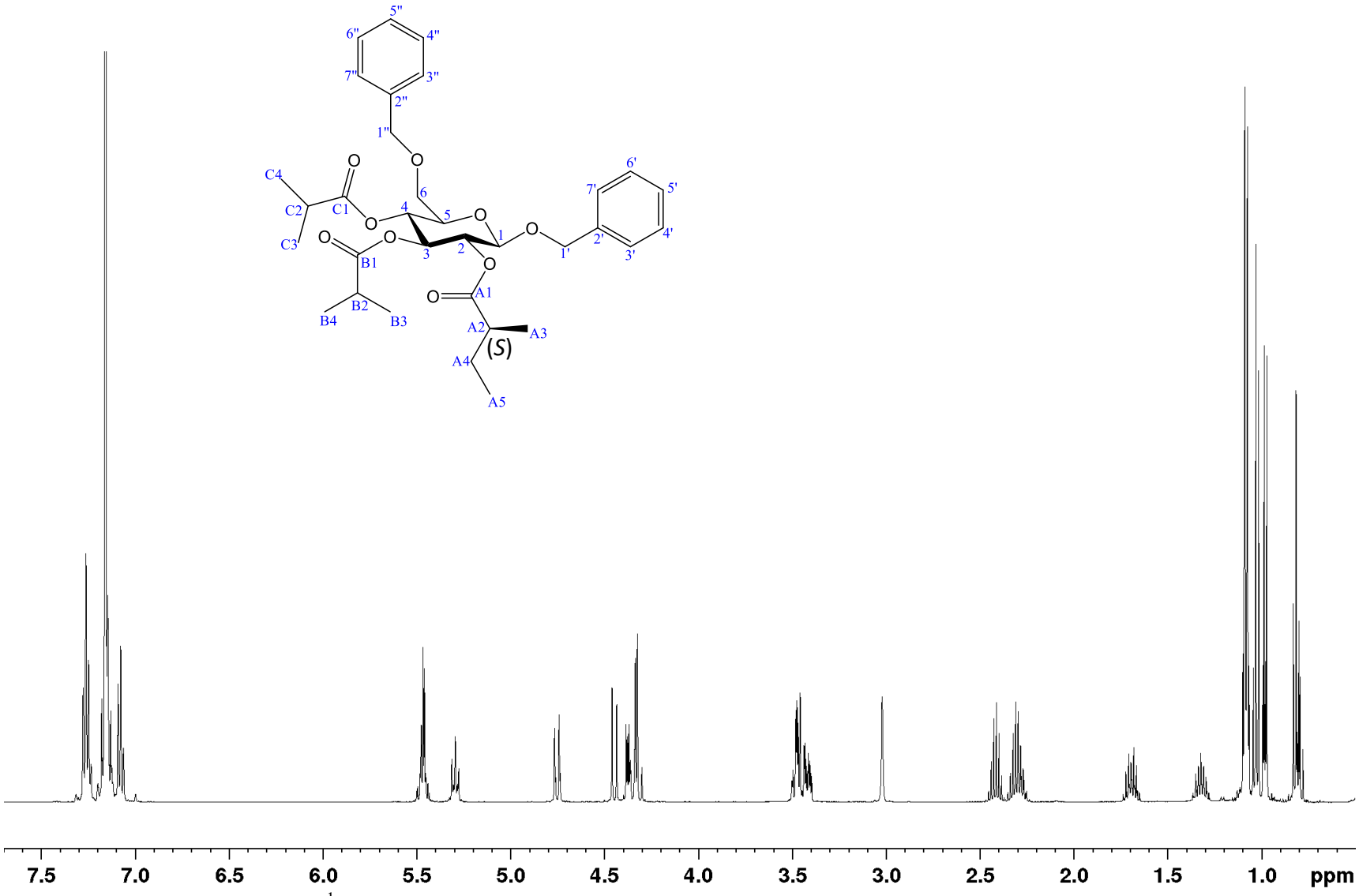

Figure S63: ^{1}H NMR spectrum of synthesized dibenzyl pennelliiside D [**2(*S*)**] (500 MHz, C_6D_6).

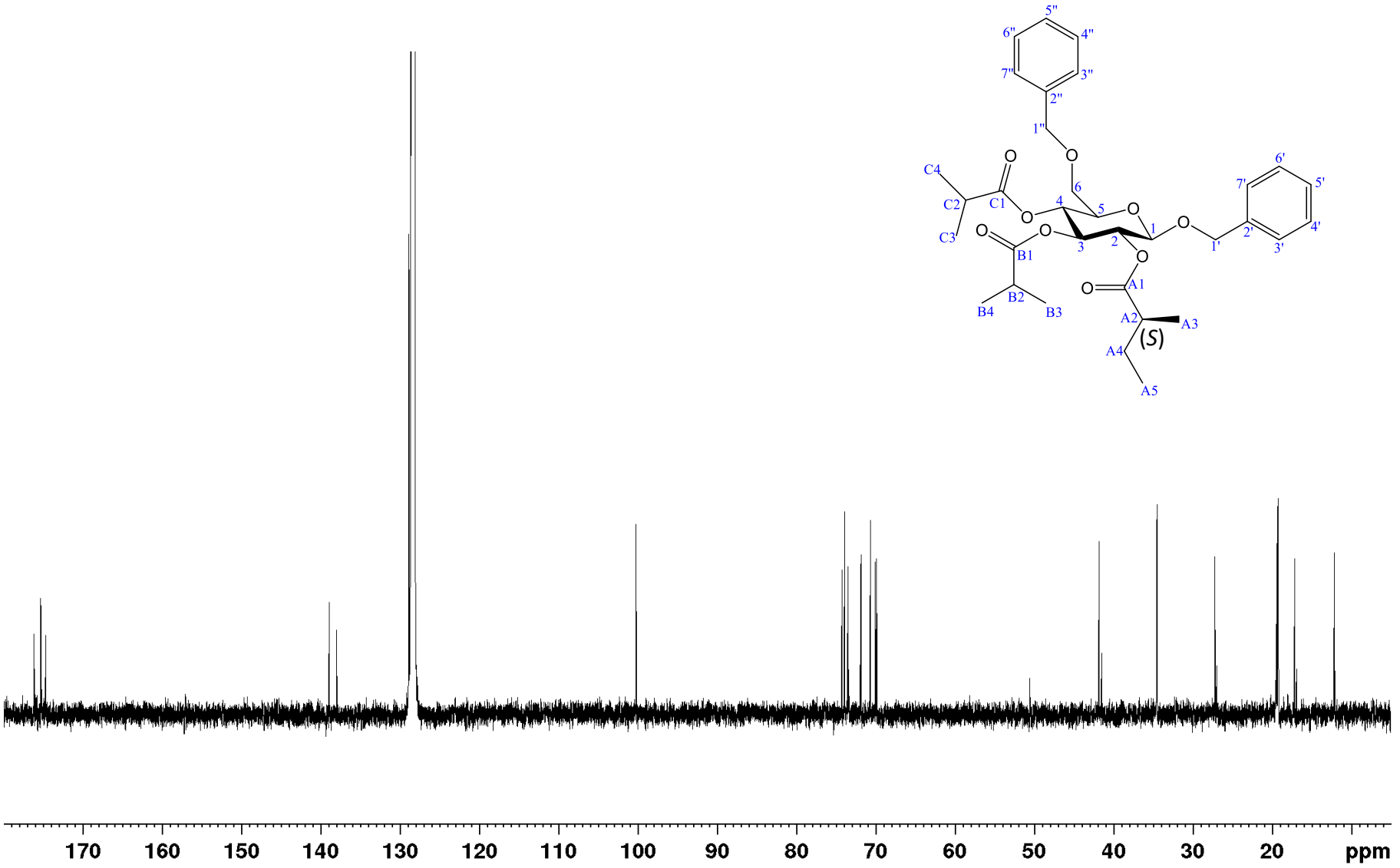

Figure S64: ^{13}C NMR spectrum of synthesized dibenzyl pennelliiside D [**2(*S*)**] (126 MHz, C_6D_6).

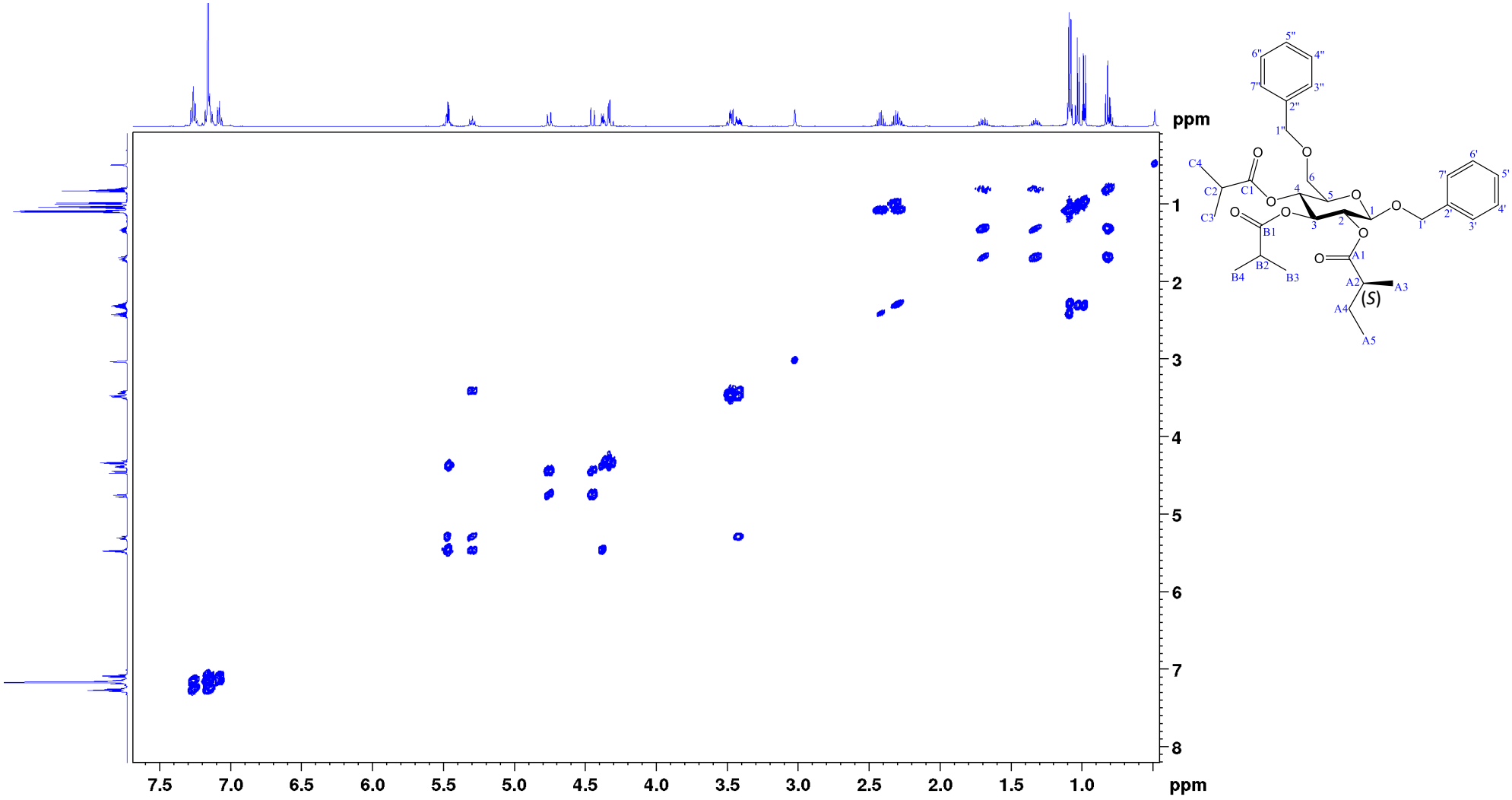

Figure S65: COSY spectrum of synthesized dibenzyl pennelliiside D [**2(*S*)**] (500 MHz, C_6D_6).

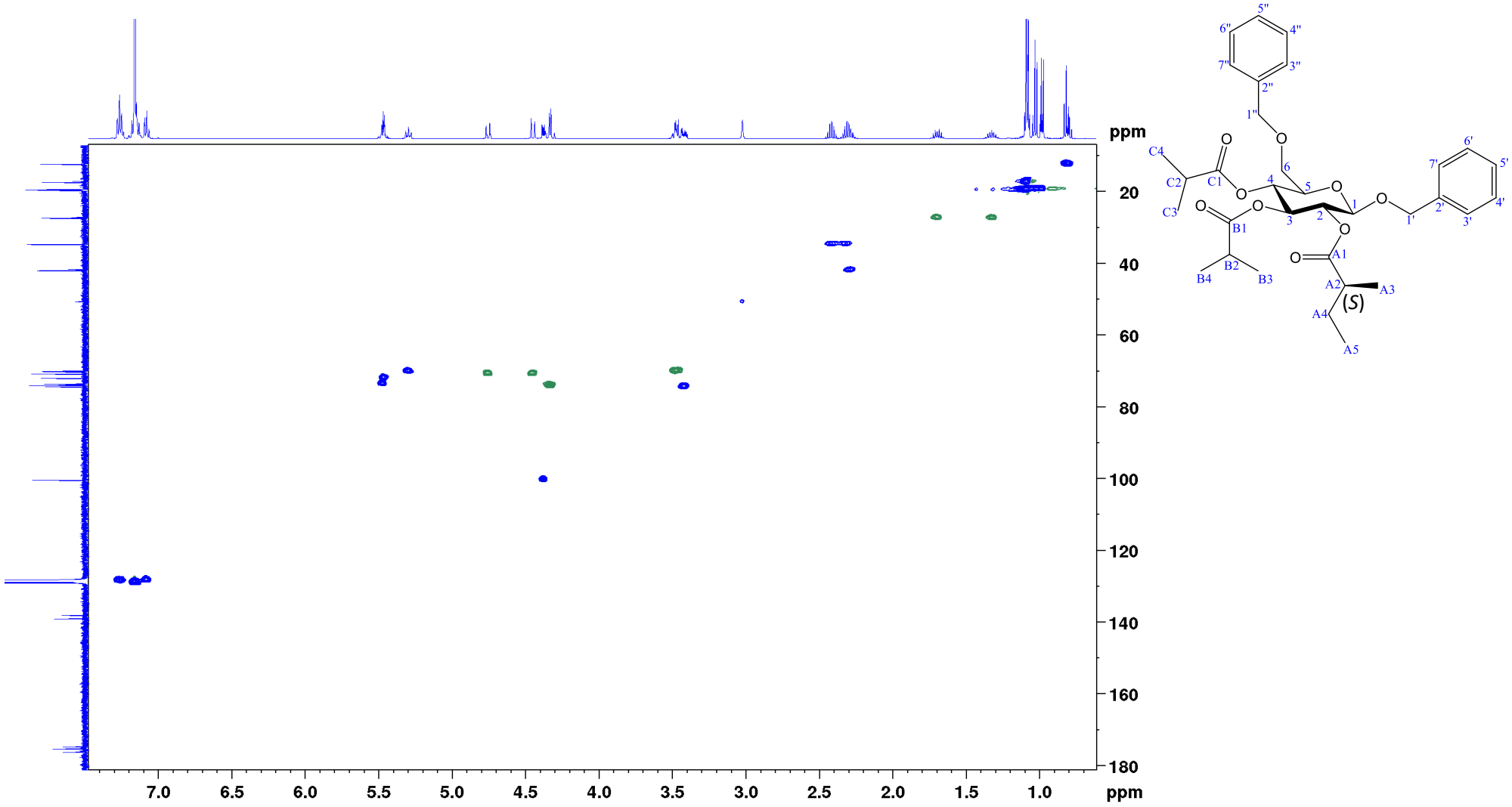

Figure S66: HSQC spectrum of synthesized dibenzyl pennelliiside D [**2(*S*)**] (500 MHz, C_6D_6).

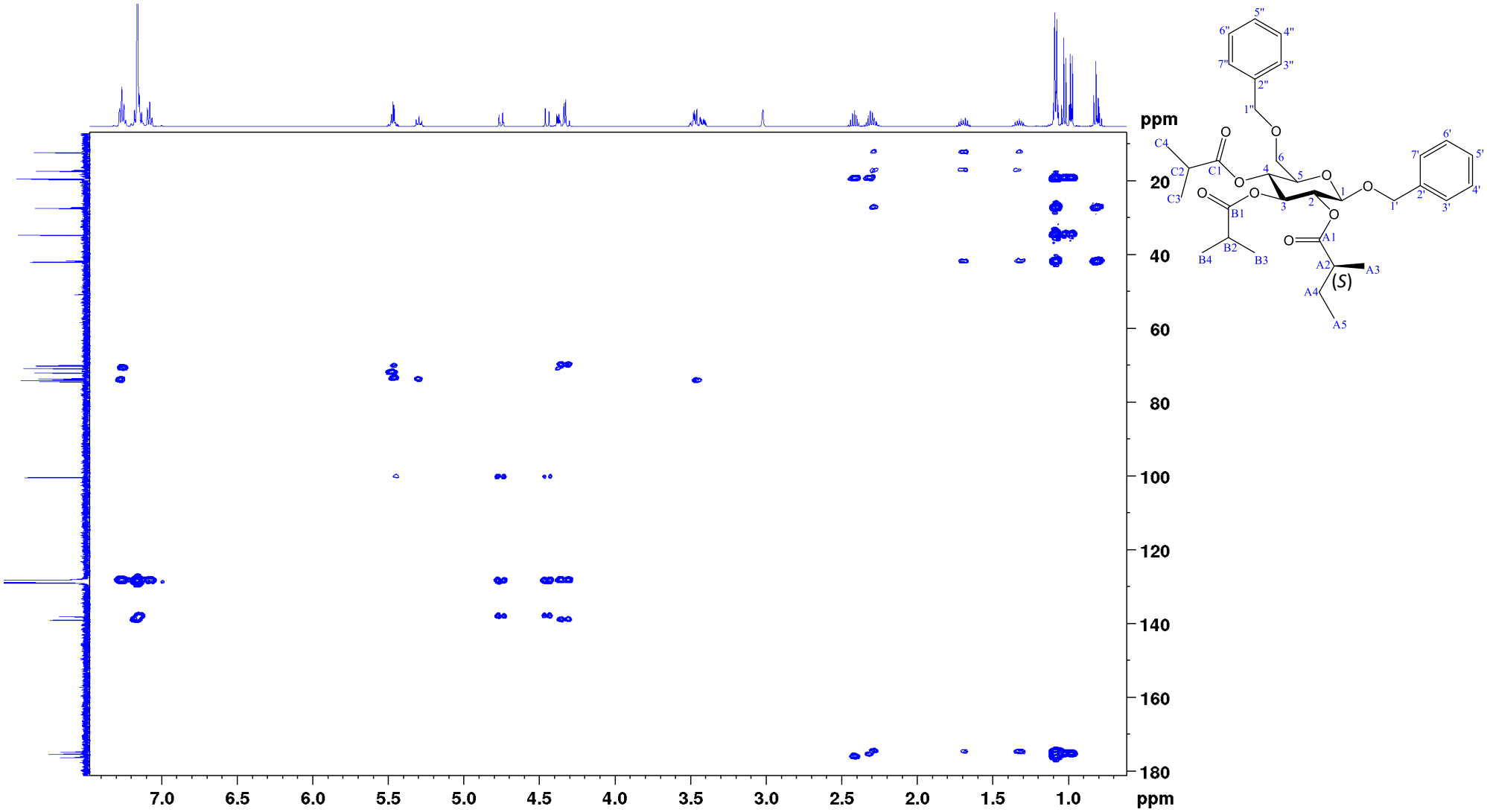

Figure S67: HMBC spectrum of synthesized dibenzyl pennelliiside D [**2(*S*)**] (500 MHz, C_6D_6).

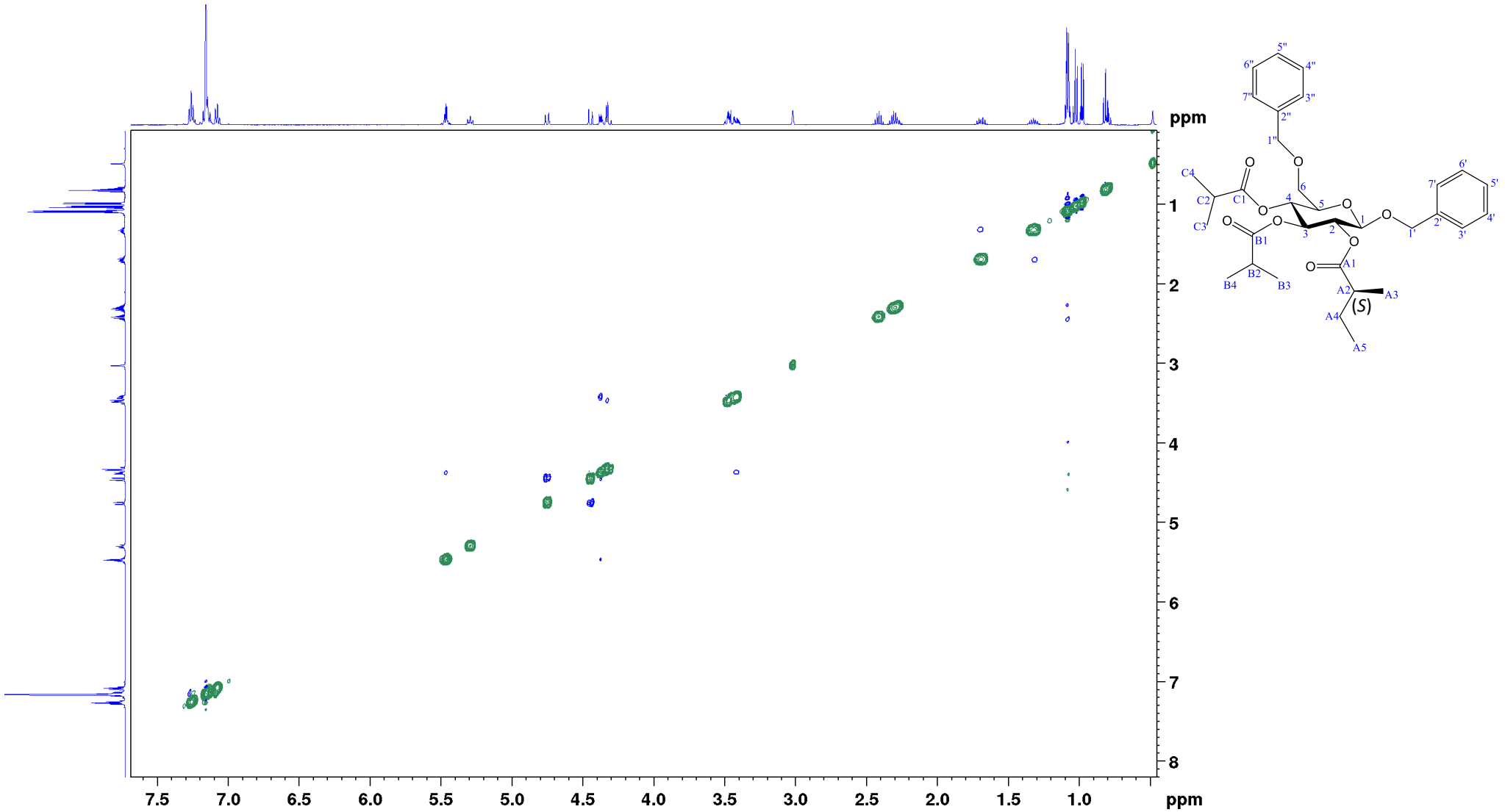

Figure S68: NOESY spectrum of synthesized dibenzyl pennelliiside D [**2(*S*)**] (500 MHz, C_6D_6).

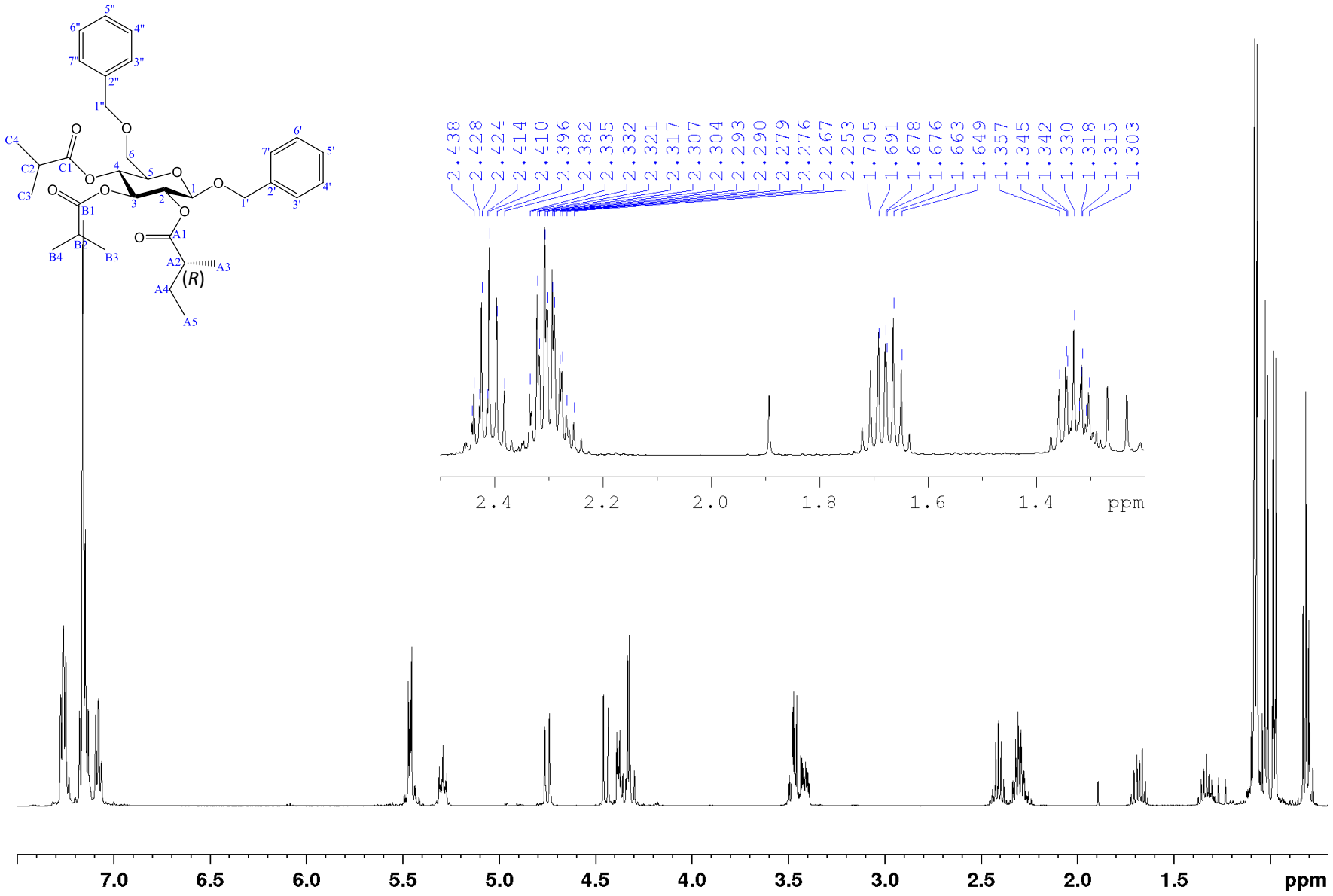

Figure S69: ^{1}H NMR spectrum of compound [**2(*R*)**] (500 MHz, C_6D_6).

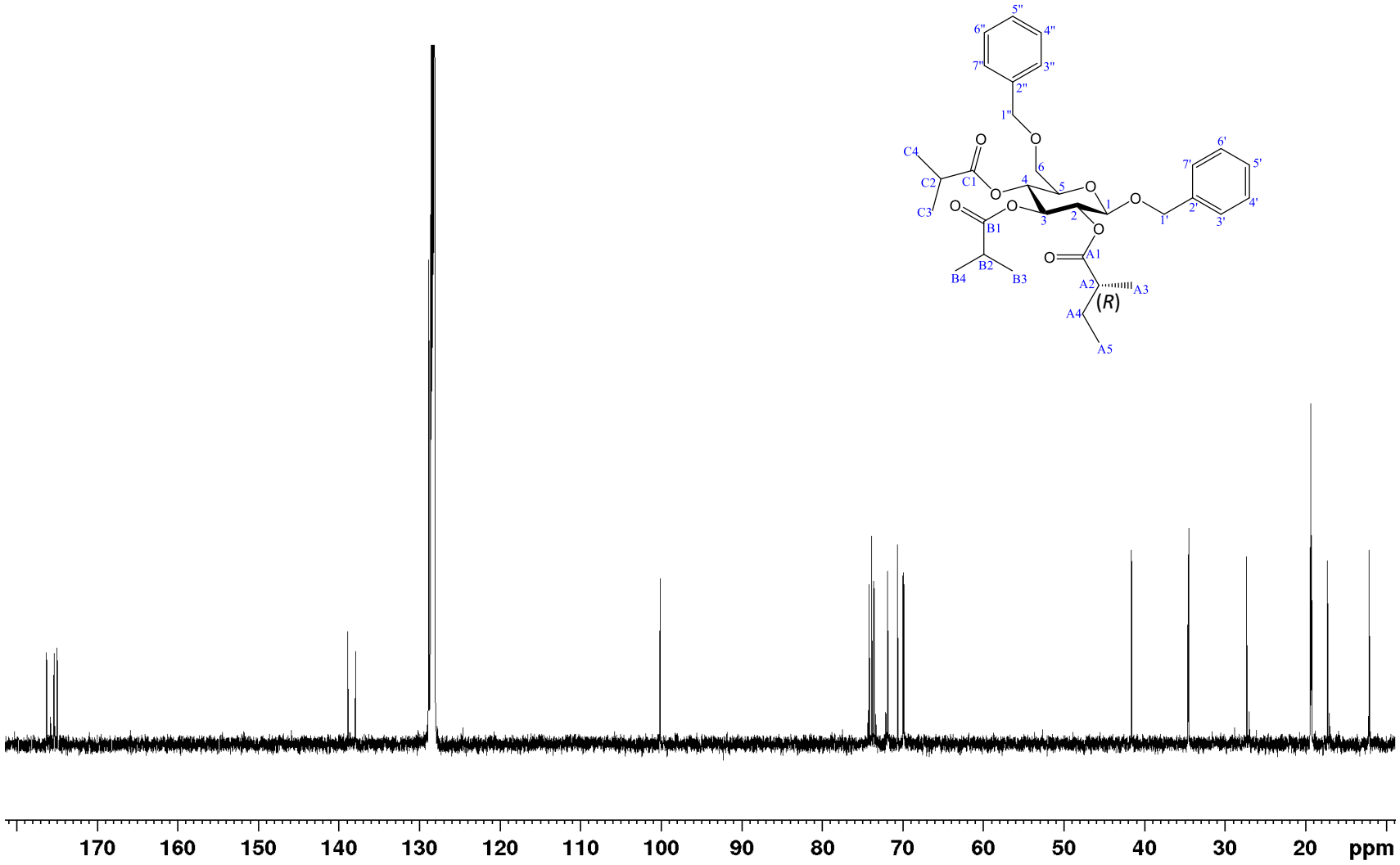

Figure S70: ^{13}C NMR spectrum of compound [**2(*R*)**] (126 MHz, C_6D_6).

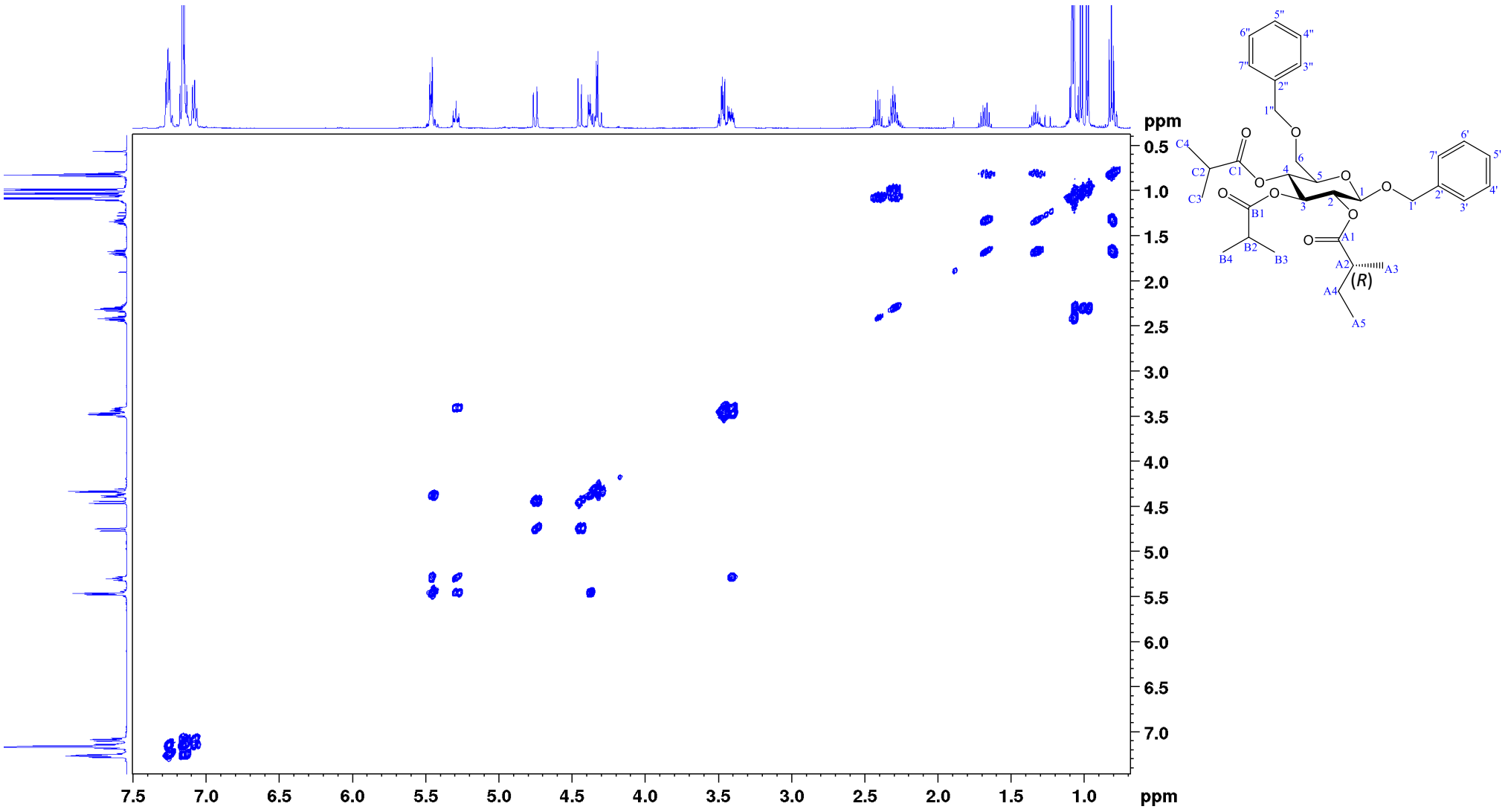

Figure S71: COSY spectrum of compound [**2(*R*)**] (500 MHz, C_6D_6).

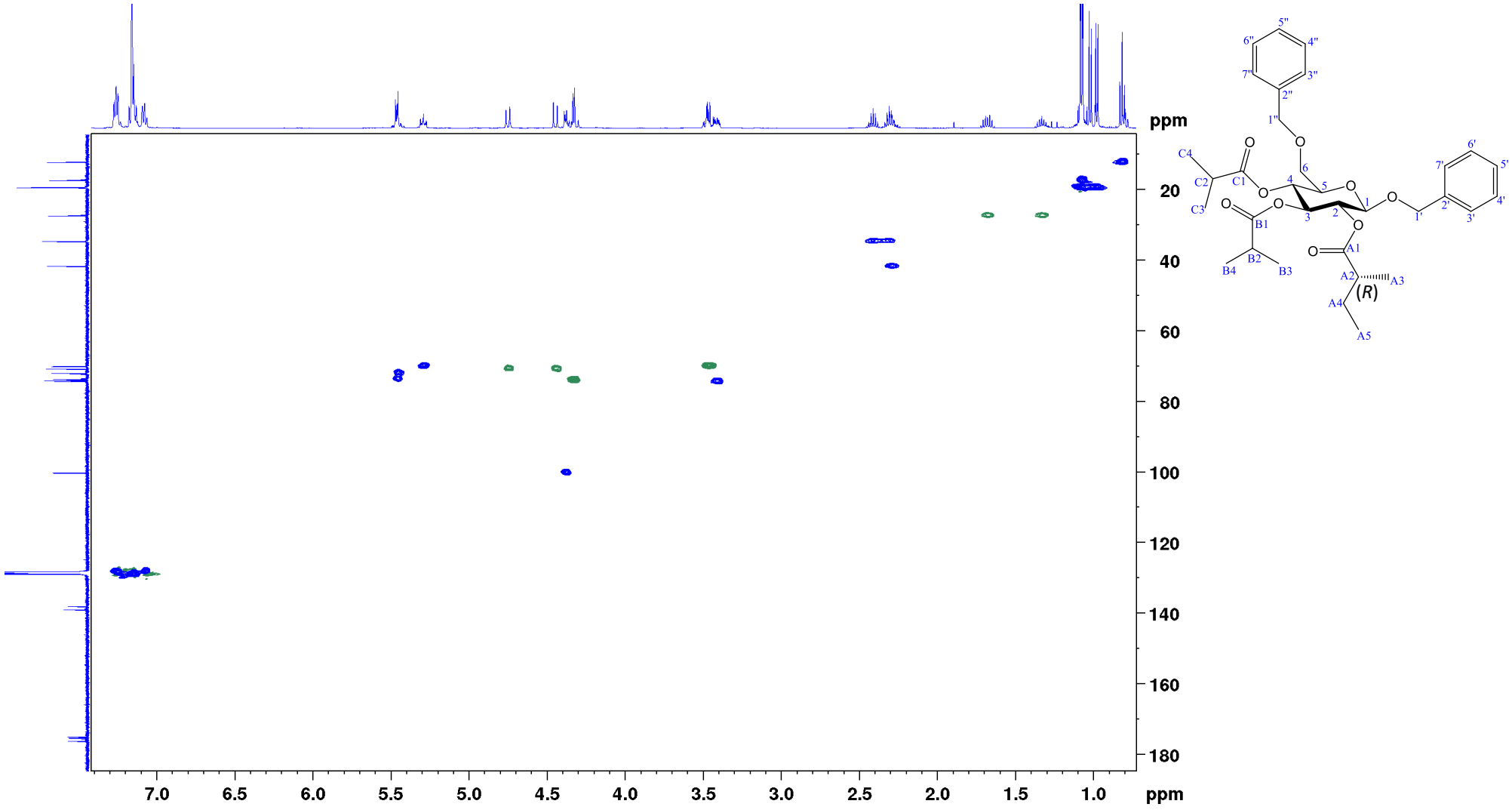

Figure S72: HSQC spectrum compound **[2(*R*)]** (500 MHz, C_6D_6).

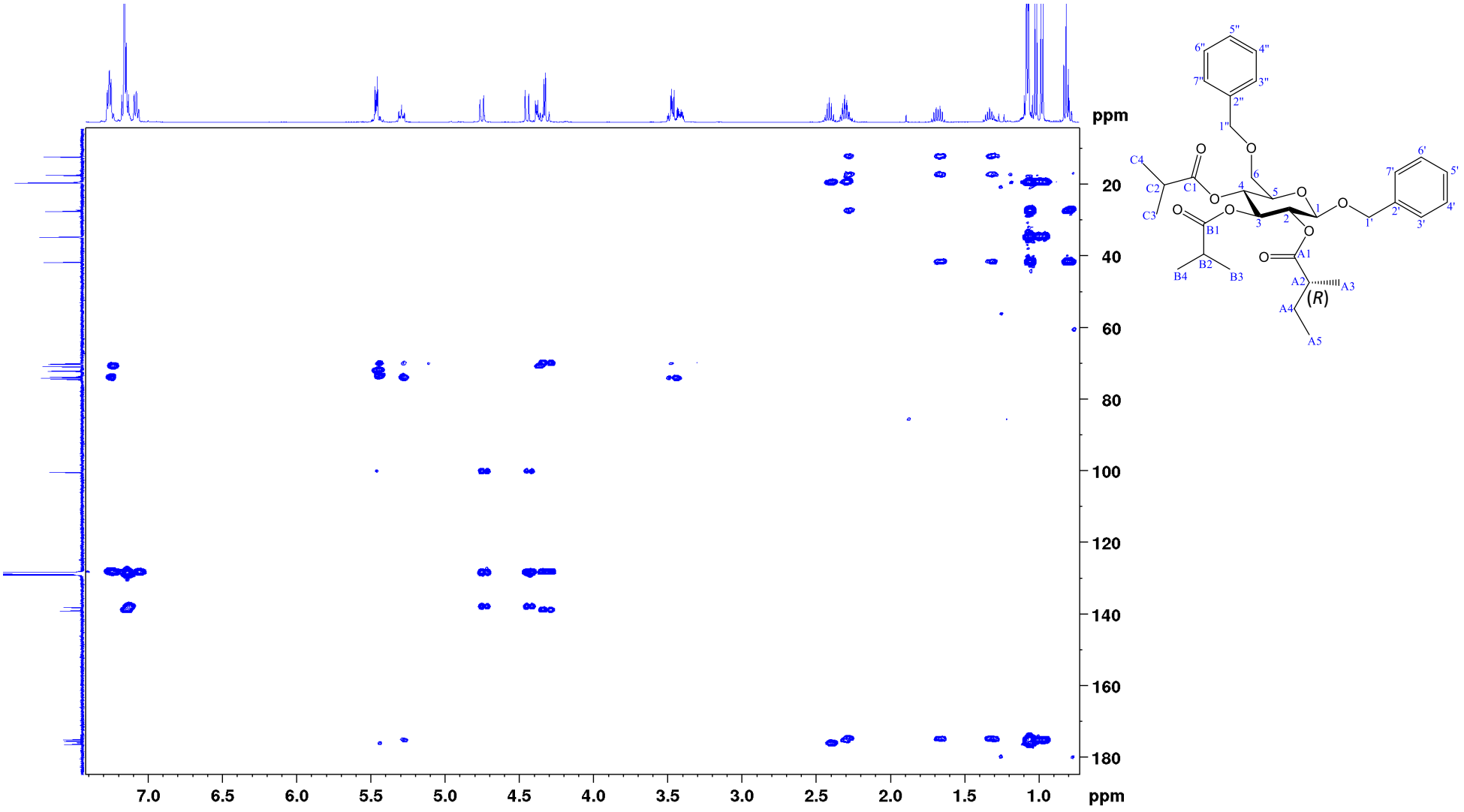

Figure S73: HMBC spectrum of compound [**2(*R*)**] (500 MHz, C_6D_6).

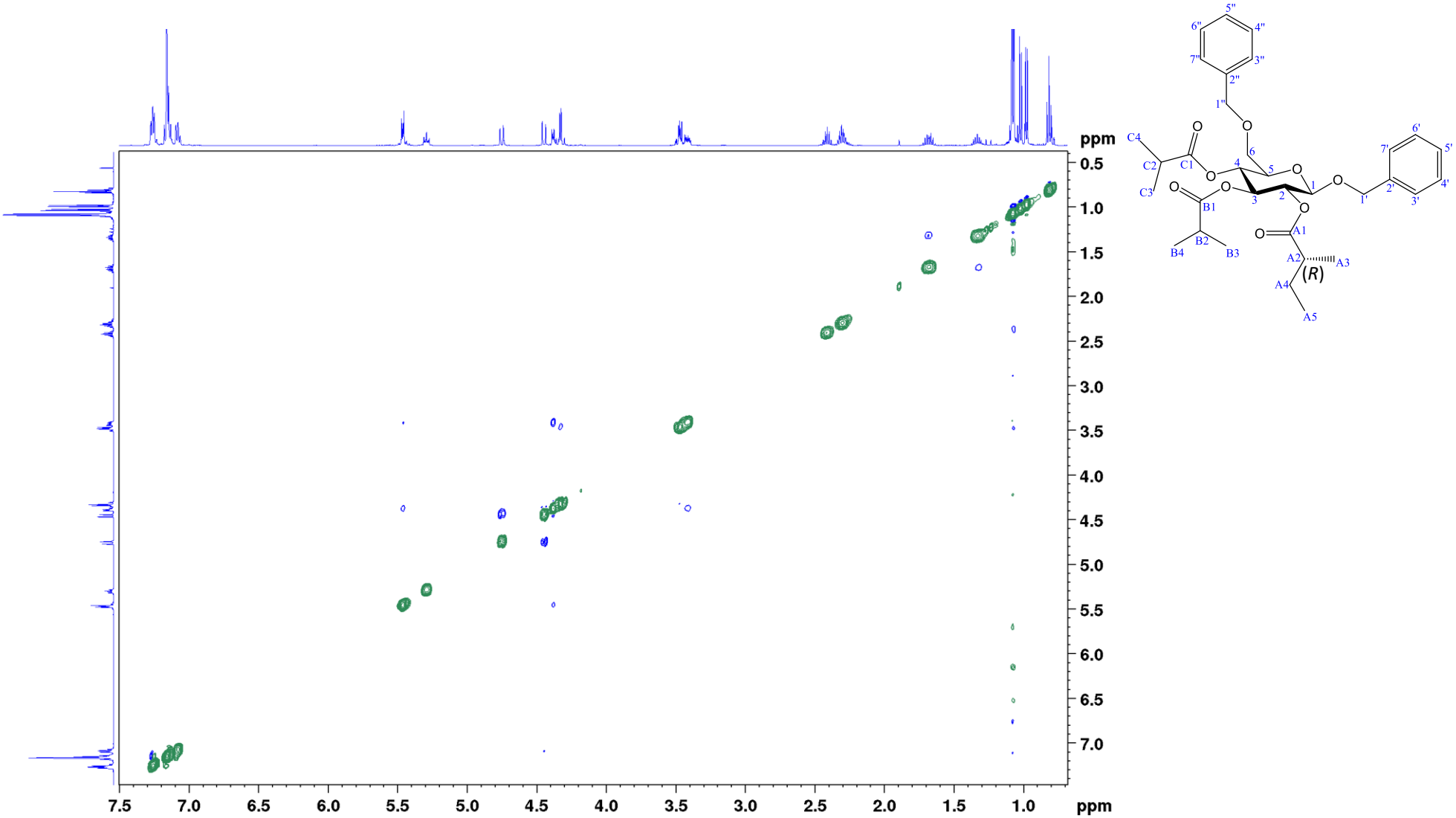

Figure S74: NOESY spectrum of compound [**2(*R*)**] (500 MHz, C_6D_6).

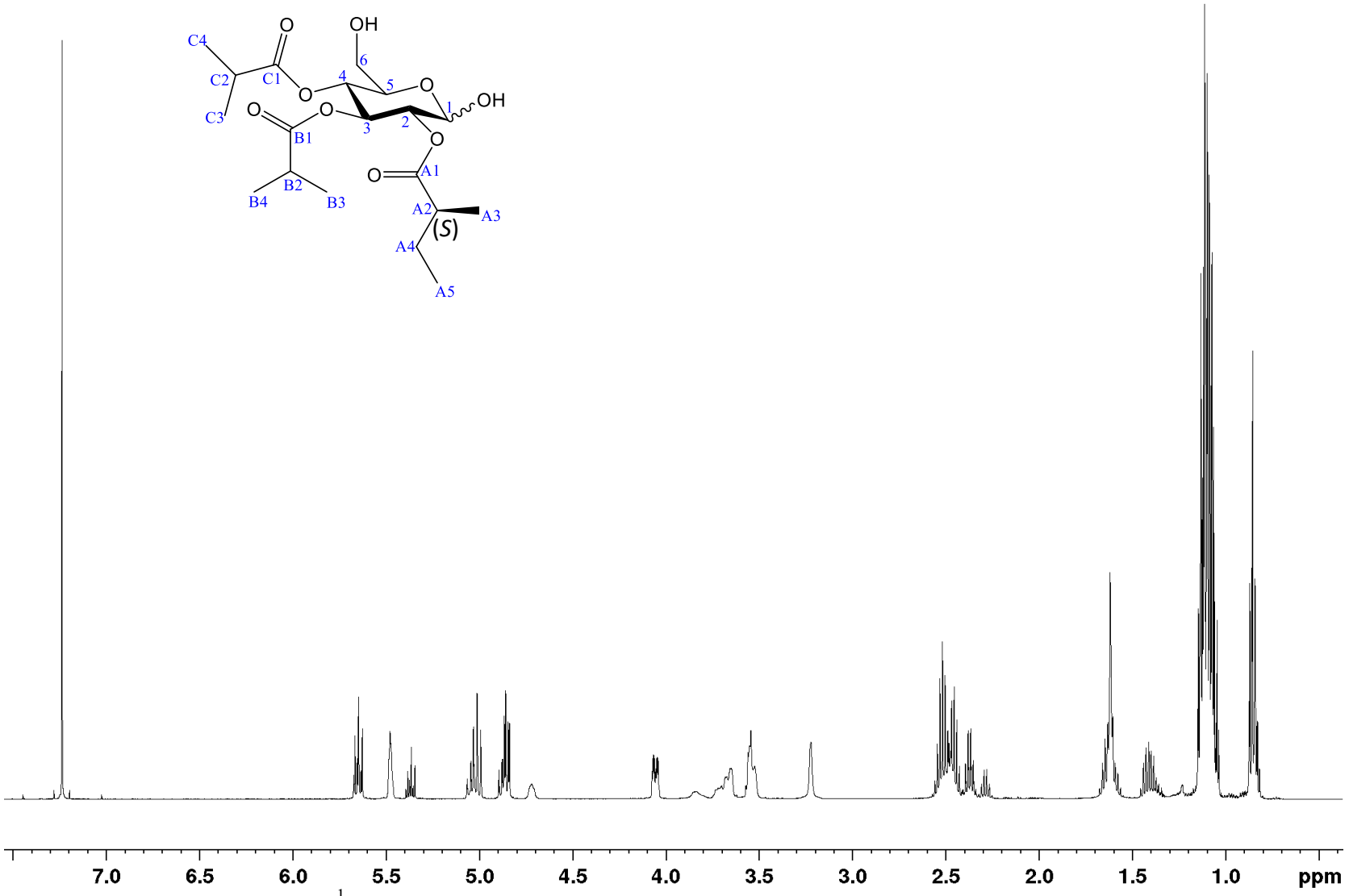

Figure S75: ^{1}H NMR spectrum of synthesized pennelliiside D (**1**) (500 MHz, $CDCl_3$).

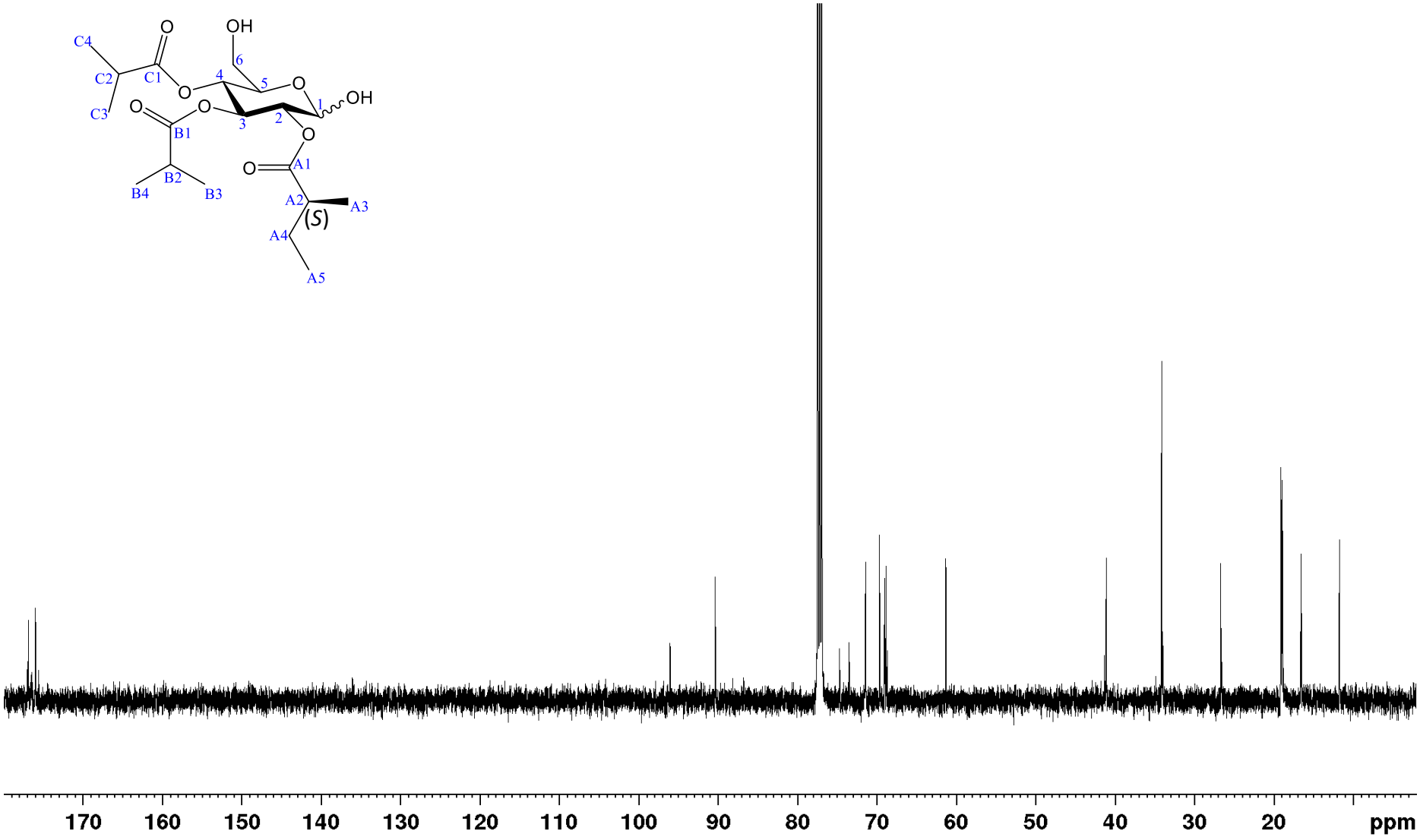

Figure S76: ^{13}C NMR spectrum of synthesized pennelliiside D (**1**) (126 MHz, $CDCl_3$).

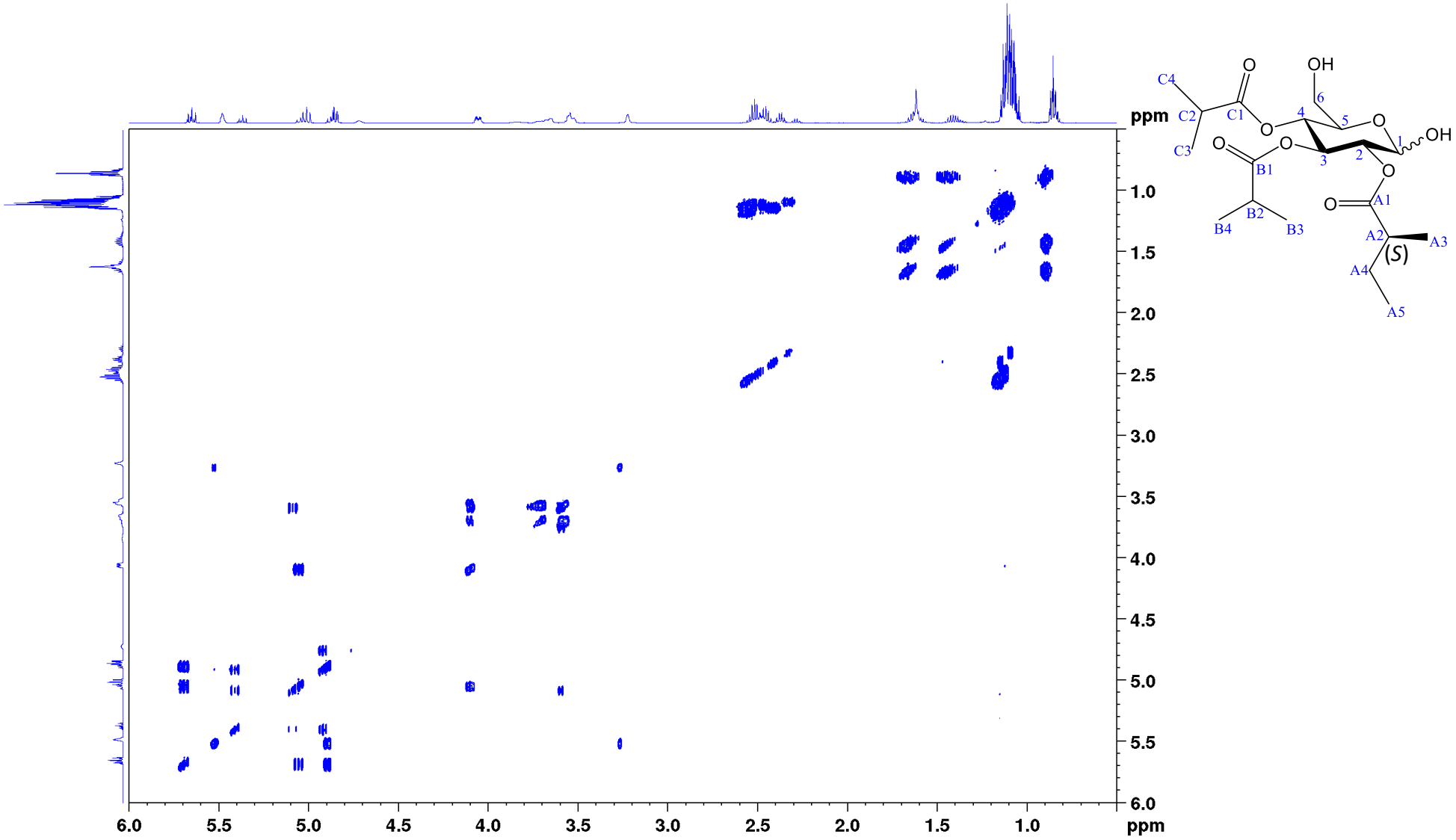

Figure S77: COSY spectrum of synthesized pennelliiside D (**1**) (500 MHz, $CDCl_3$).

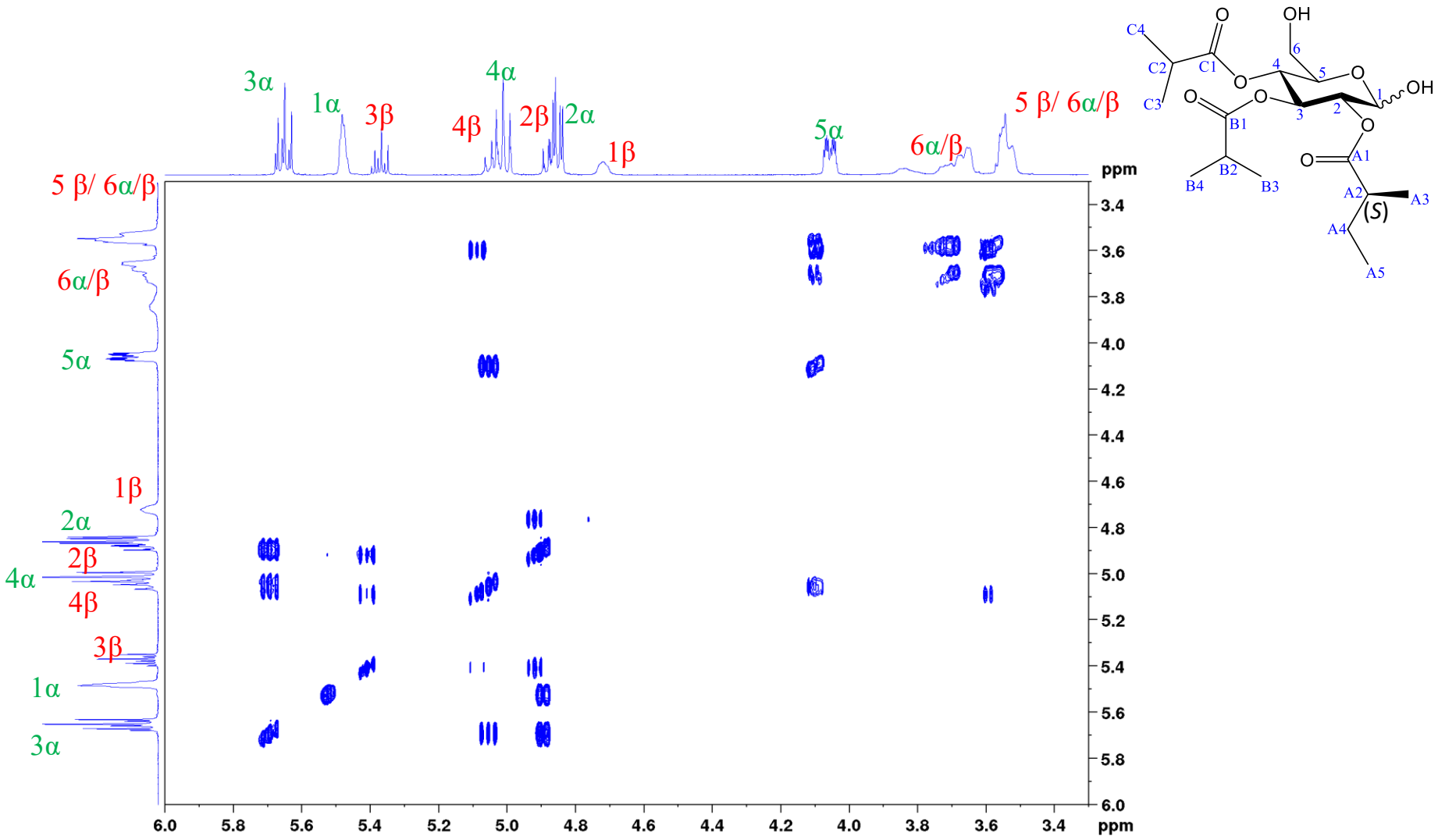

Figure S78: COSY spectrum of synthesized pennelliiside D (**1**) (500 MHz, $CDCl_3$).

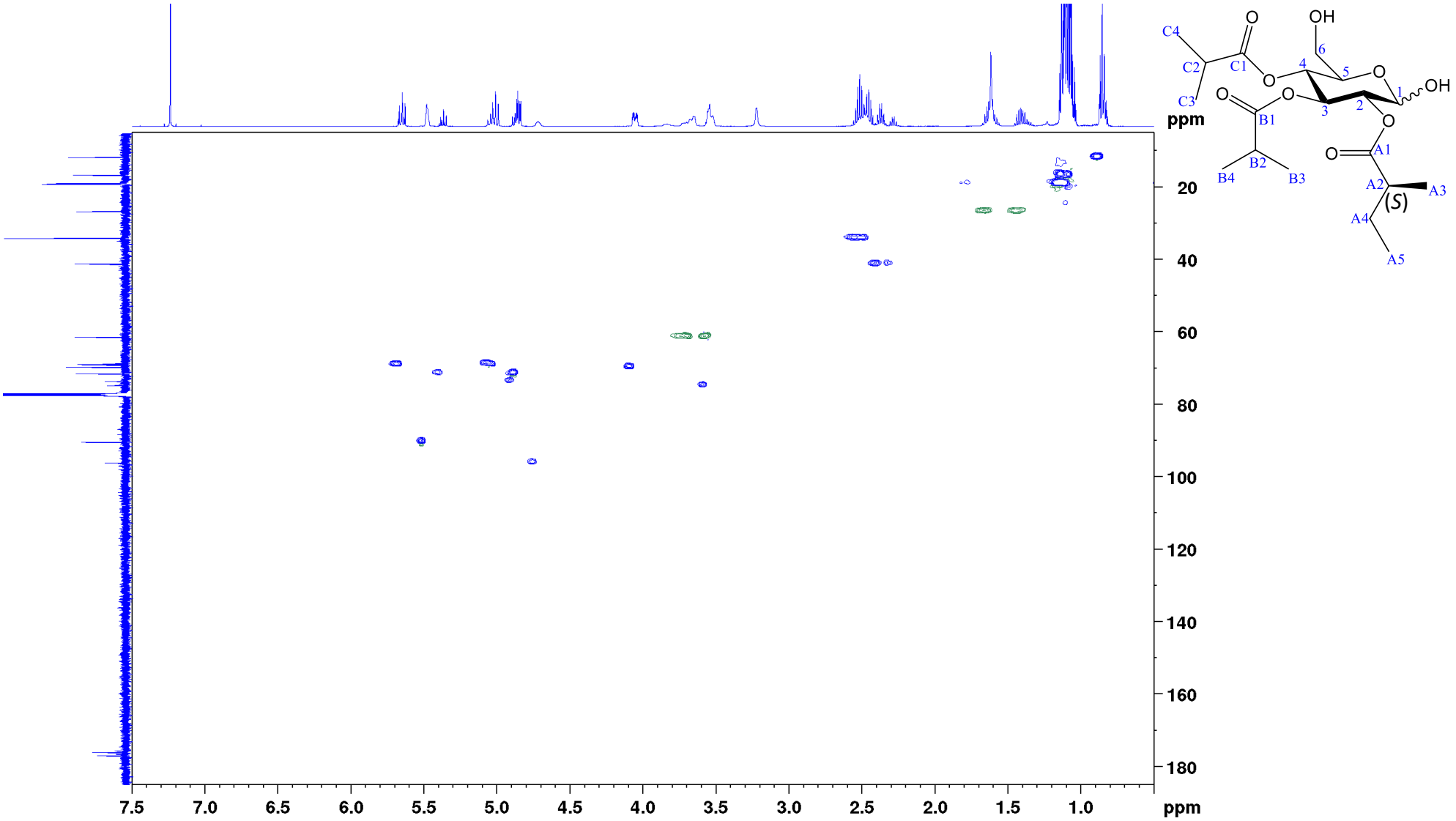

Figure S79: HSQC spectrum of synthesized pennelliiside D (**1**) (500 MHz, $CDCl_3$).

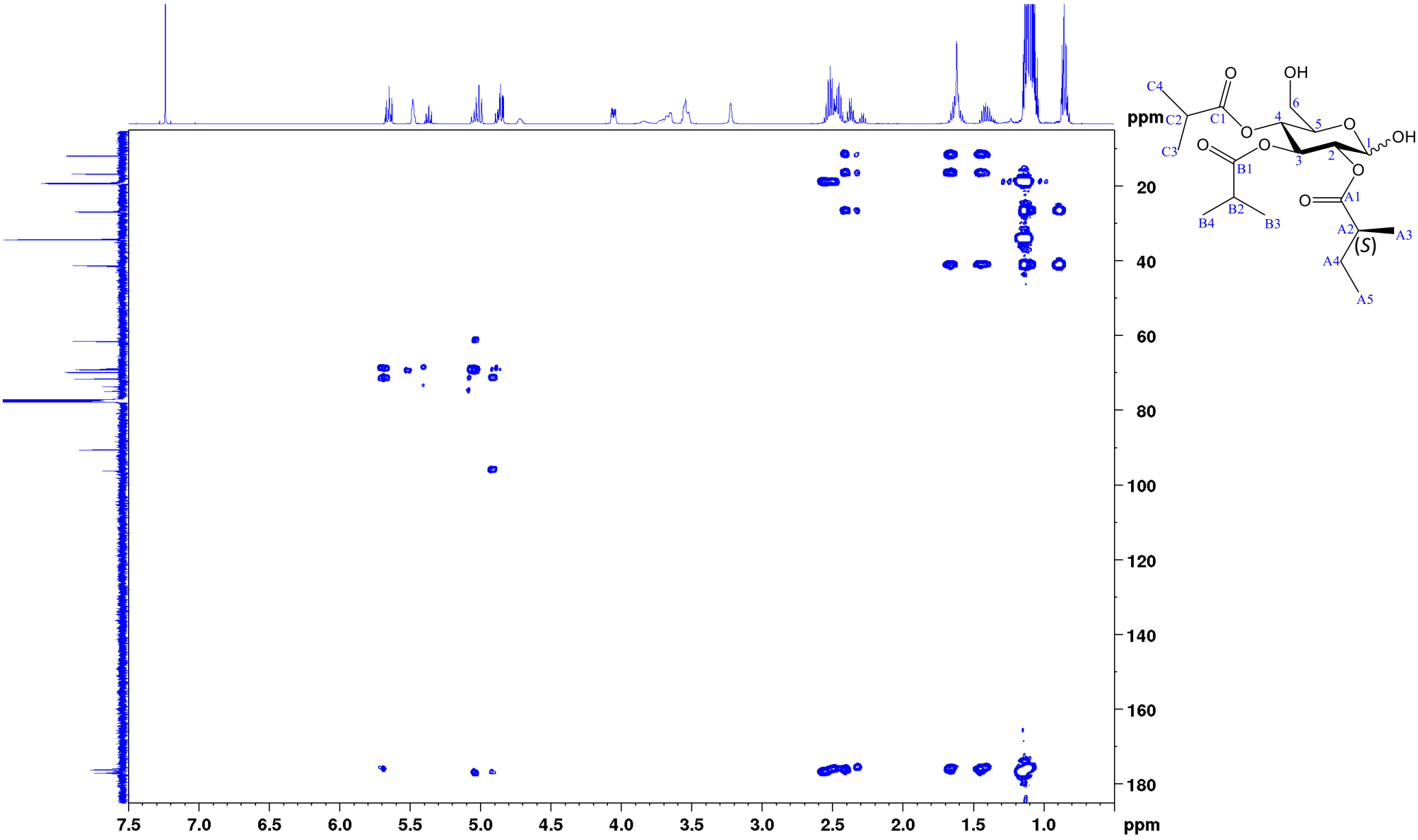

Figure S80: HMBC spectrum of synthesized pennelliiside D (**1**) (500 MHz, $CDCl_3$).

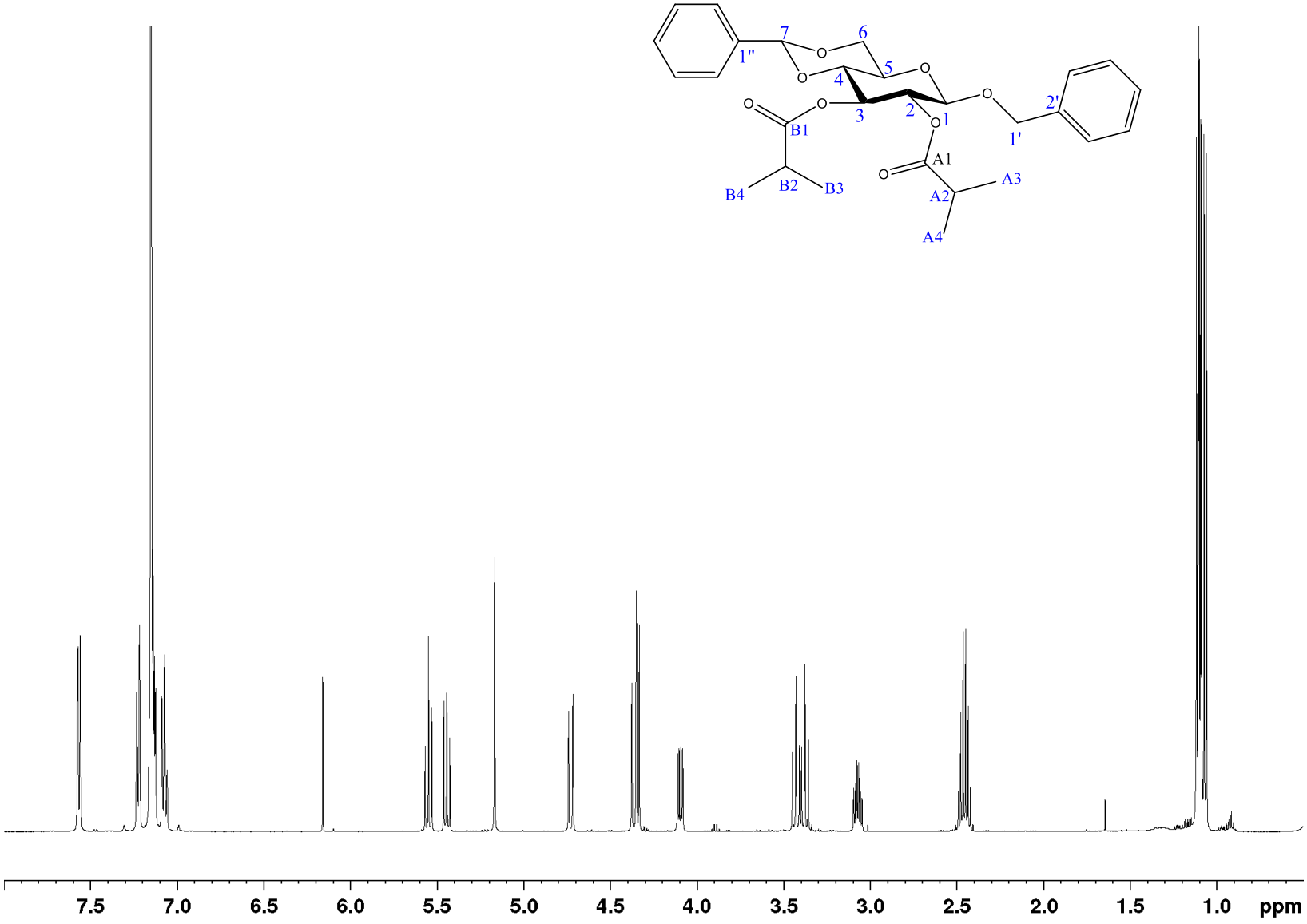

Figure S81: ^{1}H NMR spectrum of compound **10** (500 MHz, C_6D_6).

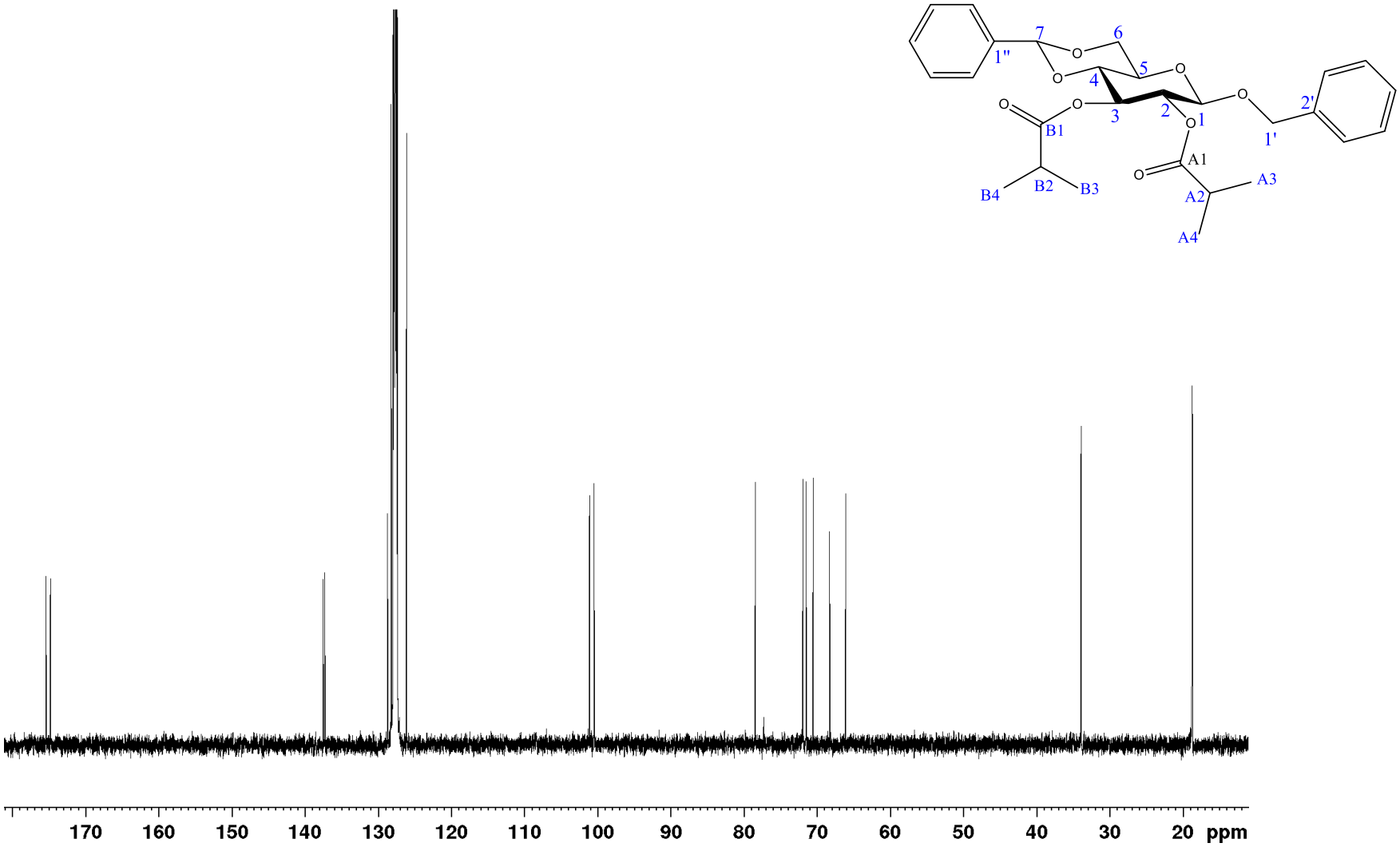

Figure S82: ^{13}C NMR spectrum of compound **10** (126 MHz, C_6D_6).

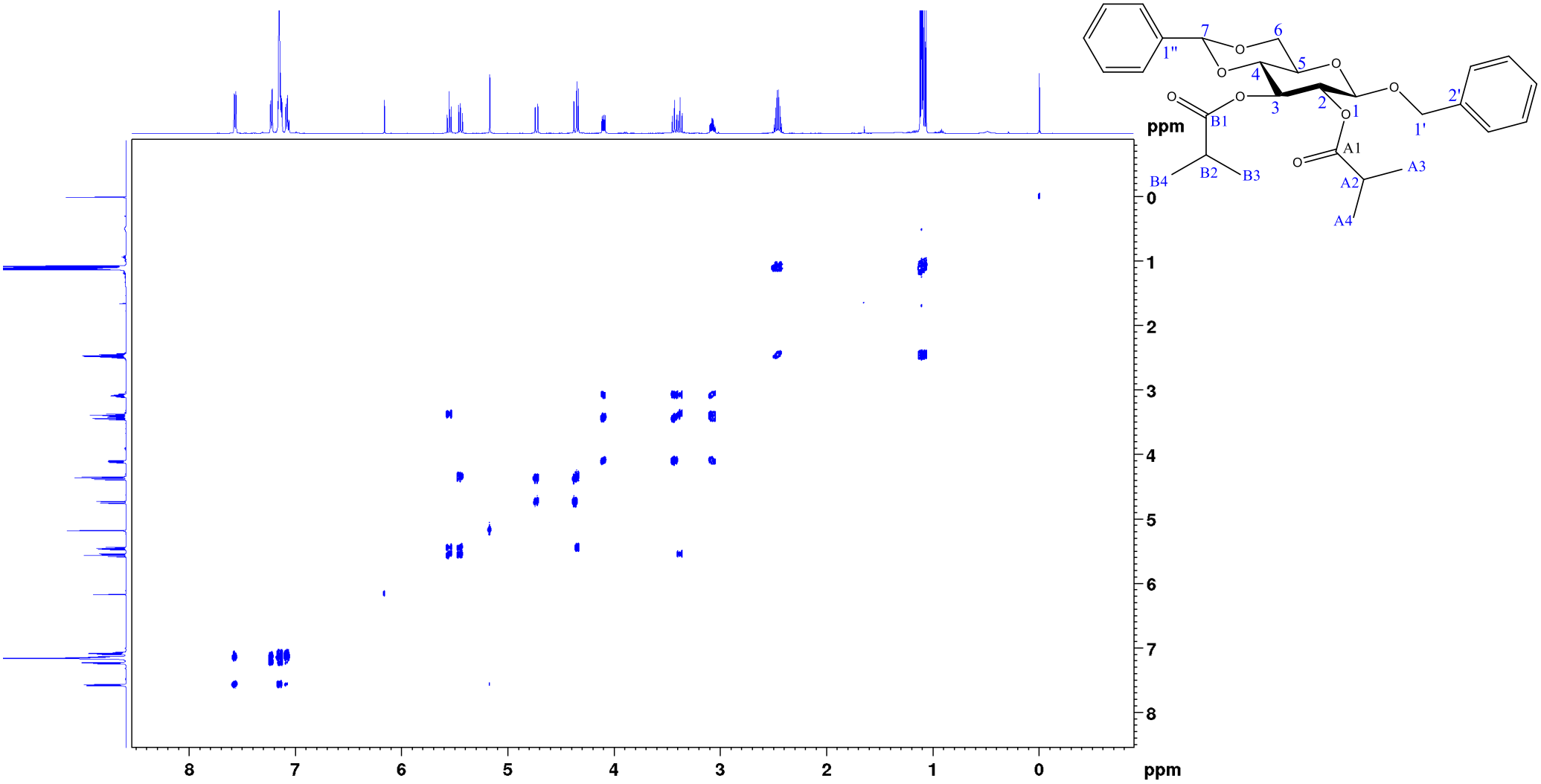

Figure S83: COSY spectrum of compound **10** (500 MHz, C_6D_6).

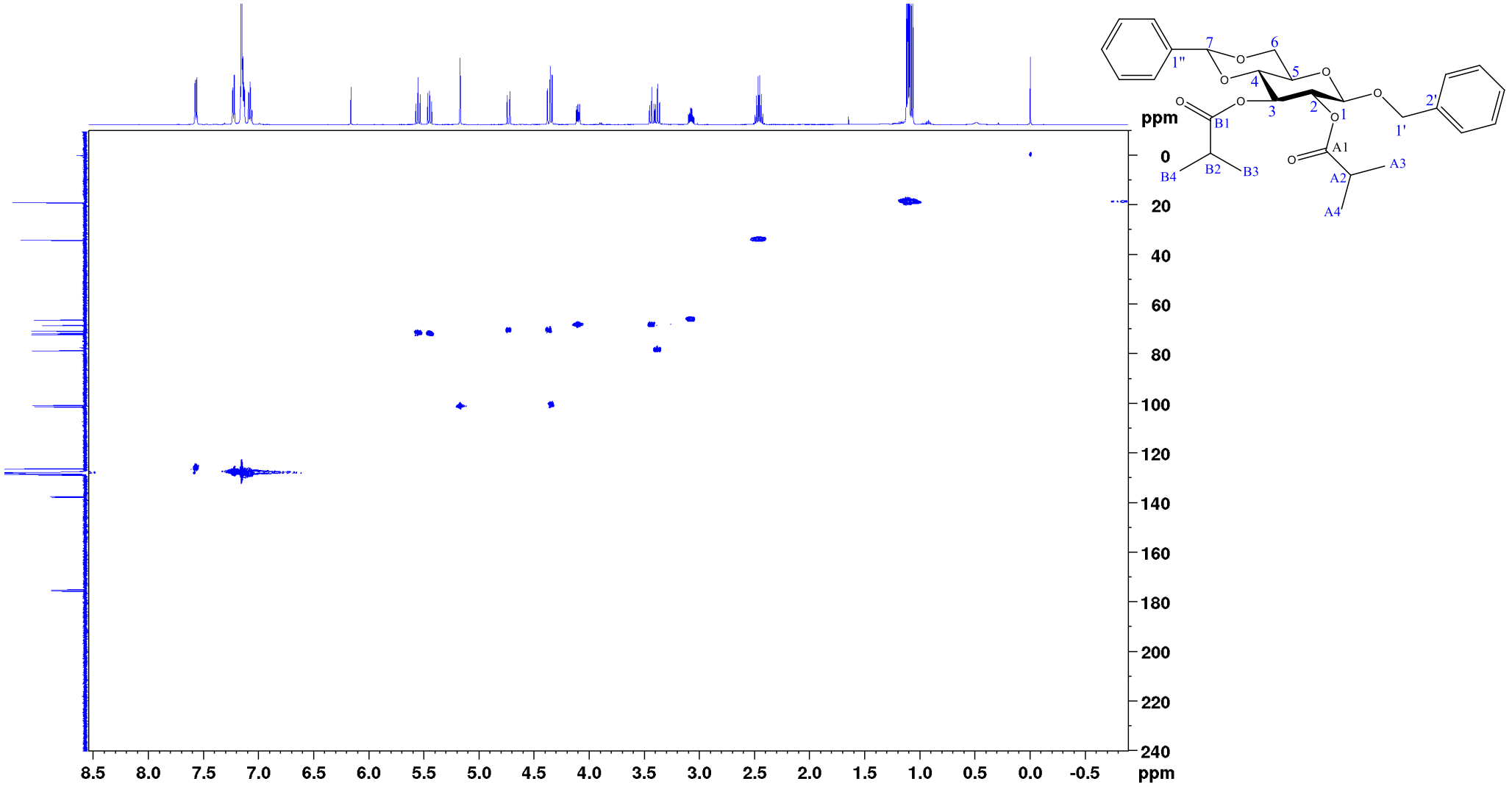

Figure S84: HSQC spectrum of compound **10** (500 MHz, C_6D_6).

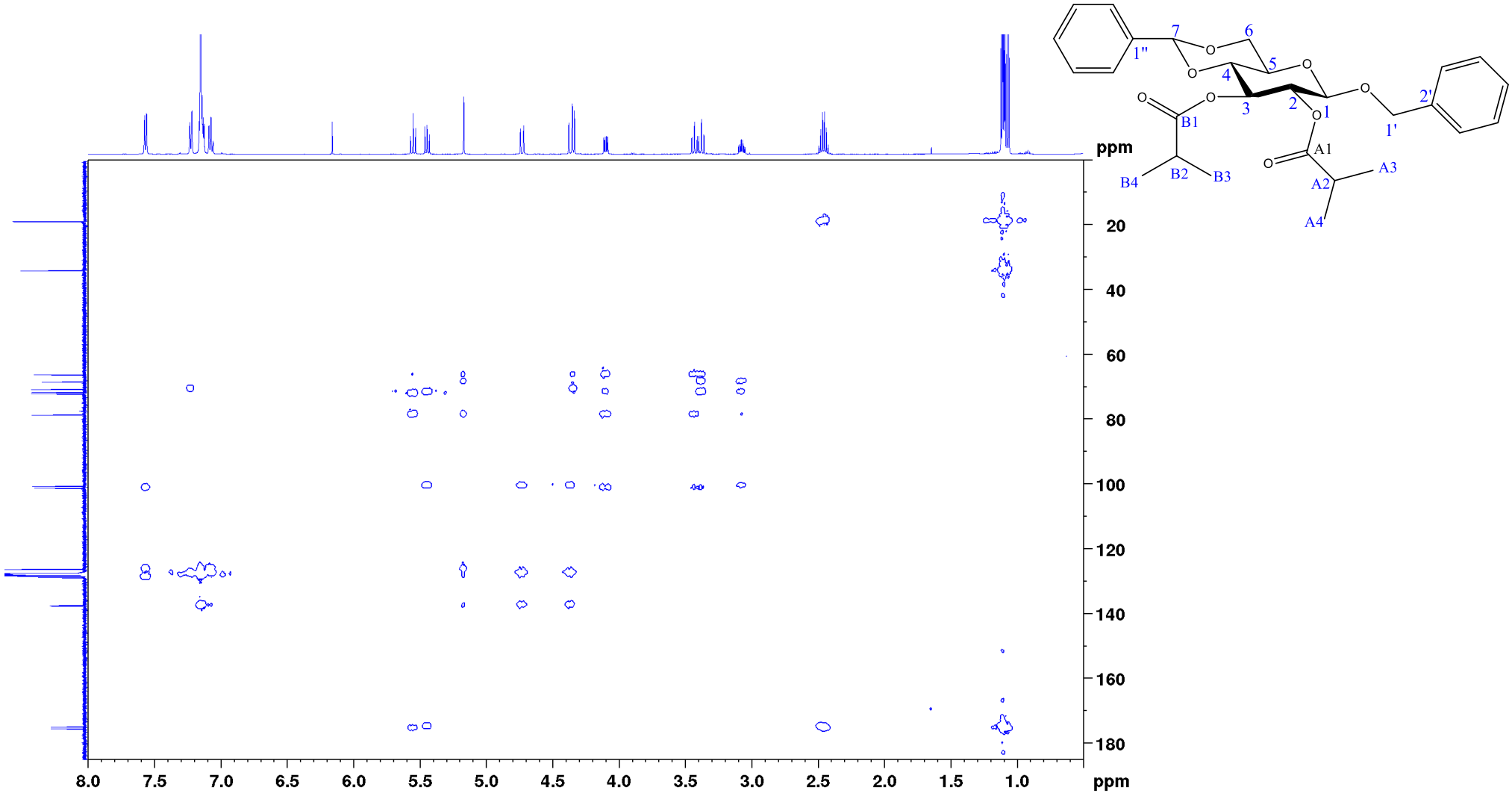

Figure S85: HMBC spectrum of compound **10** (500 MHz, C_6D_6).

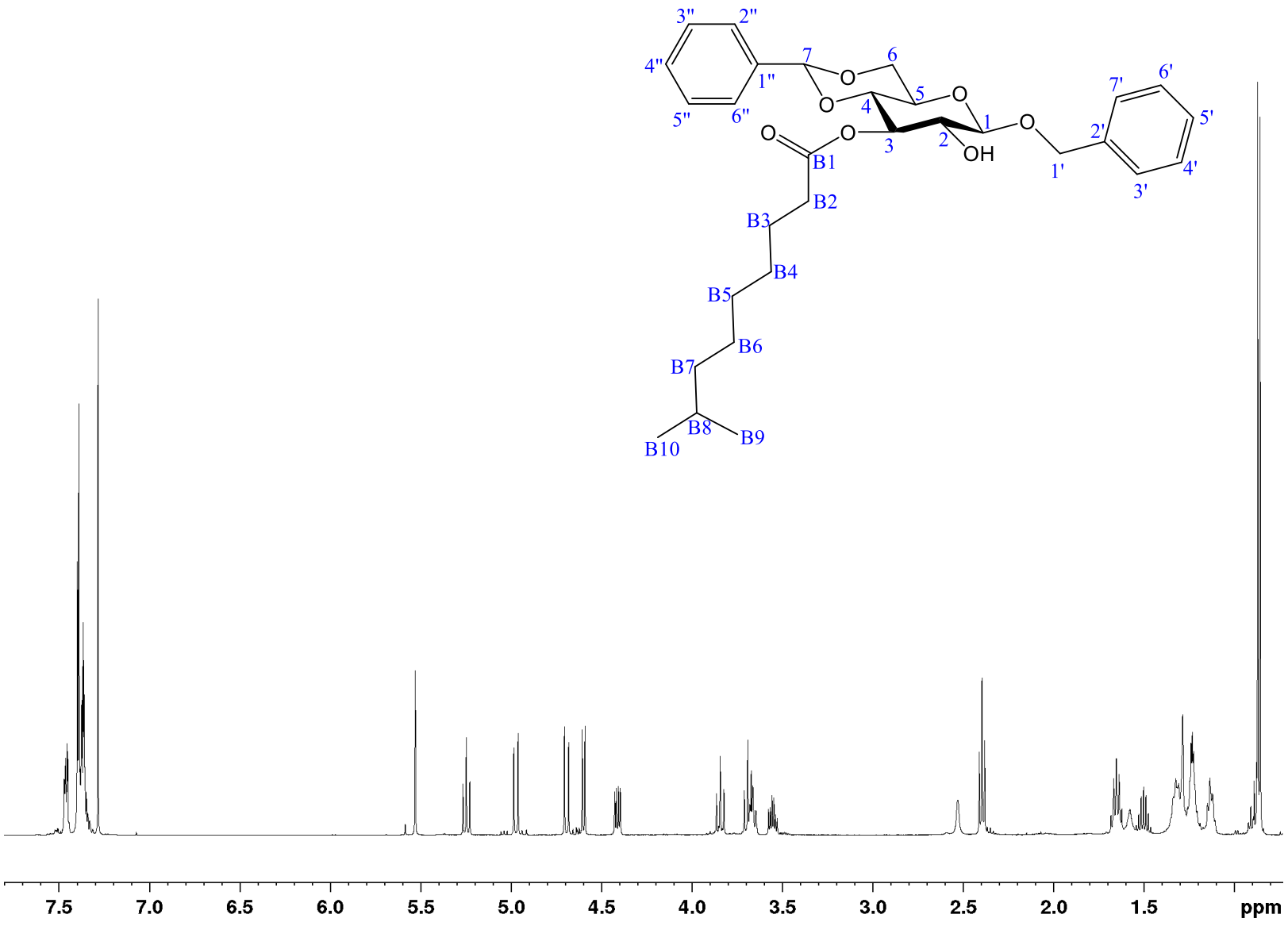

Figure S86: ^{1}H NMR spectrum of compound **11** (500 MHz, $CDCl_3$).

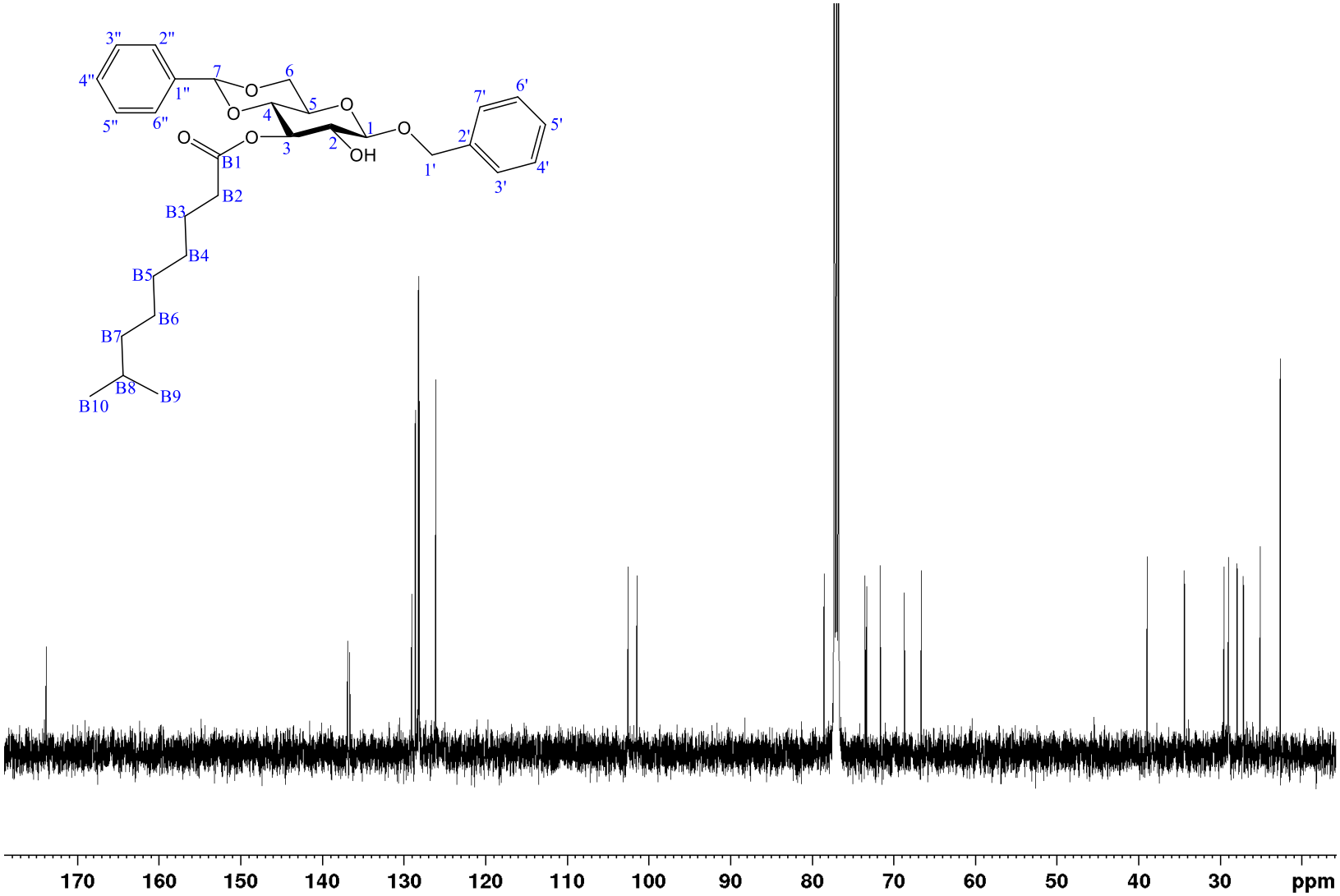

Figure S87: ^{13}C NMR spectrum of compound **11** (126 MHz, $CDCl_3$).

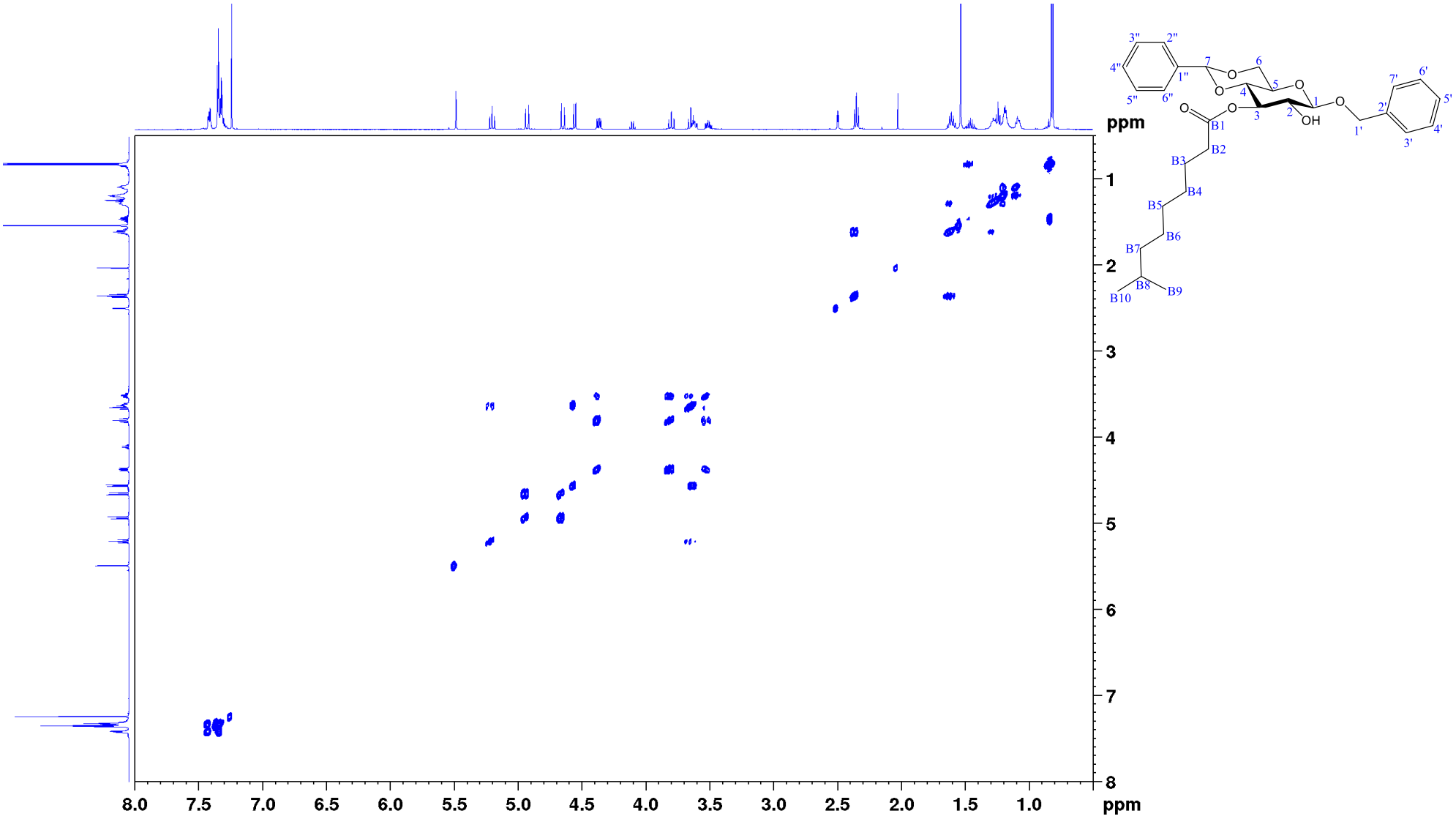

Figure S88: COSY spectrum of compound **11** (500 MHz, $CDCl_3$).

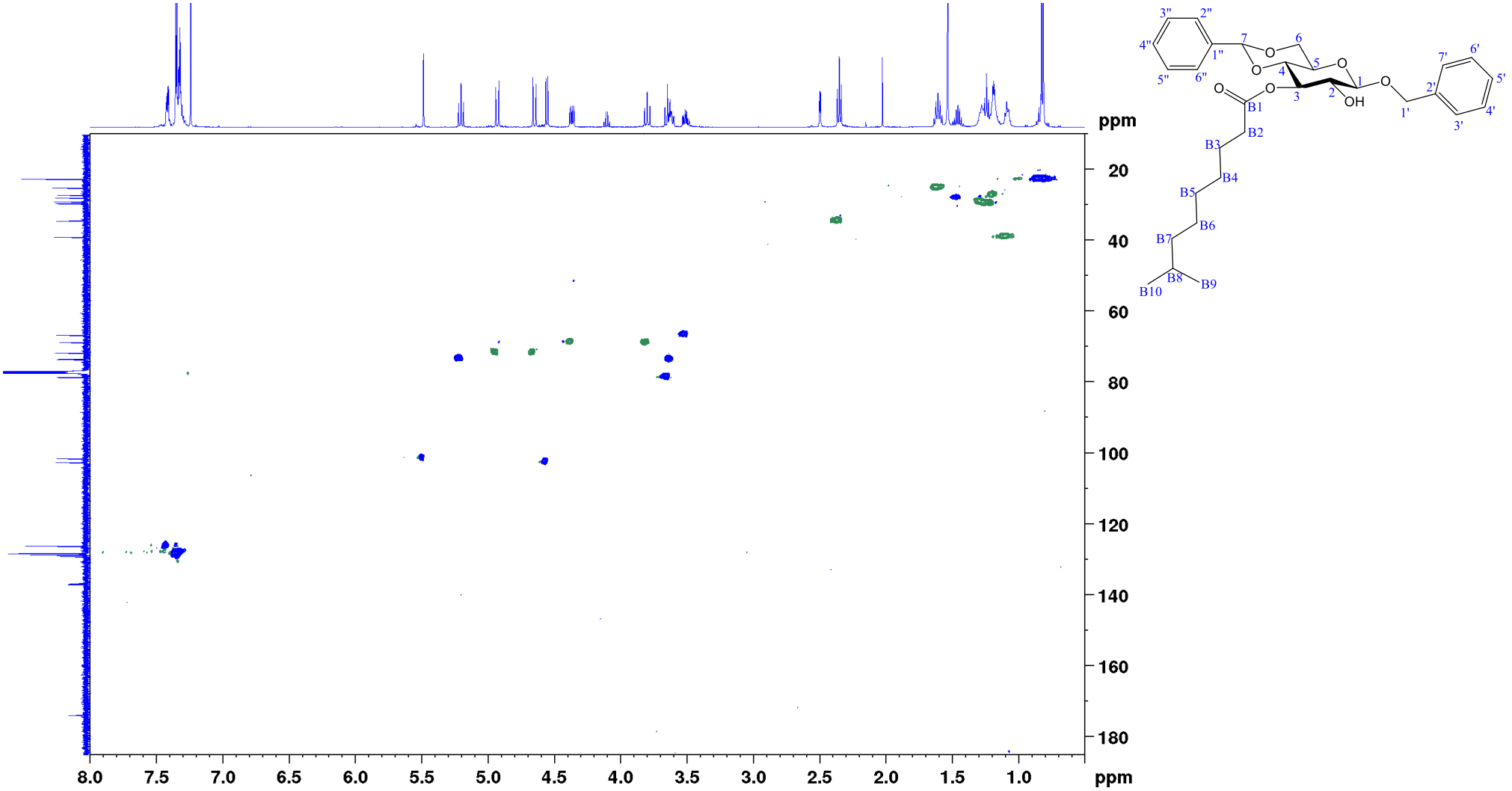

Figure S89: HSQC spectrum of compound **11** (500 MHz, $CDCl_3$).

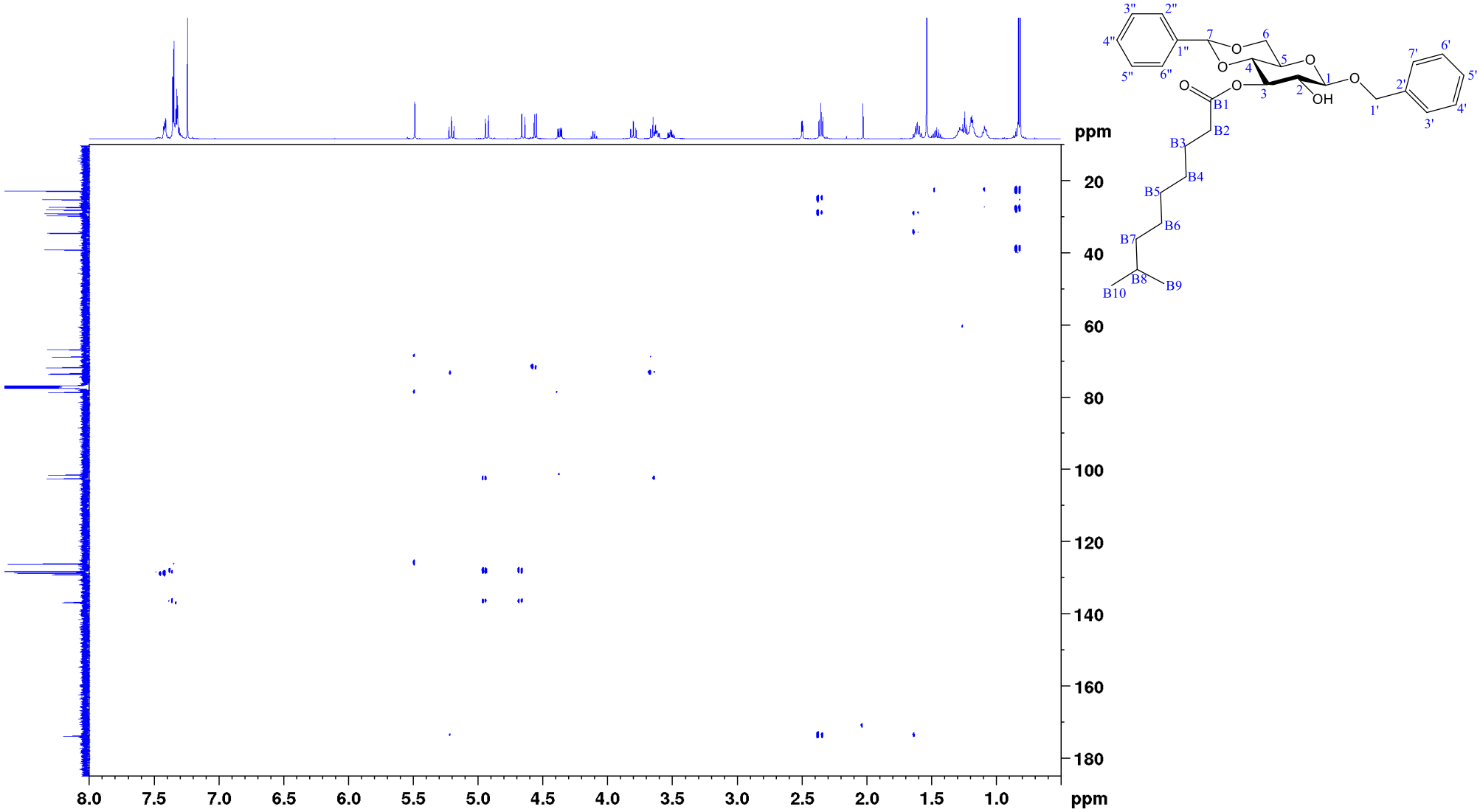

Figure S90: HMBC spectrum of compound **11** (500 MHz, $CDCl_3$).

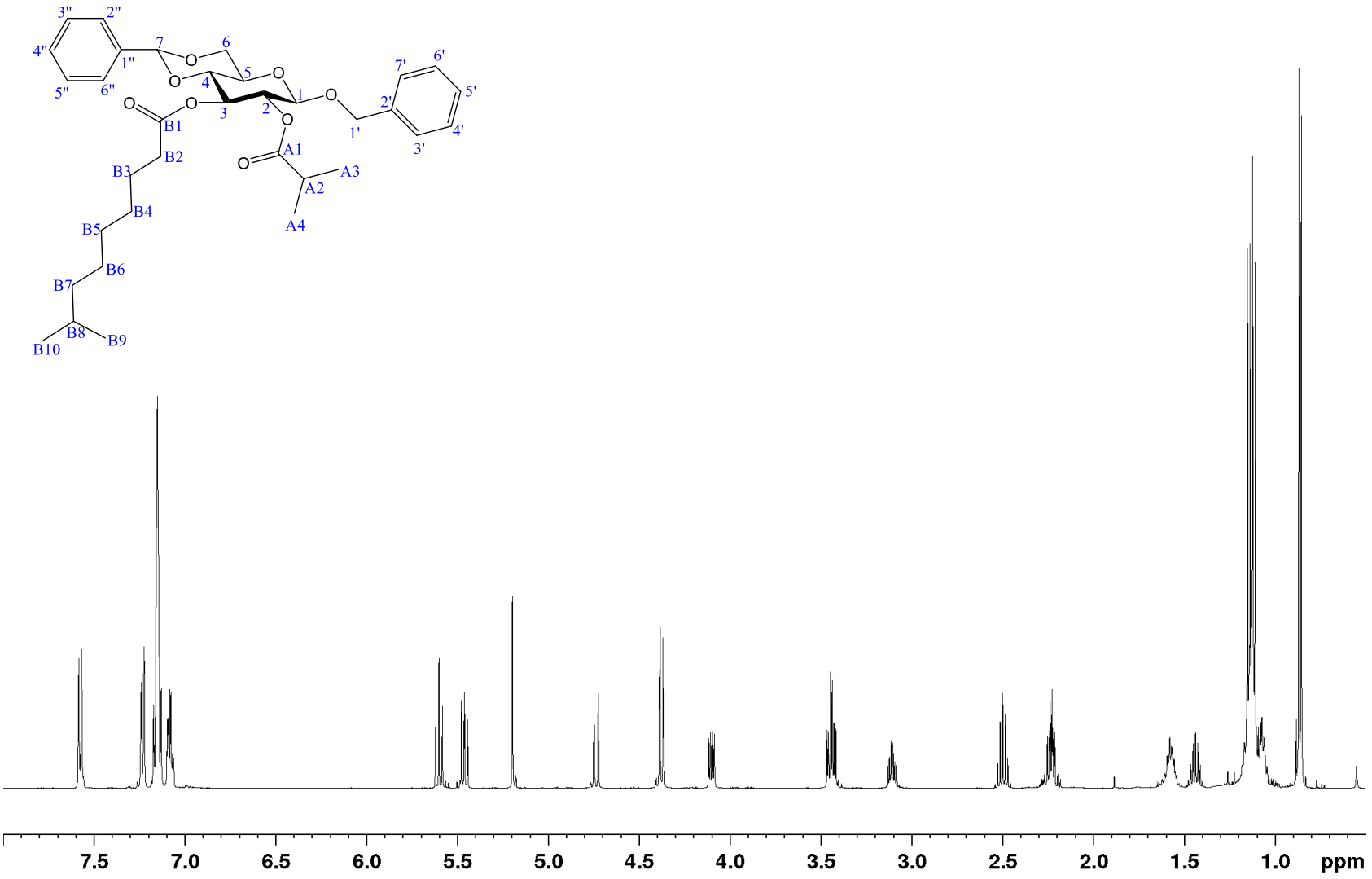

Figure S91: ^{1}H NMR spectrum of compound **12** (500 MHz, C_6D_6).

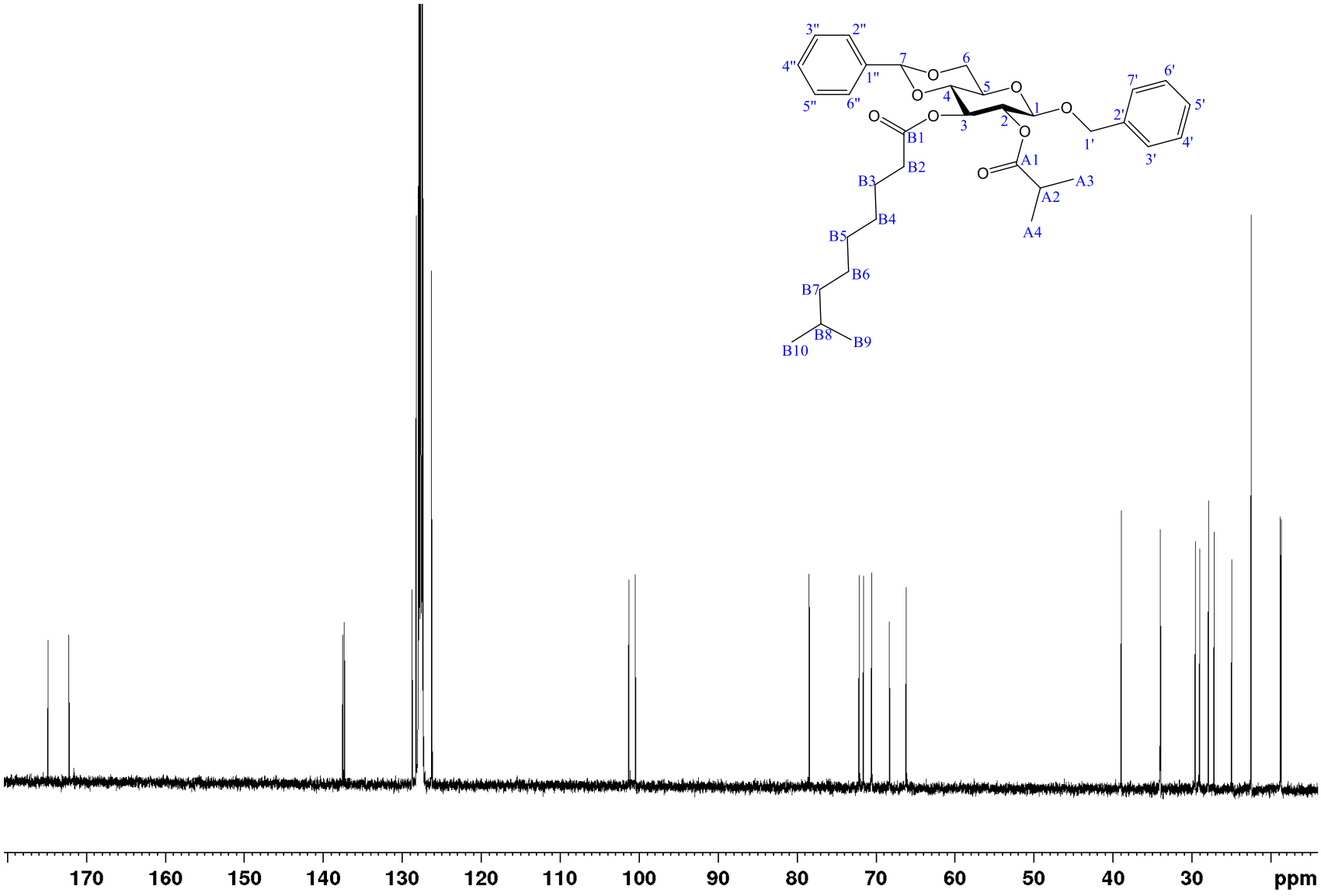

Figure S92: ^{13}C NMR spectrum of compound **12** (126 MHz, C_6D_6).

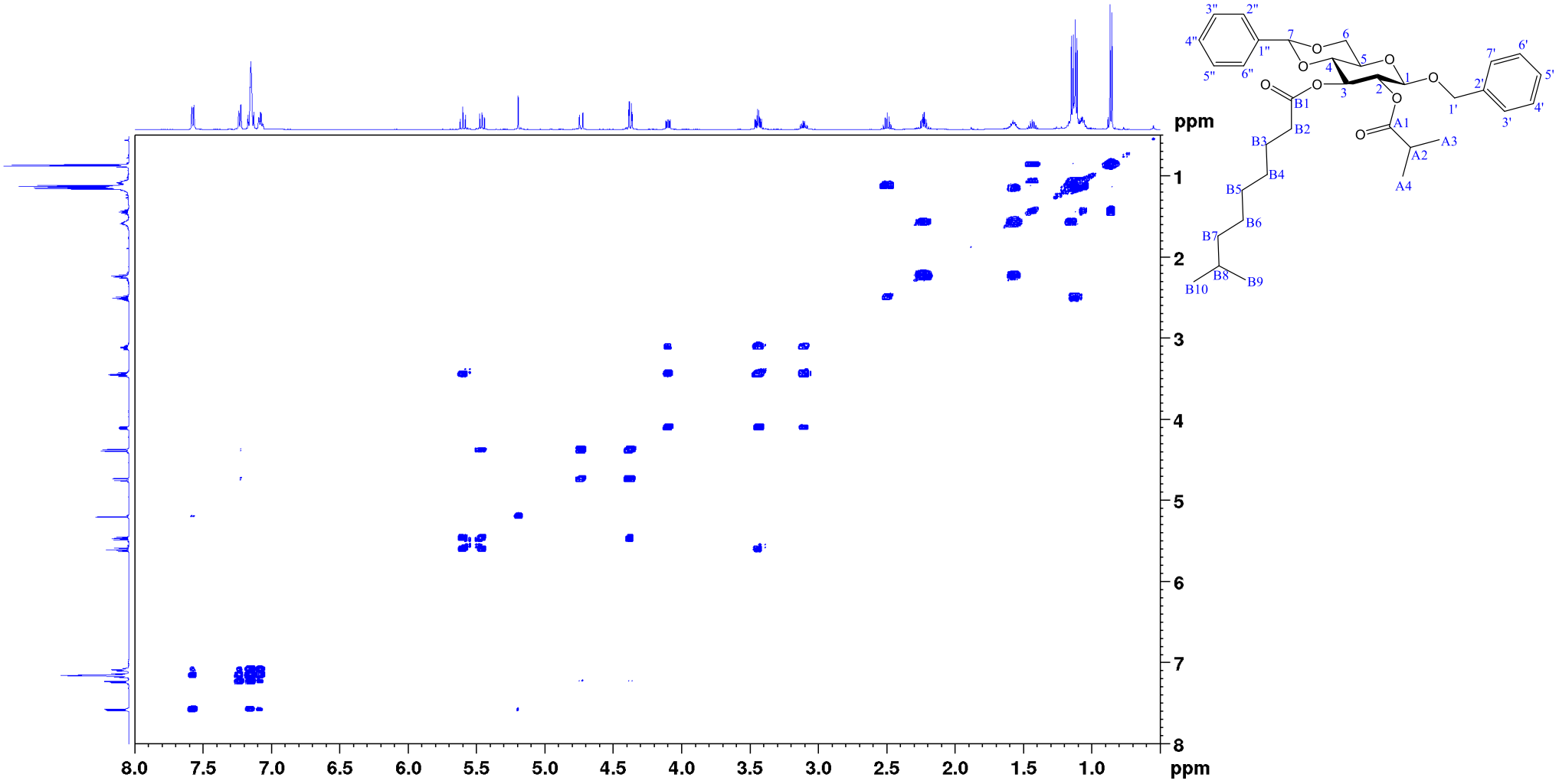

Figure S93: COSY spectrum of compound **12** (500 MHz, C_6D_6).

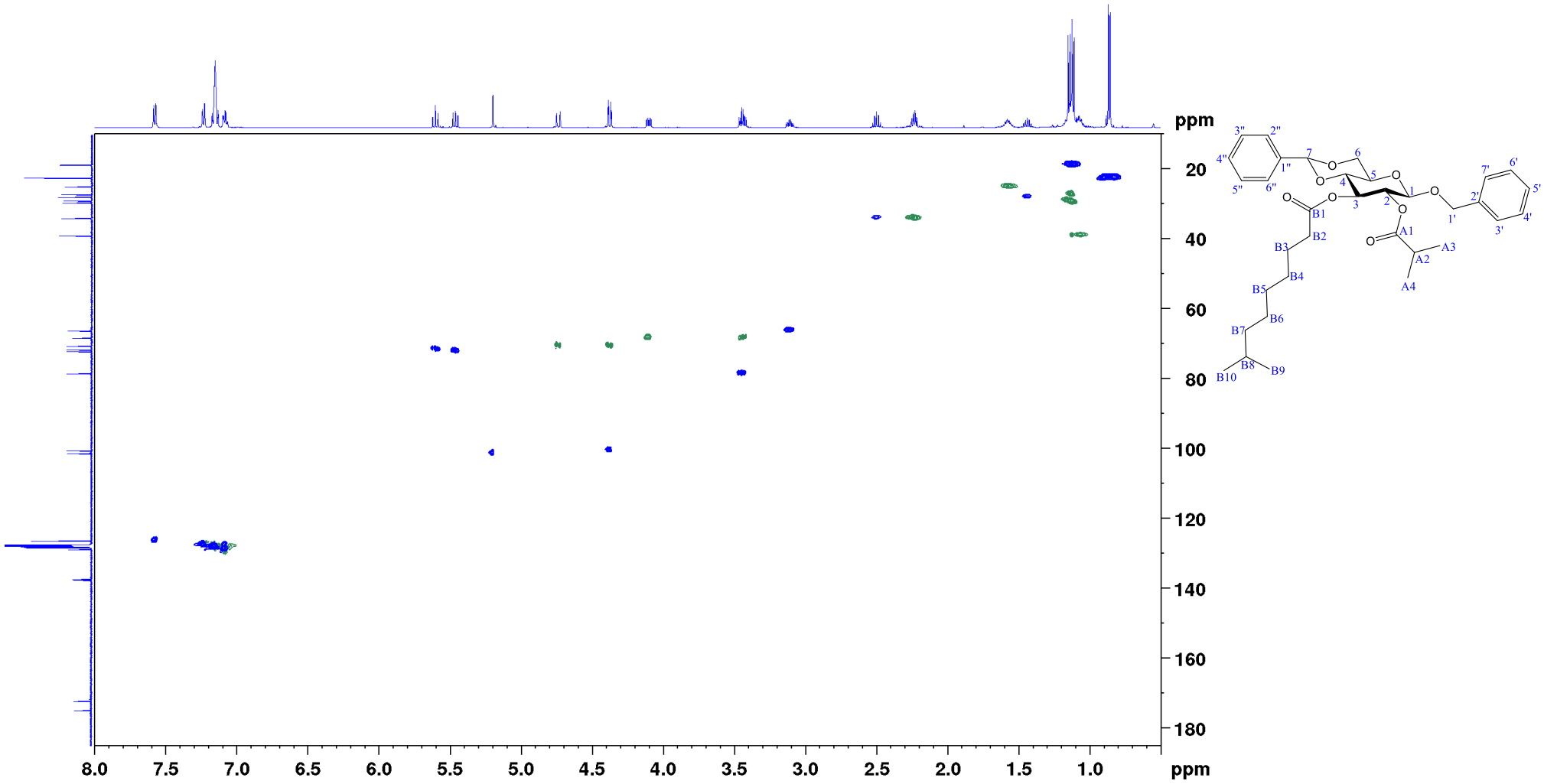

Figure S94: HSQC spectrum of compound **12** (500 MHz, C_6D_6).

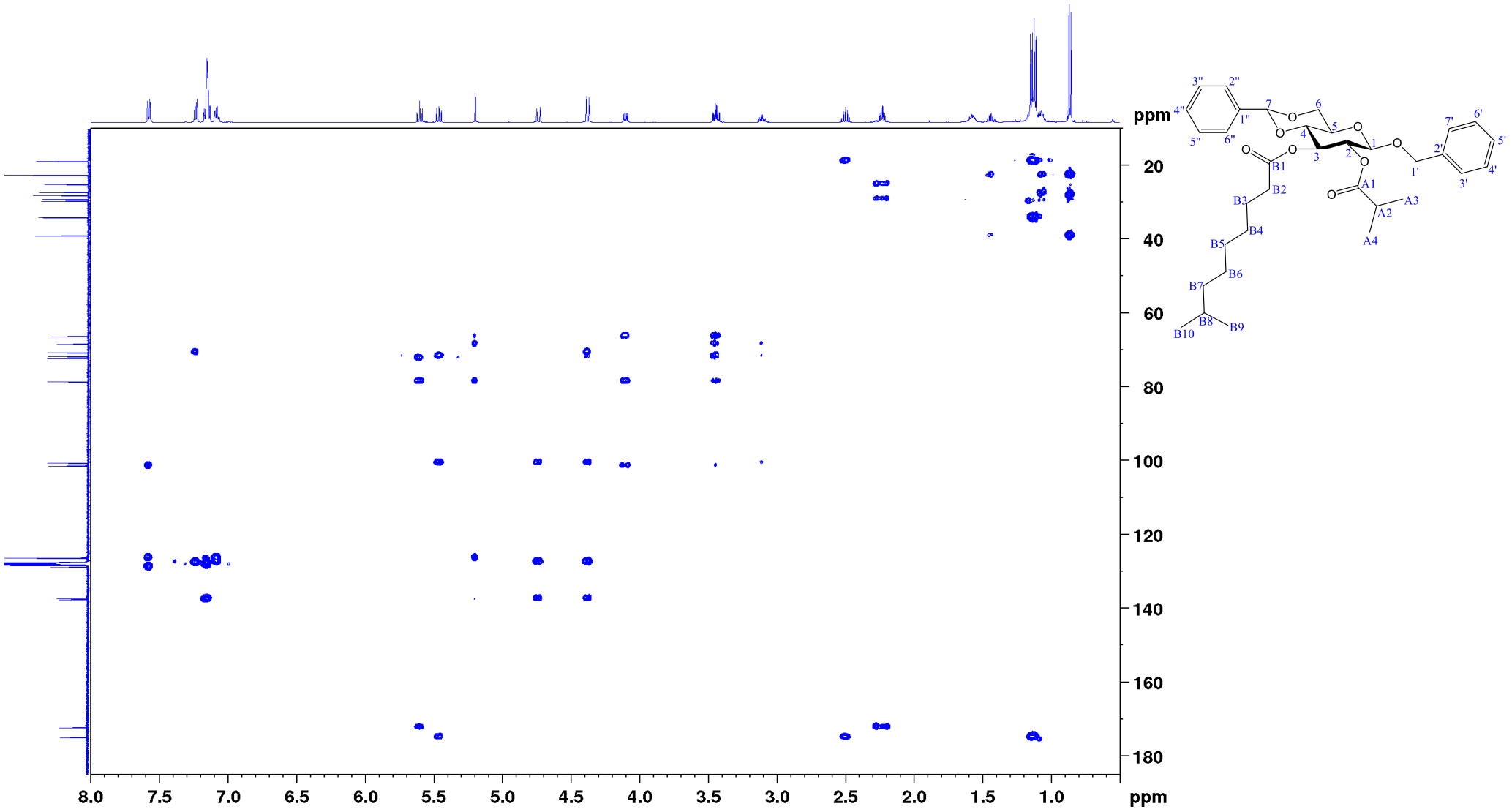

Figure S95: HMBC spectrum of compound **12** (500 MHz, C_6D_6).

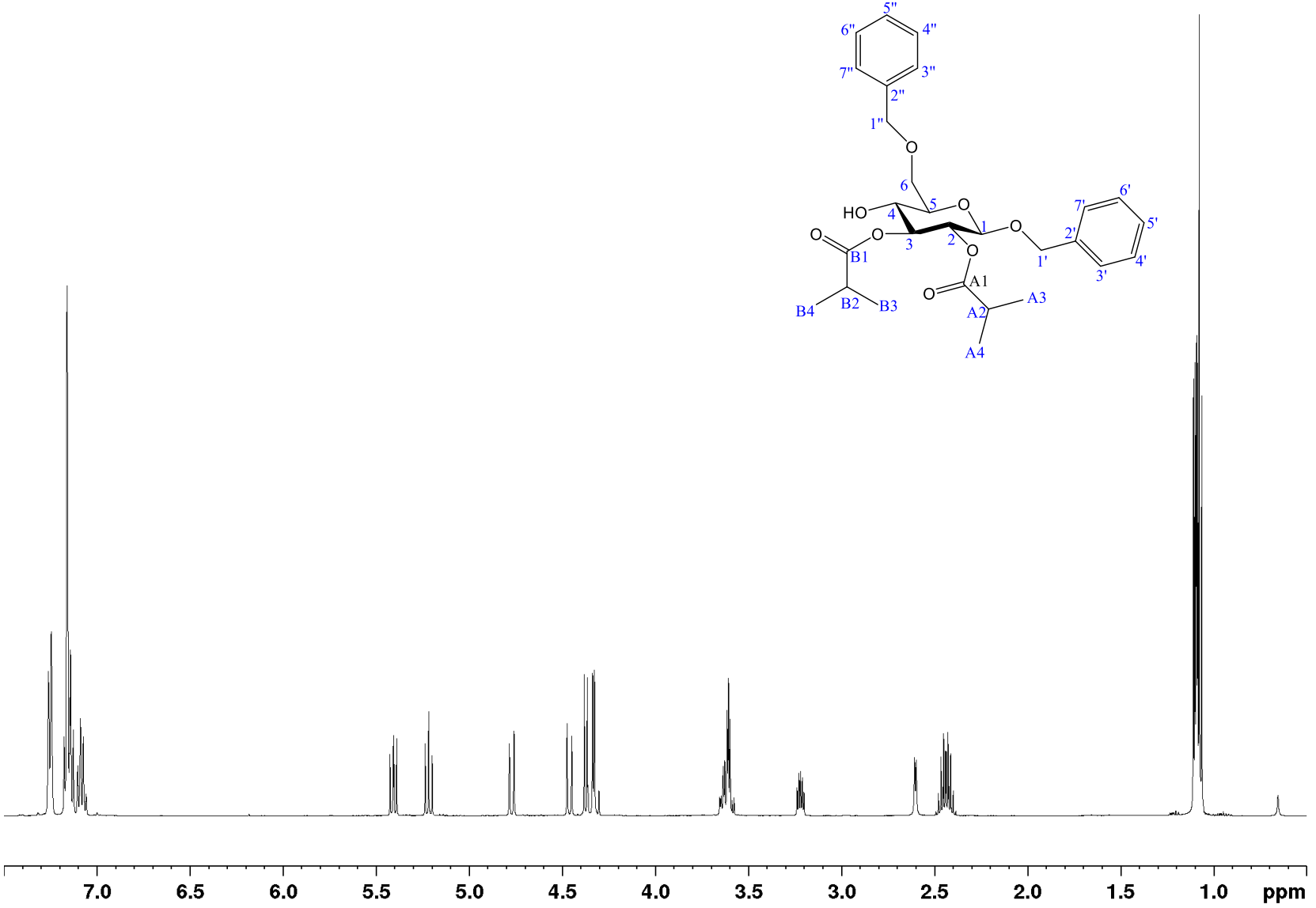

Figure S96: ^{1}H NMR spectrum of compound **13a** (500 MHz, C_6D_6).

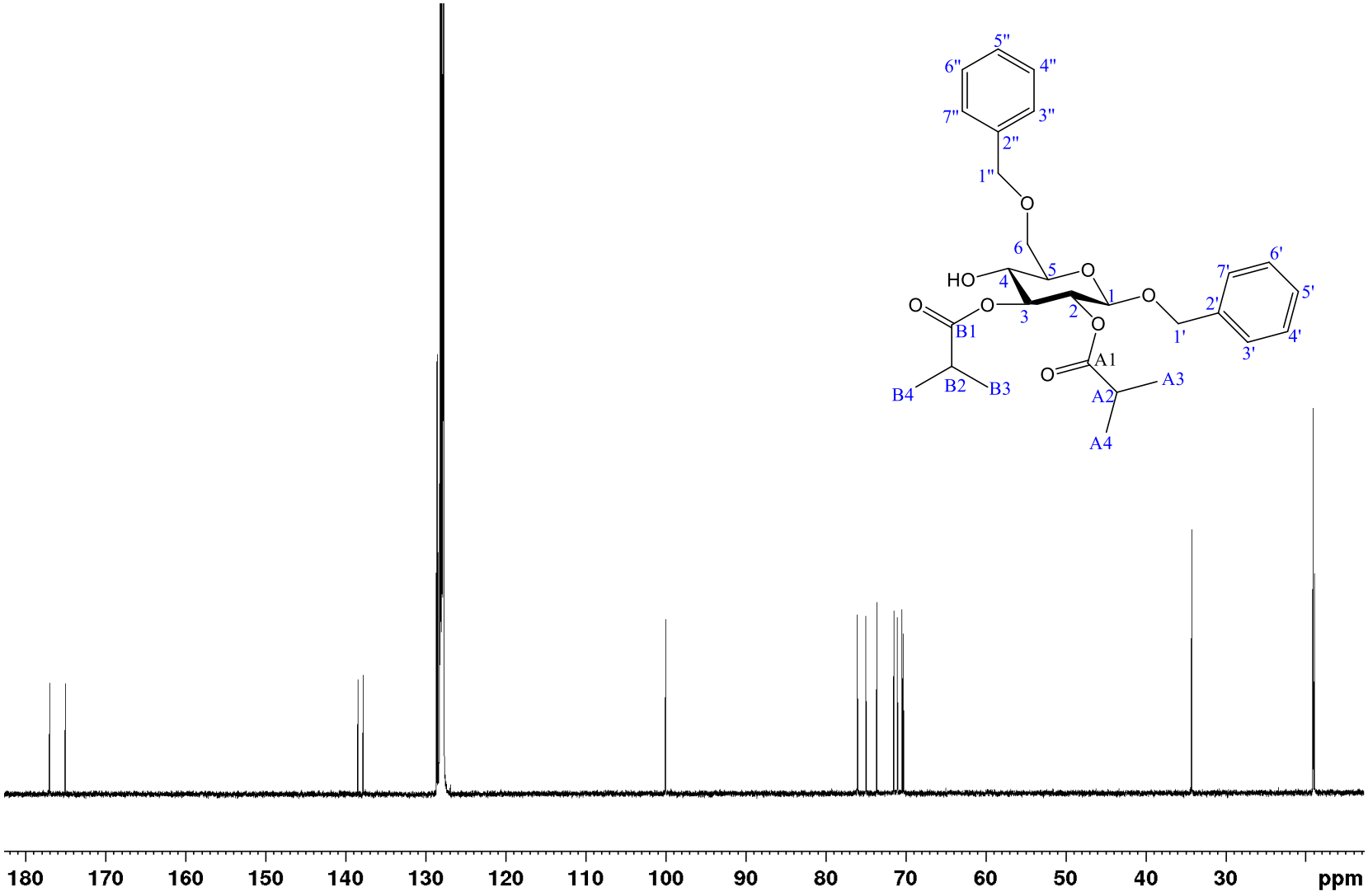

Figure S97: ^{13}C NMR spectrum of compound **13a** (126 MHz, C_6D_6).

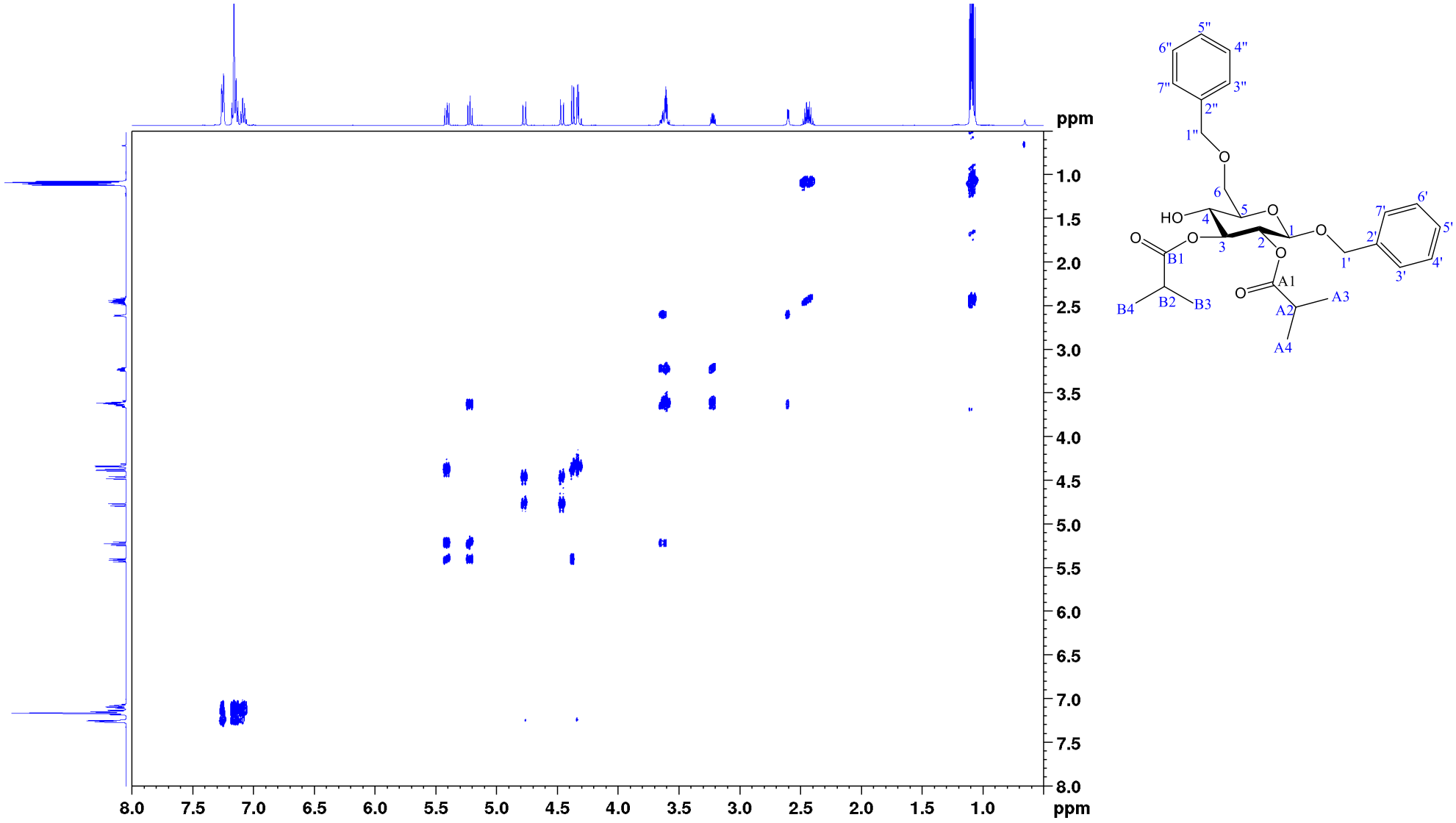

Figure S98: COSY spectrum of compound **13a** (500 MHz, C_6D_6).

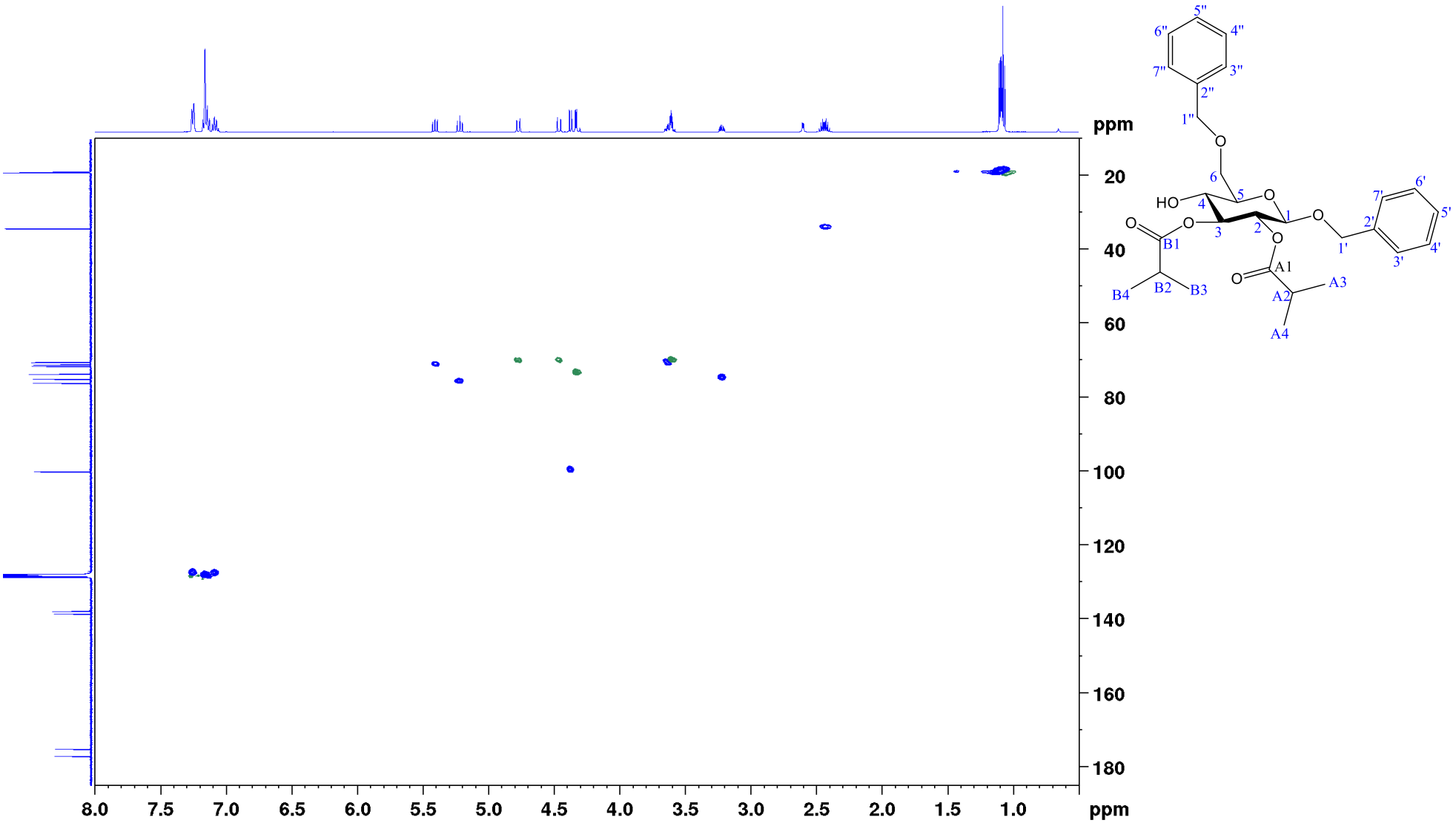

Figure S99: HSQC spectrum of compound **13a** (500 MHz, C_6D_6).

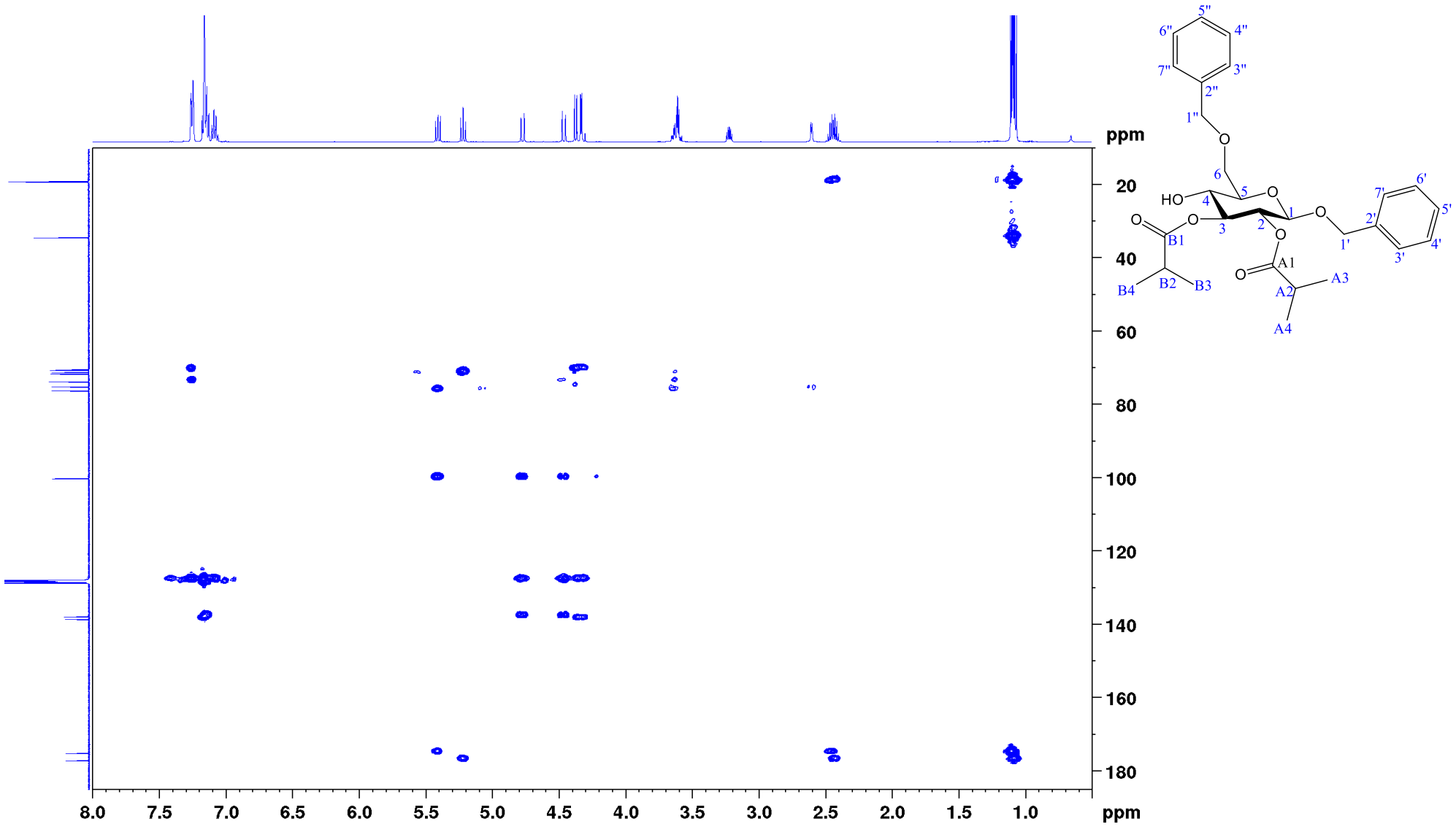

Figure S100: HMBC spectrum of compound **13a** (500 MHz, C_6D_6).

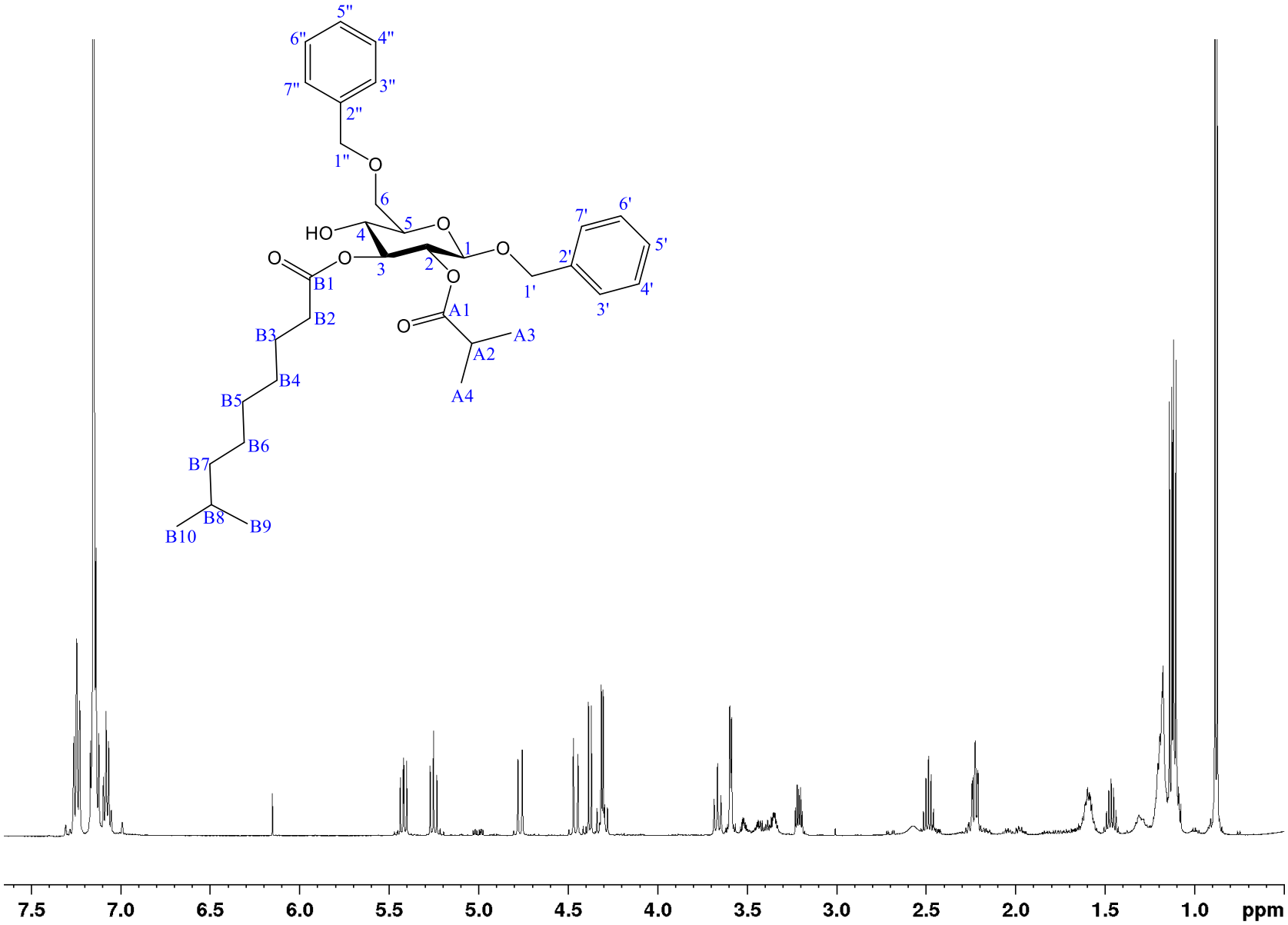

Figure S101: ^{1}H NMR spectrum of compound **13b** (500 MHz, C_6D_6).

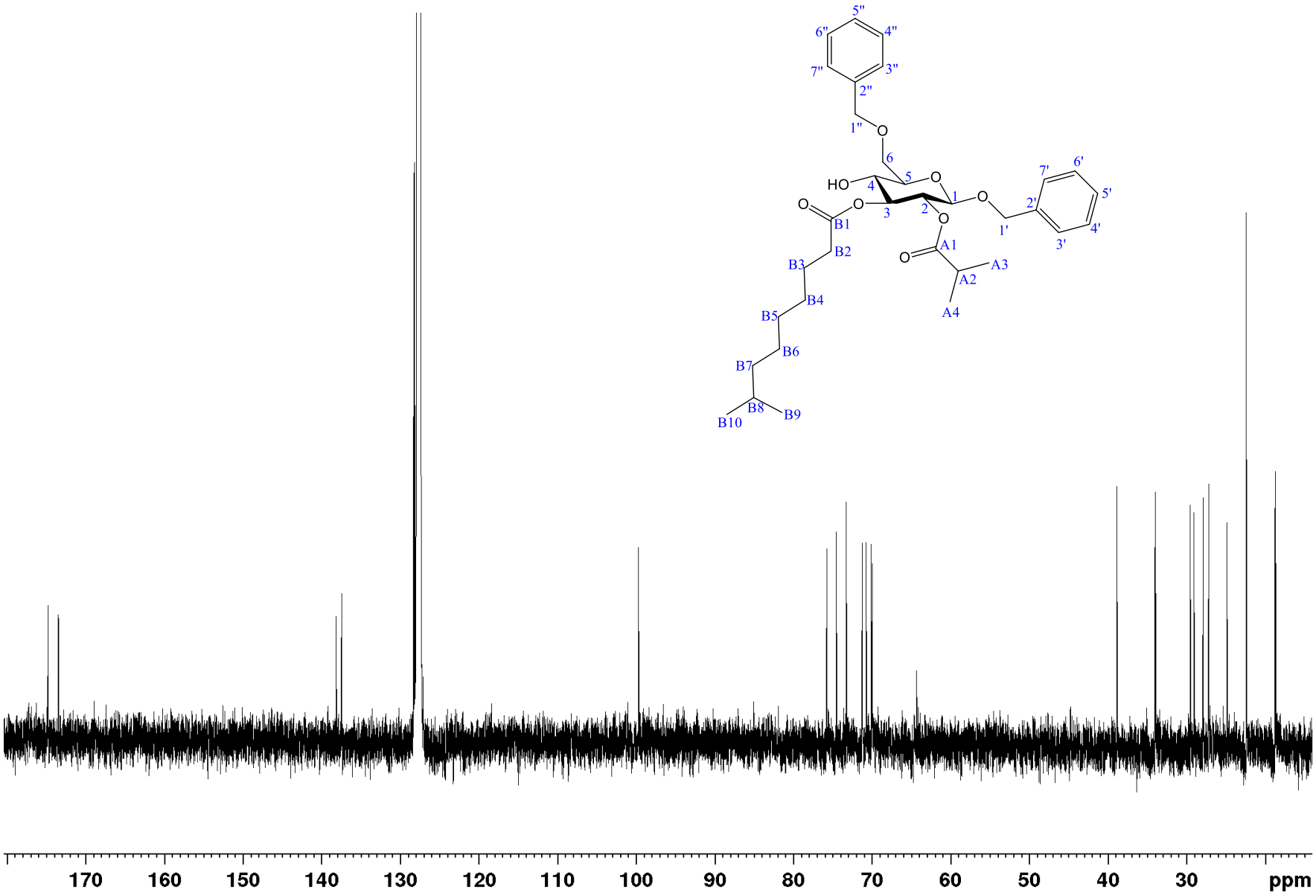

Figure S102: ^{13}C NMR spectrum of compound **13b** (126 MHz, C_6D_6).

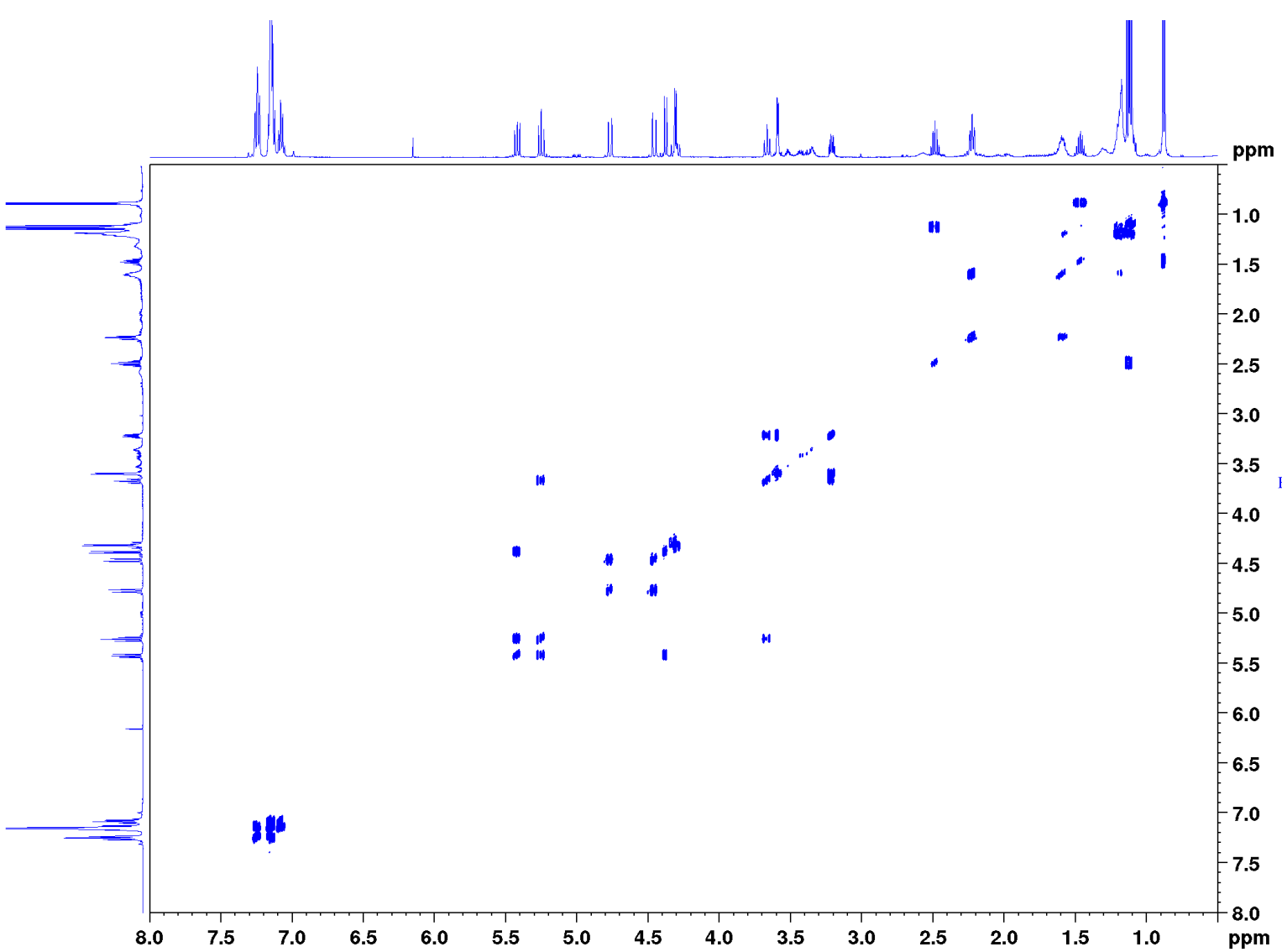

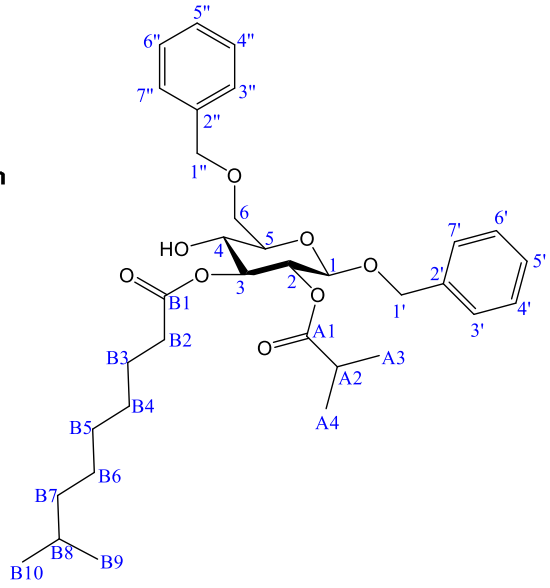

Figure S103: COSY spectrum of compound **13b** (500 MHz, C_6D_6).

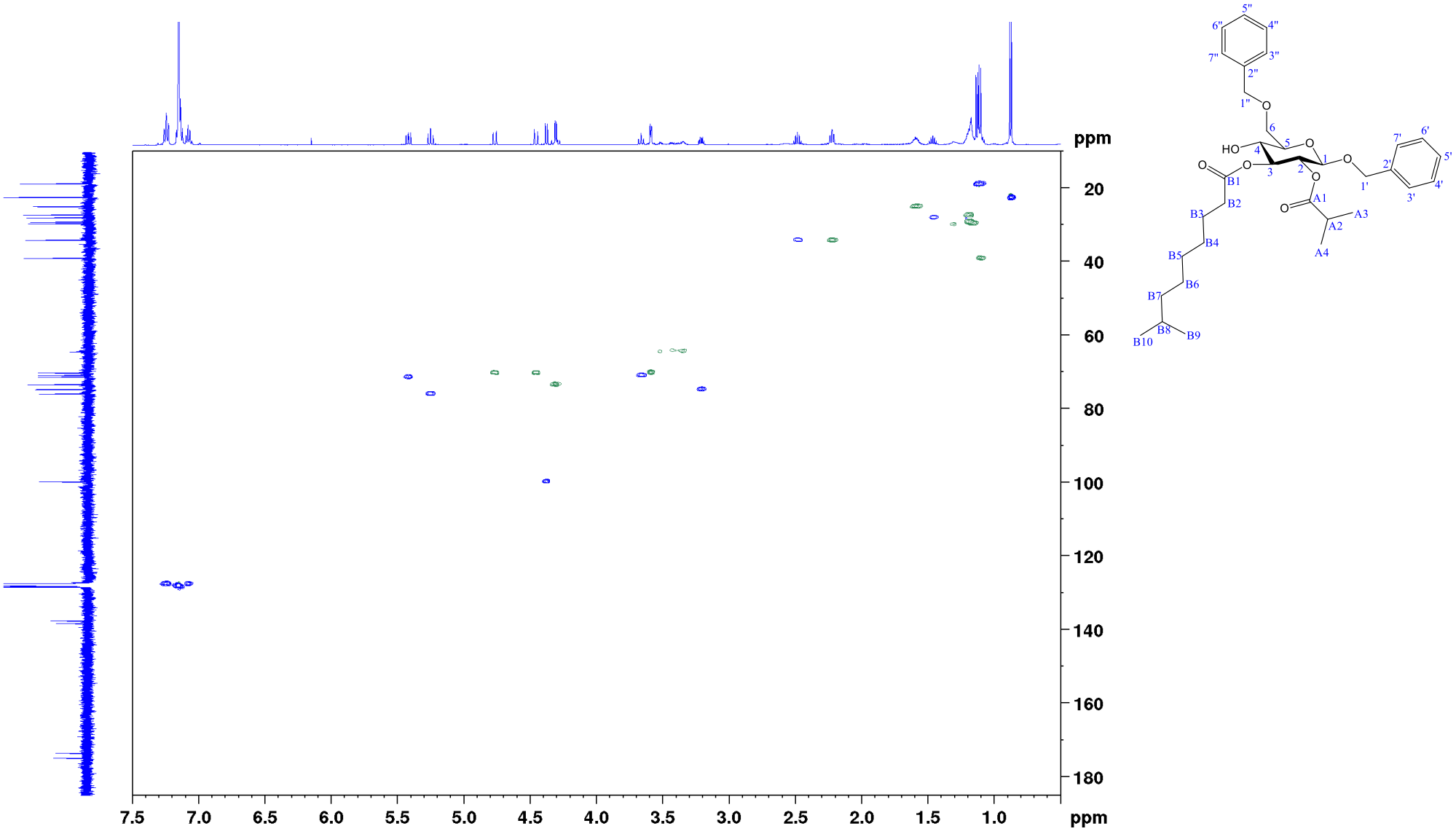

Figure S104: HSQC spectrum of compound **13b** (500 MHz, C_6D_6).

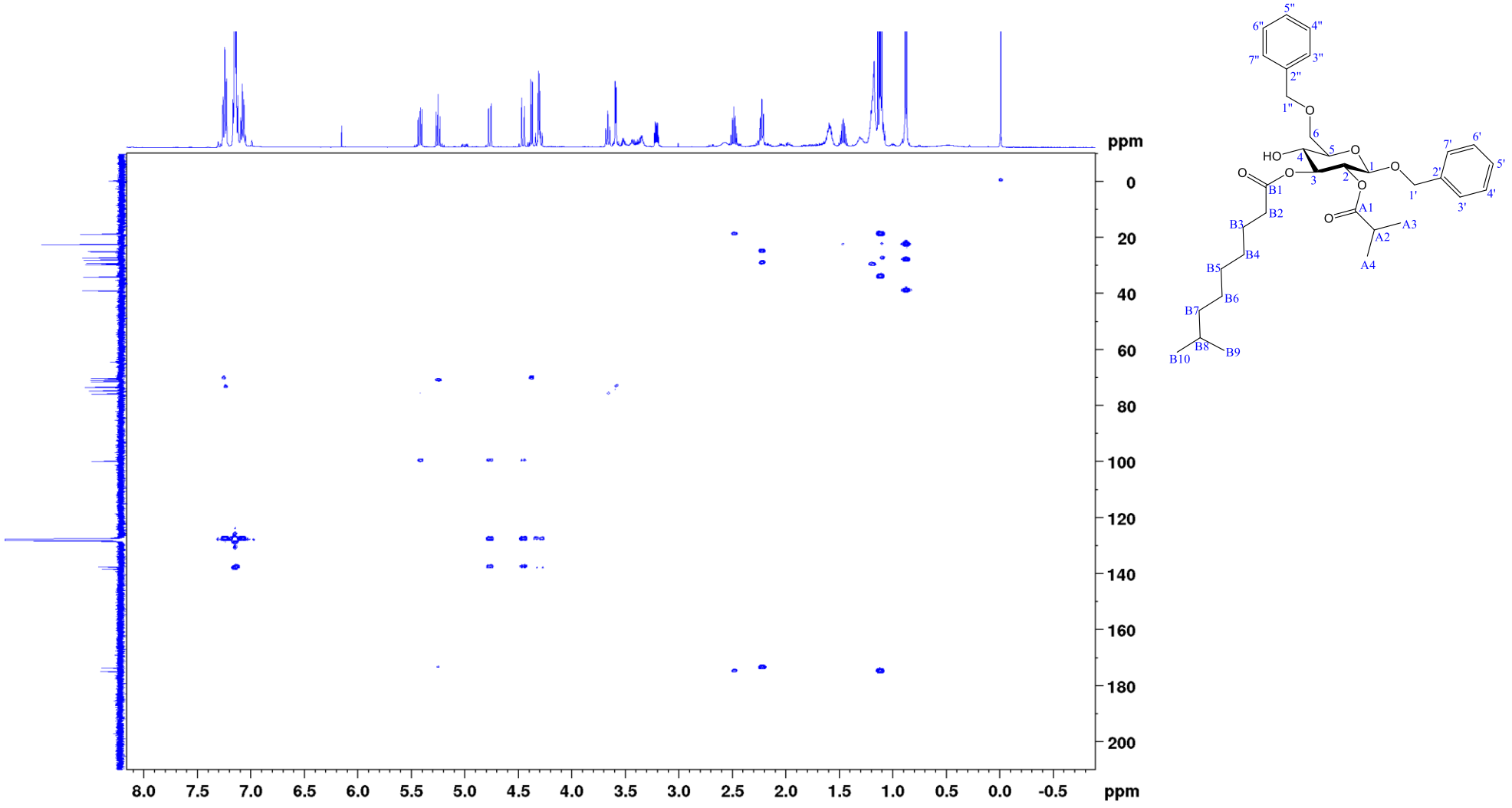

Figure S105: HMBC spectrum of compound **13b** (500 MHz, C_6D_6).

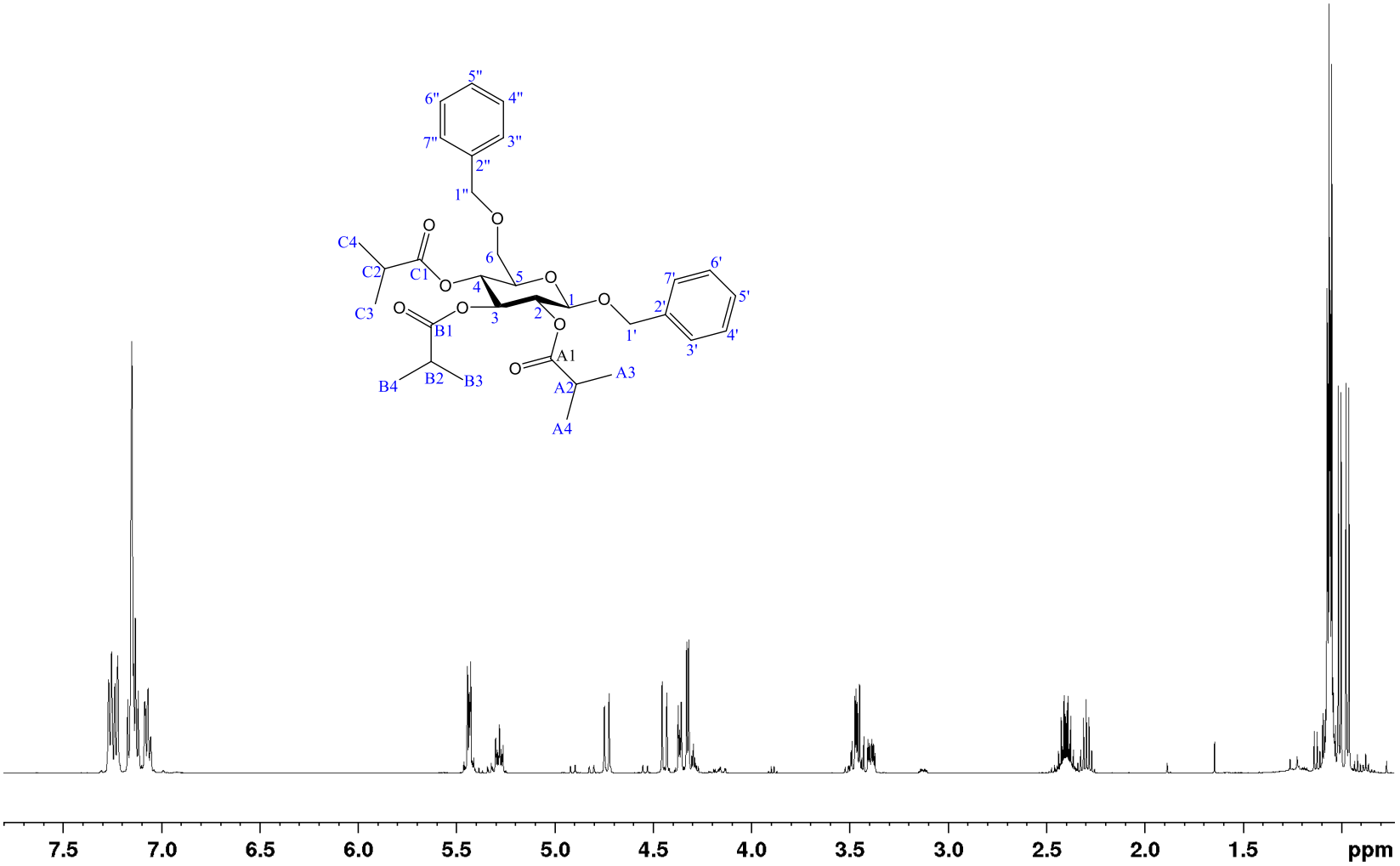

Figure S106: ^{1}H NMR spectrum of compound **14a** (500 MHz, C_6D_6).

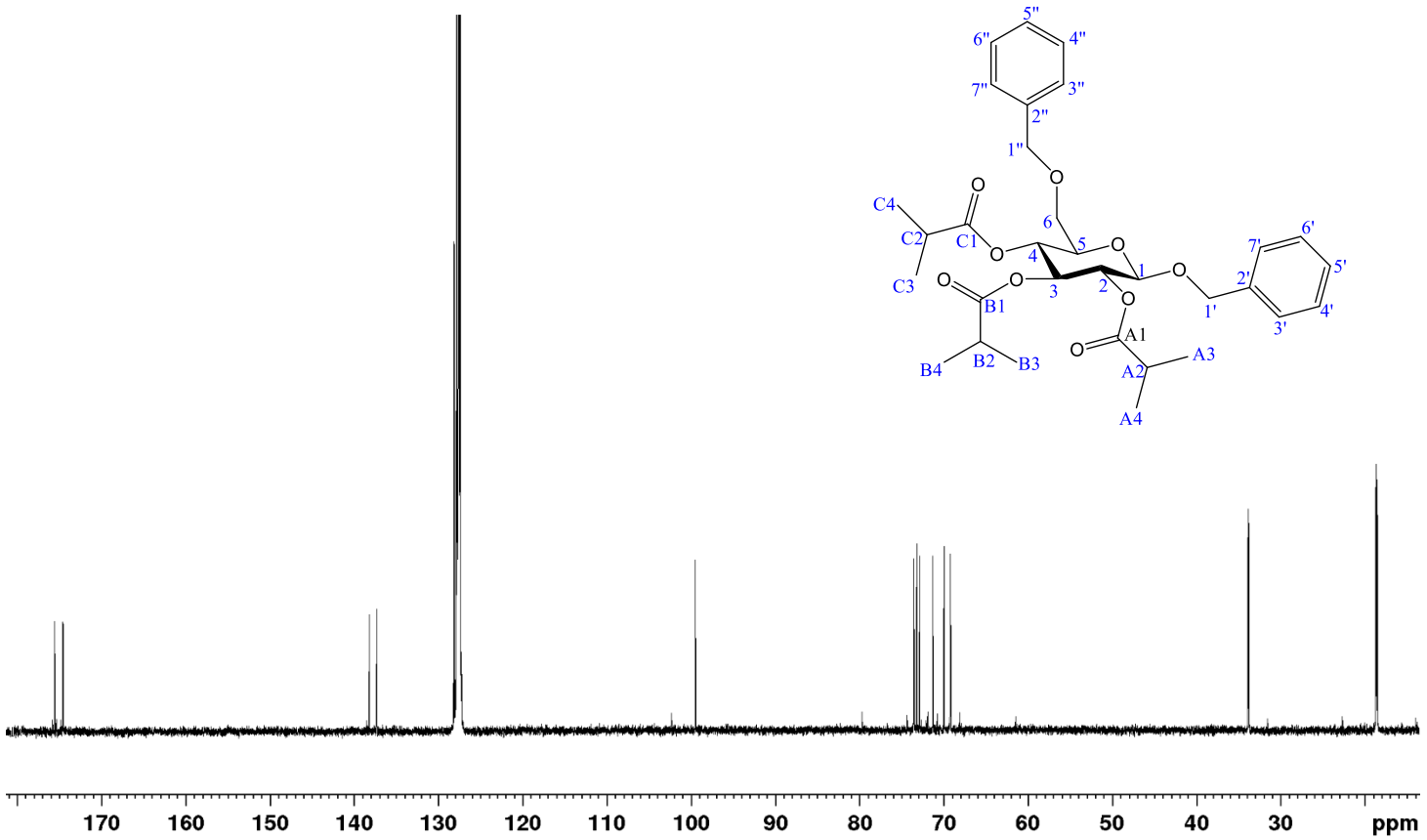

Figure S107: ^{13}C NMR spectrum of compound **14a** (126 MHz, C_6D_6).

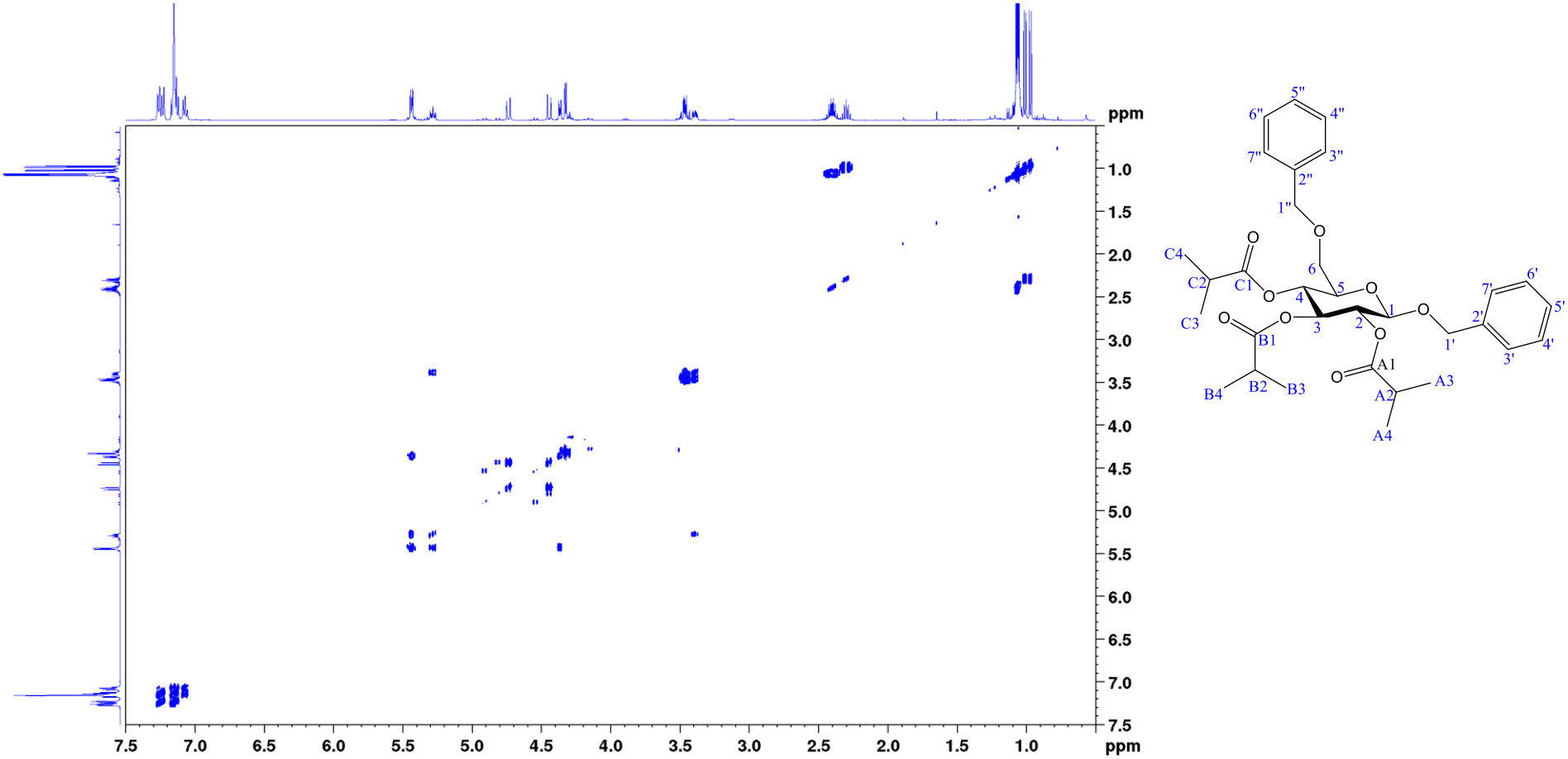

Figure S108: COSY spectrum of compound **14a** (500 MHz, C_6D_6).

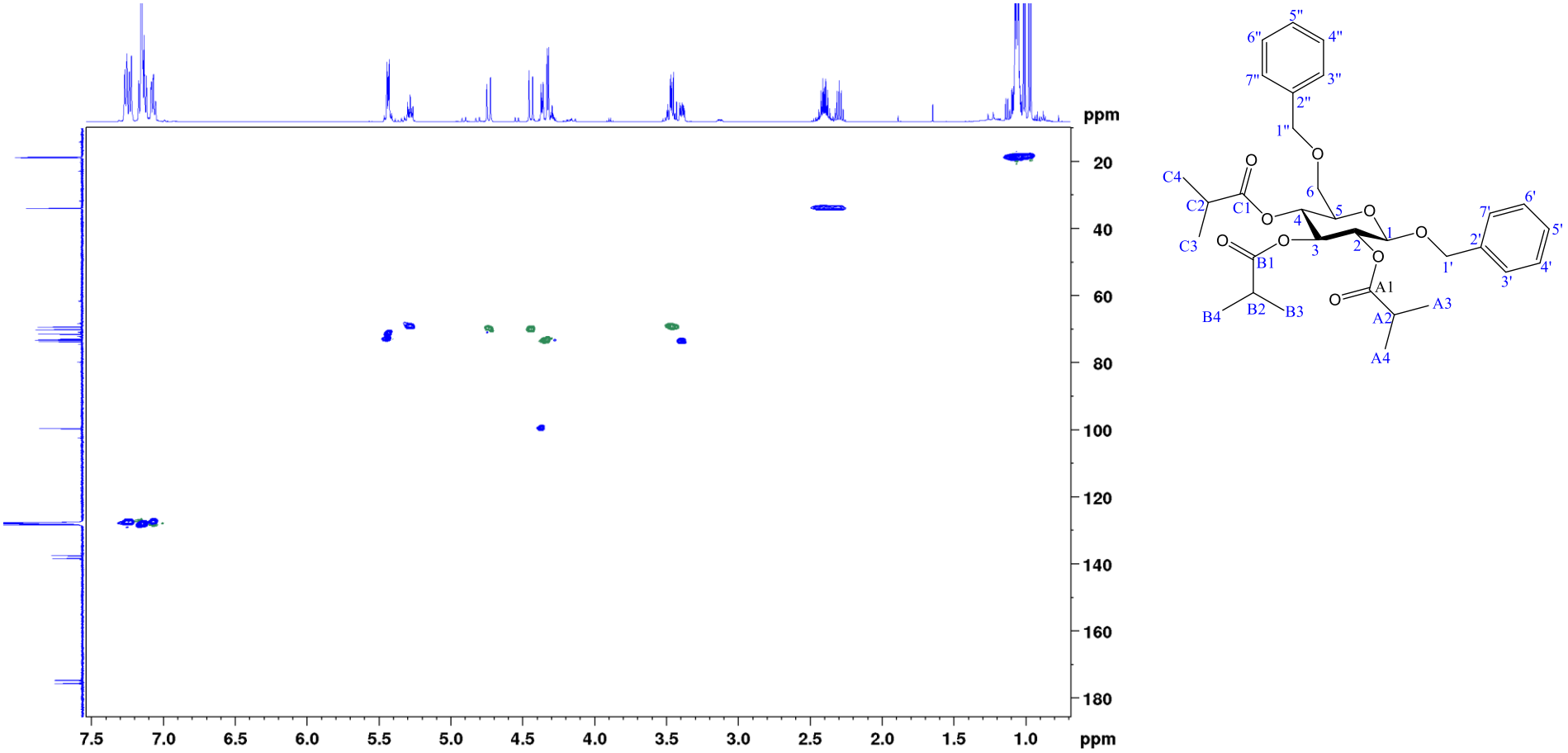

Figure S109: HSQC spectrum of compound **14a** (500 MHz, C_6D_6).

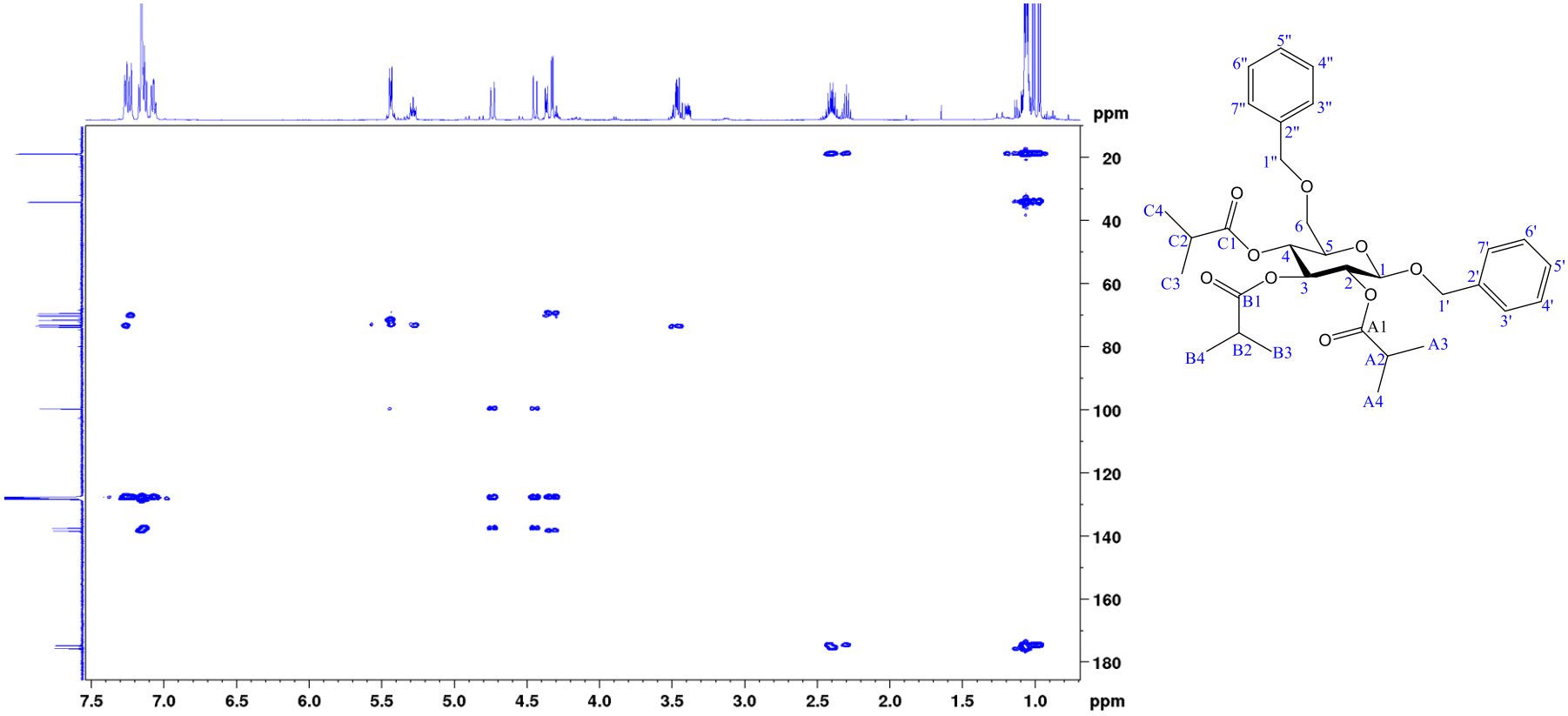

Figure S110: HMBC spectrum of compound **14a** (500 MHz, C_6D_6).

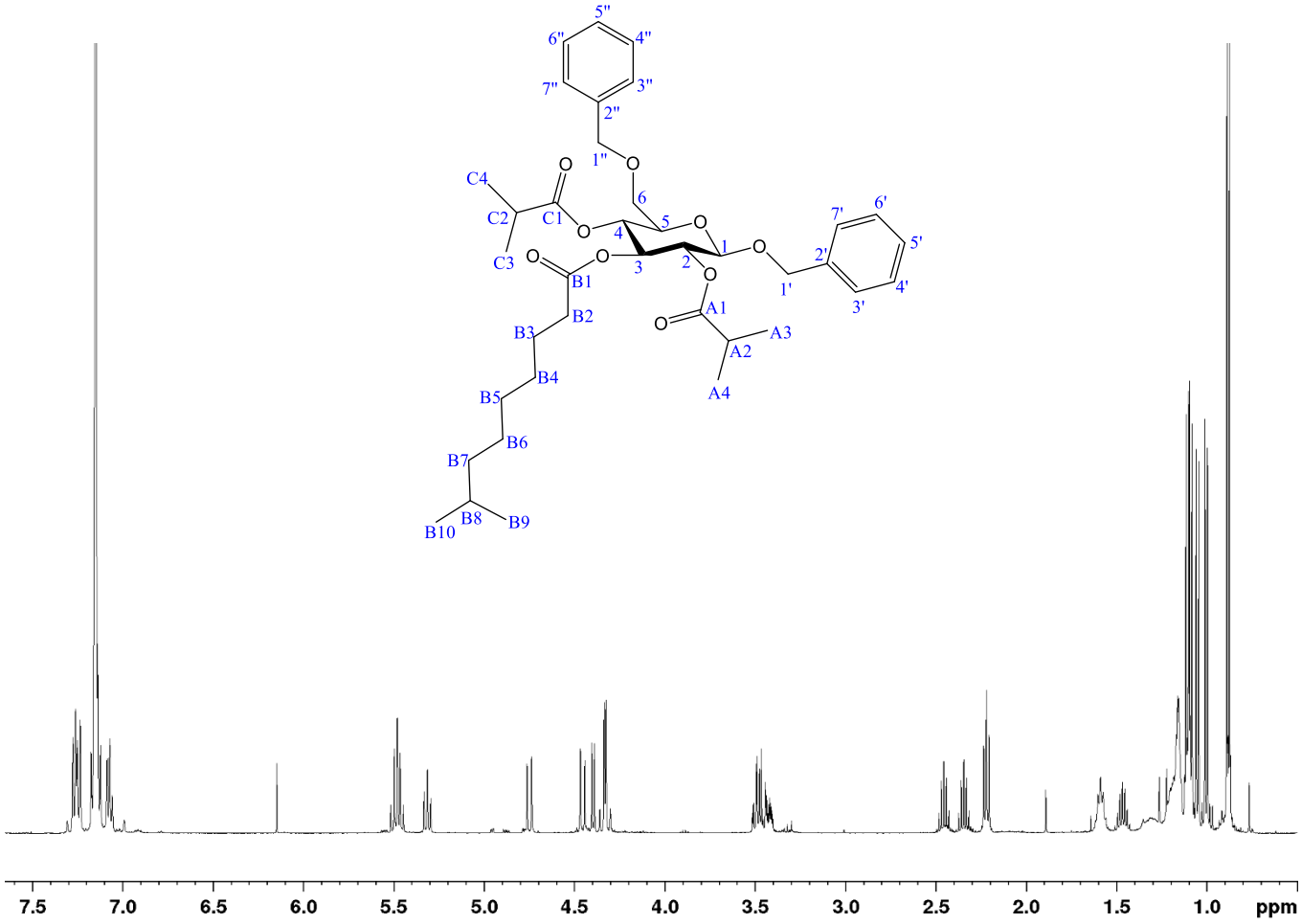

Figure S111: ^{1}H NMR spectrum of compound **14b** (500 MHz, C_6D_6).

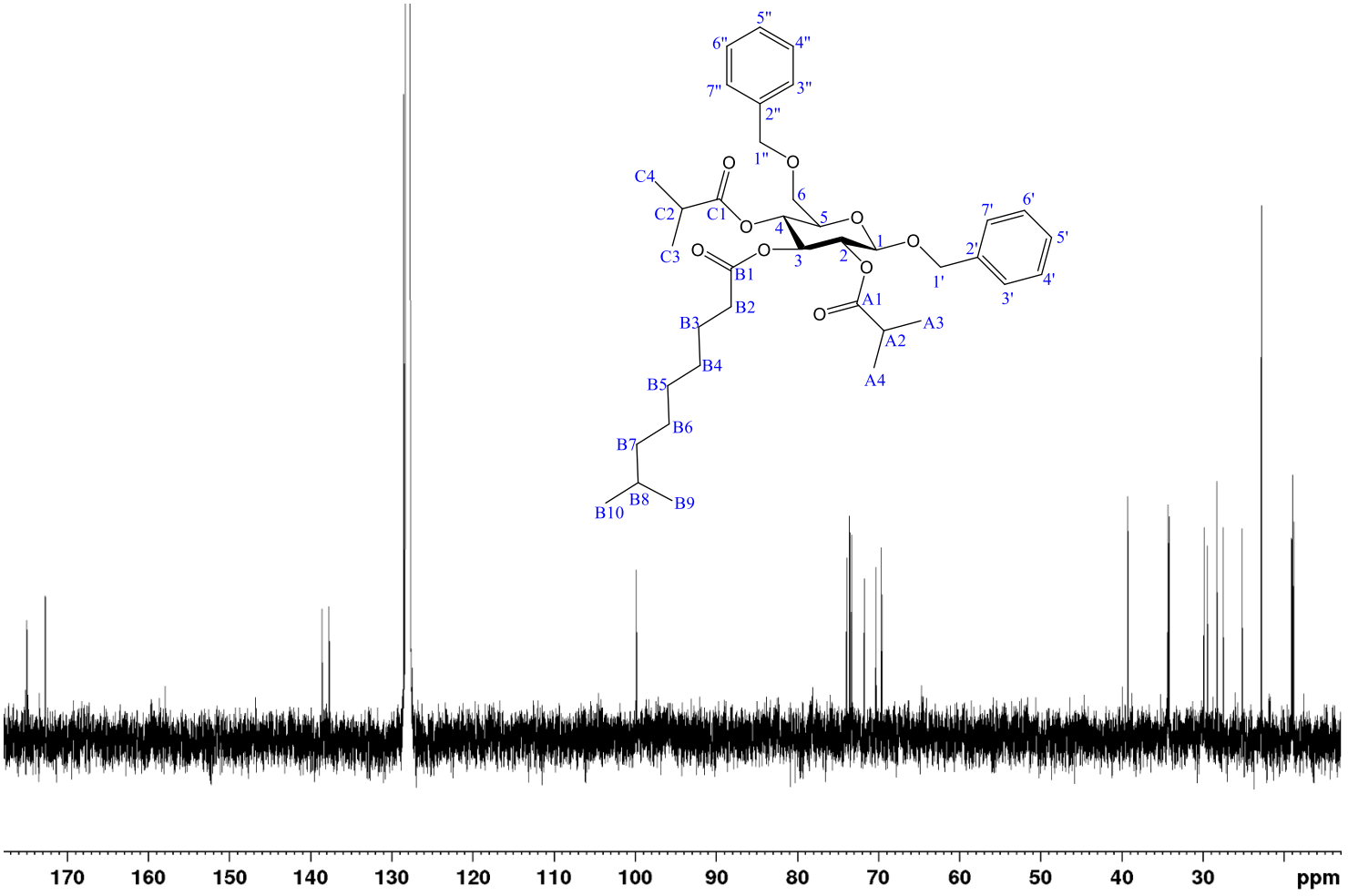

Figure S112: ^{13}C NMR spectrum of compound **14b** (126 MHz, C_6D_6).

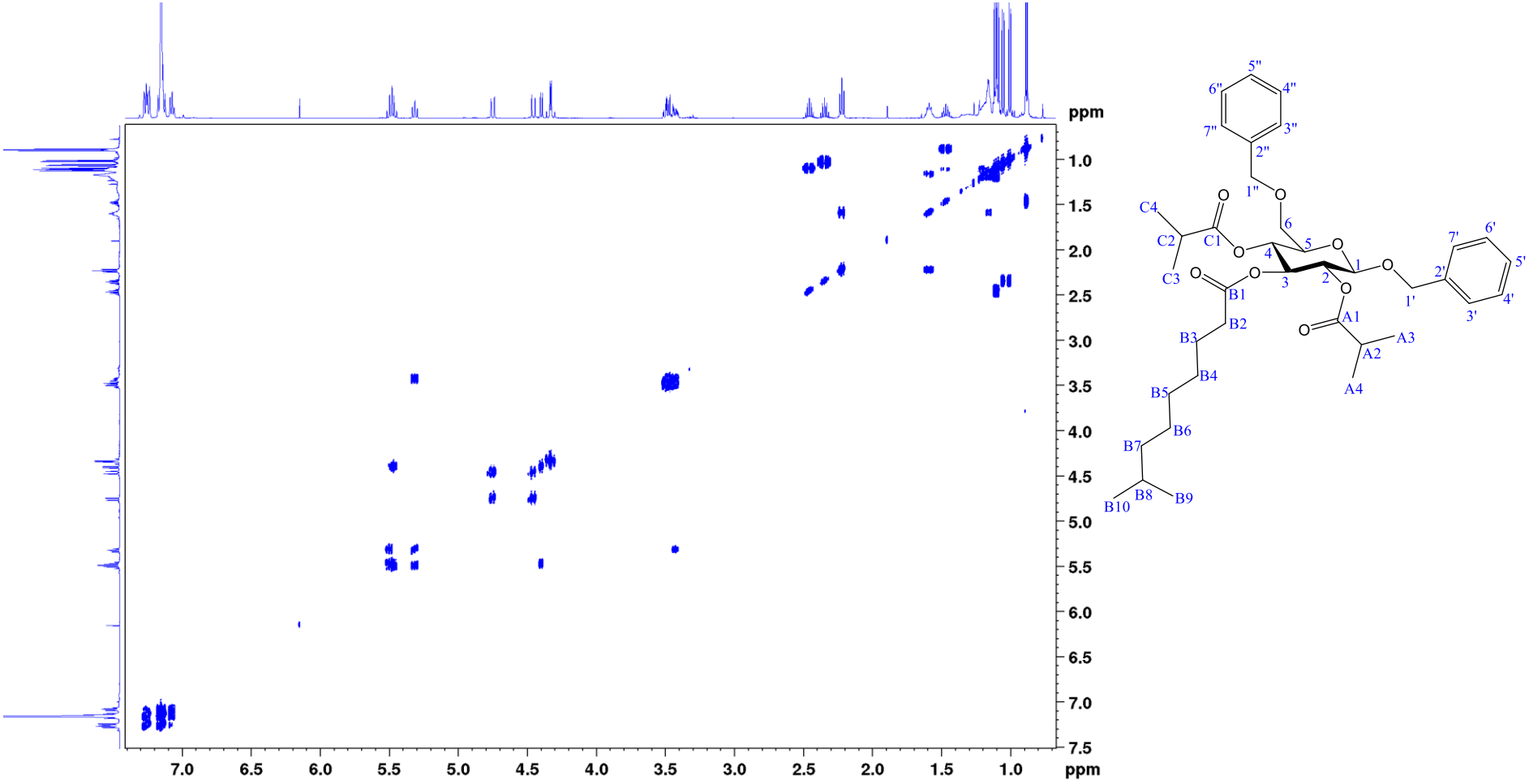

Figure S113: COSY spectrum of compound **14b** (500 MHz, C_6D_6).

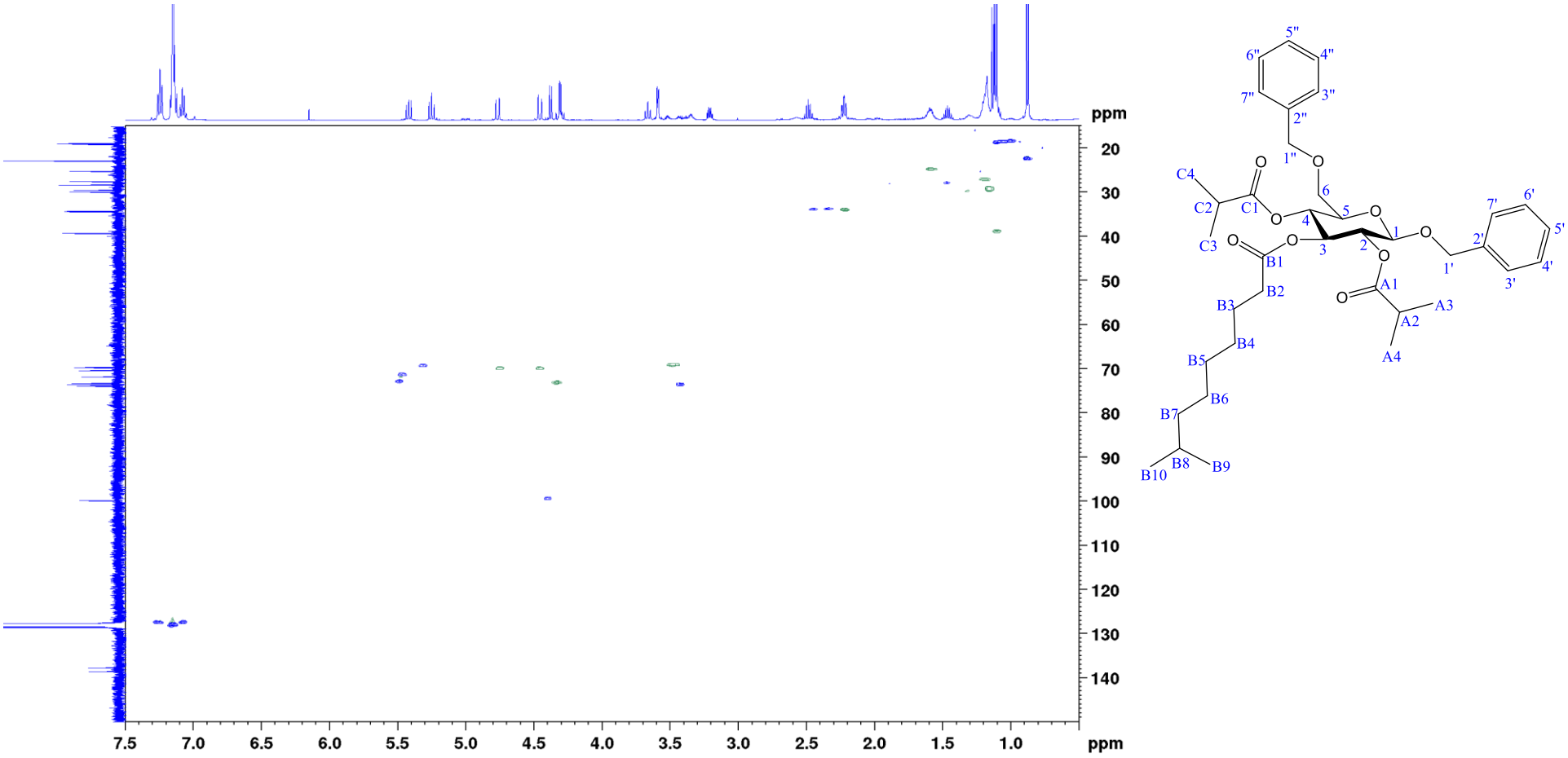

Figure S114: HSQC spectrum of compound **14b** (500 MHz, C_6D_6).

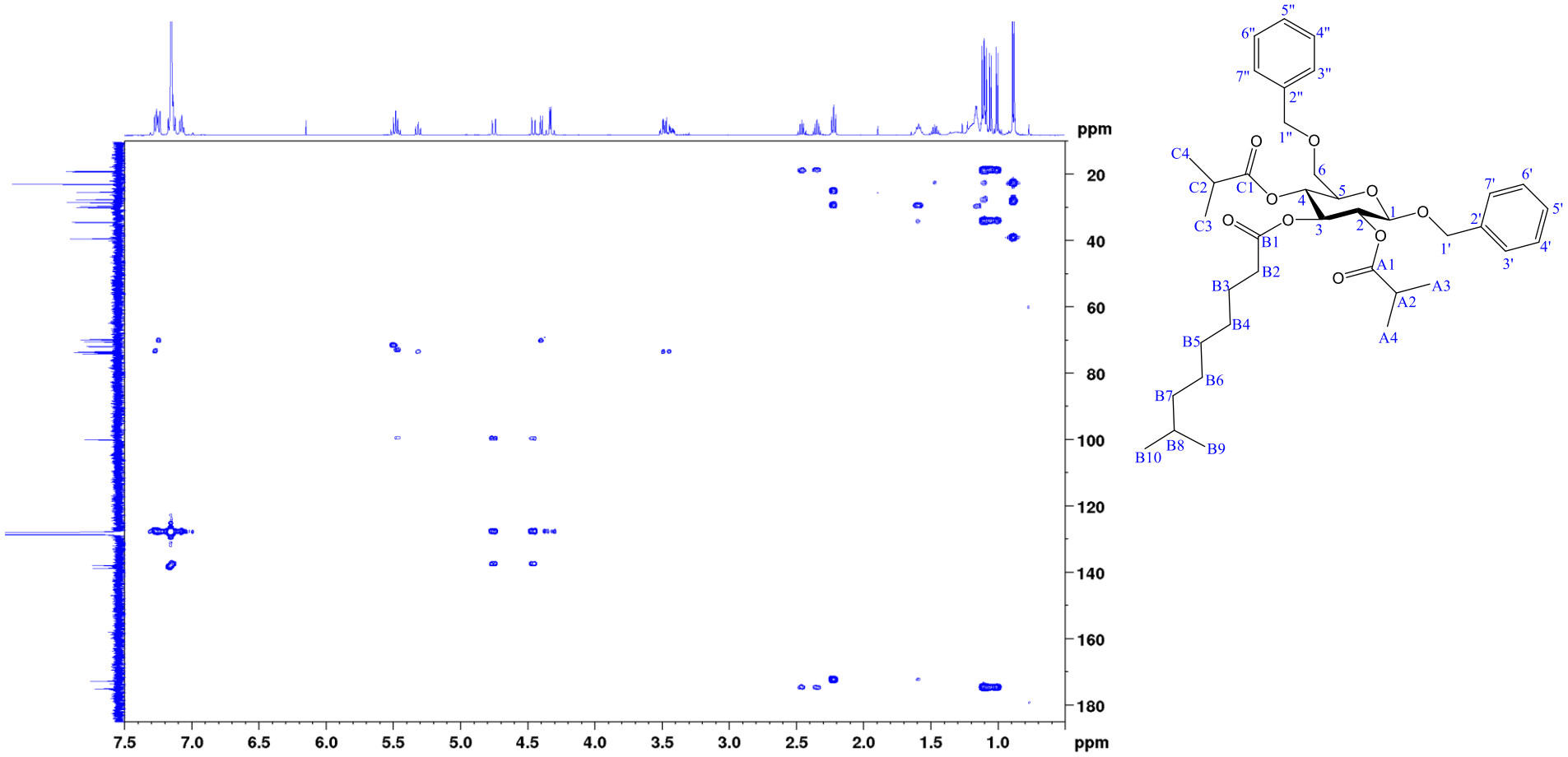

Figure S115: HMBC spectrum of compound **14b** (500 MHz, C_6D_6).